*Author:*
**Mediavilla Santos, Laura**

*Title:*
**Early postnatal development of neocortex-wide activity patterns in GABAergic and pyramidal neurons**

University of Bristol

School of Physiology, Pharmacology and Neuroscience
Ashby Lab

# Early postnatal development of neocortex-wide activity patterns in GABAergic and pyramidal neurons

Laura Mediavilla Santos

*A dissertation submitted to the University of Bristol in accordance with the requirements of the degree of Doctor of Philosophy in the Faculty of Life Sciences*

*1. Reviewer* Dr. Simon Butt
Department of Physiology, Anatomy and Genetics
University of Oxford

*2. Reviewer* Professor Clea Warburton
School of Physiology, Pharmacology and Neuroscience
University of Bristol

*Supervisor* Michael C. Ahsby

17th July 2023

Word count: 77,348

**Laura Mediavilla Santos**

*Early postnatal development of neocortex-wide activity patterns in GABAergic and pyramidal neurons*

PhD in Neural Dynamics, 17th July 2023

Reviewers: Dr. Simon Butt and Professor Clea Warburton

Supervisor: Michael C. Ahsby

**University of Bristol**

*Ashby Lab*

Biomedical Sciences Building

School of Physiology, Pharmacology and Neuroscience

University of Bristol, Tankard's Cl, University Walk

BS8 1TD Bristol

*For all I've learnt.*
*For all I've achieved.*
*This is for me.*

# Abstract

Before the onset of sensory experience, developing circuits generate synchronised activity that will not only influence its wiring, but ultimately contribute to behaviour. These complex functions rely on widely distributed cortical that simultaneously operate at multiple spatiotemporal scales. The timing of GABAergic maturation appears to align with the developmental trajectories of cortical regions, playing a crucial role in the functional development of individual brain areas. While local connectivity in cortical microcircuits has been extensively studied, the dynamics of brain-wide functional maturation, especially for GABAergic populations, remain underexplored. In this project, a dual-colour widefield calcium imaging approach was developed to examine the neocortex-wide dynamics of cortical GABAergic and excitatory neurons simultaneously across early postnatal development. This study provides the first broad description of neocortex-wide GABAergic developmental trajectories and their cross-talk with excitatory dynamics during the second and third postnatal weeks.

The observed spontaneous activity revealed discrete activity domains, reflecting the modular organisation of the cortex. Both excitatory and GABAergic population exhibited an increase in the size and frequency of activity motifs, as well as changes in motif variability. However, as they matured, the distribution of these spatiotemporal properties displayed divergent trajectories across populations and regions. These findings suggest fundamental differences in the spatial organisation of both populations, indicating potential distinct roles in cortical network function development. Moreover, while excitatory and GABAergic dynamics exhibited high correlations, brief deviations from perfect timing were observed. This correlation patterns changed significantly during development and across regions, with the two populations gradually becoming more correlated as they matured. Manipulating inhibition *in vivo* disrupted these fluctuations, impacting both local activity and the wider functional network.

These findings provide valuable insights into the developmental trajectories of spontaneous activity patterns in excitatory and GABAergic cell populations during early postnatal development. The interplay between both neuronal populations plays a critical role in shaping activity patterns, and understanding the underlying mechanisms of their development can provide valuable insights into neurodevelopmental disorders.

# COVID statement

The COVID-19 pandemic severely impacted research activities, especially for PhD students. Limited and inconsistent guidelines from the authorities led to rapid decision-making within the University of Bristol as the crisis unfolded. The Health Research Authority took control over national research priorities by suspending non-COVID research early on in the pandemic, which meant that the University of Bristol officially closed on March 18, 2020.

The Animal Support Unit (ASU) faced difficulties due to closure and lockdown decisions, resulting in the complete cessation of animal experiments and the reduction and/or termination of most animal breeding colonies. A soft reopening occurred in July 2020 for priority research, but the resumption of ASU activity was slower than expected, partly due to refurbishment works that continued until October 12, 2020. These works revealed existing ASU issues, further delaying the reopening and impacting the resumption of research activities. This meant that it wasn't until May 2021, when the first-ever piece of data was collected, two and a half years into the PhD.

The research activities curtailed by the lockdown and further ASU closure include:

- Establishment of the transgenic breeding line: two new mouse lines required for the project were purchased at end of January 2020, and arrived in Bristol at the same time the ASU implemented strict breeding restrictions. As a result, the mouse lines were maintained with limited numbers until the unit could fully reopen. Since the project relied on a triple breeding strategy, this required a longer breeding period to obtain the experimental colonies as it involved multiple breeding cycles.
- Adaption of the imaging technique: the existing equipment in the lab had to be adapted for a new dual-colour and longitudinal imaging approach. The new parts had to be purchased and the setup has to be optimised for the approach to work effectively. This involved conducting control animal experiments and accessing the imaging room, both of which were not feasible.
- Collection of pilot data: due to the exploratory nature of the project, preliminary data had to be collected in order to generate hypotheses that could contribute to the foundation of more focused research questions. The acquisition of this data relied on the establishment of the breeding line and the setup of the imaging technique.

The project was severely affected by the pandemic, particularly because it was still in its early stages and no data had been collected prior to the lockdown. As mentioned above, the project adopted an exploratory approach, incorporating two novel transgenic mouse lines, one of them previously never tested in developmental studies. This posed challenges in evaluating their reliability and exploring alternative strategies to adjust the project, as completely changing the approach was not feasible due to the uncertain nature of the pandemic. The delay on these research-related activities had a knock-on effect on the project as it was very dependent on the first set of results, which had a delay of over a year, not only affecting the type of experiments performed but also the sample size.

Hence, the initial plan during the lockdown was to shift the project's focus towards the computational and analytical aspects. The idea was to utilise the data gathered by a lab member to construct statistical models and analysis pipelines that could be readily employed once data collection resumed. However, due to the lack of supervision on that side of the project, coupled with the complexity of the methods and the large data types involved in the project, progress on computational and analytical aspects was also hindered during the lockdown. This situation resulted in frustration and demotivation, and added to the already significant toll on mental health caused by the pandemic.

# Acknowledgements

Although the PhD journey can feel like a lonely one at times, it takes a lot of people to raise a doctor. First and foremost, my supervisor Mike, who was always there to guide me and support me through this journey. Thank you for giving me the space to make my own mistakes, which allowed me to learn and grow, while still providing advice every time I felt lost and confused.

To the Ashby and Anastasiades lab members, past and present, thank you for the laughs, the gossip, for introducing me to climbing, and of course, all those insanely valuable science tips and discussions. But above all, thank you for keeping a constant snack supply in the office, you have spoiled me for life. I would like to extend a special thanks to Jini for ensuring I had proper meals even when I would have otherwise survived on potato chips and pizza. And to Naomi, for all those passionate office rants about everything and nothing which were a perfect stress release during challenging times.

I am also deeply grateful to the Inclusive Research Collective for giving me a chance to work on something I am truly passionate about. Being part of this team has been a major highlight of my journey. Specially, thank you to Amber and Luke, who consistently pulled me out of the science bubble and provided valuable perspective to both my research and life. Thank you for helping me maintain (somewhat) balance and perspective throughout this journey.

Also, a really big thank you to all the wonderful people I have met in this incredible city. who, after taking one look at my profile picture, deemed me crazy enough to be her roommate. Without you, the journey would have been a lot lonelier, and a lot less fun.

I would also like to acknowledge the many people and organisations who made my PhD research possible. To my funders and directors at the Wellcome Trust Neural Dynamics programme, thank you for providing me with the resources I needed to succeed. To the mechanical and electrical workshops, thank you for helping me bring my miniaturised designs to life. And to my uncle, thank you for patiently helping me build the electrical circuit for my neonatal setup, even when it meant sacrificing some of our precious holiday time together.

Last but certainly not least, I want to thank my family and friends back home for their unwavering support, even though they probably will never fully understand what I do, they still proudly tell

anyone who will listen, "she does something with brains and mice". So thanks for always having my back, even if you don't quite get it. A special thank you to my mom, for her gentle reminders that I should maintain a healthy work-life balance; and to my dad, who learnt what google scholar was just to help me with reference formatting. And finally, to my very best, Heng, who has been my rock throughout this journey, and having a support system is the most important thing, right? Thank you for dragging me through the finish line, both figuratively and literally, I couldn't have done it without you.

# Declaration

I declare that the work in this dissertation was carried out in accordance with the requirements of the University's Regulations and Code of Practice for Research Degree Programmes and that it has not been submitted for any other academic award. Except where indicated by specific reference in the text, the work is the candidate's own work. Work done in collaboration with, or with the assistance of, others, is indicated as such. Any views expressed in the dissertation are those of the author.

*Bristol, 17th July 2023*

Laura Mediavilla Santos

# Contents


**1 Introduction** **1**

1.1 The *emergent* brain. . . . . 1

1.2 Neocortical formation. . . . . 2

1.2.1 Primary neuronal cell types in the neocortex. . . . . 3

1.2.2 Neurogenesis, migration and laminar distribution. . . . . 4

1.2.3 Cortical arealisation. . . . . 6

1.2.4 Functional integration and wiring the cortex: short and long range connections . . . . . 9

1.3 Development of primary sensory networks. . . . . 12

1.3.1 Structural changes to developing sensory networks. . . . . 12

1.3.2 Developmental behavioural changes. . . . . 13

1.3.3 Spatiotemporal patterns of spontaneous activity during development. . . 15

1.3.4 Developmental transition to mature activity states. . . . . 17

1.3.5 Maturation of spontaneous activity and emergence of functional architecture in the developing human neocortex. . . . . 19

1.4 Critical periods of development. . . . . 21

1.4.1 Cross-modal plasticity following early sensory deprivation. . . . . 23

1.4.2 Experience-related control of critical periods. . . . . 24

1.4.3 GABAergic control of critical period plasticity. . . . . 25

1.4.4 Excitation-inhibition balance and timing of critical periods. . . . . 26

1.5 Developmental perspective on GABA polarity shift. . . . . 27

1.5.1 When are depolarising GABA responses excitatory? . . . . . 27

1.5.2 Excitatory and inhibitory GABAergic effects in the immature brain. . . . 29

1.5.3 Consequences of the GABA switch on network development. . . . . 30

1.6 Thesis outline. . . . . 31

**2 Chronic, neocortex-wide, dual-colour calcium imaging in awake behaving neonatal mice** **33**

2.1 Introduction. . . . . 33

2.1.1 Why do we care about multi-region recordings? . . . . . 34

2.1.2 Techniques and analysis methods for large-scale recordings. . . . . 36

2.1.3 Optoencephalography or widefield calcium imaging. . . . . 40

2.1.4 Aims and outline. . . . . 42

2.2 Methodological approach: technique development and preprocessing pipeline. 43
2.2.1 Custom-built macroscope for widefield imaging. . . . . 43
2.2.2 Surgical preparation to image through the intact skull. . . . . 50
2.2.3 Data preprocessing pipeline. . . . . 51
2.3 Results and validations. . . . . 61
2.3.1 Sources of widefield fluorescence. . . . . 61
2.3.2 Controls for dual-colour widefield calcium imaging. . . . . 66
2.3.3 Validation of the long-term headpost implant on neonatal mice for chronic imaging. . . . . 78
2.4 Discussion. . . . . 81
2.4.1 Possible sources of the widefield fluorescence signals across early postnatal development. . . . . 82
2.4.2 Validity of the preprocessing method. . . . . 86
2.4.3 Control experiments to assess the longitudinal dual-colour imaging approach. . . . . 87
2.4.4 Limitations of dense labelling widefield calcium imaging. . . . . 89
2.4.5 Closing remarks. . . . . 90

**3 Characterisation of developmental neocortex-wide spontaneous activity patterns 91**
3.1 Introduction. . . . . 91
3.1.1 Spontaneous activity during early brain development. . . . . 92
3.1.2 GABAergic interneurons shape the functional maturation of the cortex. . 94
3.1.3 Aims and research questions. . . . . 95
3.2 Methods. . . . . 95
3.2.1 Database summary. . . . . 96
3.2.2 Breeding the triple transgenic mice. . . . . 96
3.2.3 Surgical preparation to image through the intact skull. . . . . 98
3.2.4 Picrotoxin injections. . . . . 98
3.2.5 Protocol for widefield calcium imaging of spontaneous activity. . . . . 99
3.2.6 Preprocessing of widefield calcium imaging data. . . . . 99
3.2.7 Spatiotemporal properties and metrics to describe spontaneous motifs. 101
3.2.8 sICA motif identity assignment. . . . . 102
3.2.9 Reduction of the SNR for the recordings. . . . . 102
3.2.10 Jaccard index for EI partners and instantaneous correlation. . . . . 103
3.2.11 Statistical analysis. . . . . 104
3.2.12 Data visualisation. . . . . 105
3.3 Results. . . . . 105
3.3.1 Spatiotemporal development of spontaneous neocortex-wide activity. . . 106
3.3.2 Regionalisation of spatiotemporal activity motifs across the dorsal cortex. 113
3.3.3 Complexity of cortical population dynamics across early development. . 121

3.3.4 Developmental maturation of excitation and inhibition balanced temporal dynamics. . . . . 128
3.4 Discussion. . . . . 138
3.4.1 Defining cortical domains based on spontaneous activity patterns in early postnatal development. . . . . 138
3.4.2 Excitatory and GABAergic populations exhibited divergent trajectories of their spatiotemporal dynamics across regions and developmental age. . 140
3.4.3 Correlation patterns between GABAergic and pyramidal neuronal populations reveal developmental regional changes in cortical function. . . . . 142
3.4.4 Limitations. . . . . 144
3.4.5 Closing remarks. . . . . 147

**4 General discussion and next steps** **149**
4.1 Future experiments. . . . . 156
4.2 Closing remarks. . . . . 158

**Annex** **159**

**Bibliography** **175**

# List of Figures


2.1 Examples of distributed representation of behaviour in mouse neocortex . . . . . 35
2.2 Schematic overview of the spatiotemporal resolution and spatial coverage spectra of techniques to monitor brain dynamics . . . . . 39
2.3 Overview of the components of the custom-built macroscope . . . . . 44
2.4 Acquisition parameters for dual-colour light excitation and collection pathways . . 47
2.5 Overview of the system requirements for neonatal mice head fixation . . . . . 49
2.6 Diagram of the data processing pipeline . . . . . 53
2.7 sICA noise sorting and resolution analysis . . . . . 56
2.8 Comparison of spatial and temporal information content through sICA compression and filtering . . . . . 59
2.9 Photobleaching and temporal filtering of fluorescent signals . . . . . 60
2.10 Contribution of the Thy1-jRGECO1a;Gad2;GCaMP6f transgenic mouse line to widefield fluorescence . . . . . 65
2.11 Photoswitching effect of jRGECO1a at different blue-light frequency pulses . . . 68
2.12 Assessment of lateral brain movement during awake imaging . . . . . 70
2.13 Movement-induced blood volume artefacts in CAG-GFP mice across early postnatal development . . . . . 74
2.14 Evaluation of signals contributing to the spectrogram and hemodynamics . . . . 76
2.15 Incidence of epileptiform events observed in the longitudinal widefield calcium imaging of GABAergic and pyramidal populations . . . . . 77
2.16 Assessment of the effect of the chronic implant on developmental growth . . . . 80
2.17 Open field behaviour of the chronic implanted animals after longitudinal recordings 81
2.18 Examples of high spatial precision maps obtained with widefield calcium imaging 85

3.1 Modality-specific spatial organisation of spontaneous neuronal activity in the sensory systems during early developmental stages . . . . . 93
3.2 Breeding of the triple transgenic mouse line and experimental yield . . . . . 97
3.3 Illustration of spontaneously occurring spatial activity motifs across early postnatal development . . . . . 107
3.4 Stable coverage of the exposed cortex by spatial activity motifs during early postnatal development . . . . . 108
3.5 Developmental trajectory of activity motif size in pyramidal and GABAergic populations during early postnatal development. . . . . 109
3.6 Temporal dynamics of activity motifs across early postnatal development . . . . . 112

3.7 Developmental trajectory of activity motif frequency in pyramidal and GABAergic populations during early postnatal development . . . . . 113
3.8 Functional parcellation of developing neocortex using the TCA-RFP mouse line. . 114
3.9 Spread of the sICA motif spatial masks across cortical region boundaries . . . . 116
3.10 Proportion of sICA motifs assigned to each region of interest across development 118
3.11 Motif size and frequency per region across development . . . . . 121
3.12 Developmental changes in population and region-specific variance of cortical activity 123
3.13 Distinct developmental trajectories of activity motifs in pyramidal and GABAergic neuronal populations . . . . . 125
3.14 Influence of SNR on the sICA decomposition of GCaMP6f and jRGECO1a dynamics 127
3.15 Overlap distributions between pyramidal and GABAergic sICA motifs across development. . . . . 130
3.16 Instantaneous correlation between GABAergic and pyramidal dynamics across different temporal scales . . . . . 131
3.17 Strengthening correlation between GABAergic and pyramidal dynamics during development . . . . . 133
3.18 Region-specific tightening of correlation between GABAergic and pyramidal dynamics 134
3.19 Epileptic-like activity induced by blockade of GABAergic signalling . . . . . 136
3.20 Shift towards higher GABAergic-pyramidal correlation after blockage of GABAergic signalling . . . . . 137

# List of Tables

2.1 Overview of the multi-region recording techniques and their trade-offs . . . . . 38
2.2 Widefield macroscope specifications and optical parameters of grey matter at different wavelengths used for the simulations . . . . . 63

# 1 Introduction

Neural circuits are organised and tuned to achieve stable functions that result in robust behaviour. They must, however, strike a delicate balance between reliability and the flexibility to adapt and learn in response to changing environments. The establishment of circuits with these seemingly antagonistic properties is non-trivial, and requires an intricate developmental process, in which all of this rich repertoire of computations and spatiotemporal activity patterns is acquired. Understanding brain development is therefore critical to understanding how behaviour and cognition emerge through cortical region interactions.

## 1.1 The *emergent* brain.

The concept of *emergence* is essential to understanding brain dynamics and behaviour. In the context of this project, two different perspectives can be used to frame this concept. Firstly, the term *emergent* can refer to the process of forming and establishing nascent neuronal networks that occurs during early postnatal development. Secondly, *emergent* dynamics refer to the complex properties that arise from the collective interactions across brain regions. Characterising how dynamic interactions between distributed brain regions are established can inform the understanding of mature network function, much like observing the construction of a car engine helps in understanding how all the components work together. Consequently, it is crucial to investigate these emergent properties from early development.

The brain is a complex and adaptive system that undergoes protracted developmental changes to establish functional networks, leading to the emergence of complex behaviours (Schotten et al., 2022; Chialvo, 2010). While significant progress has been made in understanding the development of individual neural circuits within specific brain regions, our knowledge of the developmental trajectories of whole-brain functional networks, particularly in animal models, remains limited (Ackman et al., 2014b; McVea et al., 2017; Cross et al., 2021; Mojtahedi et al., 2021; Gribizis et al., 2019). Although non-invasive neuroimaging techniques are commonly used to study emergent brain dynamics in humans (Menon, 2013; Pines et al., 2022), the use of animal models provides an opportunity to employ more invasive techniques that can enable detailed investigations into the mechanisms of distributed computation and the underlying circuitry involved (Lake et al., 2022). This knowledge is crucial for advancing translational science and developing effective treatments for neurodevelopmental disorders, as disrupted

functional connectivity has been implicated as a key feature in many of these disorders (Menon, 2011).

During early postnatal development, a general feature observed in large-scale dynamics is a decrease in correlation among nearby brain regions (segregation), accompanied by an increase in the correlation between selected regions that are further apart (integration), resulting in a shift from local to distributed computations (Fair et al., 2009). While the local decorrelation and sparsification of activity have been extensively studied (Golshani et al., 2009; Rochefort et al., 2009; Chini et al., 2022), the formation of functional networks across distant regions has received less attention. Long-range connectivity is highly dynamic across early development, with both increases and decreases in correlation that are dependent on brain area and age (Ackman et al., 2014b). This progressive strengthening of intra- and inter-hemispheric connections aligns with the increase in long-range connectivity strength between distinct brain regions during brain development, which are key features in the formation of the cortical global network architecture (Fair et al., 2009). Additionally, the development of anatomical hierarchy, both at the regional level for stimulus encoding, and at the global level for distributed computations, appears to be a product of this protracted period of development (Pines et al., 2022).

It is crucial to recognise that the developing brain is not merely a smaller or less developed version of the adult brain. Instead, the immature brain exhibits distinct functions that emerge exclusively during this developmental period (Luhmann, 2022). The developing brain possesses a variety of unique characteristics, including specific cell types and structures, like the subplate and cajal-retzius cells (Luhmann et al., 2020), as well as transient circuits (Marques-Smith et al., 2016; Tuncdemir et al., 2016; Anastasiades et al., 2016) that facilitate the organisation of functional circuits within the immature brain. Moreover, brain activity patterns exhibit distinct developmental sequences that typically undergo changes at specific milestones along this trajectory, such as the initiation of active sensing or behaviour (Dehorter et al., 2012). Therefore, understanding emergent dynamics, encompassing both its conceptual meanings, is key for comprehending the underlying processes that later give rise to behaviour and cognition. Through the understanding of typical brain development, deviations from these expected trajectories can subsequently be identified and addressed, which may serve as indications of developmental disorders (Iannone et al., 2021; Tang et al., 2021). Thus, the adoption of a system-level approach to brain development and the consideration of the intricate interactions between different brain regions are essential.

## 1.2 Neocortical formation.

The neocortex is evolutionarily the youngest structure and is unique to mammals (Kaas, 2011). In humans, it constitutes over three-quarters of the brain mass (Azevedo et al., 2009). The expansion of the neocortex, particularly of the upper cortical layers, has played a significant role

in the increased cognitive abilities of humans, and appears to be influenced by the lengthening of the neurogenic period (Stepien et al., 2020; Florio et al., 2014). Remarkably, longer gestation periods result in a longer neurogenic period, producing a greater number of neocortical neurons, even across different rodent strains (Stepien et al., 2020).

The complexity of the neocortex arises from its extensive interconnections and organisation, and can be defined along two structural and functional orthogonal axes: a radial plane organised generally into six layers that run parallel to the surface of the cortex, and a tangential arrangement into functional cortical columns (Douglas et al., 2004). These layers exhibit alternating patterns of cell density, generally with layers I (L1), III (L3), and V (L5) having relatively fewer cells, while layers II (L2), IV (L4), and VI (L6) typically have relatively higher cell density (Keller et al., 2018). Cortical columns can further organise into more complex structures, from brain regions to functional networks and topographical maps (Rakic, 1988; Kätzel et al., 2011; Cadwell et al., 2019). During development, the allocation of different populations of neurons to specific layers and areas is tightly regulated, shaping the functional characteristics of the developing brain. Therefore, it is key to understand the development of both the anatomical and functional connectivity within the neocortex.

### 1.2.1 Primary neuronal cell types in the neocortex.

Although the adult brain contains as many neurons as non-neuronal cells (Azevedo et al., 2009), the focus of this introduction will be on the neuronal populations that compose the neocortex, which play a central role in the processing and transmission of information across different brain regions. The primary neuronal cell types in the mammalian neocortex can be broadly categorised into two groups: glutamatergic excitatory projection neurons, responsible for generating the circuit output, and GABA (gamma-aminobutyric acid)-ergic inhibitory interneurons, which play a crucial role in shaping that output response. Excitatory pyramidal neurons are the most common neuronal cell type in the neocortex and are characterised by their pyramid-shaped somata. These neurons are present in all cortical layers except L1 and are known for their extensive long-range synaptic projections and clustered connectivity with other excitatory neurons (Narayanan et al., 2016). On the other hand, interneurons are less abundant than pyramidal cells, interspersed amongst them in a roughly 4:1 ratio (Rudy et al., 2011). Despite their lower numbers, interneurons play a crucial role in regulating the activity of pyramidal cells by establishing dense and non-specific local connections within the neocortex (Fino et al., 2011).

The diversity of cortical GABAergic interneurons has received significant attention, given their variations in morphology, connectivity, and activity patterns (Tremblay et al., 2016; Kepecs et al., 2014), with numerous genes implicated in the diversification of these early inhibitory precursors (Mayer et al., 2018). In contrast, pyramidal neurons, due to their high morphological resemblance, have received relatively less attention. Nonetheless, recent molecular investiga-

tions have started to uncover the heterogeneity within pyramidal neurons (Lodato et al., 2015). These studies have identified at least 56 distinct transcriptome-defined cell types of glutamatergic neurons, surpassing the 30 types observed for GABAergic neurons (Yao et al., 2021). This suggests, at least by transcriptomic categorisation, a greater diversity of glutamatergic neuron subtypes in comparison to GABAergic ones. The majority of GABAergic cell types are present throughout all neocortical areas, similarly to the distribution of glutamatergic cell types, which exhibit a continuous and graded arrangement across the cortical sheet (Yao et al., 2021). When classifying these neurons into further subtypes, it is essential to consider their distinct computational roles within cortical circuits. GABAergic interneurons play crucial roles in coordinating local circuits and possess unique morphological features that contribute to their functional diversity (Tremblay et al., 2016; Kepecs et al., 2014). In contrast, pyramidal neurons are primarily involved in computations taking place on a larger spatial scale, as they generally transmit signals across distant regions of the brain (Tang et al., 2020; Mohan et al., 2023; Musall et al., 2023), and therefore, their classification may require a focus on their long-range projection patterns (Winnubst et al., 2019).

To what extent is the specification of cortical cell types constrained during development? One of the primary goals of cell type classification is to achieve a reproducible identification of different neurons and facilitate their genetic access (Zeng et al., 2017). However, such classifications are inherently arbitrary, allowing for numerous ways of categorising them. This question becomes particularly relevant during development, as neuronal properties undergo continuous changes. The use of transgenic lines has significantly improved the the capacity to identify neurons during early stages of development (Hanson et al., 2022; Di Bella et al., 2020). However, selectively targeting specific subtypes of neurons, particularly pyramidal neurons, for recording or manipulation purposes remains challenging due to the relatively limited availability of mouse driver lines compared to those designed for GABAergic interneurons (Taniguchi et al., 2011).

### 1.2.2 Neurogenesis, migration and laminar distribution.

Cortical neurons undergo neurogenesis within a specific time frame. In mice, this period of neurogenesis takes place from embryonic day 10.5 (E10.5) to E17.5 (Costa et al., 2015; Molyneaux et al., 2007). The earliest-born neurons initially form a structure called the preplate (PP) around E10.5, which later divides into the marginal zone (MZ) and subplate (SP). The cortical plate, which will give rise to the multilayered neocortex, develops between these two layers (Molyneaux et al., 2007). Pyramidal projection cells, which are the principal excitatory neurons in the cortex, originate in the dorsal telencephalon from two major progenitor populations: ventricular zone (VZ) progenitors, also known as radial glial cells (RGC), and subventricular zone (SVZ) progenitors, referred to as intermediate progenitors (IP) (Greig et al., 2013; Tarabykin et al., 2001). Once they become postmitotic, pyramidal neurons migrate radially over relatively short distances to establish themselves in the different layers (Molyneaux et al., 2007).

During neocortical development, the generation of excitatory projection neurons follows a tightly regulated temporal sequence, with distinct classes of neurons emerging in overlapping waves (Greig et al., 2013; Molyneaux et al., 2007). SP neurons reach their peak production at E11.5, while layer IV and layer V projection neurons exhibit their highest generation rates at E12.5 and E13.5, respectively (Greig et al., 2013). Additionally, some callosal projection neurons emerge to form at E12.5, migrating to deeper layers, while the majority of these projection neurons are born between E14.5 and E16.5 and migrate towards more superficial cortical layers. This migration process follows an inside-out pattern, where later-born neurons traverse past earlier-born neurons to establish their appropriate positions within the cortical plate (Greig et al., 2013; Molyneaux et al., 2007). This intricate journey is orchestrated by a complex network of molecular factors and signalling pathways (Molyneaux et al., 2007). Projection neurons can be broadly classified into two categories based on their projections, intratelencephalic (IT) neurons and corticofugal (CFu) neurons (Lodato et al., 2015). IT neurons project exclusively to targets within the forebrain and are found in L2-6 of the cortex, with a higher representation in upper L2/3 (callosal projection neurons, CPNs). On the other hand, corticofugal projection neurons consist of two main groups: corticothalamic projection neurons (CThPNs) and subcerebral projection neurons (ScPNs). CThPNs, found in L6, encompass a diverse population of projection neurons that send axonal projections to various thalamic nuclei; while ScPNs, located in L5, have extensive projections that extend to other subcortical regions (Adesnik et al., 2018; Molyneaux et al., 2007).

In contrast, GABAergic interneurons are primarily generated from progenitors in the ventral telencephalon, with the majority of interneurons generated in the medial ganglionic eminence (MGE), followed by the caudal ganglionic eminence (CGE), lateral ganglionic eminence (LGE) and preoptic area (PO) (Rudy et al., 2011). Most interneurons derived from the MGE are generated from E9.5, whereas the peak generation of interneurons derived from the CGE occurs at later stages, around E15.5 (Butt et al., 2005). Each of these progenitor regions, exhibits its own molecular signature, leading to the production of diverse interneuron populations with distinct characteristics (Fogarty et al., 2007; Butt et al., 2005; Kepecs et al., 2014; Lim et al., 2018). These interneurons can be classified into three main groups based on the expression of specific molecular markers: Parvalbumin (PV), Somatostatin (SST), or the ionotropic serotonin receptor 5HT3a (5HT3aR) (Kepecs et al., 2014). For example, MGE gives rise to interneuron subtypes that include SST and PV interneurons, while the CGE predominantly generates neurons from the 5HT3aR subgroup, ontaining subtypes further defined by expression of Reelin+, vasoactive intestinal peptide+ (VIP), and cholecystokinin+ (CCK).

The immature interneurons embark on a protracted tangential migration from the ganglionic eminences towards the pallium, entering the marginal zone (MZ) or intermediate zone/subventricular zone (IZ/SVZ) before continuing their journey towards their final location within the cortex (Marín et al., 2001). The migration of interneurons continues beyond the early postnatal stages (Faux et al., 2012; Marín, 2013). Notably, neuronal precursors from the subventricular zone (SVZ),

migrate not only towards the olfactory bulb but also to cortical and subcortical structures during the first three postnatal weeks after (Inta et al., 2008; Faux et al., 2012). The termination signal for interneuron migration to their appropriate laminar position appears to be mediated by the upregulation of the potassium-chloride cotransporter, KCC2, which reduces interneuron motility by decreasing membrane potential upon activation of $GABA_A$ receptors (Bortone et al., 2009). Although interneuron subtypes are distributed across all layers of the cortex, there are some layer preferences, with PV basket cells, the most abundant type of interneuron in the neocortex, present throughout L2 to L4, particularly abundant at L4 and L5 (Gonchar et al., 1997), while SST Martinotti cells, are predominantly found in L5, as well as layer L2/3, extending their dendrites into L1 (Lim et al., 2018). Less abundant but with a potential important role are SST/nNOS cells which function as long-range GABAergic projection neurons, predominantly located in deep layers and project to other regions within the neocortex; VIP interneurons, which are enriched in L2/3; and neurogliaform cells, which are the most abundant type of interneuron in L1(Lim et al., 2018).

One of the most fundamental questions regarding cortical layers is whether their organisation has functional significance (Adesnik et al., 2018). Research conducted on the reeler mutant mouse, a mouse model with disrupted cortical layer organisation caused by impaired neuronal migration due to the absence of reelin protein expression (Boyle et al., 2011), has questioned the necessity of layers for cortical function, as the mutant mouse did not exhibit immediate sensory deficits (Guy et al., 2017). This raises the question of whether cortical layering is primarily a consequence of early development and may lack inherent functionality in the adult brain. However, lamination is a common feature observed in various brain circuits across different species and brain regions, and it plays a crucial role in organising synaptic connectivity and function (Shepherd et al., 2017). Moreover, a recent study showed that the formation of layers speeds the functional development of neuronal circuits (Nikolaou et al., 2015). This would suggest that lamination evolved to serve specific computational goals, even though it may not be strictly essential for general computation.

### 1.2.3 Cortical arealisation.

Our current understanding of the diversity of neurons in the cerebral cortex and how their distinct properties relate to different functional areas of the cortex is still incomplete. In the adult brain, anatomical subdivisions corresponding to specialised functional areas are defined by changes in cell number, density, lamination, and the presence of unique cell types (Cadwell et al., 2019; Schleicher et al., 2000). There are species and regional variations in the abundance of different neuron types and receptors throughout the cerebral cortex, and ongoing studies are aiming to comprehensively understand the cellular composition and connectivity of cortical areas (Palomero-Gallagher et al., 2019; Ding et al., 2016), providing insights into functional variations and hierarchical organisation (Jiang et al., 2015; Markram et al., 2015).

Many of these differences, observed in the adult brain, are not apparent during development. The processes that underlie cortical arealisation involve the transformation of an initially uniform neuroepithelium into distinct cortical regions with specific functions. There has been a long-standing debate about the mechanisms that lead to the development of anatomical and functional subdivisions in the cerebral neocortex. Two different hypotheses have been proposed: the protomap and the protocortex. The protomap hypothesis suggests that intrinsic genetic factors or a pre-determined "map" guide the differentiation and positioning of neurons to form specific brain regions (Rakic, 1988). According to this hypothesis, the process of arealisation in the cerebral cortex is predominantly driven by intrinsic factors rather than external inputs or experiences (O'Leary et al., 2008). It suggests that the establishment of gradients of morphogens within the developing neuroepithelium plays a crucial role in determining the specific cell fates in the cerebral cortex (Cadwell et al., 2019). The presence of morphogen gradients triggers the activation of specific transcription factors involved in cortical patterning, which subsequently initiate region-specific neurodevelopmental processes and regulate the destiny of neurons (Charvet et al., 2015). The signalling molecule gradients, established by these patterning centres, convey positional cues and play a role in determining cell fates that are specific to particular areas within the cerebral cortex (Rakic et al., 2009; Cadwell et al., 2019). Differential expression of molecular markers associated with areal identity has been observed between the anterior and posterior regions of the brain, indicating the potential involvement of a morphogen and gene expression gradient in the formation of distinct cortical areas in the frontal, central, and occipital regions (O'Leary et al., 2007).

In contrast to the protomap, the protocortex hypothesis proposes that cortical areas are not predetermined, but rather emerge through activity-dependent processes, where sensory inputs drive their formation based on patterns of activation and neuronal connections established during development (O'Leary, 1989; Loos et al., 1973). Therefore, this hypothesis suggests that spontaneous activity and inputs from sensory systems play a crucial role in shaping the functional and anatomical organisation of the developing cortex. Neural activity generated by sensory inputs aids in the formation local circuits and connectivity patterns, which in turn refine and differentiate cortical regions based on the type of sensory information they receive (Cadwell et al., 2019). However, an early study involving Gbx-2 mutant mice, which are characterised by impaired thalamic differentiation, showed that neocortical regions can undergo normal development despite disturbances in thalamic differentiation, showing that region-specific gene expression remains unaffected (Miyashita-Lin et al., 1999). Nevertheless, a recent study has demonstrated the significance of prenatal thalamocortical calcium waves in establishing the proper organisation of barrel structures within the mouse somatosensory cortex (Antón-Bolaños et al., 2019), highlighting the influence of external factors in governing the development of the cerebral cortex.

A comprehensive model of cortical arealisation has been proposed to reconcile the protomap and protocortex hypotheses, which suggests that both genetic programs and activity-dependent

processes contribute to the development of area-specific cell types and circuit (Cadwell et al., 2019). According to this model, initial "proto-regions" are established through intrinsic genetic programs and local secreted factors in the cortical neuroepithelium (protomap). Subsequently, activity-dependent mechanisms play a crucial role in refining and defining sharp boundaries between functional areas in the mature cortex (Vue et al., 2013). These mechanisms contribute to the progressive development and specialisation of the cortex. Furthermore, signalling factors originating from the subplate or thalamocortical axons have the potential to influence gene regulatory networks, contributing to the specification of cell types and circuits after neurogenesis (Pouchelon et al., 2014; Ghosh et al., 1990). For example, the migration and distribution of Cajal-Retzius (CR) cells throughout the developing cerebral cortex has shown to regulate the size of higher-order areas, shaping the identity of local excitatory neurons beyond their mitotic phase (Barber et al., 2015). Moreover, this combined model of cortical development has found support in *in vivo* human neuroimaging studies. These studies have revealed that the relative size of the CP and SP is established early during development and remains relatively stable; while more nuanced growth differences between those regions undergo fine-tuning at later stages, particularly during periods characterised by pronounced thalamocortical growth (Vasung et al., 2020). This underscores the intricate interplay between intrinsic and extrinsic factors in the intricate process of cortical development.

As briefly mentioned, there is substantial evidence supporting the role of thalamic input in driving cortical arealisation during critical periods of postnatal development, facilitating the establishment of precise sensory maps (Feldman et al., 2005; Inan et al., 2007). The thalamus receives and modulates sensory input from the periphery before transmitting it to specific cortical areas in a modality-specific manner (El-Boustani et al., 2020; López-Bendito, 2018). Thalamocortical axons play a crucial role in cortical development by forming synapses with SP cells, thereby providing early thalamic input to the cortex (Ohtaka-Maruyama, 2020). This interaction is critical for the formation of cortical circuits (Ghosh et al., 1993). Experimental manipulations that alter thalamocortical input or reroute sensory inputs to different thalamic nuclei have been shown to impact cortical development and function (Simi et al., 2018). For instance, misrouting of retinal input to non-visual thalamic nuclei, such as the main somatosensory nucleus or auditory nucleus, resulted in the development of orientation selectivity in non-visual cortical areas (Métin et al., 1989; Roe et al., 1992). Sensory experience is therefore crucial for the appropriate development of transthalamic cortico-cortical circuits. In mice, enucleation has shown to lead to abnormal projections of L5 neurons to the dorsal lateral geniculate nucleus instead of the superior colliculus (Grant et al., 2016). Furthermore, manipulations of thalamocortical input can alter the terminal specification of neuronal identity. For example, when the thalamic input from the ventrobasalis nucleus to the primary (S1) somatosensory cortex was ablated, S1 neurons exhibited characteristics resembling those of secondary S2 neurons due to rewiring of the the posterior nucleus onto L4 neurons in S1 (Pouchelon et al., 2014). Although the complete removal of thalamocortical projections does not completely eliminate the development of area-specific gene expression domains (Miyashita-Lin et al., 1999), the establishment of

clear boundaries between these areas strongly depends on the presence of thalamocortical input (Vue et al., 2013).

### 1.2.4 Functional integration and wiring the cortex: short and long range connections

The continuous growth of the mammalian cortex over evolution has led to an increased capacity for connections between its components (Changizi, 2007). This has enabled the emergence of higher-order functions and complex behaviours by facilitating the development of intricate hierarchies among its neural connections (Lodato et al., 2015). The cortex must balance flexibility without sacrificing network robustness to mediate plasticity, which allows the brain to optimise and diversify circuits by discarding or expanding developmental programs. The process of cortical wiring initiates during embryogenesis, giving rise to a variety of neuronal types that will acquire distinct electrical properties, subsequently impacting their patterns of connectivity (Bragg-Gonzalo et al., 2021). This process involves an initial overproduction of neurons and connections, which is crucial for coordinating network wiring during various developmental stages (Innocenti et al., 2005), including the establishment of transient circuits that play a key role in the formation of circuits (Tuncdemir et al., 2016; Anastasiades et al., 2016; Marques-Smith et al., 2016).

It was initially thought that the specific and stereotyped connections between neurons were established early on due to molecular programs, leading to diversity at the progenitor level, as seen in the pre-mitotic model (Srinivasan et al., 2012). Conversely, the post-mitotic model suggested that neurons gain subclass-specific characteristics during differentiation (Greig et al., 2013). A mixed-model has now emerged, where progenitors give broad transcriptomic profiles, and additional genetic modifications are added during differentiation to diversify those profiles (Jabaudon, 2017; Telley et al., 2019). Therefore, neuronal differentiation trajectories, instead of neuronal fates, better describe the process (Bragg-Gonzalo et al., 2021). Additionally, neuronal differentiation often depends on activity, highlighting the significance of understanding the neuronal context in predicting future wiring (Pouchelon et al., 2014). The establishment of connections between different brain areas occurs in early development and has been extensively studied in relation to the development of the visual cortex in cats (Callaway et al., 1990; Katz et al., 1992). Classical studies using neuronal tracers have shown that there is an abundance of projections during development compared to the adult stage, which indicates that a developmental selective loss of specific connections occurs after an initial overproduction of these cortico-cortical connections (Innocenti et al., 2005).

Additionally, there is an excess of neurons generated during development, which undergoes programmed cell death at predetermined cellular ages, playing a crucial role in shaping and refining connectivity (Mosley et al., 2017; Southwell et al., 2012). This process of developmental apoptosis disproportionately affects interneurons compared to excitatory neurons, with estimates

suggesting that around 30% of interneurons are lost compared to approximately 12% of excitatory neurons (Wong et al., 2018). Activity-dependent mechanisms play an important role in regulating this process (Priya et al., 2018; Wong et al., 2018; Blanquie et al., 2017b; Duan et al., 2020; Warm et al., 2022a). For example, increased neuronal activity is typically correlated with high survival rates in both principal neurons and interneurons, whereas reduction or inhibition of activity tends to be associated to higher rates of apoptosis (Heck et al., 2008; Southwell et al., 2012). Current research is focused on understanding whether the influence of neuronal activity on cell survival is governed by intrinsic processes within individual cells or by network-level mechanisms (Southwell et al., 2012; Blanquie et al., 2017b; Wong et al., 2018). Recent findings indicate that the impact of neuronal activity on cell survival is not solely determined by the overall level of activity but also by its specific temporal patterns (Blanquie et al., 2017b; Wong et al., 2018). Notably, GABAergic interneurons, which play a crucial role in modulating cortical activity patterns, have been found to regulate apoptotic rates in both interneurons and pyramidal neurons (Wong et al., 2018; Duan et al., 2020). High-frequency oscillatory activity, resembling patterns observed during the later stages of the first postnatal week (Luhmann et al., 2018), appears to be particularly effective in promoting neuronal survival, with GABAergic neurons playing a pivotal role in modulating these activity patterns (Isaacson et al., 2011; Modol et al., 2020). The reciprocal relationship between activity and apoptosis in interneurons is mediated by activity-dependent mechanisms (Wong et al., 2018), which can function as a homeostatic system (Blanquie et al., 2017a), displaying region-specific characteristics (Blanquie et al., 2017b). These findings highlight the critical role of neuronal activity in cortical development, which contributes significantly to determining the final number of neurons present in different brain regions, and therefore shaping their connectivity.

The functional columnar organisation of the cerebral cortex was first demonstrated by Hubel and Wiesel in the primary visual cortex (Hubel et al., 1959), and similarly by Mountcastle in the primary somatosensory cortex of cats (Mountcastle, 1997). These studies revealed that columns of cells oriented perpendicular to the cortical surface exhibit similar selectivity for sensory stimuli, suggesting that the segregation of the cortex into functional columns is a widespread phenomenon observed across different species and brain regions. These interconnected columns develop during corticogenesis in an activity-dependent manner, when neurons are electrically coupled via gap-connections, forming columnar syncytia (He et al., 2015; Niculescu et al., 2014). Early synchronous firing within these columns is required for the formation of sensory maps, since blockage of these gap-junctions disrupts the development of orientation stimulus selectivity in primary visual cortex (Li et al., 2012). Gap junction connectivity among pyramidal neurons reaches its maximum during the early postnatal period (P1-2) and gradually declines, until it nearly disappears by P14 (Yu et al., 2012b). In contrast, the presence of gap-junctions between GABAergic interneurons increases during the second postnatal week and reaches its peak at P14 (Parker et al., 2009). These electrically coupled inhibitory interneurons have shown to modulate spontaneous activity between distant regions (Kraft et al., 2020).

GABAergic interneurons play a crucial role in sculpting cortical circuitry (Dehorter et al., 2017; Le Magueresse et al., 2013; Cardin, 2018), shaping the maturation of the columnar organisation of the neocortex (Lim et al., 2018). During the first week of postnatal development, transient circuits formed between GABAergic interneurons and excitatory neurons contribute to the development of mature local and thalamocortical microcircuits (Anastasiades et al., 2016; Marques-Smith et al., 2016; Tuncdemir et al., 2016). L5 SST interneurons receive dense and transient thalamic inputs and establish connections not only with L5 pyramidal cells and immature PV interneurons but also with L4 excitatory neurons (Marques-Smith et al., 2016; Tuncdemir et al., 2016). These early transient connections provide a scaffold for the maturation of L4 cells and regulate early sensory-evoked activity before the establishment of the canonical feedforward inhibitory circuit mediated by PV basket cells (Marques-Smith et al., 2016). Moreover, the transient connections formed by this early-born SST interneurons are crucial for the maturation of PV basket cells in deeper layers (Tuncdemir et al., 2016), indicating their critical role in the development of intracortical circuits in deep layers during the early postnatal stages. Therefore, the connectivity between PV interneurons and excitatory neurons in L4 is initially weak but strengthens during the second postnatal week, when PV basket cells start receiving direct inputs from thalamic neurons (Chittajallu et al., 2010; Daw et al., 2007). The maturation of this PV interneurons coincides with the arrival of sensory experience-derived inputs, rendering them more susceptible to environmental stimuli (Gabernet et al., 2005; Tuncdemir et al., 2016).

Most GABAergic neurons primarily project within local regions, forming connections within the same or multiple neighbouring cortical columns (Thomson et al., 2003). A subset of GABAergic neurons can extend their projections over long distances to connect with remote cortical areas (Tamamaki et al., 2010; Urrutia-Piñones et al., 2022; Caputi et al., 2013). However, little is known about their development and functions in the neocortex. Recent studies have shown that a small population of GABAergic subplate cells can send these long-range axonal projections to subcortical structures (corticofugal), such as the thalamus, through the internal capsule; and to other cortical regions through the corpus callosum (Boon et al., 2019). Interestingly, these two different projection groups have shown opposite expression patterns. While the corticofugal projection neurons were most abundant during the perinatal period, decreasing in number postnatally, the contralateral callosal projecting GABAergic neurons showed an increase in numbers during the first postnatal week (Boon et al., 2019). In the hippocampus, long-range GABAergic neurons originate during embryonic development (Christenson Wick et al., 2019), and could be related to the hub neurons found in the developing hippocampus, which coordinate and synchronise neuronal assemblies (Bonifazi et al., 2009; Picardo et al., 2011). Understanding the role of these projections is important due to their potential contribution to cortical feedback processing and synchrony across brain regions (Mazo et al., 2022; Tamamaki et al., 2010).

## 1.3 Development of primary sensory networks.

The development of primary sensory networks involves a complex interaction of molecular, cellular, and physiological mechanisms (Cang et al., 2013). These networks are crucial for sensory perception and interactions with the external world, with genetic factors initially guiding their formation and activity-dependent mechanisms subsequently fine-tuning them (Bragg-Gonzalo et al., 2021). Sensory experience plays a crucial role in shaping the organisation of sensory cortices during critical periods, when immature sensory networks display high plasticity and can adapt their connectivity and properties in response to the input patterns received (Berardi et al., 2000; Hensch, 2005). This allows for the development of stable and adaptable representations of the outside world. This developmental process is not unique to sensory areas but is similarly followed in other brain regions, such as the cerebellum (White et al., 2014).

### 1.3.1 Structural changes to developing sensory networks.

The brain systematically and topographically represents the external world through sensory maps, which are established during development and refined by sensory experience, and enable the perception of incoming stimuli and interaction with the environment. These topographic sensory maps are the best models for studying the organisation of brain circuitry, as they represent discrete activation domains to different sensory stimuli, e.g. barrel activation, orientation tuning, and odorant coding (Cang et al., 2013). Thalamocortical afferents, which the relay sensory information to the cortex, play a crucial role in the development and maturation of these maps (Lokmane et al., 2013; Colonnese et al., 2018; Antón-Bolaños et al., 2019). For example, disruption of thalamocortical glutamatergic transmission leads to malformation of these maps, affecting not only the cytoarchitecture, but also the gene expression, and differentiation (Li et al., 2013).

The primary sensory regions are typically associated with a specific function that aligns with the type of sensory information they receive. Excitatory neurons have traditionally been the main focus in studying sensory maps (Cang et al., 2013; Hanganu-Opatz, 2010; Martini et al., 2021; Nakazawa et al., 2021), as they played a key role in establishing the topographical organisation of brain areas and understanding the stereotyped response of them to external stimuli. This approach has been favoured due to limitations in certain techniques such as fMRI, lesions, and intrinsic imaging, which lacked genetic specificity, making it difficult to distinguish between different cell types. However, the role of GABAergic interneurons in topographic map formation should not be overlooked. While they are traditionally thought to lack the structured mapping seen in excitatory neurons, recent studies have shown that inhibitory maps play a significant role in sensory processing (Che et al., 2018; De Marco García et al., 2015; Baruchin et al., 2022). For example, in the visual cortex, PV interneurons, unlike their excitatory counterparts, initially have a narrow orientation selectivity, which broadens with maturation (Kuhlman et al., 2011). Similarly,

inhibitory interneuron sensory maps in the olfactory system broaden with maturation and sensory experience (Quast et al., 2017). Therefore, in contrast to the consolidation and refinement of the connectivity patterns observed in excitatory neurons during maturation, interneurons seem to show a significant expansion and broadening of their connectivity. This expansion may be involved in facilitating associative learning across diverse sensory inputs, such as odours (Quast et al., 2017). Moreover, the ability of experience and learning to modify inhibitory maps suggests that these maps may play a significant role in supporting behaviour. For instance, during the critical period of somatosensory cortex map formation, when active sensation begins, there is a significant remodelling of structural and functional inputs onto interneurons. This remodelling leads to divergent responses in VIP and SST interneurons to multi-whisker stimuli, with VIP interneurons losing their multi-whisker responses and SST interneurons enhancing theirs (Kastli et al., 2020), supporting the distinct roles of these interneurons subtypes in emergent sensory processing (Baruchin et al., 2022).

### 1.3.2 Developmental behavioural changes.

Sensory processing is influenced by behavioural state, which varies depending on sensory modality and developmental stage (Dooley et al., 2019; McCormick et al., 2015). Behavioural brain states can be described as a brain-wide activity patterns that emerge from, and have consequences for, the physiology and/or behaviour (Greene et al., 2023). In neonatal rodents, the primary behavioural states are sleep-wake cycles and active or non-active rest (Dooley et al., 2019; Rensing et al., 2018). These states predominate until rodents start actively using their senses and developing conscious behaviours that require other states, such as arousal and attention (Dooley et al., 2019; McCormick et al., 2020). It remains unclear whether sleep-wake cycles modulate cortical activity similarly in neonates as they do in adults, given that most neonatal cortical activity is driven peripherally. For instance, in the developing visual system (Mukherjee et al., 2017), sleep-wake states modulate ongoing activity, and this modulation abruptly changes during the second postnatal week when the thalamus becomes more disconnected from the cortex (Murata et al., 2018). This transition in activity observed during the second postnatal week coincides with the emergence of early social behaviours in rats. The modulation of neurotransmission in the supragranular cortical layers has been identified as a critical factor in this developmental process (Naskar et al., 2019).

Behavioural state plays a crucial role in sensory processing. For example, a controlled brain state such as light anaesthesia has shown to interfere with both spontaneous activity patterns and sensory stimuli (Colonnese et al., 2010; Chini et al., 2019). Neonatal rodents spend a significant portion of their time sleeping, exhibiting sleep patterns characterised by increased fragmentation compared to adult rodents (Blumberg et al., 2005). During early development, while mice cycle rapidly between sleep and wake, with individual bouts typically much shorter than a minute (Blumberg et al., 2005), active sleep is the predominant behavioural state (Jouvet-Mounier et al., 1969; Rensing et al., 2018). Research in neonatal rats has demonstrated that

active sleep, not active wake, is the optimal state to promote developmental plasticity, at least in the somatosensory system, due to spatiotemporal features of twitches and dampening of neuromodulatory activity during this state (Dooley et al., 2019; Blumberg, 2015). On the other hand, during active wake, early sensory responses are inhibited at the thalamic level (Murata et al., 2018; Dooley et al., 2018), and only transition to adult-like behaviour, characterised by enhanced sensory responses during wakefulness, towards the end of the second postnatal week (Dooley et al., 2018).

The activity of the visual system during the early stages of development has shown to be heavily influenced by the animal's behavioural state. Prior to the emergence of patterned vision in mice at P14 (when the eyes open), retinal waves lead to an organised activation of visual circuits, regardless of behavioural state (Ackman et al., 2012). As mentioned above, during this period, the visual cortex (Mukherjee et al., 2017) shows inhibited activity during active wakefulness, but not during active sleep. This reverses at the time of eye opening, due to a change in the modulation of the thalamic inputs (Murata et al., 2018). In the somatosensory cortex, behavioural state modulation is a key aspect, as it plays a central role in the development of the sensorimotor system while simultaneously being involved in crucial infant behaviours like suckling, huddling, and locomotion (Alberts, 2007; Westneat et al., 1992). The primary motor cortex is not involved in the production of movement until later stages ($\sim$P35), but it acts like a prototypical somatosensory area, similar to S1 (Dooley et al., 2018). During early postnatal development, in somatosensory and motor cortices, neural activity consists mainly of spindle bursts triggered by somatosensory stimuli (Tiriac et al., 2014; Khazipov et al., 2004). Myoclonic twitches during active sleep provide organised input to the developing somatosensory system (Blumberg et al., 2013), while the activity from wake movements is inhibited by thalamic sensory gating (Tiriac et al., 2016). This dependence on behavioural state continues until P10, suggesting that myoclonic twitches play a crucial role in initiating spindle bursts in S1 and M1 during early development (Tiriac et al., 2014; Tiriac et al., 2016). However, by P11, the inhibition of wake-related reafference diminishes, enabling neurons in S1 and M1 to respond to the sensory consequences of wake movements (Dooley et al., 2018). The influence of behavioural state on activity in the auditory system remains uncertain. However, prior to the opening of the ear canal, the cochlea generates localised activity patterns that resemble the patterns observed during twitches and retinal waves (Tritsch et al., 2007).

Behavioural state-specific activity patterns in neonatal animals has shown to be tightly regulated and highly conserved across individuals (Mojtahedi et al., 2021). A recent study has demonstrated that the neocortex-wide patterns of activity associated with motion and rest exhibit distinct spatial organisation, with somatosensory-motor regions being active during motion, while auditory-visual regions exhibited increased functional connectivity during rest (Mojtahedi et al., 2021). Moreover, the retrosplenial cortex (RS) showed a behavioural state-specific engagement in coherent activity with visual cortex at rest and somatomotor cortices during motion (Mojtahedi et al., 2021). Indeed, RS has been shown to play an important role in dictating

cortical dynamics and regulating REM (Rapid Eye Movement) sleep progression in adults (Dong et al., 2022). Moreover, recent research has suggested that there may be a common inhibitory circuit for regulating sensory processing by behavioural state. In this proposed circuitry, which was originally studied in mouse V1, locomotion would activate VIP neurons independently of visual stimulation, while decreasing SST neuron activity, and thereby disinhibiting excitatory neurons and enhancing visual responses (Fu et al., 2014). Additionally, inhibitory circuits have been shown to be modulated by behavioural state in a cell type-specific and context-dependent manner (Pakan et al., 2016), serving as a potential gate for cortical state transitions (Zucca et al., 2017).

### 1.3.3 Spatiotemporal patterns of spontaneous activity during development.

During early development, the topographic organisation of spontaneous activity is essential for facilitating sensory processing. The formation of topographical maps in sensory systems depends on complex spatiotemporal patterns of spontaneous activity, which play a crucial role in refining specific features of neural circuits (Thivierge, 2009; Leighton et al., 2016; Nakazawa et al., 2021). The visual and auditory cortex experience a pre-sensory period during the first postnatal week due to the closure of the eye lids and ear canal (Crowley et al., 1966; Tkatchenko et al., 2010), and they only attain functional maturity by the end of the third week after birth. This is in contrast to olfaction and somatosensation, which are present even before birth (Liu et al., 2017; Antón-Bolaños et al., 2019).

While the basic structure of sensory systems is established prior to birth through genetic programming (Yogev et al., 2014; Hoffpauir et al., 2009), the refinement of sensory maps and neural circuits occurs in an activity-dependent manner (Kirkby et al., 2013; Espinosa et al., 2012; Okawa et al., 2014). This activity-dependent process organises and stabilises the initial topographical arrangement of thalamocortical projections in primary sensory cortical regions (Colonnese et al., 2018). Even at the earliest developmental stages, patterned spontaneous activity is necessary for the formation of functional sensory maps (Antón-Bolaños et al., 2019). For example, in the olfactory system, a rough map forms initially independent from neuronal activity (Mori et al., 2011), but the sensory environment experienced prenatally significantly impacts the structure of the olfactory bulb and the responsiveness to odours (Liu et al., 2017), highlighting the existence of a critical period for olfactory bulb development before birth.

In the sensory cortices, the activity at early stages of development is largely spontaneously generated (Martini et al., 2021). This synchronised spontaneous activity plays a crucial role in brain maturation by regulating various processes that include neuronal migration (Komuro et al., 1998), differentiation (Gu et al., 1997), influencing dendritic growth (Wong et al., 2002) and connection patterning (Penn et al., 1998). The blockage or disruption of this activity has shown to lead to defects in the arrangement of the sensory maps. For example, genetically interfering with spontaneous activity patterns coming from the retina has shown to lead to

inaccurate mapping in the visual cortex (Cang et al., 2005); while suppression of spontaneous activity in the somatosensory cortex leads to abnormal development of both thalamocortical (Yamada et al., 2010) and callosal projections (Wang et al., 2007). Particularly, the formation of inter-hemispheric connections, which develop during the first postnatal week in rodents (Wang et al., 2007), requires further refinement by spontaneous activity (Wang et al., 2007; Suarez et al., 2014; Tagawa et al., 2008), in which, for example, the proper development of the corpus callosum relies on maintaining a balance in interhemispheric cortical activity (Suarez et al., 2014). Furthermore, these callosal fibres play a role in patterning spontaneous activity, highlighted by the increased bilateral activity observed in the primary somatosensory cortex following lesions in these fibres during the first postnatal week (Marcano-Reik et al., 2008).

In addition, synchronised spontaneous activity plays a crucial role in shaping the organisation of the cortex in both the radial and tangential planes. This activity generally originates from peripheral sensory organs and the thalamus, manifested as calcium waves (Ackman et al., 2012; Tritsch et al., 2007) that propagate through the subplate and gap-junctions (Hanganu et al., 2009; Molnár et al., 2020; Roerig et al., 2000), which amplify these calcium waves leading to oscillatory bursts (Hanganu et al., 2009). In rodents, this activity gradually transitions from spindle bursts and early gamma oscillations (EGOs) to more restricted local radial columns around P5-P6, until eventually culminating in mature sparse synaptic transmission around P20-P21 (Antón-Bolaños et al., 2019; Minlebaev et al., 2011). As development progresses, there is a reduction in synchronised neurons, indicating a shift from electrical to chemical communication and from intrinsic to stimuli-evoked activity (Valiullina et al., 2016).

In the early stages of development, activity is characterised by discontinuous bursts of activity interspersed with periods of relative silence (Colonnese et al., 2010; Seelke et al., 2010), low firing rates (Shen et al., 2016), loose temporal coordination between EI (Dorrn et al., 2010) and weak modulation by behavioural state (Chini et al., 2019; Cirelli et al., 2015). This seems to be conserved across different organisms, from fish (Avitan et al., 2017) to flies (Akin et al., 2019) and rodents (Khazipov et al., 2004) and even organoids (Trujillo et al., 2019), as well as humans (Vanhatalo et al., 2006). These bursts of activity, known as spindle bursts, occur in all behavioural states and are believed to be either triggered by sensory inputs or generated spontaneously by thalamocortical circuits (Khazipov et al., 2004; Mizuno et al., 2018). Spindle bursts have been observed in virtually all cortical areas, including S1 (Khazipov et al., 2004), V1 (Murata et al., 2016), A1 (Chipaux et al., 2013), M1 (Tiriac et al., 2014), and PFC (Brockmann et al., 2011). During the developmental stages, there is a complex interaction between peripheral and central spontaneous activities (Avitan et al., 2021; Luczak et al., 2013), which has been extensively investigated in V1 (Siegel et al., 2012; Gribizis et al., 2019; Ackman et al., 2014a). The disappearance of spindle bursts is related to the decreased engagement of the thalamus with the cortex, as these bursts rely on corticothalamic feedback, which amplifies the sensory signal (Murata et al., 2016).

Prior to the onset of vision, two distinct and independent patterns of activity emerge. One pattern, known as L-events, is locally generated and exhibits low synchronicity (Siegel et al., 2012; Gribizis et al., 2019; Ackman et al., 2014a). These L-events resemble the spindle bursts and are believed to originate from the retina. The second pattern, referred to as H-events, is globally synchronised and is generally mediated by gap junctions (Siegel et al., 2012; Gribizis et al., 2019; Hanganu et al., 2006). During the pre-eye-opening period (around P8-P10), the frequency of L-events increases, conveying information about the position and function of retinal ganglion cells (Siegel et al., 2012; Gribizis et al., 2019). This information aids in the refinement of retinotopic maps in the visual cortex. In contrast, H-events decrease in occurrence with age and do not carry selective information for specific groups of neurons. Instead, their function may be to regulate the downregulation of synaptic weights, ensuring optimal levels of global activity (Siegel et al., 2012). These patterns are gradually replaced by L-events that are driven by peripheral inputs, indicating a shift towards more visually guided activity patterns. For instance, in Fmr1 knockout mice, spontaneous activity patterns are altered during development (Gonçalves et al., 2013), with retinally driven activity in V1 found to be reduced, resulting in a relative decrease in L-events compared to H-events (Cheyne et al., 2019). Therefore, while local events play a crucial role in shaping the selectivity and topography of cortical inputs, influencing sensory processing, global events have shown to regulate the strength of connections in a homeostatic manner (Siegel et al., 2012). The magnitude of these events can be adjusted in response to previously occurring patterns of cortical activity, ensuring an optimal balance between local selectivity and global regulation (Siegel et al., 2012; Wosniack et al., 2021). H- and L-events exhibit different ratios of excitatory and inhibitory inputs, primarily driven by the stronger excitatory drive in H-events, rather than differences in inhibitory inputs (Leighton et al., 2021). Additionally, it has been observed that SST interneurons play a role in regulating the recruitment of cells to retinally driven spontaneous activity, limiting the lateral spread of these L-events (Leighton et al., 2021), which may potentially contribute to the fine-tuning of retinotopy.

### 1.3.4 Developmental transition to mature activity states.

Spontaneous activity undergoes several transitions in activity dynamics during early brain development, from immature to more mature states (Nakazawa et al., 2021; Martini et al., 2021), playing a crucial role in shaping the topography of cortical networks (Molnár et al., 2020). In rodents, there is a shift from scattered and uncorrelated activity to more correlated patterns in the last days of embryonic life (Corlew et al., 2004). This correlated activity is important for strengthening and fine-tuning the connections across neuronal circuits (Winnubst et al., 2015) and is generally dependent on thalamic input arriving via the subplate (Higashi et al., 2002), which is itself involved in creating this patterned activity (Tolner et al., 2012).

During early postnatal development, there is a second developmental shift in neocortical activity from highly synchronised patterns to more desynchronised and sparse neocortical activity, which is better suited for efficient sensory coding (Minlebaev et al., 2011). In mice, this change

happens around the second postnatal week and coincides with the onset of active sensing, when the ear canals and eyelids open and active whisking behaviour begins (Colonnese et al., 2010; Mizuno et al., 2018; Rochefort et al., 2009). While this transition can occur in the somatosensory cortex in the absence of external sensory input (Golshani et al., 2009), sparsification in the visual cortex is delayed by dark rearing (Rochefort et al., 2009), indicating a discrepancy between modalities. This suggests that while transition may be internally generated in the somatosensory cortex, sensory input may act as a catalyst for its occurrence in the visual cortex. Therefore, this developmental desynchronisation is generally independent of thalamic input, involving changes in synaptic properties, such as the transition from electrical to chemical synaptic coupling between excitatory neurons (Valiullina et al., 2016), as well as changes in inhibitory circuits, including the decline of transient circuits and the maturation of feedforward inhibition (Chini et al., 2022; Marques-Smith et al., 2016; Tuncdemir et al., 2016). Recently, an increase in inhibition has shown to drive these activity desynchronisation *in vivo*, which tilts the excitation-inhibition ratio towards inhibition (Chini et al., 2022). Disruptions in this ratio can lead to long-lasting problems in adulthood and are a hallmark of many neurodevelopmental disorders (Markicevic et al., 2020). Moreover, a gradual change in inhibitory synaptic properties can induce these rapid developmental switches, causing an abrupt change in network dynamics resembling a bifurcation-like behaviour (Romagnoni et al., 2020). This supports the idea that the maturation of GABAergic transmission governs sparsification of activity (Rahmati et al., 2017).

The desynchornisation and sparsification of spontaneous activity during development is observed throughout different regions of the mammalian neocortex, as well as layers and types of cells (Luhmann et al., 2018; Colonnese et al., 2010; Golshani et al., 2009; Rochefort et al., 2009; Modol et al., 2020). This activity phase transition has been extensively researched in the rodent barrel system. The barrel-specific immature patchwork activity (phase I) (Mizuno et al., 2014; Mizuno et al., 2018) changes around P11-13, becoming sparse, with no clear spatial organisation (phase III), similar to those observed in the adult cortex (Berkes et al., 2011). Interestingly, at P9 there is an intermediate activity pattern in which all neurons seem to be widely synchronised (phase II), even across barrels (Nakamura et al., 2020). Generally, cross-barrel activations are restricted by SST+ neurons, which can help limiting the activity spread across barrels in phase I activity (Modol et al., 2020). However, the disappearance of the transient SST-thalamus circuit (Marques-Smith et al., 2016), in favour of feedforward inhibition by PV neurons (Daw et al., 2007; Modol et al., 2020) could be driving this switch to highly synchronised bursts of activity across barrels (Shigematsu et al., 2019). The extent of thalamic recruitment of feedforward inhibition in L4 of the primary somatosensory cortex in mice has shown to be significantly greater during the P9-P11 period compared to the P6-P8 period (Chittajallu et al., 2010).

These different phases of activity are shared across different neuronal pyramidal cell types (Nakamura et al., 2020; Golshani et al., 2009; Mizuno et al., 2018), as well as GABAergic cells (Modol et al., 2020), although the sparsification of GABAergic patterns seems to happen slightly

earlier (Mòdol et al., 2017). GABAergic cells are strongly driven by the thalamus during early stages, which results in similar assemblies for both spontaneous and whisker-evoked activity during this immature phase I (Modol et al., 2020). However, in phase II, these assemblies become different across spontaneously and stimulus-evoked activity, leading to the activity sparsification in phase III (Modol et al., 2020). Given that whisker plucking from birth stopped the transition to phase II, sensory input is required to reduce the dependency of GABAergic neurons on the thalamic input (Modol et al., 2020).

Although other sensory systems also undergo sparsification of cortical activity, they do not exhibit the same distinct phase transitions as the somatosensory cortex, which may be due to the less organised thalamus in these systems making it difficult to distinguish between phase II and III (Nakazawa et al., 2021). In the case of the mouse visual cortex, this loss of thalamic dependency occurs around P10 (Gribizis et al., 2019), with sparsification in L2/3 neurons occurring around P13 (Siegel et al., 2012; Rochefort et al., 2009), while in the auditory cortex it occurs between P12 and P20 (Rochefort et al., 2009). This loss of thalamic dependency may be thus associated with the development of intracortical dependency. Therefore, generally, the patterns of cortical activity transition from being primarily gap junction-dependent and thalamus-driven (bottom-up) to being synaptically driven and integrated in the wider network, originating in the thalamus, the periphery, or other cortical areas (top-down) (Bragg-Gonzalo et al., 2021). As the brain networks mature, there is an increase in the rhythmicity and complexity of oscillatory events (Trujillo et al., 2019), accompanied by an increase in both their amplitude and average frequency (Bitzenhofer et al., 2020). Furthermore, there is a decrease in the ratio of excitatory and inhibitory conductances (Zhang et al., 2011b), and a tightening of their temporal responses (Dorrn et al., 2010; Moore et al., 2018).

### 1.3.5 Maturation of spontaneous activity and emergence of functional architecture in the developing human neocortex.

The fundamental stages of cortical development during the formation of the fetal brain are conserved across mammalian species (Molnár et al., 2012; Clancy et al., 2007). The synchronised oscillatory network activity in the cerebral cortex, believed to be crucial for the formation of neuronal cortical circuits, exhibits several similar features across rodents and humans, such as delta brushes, spindle bursts, and spindle-like oscillations (André et al., 2010; Vanhatalo et al., 2006; Khazipov et al., 2006; Minlebaev et al., 2011; Hanganu et al., 2006), transitioning towards more mature patterns at later stages of development (André et al., 2010). These shared oscillatory patterns suggest that the fundamental functional properties of immature cortical neuronal networks are conserved across evolution. Thus, the postnatal rodent brain can serve as a model to study fetal stage activity in humans.

In the immature human brain, there is a rich repertoire of spontaneous patterns characterised by intermittent bursts of activity, separated by periods of complete silence, which give rise to a

highly discontinuous temporal organisation (Vanhatalo et al., 2006). These activity bouts are characterised by ultra-slow delta waves (Khazipov et al., 2006), in which faster rhythms are nested towards the third semester of gestation, like the delta-brush pattern, becoming more synchronised with development (Vanhatalo et al., 2006). This activity is particularly prominent in primary sensory cortical regions around 30 weeks, coinciding with the entry of thalamocortical projections into the cortex (Vanhatalo et al., 2006). These delta-brushes disappear at 38-42 weeks, resembling the developmental transition observed in rodents during the onset of sensory experience (Whitehead et al., 2017). Moreover, this progression closely corresponds to the maturation of functional GABAergic inhibition, highlighting the significant involvement of GABA dynamics in their generation (Dzhala et al., 2005). Spontaneous activity in preterm infants has shown to correlate positively with brain growth (Benders et al., 2015), and has shown to reflect shifts in subplate-cortex interactions (Leikos et al., 2020). Therefore, since the emergence of spontaneous activity is associated with important biological processes that are involved in typical brain development, understanding and describing spontaneous activity is essential for the diagnosis and prediction of potential neurodevelopmental disorders (Iyer et al., 2015).

In human postnatal cortical development, sensory and motor cortices mature earlier than association cortices, resulting in heterochronous patterns of development (Sydnor et al., 2023; Sydnor et al., 2021). Intrinsic fMRI activity has been identified as a reliable functional marker of plasticity in the human brain (Newbold et al., 2020), showing that its amplitude is correlated with the maturation of intracortical myelin, a crucial regulator of developmental plasticity (Sydnor et al., 2023). This intrinsic activity undergoes a transition from synchronised and high amplitude patterns to sparse and low amplitude patterns, as plasticity declines and the cortex matures, mirroring findings observed in animal models (Sydnor et al., 2023). Moreover, the developmental trajectory of intrinsic activity changes showed unique increases in amplitude in association regions during adolescence, while it decreased in sensorimotor cortices (Sydnor et al., 2023). This variability in maturational trajectories of different regions follows the sensorimotor-association axis (Sydnor et al., 2023), supporting the hypothesis of a gradient in developmental change across the hierarchy of the cortical sheet (Harris et al., 2019; Dong et al., 2021; Gu et al., 2021).

The hierarchical organisation of the brain along the sensorimotor-association axis is not established during youth but instead develops gradually over time (Harris et al., 2019; Dong et al., 2021), providing a scaffold for bottom-up sensory integration and top-down control of cortical activity (Pines et al., 2023). Slow and widespread activity propagates across the cortex-wide functional hierarchy and is directionally constrained along this axis of cortical hierarchy, either bottom-up or bottom-down directions (Gu et al., 2021). Top-down direction of propagation of activity increases during cognitive task demands and becomes more prevalent with age, whereas bottom-up propagations show a larger decline with age (Pines et al., 2023). This spatial directionality is a key feature of perception and task execution in other mammals (Rubino et al., 2006; Aggarwal et al., 2022). Moreover, critical periods of plasticity are thought to follow

as well a hierarchical sequence during development, beginning with primary sensory cortices and progressing to secondary and higher-order cortical areas (Takesian et al., 2013a; Reh et al., 2020). A recent study employed non-invasive neuroimaging methods and pharmacology to generate an empirical model of the excitatory-inhibitory (EI) ratio, and predicted a decline in the EI ratio in the association cortices during adolescence in humans (Larsen et al., 2022), providing support for the notion that critical period mechanisms play a role in shaping the development of association cortices during this period.

## 1.4 Critical periods of development.

Critical periods are specific time windows during postnatal development when the functional properties of the brain rapidly and specifically change in response to environmental stimuli and experience. These periods are characterised by heightened plasticity, making the connections between neurons particularly sensitive to external influences, which can have significant and lasting effects on brain development (Hensch, 2005). Critical periods play a crucial role in establishing and refining sensory circuits, allowing the brain to efficiently acquire and process sensory information. The length of these critical periods is correlated with the lifespan and complexity of the brain, with longer periods observed in species with longer lifespans and larger brains (Berardi et al., 2000).

Critical periods have been observed in all major sensory modalities, including vision, audition, and somatosensation, as well as in various species, including not only mammals (Hensch, 2005) but also invertebrates like Drosophila (Golovin et al., 2019; Coulson et al., 2022). The presence of critical periods has been well-established through studies that manipulate sensory experiences during specific time windows (Barkat et al., 2011; Berardi et al., 2000). Furthermore, critical periods are not limited to sensory modalities and have also been observed in more complex processes like birdsong learning in birds and language acquisition in humans (Doupe et al., 1999). This evidence supporting the existence of critical periods often comes from cases where the absence of specific experiences during early life results in compromised development of related brain functions, and subsequent exposure to those experiences during later stages does not fully compensate for the earlier deprivation. This classical definition of critical period stems from Hubel and Wiesel's work, who observed that, depriving an eye from of visual stimulation during a specific window of development, caused cortical visual responses to be biased towards the open eye, what it is known now as the ocular dominance plasticity (Wiesel et al., 1963). Sensory deprivation can occur as a result of various factors, such as natural events, traumatic events, or a lack of sensory stimulation. For example, in the context of visual deprivation, it can be caused by early blindness, enucleation (removal of the eye), or dark rearing (keeping the individual in complete darkness). For example, neonatal hypoxic-ischemic injury, which involves oxygen deprivation and reduced blood flow to the brain, has been found to diminish plasticity during critical periods of development in both the visual (Failor et al., 2010)

and somatosensory cortices (Ranasinghe et al., 2015). Similarly, in the rodent somatosensory cortex, a critical period plasticity was observed following whisker deprivation, where the structure of the L4 barrel field became completely disorganised (Loos et al., 1973), with an age-dependent decline in the capacity to induce long-term potentiation of thalamocortical excitatory synapses (Crair et al., 1995).

The timing and duration of critical periods may vary across sensory modalities and individuals, and the proper timing of these periods, aligned with the expected experiences, is crucial to ensure proper formation of neural circuits, like the acquisition of higher-order functions (Werker et al., 2015). Therefore, normal brain development relies on the synchronisation of intrinsic maturational processes and environmental input (Reh et al., 2020). Critical periods are commonly studied at the millisecond timescale to understand the physiological aspects of plasticity. However, it is important to consider that these developmental trajectories are also influenced by longer timescales, including developmental time and evolutionary processes, which play a role in shaping the neural architectures that support plasticity (Reh et al., 2020).

Additionally, while critical periods are characterised by heightened plasticity, sensory development continues beyond these periods, albeit with reduced plasticity. Interestingly, the ability of the adult cortex to adapt to changes can be influenced by previous experiences, with prior exposure to similar sensory changes earlier in life enhancing the capacity for adaptation (Hofer et al., 2006). Moreover, several studies have shown that the adult brain still possesses a significant degree of plasticity (Thomas et al., 2013; Heimler et al., 2020; Kätzel et al., 2014), from the recovery of higher order abilities such as language to the improvement of sensory abilities as a consequence of a lesion (Reetzke et al., 2018; Bherer, 2015). Hence, a novel theory called the Reversible Plasticity Gradient (RPG) theory has emerged, challenging the traditional strict definition of critical periods. According to this theory, the development of brain specialisations is not exclusively dependent on specific sensory inputs, as previously thought, but rather influenced by sensory-independent computations that can be triggered by atypical sensory inputs (Heimler et al., 2020). So, while brain plasticity typically declines with age, it remains reversible in adulthood, even in cases where individuals have not been exposed to specific sensory experiences during childhood due to full or partial sensory deprivations (Heimler et al., 2020).

Manipulating sensory inputs during the critical periods of plasticity can lead to significant changes in sensory maps. In the primary somatosensory cortex, for example, early whisker manipulations during the first postnatal week result in rapid plasticity in L4, which corresponds to the plasticity observed at thalamocortical synapses (Crair et al., 1995; Erzurumlu et al., 2012). Whereas, sensory deprivation at the end second postnatal week, neurons form L2/3 developed broad receptive fields, along with a disordered whisker map (Stern et al., 2001), while the whisker map in L4 remains unaffected. This suggests that L4 thalamocortical synapses undergo a critical period of plasticity early in development, while the critical period of L2/3 coincides with

their synaptic development (Stern et al., 2001). In contrast, synapses within other layers of the cortex retain a higher degree of plasticity and continue to be the primary sites of rapid plastic changes throughout life (Feldman et al., 2005; Polley et al., 2004). Conversely, overstimulation of whiskers decreases their representation in the adult brain (Welker et al., 1992), primarily due to an increase in the number and density of GABAergic synapses onto L4 spines (Knott et al., 2002). Many synapses in the primary somatosensory cortex exhibit N-methyl-D-aspartate (NMDA) receptor-dependent long-term potentiation (LTP) and long-term depression (LTD), and the capacity for LTP and LTD correlates with critical periods for map plasticity in each layer (Feldman et al., 1999). Pharmacological blockade of NMDA receptors has also shown to impair the development of barrels in the somatosensory cortex (Fox et al., 1996).

The initiation of the critical period is typically influenced by a combination of genetic factors and sensory experience (Hensch, 2003; Hensch, 2005; Berardi et al., 2000). These triggers can include the establishment of important synaptic connections (Feldman, 2009), the activation of critical genes (Kobayashi et al., 2015), or the development of specific neurotransmitter systems (Xu et al., 2020a). However, sensory experience plays a vital role in initiating and shaping critical periods (see subsection 1.4.2). When relevant sensory information, such as visual stimuli, auditory sounds, or tactile sensations, is present, it provides the environmental cues necessary to activate and modulate the plasticity of developing sensory circuits. Additionally, the onset of critical periods appears to be marked by the maturation of intracortical inhibition (see subsection 1.4.3).

### 1.4.1 Cross-modal plasticity following early sensory deprivation.

Cross-modal plasticity refers to the brain's ability to adapt and reorganise when one sensory modality is absent, leading to the involvement of other sensory modalities in the information processing (Mezzera et al., 2016). This phenomenon can occur during critical periods, when sensory deprivation causes the primary sensory cortices associated with the deprived modality to be taken over by the remaining sensory modalities, having profound effects on development (Bronchti et al., 2002; Piche et al., 2007; Karlen et al., 2006). Therefore, this sensitivity of the sensory systems to deprivation extends beyond the deprived modality and affects the non-deprived modalities as well. Examples of cross-modal plasticity include increased spine density in the auditory cortex following the removal of eyes or whiskers (Ryugo et al., 1975), enlargement of the whisker representation in the somatosensory cortical barrel field after bilateral enucleation (Bronchti et al., 1992), which results in improved maze performance in adult mice (Toldi et al., 1994), and activation of primary auditory cortex upon visual stimuli (Chabot et al., 2007). Cross-modal plasticity is not limited to sensory areas but also extends to association areas following sensory deprivation (Mezzera et al., 2016). For instance, visual deprivation can increase the number of neurons in multimodal areas that respond to somatosensory and auditory information (Karlen et al., 2009).

The mechanisms responsible for triggering neuroplastic changes in the brain are still a subject of debate. One factor contributing to the controversy is the variation in results obtained from different animal models and sensory deprivation paradigms, as well as the timing of sensory loss (Mezzera et al., 2016). The brain shows more pronounced adaptive effects when the peripheral lesion occurs earlier in development, while it becomes less responsive to changes as development progresses. The plasticity observed in sensory areas, such as the auditory and somatosensory cortices, following visual deprivation, is believed to be influenced by the homeostatic scaling of synaptic plasticity (Goel et al., 2006; He et al., 2012). Studies have shown that this form of plasticity can occur not only during early development but also in adulthood. For instance, visual deprivation in adult mice leads to enhanced thalamocortical synapses in the auditory cortex, resulting in improved auditory processing (Petrus et al., 2014). Further research on cross-modal plasticity is needed to gain a deeper understanding of how critical periods shape sensory and higher-order brain functions during early brain development (Nardou et al., 2019).

### 1.4.2 Experience-related control of critical periods.

Neural circuits are laid down by early experience. Primary sensory areas serve as the initial filters for processing sensory information from the external world and undergo specific periods of experience-dependent plasticity, allowing for the establishment of optimal neural representations of sensory stimuli (Ribic, 2020). Silent synapses, which are glutamatergic synapses containing NMDA receptors (NMDAr) but lacking AMPA receptors (AMPAr), have been implicated as a cellular mechanism involved in critical periods of development (Xu et al., 2020a). The role of NMDAr in critical periods has been observed in various sensory modalities, including somatosensory (Crair et al., 1995; Iwasato et al., 2000), visual (Erisir et al., 2003), auditory (Feldman et al., 1996), and olfactory cortices (Poo et al., 2007).

The critical period of plasticity generally corresponds to the maturation of thalamocortical connections in primary sensory areas or even prefrontal cortex (Takesian et al., 2013a; Barkat et al., 2011). Thalamocortical synapses exhibit specific changes that occur only during the critical periods. For example, in the barrel cortex, the thalamocortical afferents projecting to L4 peak around P3 and decrease by P8 (Crair et al., 1995). This coincides with the transition from early gamma oscillations, transient activity patterns observed in the developing rat barrel cortex, to mature activity patterns, characterised by inhibition-dependent gamma oscillations that arise towards the end of the second postnatal week (Minlebaev et al., 2011). This transition also aligns with the onset of the active whisking period (Arakawa et al., 2014). Similar changes in thalamocortical synapses have been observed across sensory modalities, including visual (Jiang et al., 2007), and auditory (Chun et al., 2013; Barkat et al., 2011). For instance, monocular deprivation specifically induces a depression of thalamic inputs to L4 in the visual cortex while leaving the inputs to L6 and cortico-cortical connections unaffected (Wang et al., 2013).

Although it was previously believed that thalamocortical synaptic plasticity is lost in adulthood, it has been shown that modulatory systems play a role in gating thalamocortical synaptic plasticity (Chun et al., 2013; Blundon et al., 2011), allowing them to provide a substrate for adult plasticity even after the critical period has ended (Yu et al., 2012a).

### 1.4.3 GABAergic control of critical period plasticity.

Different types of GABAergic interneurons exhibit distinct responses to early sensory experience (Baruchin et al., 2022; Kastli et al., 2020). The development of inhibitory circuits typically occurs later than that of excitatory pyramidal cells (Lodato et al., 2011). Mature PV fast-spiking cells are the first interneurons to exhibit a response to sensory deprivation (Kuhlman et al., 2013). This particular interneuron subtype plays a critical role in regulating the timing of neuronal circuits by forming densely interconnected networks that inhibit nearby pyramidal cells (Packer et al., 2011). This inhibition affects the generation and propagation of action potentials in dendrites, as well as contributes to the coordination of rhythmic oscillations (Kirmse et al., 2022; Sohal et al., 2009). Multiple lines of evidence support the involvement of PV basket cells as key triggers of the critical period (Feese et al., 2018; He et al., 2014). As these cells emerge at distinct time points across brain regions (Takesian et al., 2013a), they could be capable of contributing to and driving the sequential trajectories of critical periods in primary sensory areas (Takesian et al., 2013a; Condé et al., 1996). The maturation of PV cells, which serve as the main feedforward inhibitors in the system, is delayed compared to other inhibitory subtypes, developing in tight correlation with plasticity onset (Jiang et al., 2005). For example, accelerating the maturation of PV cells through overexpression of the nerve growth factor BDNF alters the timing of the critical period for ocular dominance (Huang et al., 1999). Conversely, delaying the maturation of GABAergic transmission through dark rearing has been shown to delay the onset and prolong the duration of the critical period (Morales et al., 2002). Moreover, the removal of the perineuronal nets that wrap these cells in adulthood has shown to reactivate plasticity (Lensjø et al., 2017).

Inhibitory circuits undergo experience-dependent changes that are crucial for critical periods. Early sensory experiences can lead to a downregulation of GABAergic transmission in sensory cortices, while excitatory cells remain unaffected, as observed in various experimental conditions such as dark rearing (Morales et al., 2002) or occluding one eye (Kuhlman et al., 2013), whisker trimming (Jiao et al., 2006; Modol et al., 2020; Chittajallu et al., 2010), and hearing loss (Kotak et al., 2008; Takesian et al., 2013b). Unilateral whisker deprivation leads to a decreased strength and spatial extent of inhibitory input from PV interneurons onto pyramidal neurons in L2/3, L4, and L5 of the somatosensory cortex (Lo et al., 2017). These effects are observed only when the sensory manipulation occurs during the first two postnatal weeks, which therefore, corresponds to the critical period for plasticity in the inhibitory circuit (Lo et al., 2017).

These transient, sensory-evoked changes in inhibition are fundamental mechanisms underlying cortical plasticity, even in adulthood. The initiation of the critical period relies on the development

of specific inhibitory circuitry, and this process can be accelerated by the activation of inhibitory $GABA_A$ receptors using modulators such as benzodiazepines (Fagiolini et al., 2000; Iwai et al., 2003). For example, mice lacking the ability to synthesise GABA, which results in impaired GABAergic transmission, are insensitive to monocular deprivation throughout their lives (Fagiolini et al., 2000). However, when GABAergic transmission is restored using GABA agonists, the effects of monocular deprivation become apparent (Fagiolini et al., 2000). Furthermore, the critical period can be induced by tonic inhibition in visual cortex (Iwai et al., 2003). Similarly, transplantation of inhibitory neurons after the end of the critical period is capable of inducing ocular dominance plasticity (Southwell et al., 2010). This suggests that GABAergic transmission plays a direct role in controlling the timing of the critical period and engaging plasticity within the system, and therefore, it is important to understand these transient, sensory evoked changes in inhibition, as they have shown to be a fundamental mechanism for cortical plasticity even in adults (Chen et al., 2011). The critical period can be reactivated in adulthood by pharmacologically reducing inhibition (Harauzov et al., 2010) or by suppressing the expression of Otx2 (Spatazza et al., 2013), a homeoprotein involved in both the initiation and termination of critical period plasticity. Additionally, chemogenetic inactivation of PV interneurons alone is capable of restoring critical period plasticity in the adult auditory cortex (Cisneros-Franco et al., 2019)

### 1.4.4 Excitation-inhibition balance and timing of critical periods.

The majority of the effects observed when disrupting GABAergic networks during critical period plasticity appear to stem from changes in the equilibrium between excitatory and inhibitory signalling, which is known to be essential for the proper functioning of the brain (Hensch et al., 1998; Southwell et al., 2010; Hensch et al., 2005; Jiao et al., 2006; Keck et al., 2011; Kätzel et al., 2014; Kannan et al., 2016). Manipulating the balance between local circuit inhibition and excitation through pharmacology, sensory stimuli and/or genetic factors, among others, can influence the timing of critical periods in both animals and humans (Putignano et al., 2007; Maya Vetencourt et al., 2008). Slight modifications in the relative levels of excitation and inhibition can significantly impact information processing (Liu, 2004). This precise balance is dynamically regulated by cortical circuitry (Turrigiano et al., 2004), with inhibitory connections maturing later than excitatory ones during the pre-critical period of ocular dominance (Long et al., 2005). Developmental or environmental imbalances to the synaptic EI ratio (Rubenstein et al., 2003; Nelson et al., 2015) can lead to shifts in critical period timing that further disrupt circuit development (Weikum et al., 2012). Interestingly, cortical lesions or retinal abnormalities occurring in adulthood can temporarily alter the local balance between excitation and inhibition, configuring the system to an immature state of the circuitry (Arckens et al., 2000)

Maintaining a balance between excitation and inhibition is crucial during development and has shown to have implications for neurodevelopmental disorders such as epilepsy (Möhler et al., 2004), autism(Rubenstein et al., 2003), Rett syndrome (Dani et al., 2005) and schizophrenia (Lewis et al., 2005). Unravelling the mechanisms underlying critical period plasticity could

thus open doors to novel therapies to treat these conditions, as interventions targeted at the appropriate critical periods have the potential to redirect atypical developmental trajectories (Marín, 2016).

## 1.5 Developmental perspective on GABA polarity shift.

GABA, the primary inhibitory neurotransmitter in the adult brain, has been shown to depolarise and often excite immature neurons in virtually all animal species investigated, from frogs to rodents, and most likely humans (Ben-Ari et al., 2007). This depolarising effect is later reversed to hyperpolarising as the brain matures, which is partly attributed to a developmentally regulated decrease in intracellular chloride concentration (Shimizu-Okabe et al., 2002). This change in GABA response, referred to as the GABA polarity shift, arises from changes in the expression of the two primary chloride cotransporters: Na-K-2Cl cotransporter isoform 1 (NKCC1) and K-Cl cotransporter isoform 2 (KCC2) (Shimizu-Okabe et al., 2002; Blaesse et al., 2009). During early development and until the third postnatal week, there is an upregulation of the KCC2 channel that leads to a reduction in intracellular chloride levels, which occurs in a layer, region, and species-specific manner, resulting in differences in the timing of the GABA switch (Shimizu-Okabe et al., 2002; Ben-Ari et al., 2007). The upregulation of KCC2 follows the caudal-to-rostral pattern of neuronal differentiation (Wang et al., 2002; Stein et al., 2004).

The role of NKCC1 in this process is less well understood (Virtanen et al., 2020). Recent studies have suggested that the involvement of NKCC1 in establishing functional networks may not be essential, as even in the absence of NKCC1 in glutamatergic hippocampal neurons, which leads to lower intracellular chloride concentration, mice still demonstrated the ability to perform hippocampus-dependent behavioural tasks (Graf et al., 2021). Thus, the timing of the GABA switch is not solely governed by genetic programming but can also be influenced by neurotrophic factors (Wardle et al., 2003) and neuronal activity (Ganguly et al., 2001). For instance, repetitive excitation has been shown to impact the expression of KCC2 (Fiumelli et al., 2005), whereas blocking $GABA_A$ receptors can inhibit the upregulation of this transporter (Leitch et al., 2005).

### 1.5.1 When are depolarising GABA responses excitatory?

The direction of chloride flux, which depends on the chloride reversal potential, will determine whether GABA, acting through $GABA_A$ receptors, has a depolarising or hyperpolarising effect. The reversal potential represents the membrane potential at which the net flow of ions through a specific ion channel or receptor becomes zero. If the chloride reversal potential is higher than the resting membrane potential, which is generally the case during early postnatal development due to high internal chloride concentration (Shimizu-Okabe et al., 2002; Blaesse et al., 2009), chloride ions will leave the cells, resulting in depolarisation. Conversely, if the chloride reversal potential is below the resting membrane potential, chloride ions will enter the cells, leading to

hyperpolarisation. The GABA reversal potential, in this context, is defined as the membrane potential at which GABAergic inhibition turns to excitation (Lombardi et al., 2021). In this regard, it is important to distinguish between depolarising and excitatory actions of GABA, as GABA-induced depolarisation and calcium influx do not necessarily go hand in hand with neuronal excitation. Generally, an activation of the $GABA_A$ receptor could lead to either hyperpolarisation or a weak depolarisation. However, when a second $GABA_A$ receptor opens adjacent to the first one, it will reduce the input resistance of the cell, as the cell membrane becomes *leaky* increasing conductance, inducing shunting inhibition. This shunting inhibition short-circuits excitatory currents in nearby synapses, decreasing the firing probability of the cell (Destexhe et al., 2003; Egawa et al., 2013). Therefore, while GABA may induce a modest depolarisation at the synaptic level, its net effect remains inhibitory and is contingent upon the intricate interplay between chloride levels, neuronal activity, and the synaptic connectivity onto developing neurons (Le Magueresse et al., 2013; Morita et al., 2006; Staley et al., 1992). Therefore, referring to GABA as excitatory means that GABA generated a depolarisation sufficient to trigger an action potential.

Generally, for GABA to mediate an excitatory effect, the GABA reversal potential would need to be close to the action potential threshold (Owens et al., 2002; Lombardi et al., 2021; Kilb, 2021). Measuring the GABA reversal potential experimentally is challenging, but recent computational modelling by Lombardi et al., 2021 has shed some light on the conditions under which GABA could be inducing an excitatory effect. For example, if GABAergic signalling happened in the absence of other inputs and close to the soma and axon initial segment, the GABA reversal potential was close to the action potential threshold, while the further away the synapse moved along the dendrite, the more positive the reversal potential got (Lombardi et al., 2021). However, the impact of GABA on AMPA-mediated inputs showed a complex spatiotemporal dependency. Spatially and temporally correlated inputs led to a GABA reversal potential consistently below the action potential threshold, indicating that excitatory actions of GABA could happen at membrane potentials below this threshold (Lombardi et al., 2021). Moreover, if AMPA-mediated inputs appeared after the GABAergic input, the reversal potential converged close to the resting membrane potential, making GABA have a striking excitatory effect at very negative potentials (Lombardi et al., 2021). Therefore, even with considerably hyperpolarised potentials, GABA could mediate an excitatory effect.

As a result, this transition from depolarising to hyperpolarising GABA signalling does not solely correspond to a shift from GABAergic excitation to inhibition. In certain conditions, such as low neuronal activity in brain slices, depolarisation caused by GABA could more easily trigger action potentials (Kilb, 2021). However, in the intact brain, regional differences in spatiotemporal activity patterns could play a crucial role, determining whether depolarising GABA responses will lead to prominent excitatory effects.

### 1.5.2 Excitatory and inhibitory GABAergic effects in the immature brain.

The excitatory effect of GABA during development remains a topic of debate (Ruusuvuori et al., 2010; Ben-Ari et al., 2012; Bregestovski et al., 2012; Sulis Sato et al., 2017; Ben-Ari et al., 2022). Several studies conducted *in vitro* have provided evidence that the activation of $GABA_A$ receptors can produce excitatory effects in immature neurons, showing suprathreshold GABAergic responses in neocortical, hippocampal and hypothalamic neurons (Valeeva et al., 2013; Wang et al., 2001; Sava et al., 2014). Furthermore, optogenetic activation of GABAergic neocortical and hippocampal interneurons in slices has provided direct evidence of the excitatory effects of GABA, leading to an increase in the frequency of excitatory postsynaptic currents and synchronous network activity (Flossmann et al., 2019; Valeeva et al., 2016). However, contrasting findings from several *in vitro* studies suggest that GABA may exert a net inhibitory effect on immature neurons, as the inhibition of $GABA_A$ receptors has been shown to induce epileptiform activity (Kolbaev et al., 2012; Sharopov et al., 2019). Nonetheless, depolarising GABAergic responses have also shown to contribute significantly to epilepsy during early brain development (Khalilov et al., 2005; Nardou et al., 2009). This discrepancy highlights the complex functional implications of depolarising GABAergic responses, where the net effect depends on the balance between GABAergic depolarisation and shunting (Winkler et al., 2019).

*In vivo* experiments have provided further evidence of the functional effects of GABA during early developmental stages. The exogenous application of GABA in the developing cortex has shown to generate a depolarisation in single neurons, while leading to a network decrease in neuronal activity (Kirmse et al., 2015). Similarly, the activation of GABAergic interneurons through optogenetics in animals under urethane anaesthesia resulted in a decrease in the frequency of excitatory postsynaptic currents in the neocortex and hippocampus (Valeeva et al., 2016). Correspondingly, the administration of the GABA antagonist gabazine enhanced the frequency of spindle burst oscillations in the neocortex (Minlebaev et al., 2007), suggesting an inhibitory effect of GABA on neuronal networks during this early stage of development. Nonetheless, there are some recent studies that have shown that activation of GABAergic interneurons in the hippocampus can actually enhance network activity during early development, indicating a potential excitatory effect of GABA in this region even under *in vivo* conditions and non anaesthetised mice. Using DREADD and optogenetic techniques, Murata et al., 2020 showed that activating GABAergic interneurons led to an increase in network activity in the hippocampus, while inhibiting GABAergic interneurons suppressed it. This excitatory effect of GABA switched to inhibition by P7 (Murata et al., 2020). Similarly, the minimisation of potential depolarising GABAergic responses by selective removal of NKCC1 in pyramidal neurons resulted in a decrease in correlated spontaneous network activity within the hippocampus (Graf et al., 2021), and therefore suggesting a potential excitatory role of depolarising GABAergic responses in the developing hippocampus. However, these studies also demonstrated that the activation of GABAergic interneurons in the visual cortex already led to inhibition as early as P3 (Murata et al., 2020), with the NKCC1 knockout in the visual cortex having no impact on the typical

network activity (Graf et al., 2021). The neocortex and hippocampus have previously shown differences in their maturation processes, for example, excitatory glutamatergic transmission in the neocortex maturing earlier compared to the hippocampus (Garaschuk et al., 2000).

Hence, despite GABA potentially triggering a calcium influx in immature neurons, it ultimately reduces neuronal firing through shunting, exerting a net inhibitory effect (Murata et al., 2020; Kirmse et al., 2015; Che et al., 2018). These findings align with studies demonstrating that depolarising GABA does not contribute to early oscillations observed in the developing cortex *in vivo* (Minlebaev et al., 2011; Kirmse et al., 2015), and instead, such oscillations rely on AMPA receptors and cholinergic activity (Yang et al., 2016). These observed differences in the excitatory or inhibitory effects of GABA during early development could be attributed to the timing of the polarity shift in different brain regions (Ben-Ari et al., 2007). Sensory regions could be experiencing an earlier switch, while cortical regions with more protracted development may still exhibit excitatory effects of GABA postnatally. This would make the medial prefrontal cortex (mPFC) a perfect candidate to observe this switch at later ages. However, a recent study showed that inhibition is already functionally present in the newborn mPFC (Chini et al., 2022).

GABA signalling and elevated chloride levels are already present in embryonic neurons, even before the maturation of synaptic transmission; and these factors have shown to play crucial roles in early network development, including processes such as proliferation, migration, and synapse formation (Peerboom et al., 2021; Wang et al., 2011). Therefore, it still remains possible that GABA might exhibit depolarising effects at earlier and very specific stages of development. In order to evaluate that, it would be crucial to determine the direction of chloride flux through $GABA_A$ receptors by measure chloride levels *in vivo*. However, conducting such measurements is generally challenging as many techniques can influence the results (Ben-Ari et al., 2012). Therefore, to obtain reliable data, it would be necessary to employ single-channel, cell-attached recordings, ideally following a similar technique as described in Munz et al., 2023, to measure chloride levels during embryonic development.

### 1.5.3 Consequences of the GABA switch on network development.

The shift in GABA polarity is crucial for proper synaptic plasticity, which relies on the inhibitory effects of GABA signalling (Capogna et al., 2021). The timing of this shift plays a crucial role in the network's capacity to undergo developmental changes in response to sensory input. Accelerating the GABA switch to an earlier time point, achieved by increasing or decreasing the expression of KCC2 or NKCC1, respectively, has been shown to induce hyperpolarising GABAergic responses at birth and reduce the number of glutamatergic synapses, which persists into adulthood (Wang et al., 2011; Awad et al., 2018; Wang et al., 2008), due to the role of depolarising GABA in synapse formation through NMDA receptor activation (Wang et al., 2008). The overexpression of KCC2 enhances GABAergic transmission (Chudotvorova et al., 2005),

while temporarily reducing NKCC1 leads to a decrease in the number of inhibitory synapses (Wang et al., 2011; Deidda et al., 2015a). GABAergic interneurons in the neocortex generally exhibit more depolarised GABA reversal potentials compared to glutamatergic neurons (Martina et al., 2001) due to the lower expression of KCC2 in the former (Elgueta et al., 2019), which can potentially limit the formation of inhibitory synapses during the early stages of postnatal development. A delay in the timing of the GABA switch, achieved by reducing KCC2 expression levels or its activity, has also been found to affect both glutamatergic and GABAergic signalling (Woo et al., 2002; Pisella et al., 2019), and seems to last until the GABA switch is completed (Pisella et al., 2019).

Therefore, modifying the timing of the GABA switch can lead to long-lasting changes in brain connectivity, function, and behaviour that persist into adulthood, ranging from developmental delays in motor coordination and an improved learning rate and long-term memory function when the GABA switch is accelerated (Wang et al., 2011; Moore et al., 2019), to almost opposite effects for a delay on this process (Moore et al., 2019; Pisella et al., 2019). These findings emphasise the importance of the timing of the postnatal GABA switch to ensure proper network development and lifelong functioning. Furthermore, dysregulation of the GABA shift is associated with various neurodevelopmental disorders, including autism spectrum disorder (Buckley et al., 2016) and Down syndrome (Deidda et al., 2015b). Given that there is a developmental increase in the function of the KCC2 transporter relative to the NKCC1 transporter in humans (Kharod et al., 2019), the delay or absence of this GABA switch may contribute to a persistent GABAergic depolarisation that will impact early postnatal activity levels. This, in turn, could potentially contribute to the behavioural symptoms observed in these disorders (Peerboom et al., 2021; Hui et al., 2022).

## 1.6 Thesis outline.

Excitatory and GABAergic synapses, as well as the maturation of of different neuronal subtypes and their connectivity, play crucial roles in postnatal development and can mutually influence each other. Moreover, it is known that the formation of local and global networks is experience-dependent and contributes to the establishment of mature neural activity patterns. However, our understanding of how the coordination between excitatory and GABAergic neuronal populations changes within the context of these broader networks is limited. Furthermore, while the role of GABAergic neurons in the functional maturation of specific areas of the neocortex has been extensively studied, their influence on the development of cortex-wide functional networks, which are essential for lifelong cognitive function and behaviour, remains poorly understood. Therefore, the primary aim of this project was to investigate how the dynamics of GABAergic neural activity, in relation to ongoing excitatory activity, contribute to the maturation of the entire mammalian cortex.

**Chapter 2** focuses on the development of a novel dual-colour widefield imaging technique for investigating the postnatal development of neocortex-wide networks in neonatal mice. The chapter begins by examining the feasibility of this technique for studying the early stages of cortical development and establishing suitable controls for simultaneous imaging of neuronal populations labelled with two distinct calcium indicators. Additionally, the chapter explores innovative methodologies for preprocessing and analysing the extensive high-dimensional data acquired through widefield calcium imaging, addressing the computational challenges associated with such data processing.

**Chapter 3** delves into the spatiotemporal activity dynamics in the GABAergic and excitatory populations during the second and third postnatal weeks of development. The chapter focuses on tracking the developmental trajectories of each neuronal population, examining how they change over time and vary across different cortical regions. Additionally, the chapter investigates the impact of manipulating ongoing activity on these developmental trajectories, shedding light on the effects of activity perturbations during this critical period of development.

**Chapter 4** integrates the findings from the previous chapters, providing a comprehensive understanding of the results obtained within the context of known changes in GABAergic and excitatory circuits during postnatal development. Additionally, the chapter identifies remaining unanswered questions that could be addressed using the dataset and proposes potential future experiments to further elucidate intriguing aspects of early postnatal development.

# 2

# Chronic, neocortex-wide, dual-colour calcium imaging in awake behaving neonatal mice

Animal behaviour and cognition are generated by the collective activity of many neurons (Arandia-Romero et al., 2017), and thus, constitutes an emergent property of the brain, which might not be apparent at the individual level single cells or even isolated anatomical regions (Pillow et al., 2017; Schotten et al., 2022). Furthermore, these collective interactions and patterns of activity across neuronal populations and brain regions are not fixed but dynamically shaped over multiple timescales by many different processes, such as learning (Makino et al., 2017). These features suggest that the behaviour of such complex dynamical systems, which arises from this collaborative function, cannot be fully understood by independently analysing each of its constituents. Therefore, to explore these interactions across distributed cortical regions and understand their relationship with behaviour, it is essential to characterise multi-region neuronal activity.

## 2.1 Introduction.

Neuronal activity is generated and organised on a wide range of spatial and temporal scales, from single cells assembled into microcircuits to dynamic large-scale networks that span spatially distant regions and serve as the basis for complex behaviour and cognition. Determining which scale or dimension the relevant brain activity is organised into is an ongoing challenge. Nonetheless, the field of neuroscience is experiencing a dramatic increase in the number of simultaneously recorded neurons and brain areas, in increasingly larger brains (see Box 1 in Urai et al., 2022), outpacing even the most optimistic projections (Stevenson et al., 2011). For example, in the case of the rodent research, it is hypothesised that single neuron recordings of the entire mouse brain may be possible between two decades and a century from now (Urai et al., 2022). This exponential growth has led to a transition in the field, which is increasingly embracing the population doctrine (Yuste, 2015; Saxena et al., 2019), and a multi-region approach to understanding brain dynamics (Urai et al., 2022; Machado et al., 2022).

However, the current interest in population-level dynamics is not new and has been prevalent throughout the history of neuroscience (Yuste, 2015; Saxena et al., 2019). Despite technical

limitations that allowed only a handful of neurons to be recorded at a time, the importance of studying larger populations of neurons can be traced back to Hebb's cell assemblies (Loring et al., 2020) and early investigations into coherence and synchronicity in the motor cortex (Georgopoulos et al., 1983). Furthermore, populations of neurons have always had an influential role in computational neuroscience (Shenoy et al., 2021; Vyas et al., 2020). This shift is leading to a reevaluation of the types of questions being posed and the ways neural activity is analysed, opening up new avenues for understanding population level neural behaviour.

### 2.1.1 Why do we care about multi-region recordings?

Sensory, motor and cognitive behaviours require the processing and integration of information across multiple brain regions. The importance of multi-scale and multi-region recordings in studying animal behaviour, as local circuits or even individual regions do not function independently but rather are highly interconnected, has been widely emphasised (Wang et al., 2022; Machado et al., 2022; Kim et al., 2022; Urai et al., 2022; Higley et al., 2022; Markicevic et al., 2021; Lake et al., 2022). These interconnected regions form deeply recurrent systems that span spatially distant regions, highlighting the need for a comprehensive multi-regional approach to understanding animal behaviour.

Traditionally, starting with the definition of Brodmann's areas, the brain has been described as a modular structure, segregated into modules or brain regions (Mountcastle, 1997). Each of these regions are thought to be anatomically and functionally different, carrying out specific computations within a given process of interest. For example, object processing involves a set of regions that form the ventral visual stream with each region performing a specific function, ranging from processing of basic level visual features such as edges and contours, to colour and complex shapes (Ungerleider et al., 1994). Consequently, understanding how an object's appearance is processed, requires the consideration of how each of these different regions collectively interact. This cannot be fully accessed by analysing each individual region in isolation. Many deep neural networks that seek to model some of these processes construct their network architectures based on this concept, where each layer can be thought of as an approximation to a single region, for example a visual area within the ventral stream hierarchy, and will display its own feature maps, which capture various aspects of visual information such as edges, textures, shapes, and object parts (Lindsay, 2021). In this context, since regions are separated into distinct elements with defined functions, removing or lesioning one of these regions will result in a network deficit and loss of function. However, we know that, in many cases, this is not true, particularly during development, when deprived areas can be reactivated by other sensory systems (Charbonneau et al., 2012) or discrete functions can be largely taken over by other brain regions when the one in question is absent (Collignon et al., 2009).

These observations challenge the traditional assignment of distinct computations to specialised brain regions, and instead point towards a brain-wide distribution of functions and/or information

that are context-dependent and task relevant (Pessoa, 2023; Machado et al., 2022). In the adult brain, even simple motor and sensory tasks involve the processing of information across multiple cortical areas. For example, a whisker deflection results in the activation of a distributed sensorimotor network (Ferezou et al., 2007; Cross et al., 2021, Figure 2.1, left panel). Locomotion engages much of the cortex (Schneider, 2020; Stringer et al., 2019b; Clancy et al., 2019), particularly observed in the extensive modulation of the primary visual cortex (Saleem et al., 2013). Attention and arousal also activate widely distributed networks (Shimaoka et al., 2018; Lohani et al., 2022, Figure 2.1, right panel). Functional magnetic resonance imaging (fMRI) studies were the first to show how changes in behavioural states influence cortical processing and lead to a dynamic routing of information across brain regions based on task demands (Raichle, 2015). This dynamic routing of information, for example, can result in the distributed signatures of subjective experiences, such as fear (Zhou et al., 2021). Most importantly, learning also causes widespread changes in cortical dynamics (Makino et al., 2017; Gilad et al., 2020; Sych et al., 2022) that are subsequently translated into distributed memory engrams (Roy et al., 2022). These representations and brain states are broadcast across brain regions that coordinate and work together. As such, the resulting behaviour constitutes an emergent property of the interconnected brain that cannot be observed or predicted solely from the constituent parts of the system (Elsayed et al., 2017; Pillow et al., 2017).

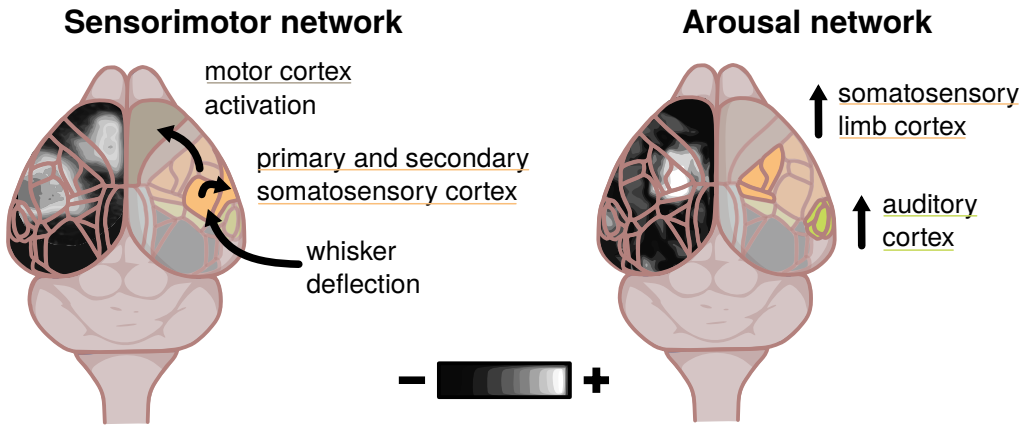


**Fig. 2.1 Examples of distributed representation of behaviour in mouse neocortex.** Left panel shows the activation of the sensorimotor network (primary barrel and secondary somatosensory cortex - orange, motor cortex - brown) after a whisker deflection. Adapted from Ferezou et al., 2007; Hubatz et al., 2020. The right panel shows the correlation of neuronal activity with running speed/pupil dilation as a proxy of arousal (auditory cortex - green, somatosensory limb cortex - orange). Adapted from Shimaoka et al., 2018.

Although this new perspective does not invalidate what it is already known about local function, what it is known about single neurons or regions may not apply directly to the dynamics of multi-region recordings. Furthermore, the observation of distributed computations has raised new questions about why the activity is so widespread and what role it plays in guiding behaviour. It has long been assumed that regional functional specialisations result from the selective strengthening of some brain circuits over others. However, it has been proposed that such regional specialisations are more likely to emerge from dynamic changes in inter-regional

communication, which will lead to changes in functional specialisation (Menon et al., 2021). Therefore, regional function might be less dependent on the input for its processing but more on its engagement with the rest of the network. This is particularly important during development as the cortex is undergoing rapid growth and the regional boundaries are not yet hard-defined (Baloch et al., 2009). This early postnatal period characterised by significant structural and functional changes that pose challenges in studying the developing cortex. These changes include the existence of transient thalamocortical circuits (Marques-Smith et al., 2016; Tuncdemir et al., 2016), programmed cell death waves (Wang et al., 2019; Duan et al., 2020), shifts from primarily periphery-driven to cortically-driven dynamics (Gribizis et al., 2019; Siegel et al., 2012), and the formation, refinement, and broadening of sensory maps during critical periods (Quast et al., 2017; Berardi et al., 2000), among others.

Despite recent efforts to study multi-region interactions throughout development (Ackman et al., 2014b; Linden et al., 2021; Smith et al., 2018; Tabuena et al., 2022; Gribizis et al., 2019; Wang et al., 2021; Hamodi et al., 2020; Ma et al., 2016; Babij et al., 2023; Mojtahedi et al., 2021; McVea et al., 2017; McVea et al., 2016; McVea et al., 2012), much of the developmental inter-regional communication, particularly that of GABAergic interneurons, remains underexplored. This major group of neurons is generally assumed to participate in local microcircuits (Baruchin et al., 2022; Modol et al., 2020; Leighton et al., 2021; Anastasiades et al., 2016) but has repeatedly been shown to play important roles as well in long-distance connectivity (Tomioka et al., 2005; Tamamaki et al., 2010; Hafner et al., 2019; Naskar et al., 2021; Urrutia-Piñones et al., 2022; Caputi et al., 2013; Lee et al., 2014; Vagnoni et al., 2020), suggesting that those connections should be developmentally regulated (Boon et al., 2019; Mòdol et al., 2017). Since learning has shown to cause dramatic changes in brain-wide dynamics (Makino et al., 2017; Gilad et al., 2020; Sych et al., 2022), characterising these widespread changes will be critical for understanding circuit formation during development, the time at which the brain *learns* the most.

### 2.1.2 Techniques and analysis methods for large-scale recordings.

Recent advances in the measurement of *in vivo* neuronal activity allow for a global and more unbiased way to explore neural dynamics across many brain regions with more naturalistic behaviours and environments (Machado et al., 2022; Urai et al., 2022). Particularly, the rodent literature has seen the greatest explosion in these techniques (Kim et al., 2022; Wang et al., 2022), which has contributed to the growing consensus that cortical processing is more widely distributed in nature. Various imaging modalities have emerged in the recent years to monitor the activity of populations at different scales (Machado et al., 2022; Kim et al., 2022). However, only a limited subset can provide high spatiotemporal resolution as well as enough spatial coverage to be able to understand distributed network function and answer questions about brain-wide computation. Each technique provides information about different aspects of the

neuronal activity and dynamics; therefore, the right match between the tool of choice and the question to answer is critical.

There are three main groups of techniques to probe large-scale dynamics: electrical, optical and metabolic. Differences between the recording techniques arise from trade-offs in spatiotemporal resolution, spatial coverage and invasiveness. Electrical techniques can measure the neural activity directly and provide high temporal resolution, with varied spatial resolution and coverage (Machado et al., 2022): going from single cells within a few selected regions using electrode/neuropixel recordings, to superficial whole-brain populations using EEG/MEG measurements (Figure 2.2, panel A, Table 2.1). However, electrical techniques that offer single cell resolution are invasive and make it challenging to identify the same cell across imaging sessions. Metabolic methods, like fMRI, offer a proxy read-out of the ongoing neuronal activity that relies on the relationship between neuronal spiking and local blood flow, and thus have a low temporal resolution, limited by the dynamics of the blood oxygen level dependent (BOLD) response (Wang et al., 2022; Lu et al., 2021). Nonetheless, they are noninvasive techniques with low spatial resolution but a large and deep spatial coverage (Figure 2.2 panel A, Table 2.1).

The remaining optical techniques constitute the broader group, spanning all the spatiotemporal axes (Figure 2.2, panel A). In recent years, large-scale fluorescence imaging techniques have gained popularity due to their ability to simultaneously observe the activity of genetically identified neurons across multiple brain regions in awake and behaving animals for extended periods of time (Kim et al., 2022). Fluorescence generally comes from the use of genetically encoded calcium indicators (GECIs), which track the levels of intracellular calcium altered by neural excitation and, therefore, provides an indirect read-out of electrical activity (Lin et al., 2016). While genetically encoded voltage-sensitive indicators (GEVIs) provide better temporal resolution and report sub-threshold information, GECIs are more widely used because they provide higher signal-to-noise ratio (SNR) (Knöpfel, 2012). Other optical indicators include those that report vesicle release and changes in neurotransmitter concentrations (Lin et al., 2016), such as glutamate, acetylcholine, and norepinephrine (Labouesse et al., 2021; Wang et al., 2022), offering a different read-out of the neuronal activity.

Most optical fluorescence techniques are temporally limited by the dynamics of the fluorescent indicator (Lin et al., 2016). They can be broadly divided into single-photon and multi-photon techniques, which can have very different spatial resolutions, coverage and imaging depth. Single photon fluorescence techniques use short wavelength excitation light, allowing for the illumination of large FOVs (large spatial coverage) with either single cell resolution (miniscopes, Ghosh et al., 2011; Rynes et al., 2021), near-single cell resolution (COSMOS, Kauvar et al., 2020) or population/brain regions resolution (optoencephalography, Figure 2.2, panel B, Cardin et al., 2020). Multi-photon techniques, on the other hand, use long wavelength excitation light to image deep within the tissue with high spatial resolution while compromising the spatial

**Tab. 2.1 Overview of the multi-region recording techniques and their trade-offs.**

| Methods | Type signal | Temporal resolution | Spatial resolution | Spatial coverage | Genetic specificity | Invasiveness | Behaviour |
|---|---|---|---|---|---|---|---|
| neuropixel probes | electrical | >1 kHz ms to days | single cell | few regions, linear trajectory *(~10 mm/shank)* | possible with optotagging | invasive, *(probe insertion)* | awake, freely moving *(up to 2 probes)* |
| 2-photon mesoscope | electrical, calcium proxy | ~1-10 Hz ** *(depending on spatial resol. and coverage)* | single cell | few adjacent regions, *(~5-8 mm)* | viral or transgenic | invasive *(cranial window)* | awake, head-fixed |
| multi-objective 2-photon | electrical, calcium proxy | >10 Hz ** *(depending on spatial resol. and coverage)* | single cell | few select cortical regions | viral or transgenic | invasive *(cranial window)* | awake, head-fixed |
| COSMOS * mesoscope | electrical, calcium proxy | 10-100 Hz ** | few cells/ clusters | entire dorsal cortical surface *(>10 mm diameter)* | viral or transgenic | minimally invasive *(scalp removal)* | awake, head-fixed |
| Widefield mesoscope *(optoence-phalography)* | electrical, calcium proxy | 10-100 Hz ** | populations | entire dorsal cortical surface *(>10 mm diameter)* | viral or transgenic | minimally invasive *(scalp removal)* | awake, head-fixed |
| fibre photometry | electrical, calcium proxy | >10 Hz ** | populations | one region/fibre | viral or transgenic | invasive *(fibre insertion)* | awake, freely moving |
| optoacoustic imaging | electrical, calcium proxy | >10 Hz ** | populations | whole brain | viral or transgenic | non-invasive | anesthetised *(whole brain)*, awake-behaving *(smaller areas)* |
| miniscopes | electrical, calcium proxy | ~10-36Hz ** | single cell | very few adjacent regions *(< 2.5 mm diameter)* | viral or transgenic | invasive *(lens insertion)* | awake, freely moving |
| EEG/MEG | electrical | >10 Hz | populations | most brain regions | no | minimally invasive *(screw implant)* | awake, freely moving |
| fMRI | metabolic *(BOLD*)* | <10 Hz | populations | whole brain | no | non-invasive | awake, body restrained |
| intrinsic optical imaging | metabolic *(haemoglobin)* | <10 Hz | populations | few adjacent regions, *(~4-6 mm)* | no | invasive *(cranial window)* | awake, head-fixed |

*COSMOS, Cortical Observation by Synchronous Multifocal Optical Sampling
*BOLD, blood-oxygen-level-dependent
** Limited by the calcium indicator dynamics
*Adapted from Machado et al. 2022 and Wang et al. 2022*

coverage (Table 2.1). Moreover, the simultaneous illumination/detection of the entire FOV and the relatively high excitation probability of single photon fluorescence microscopy permits faster image acquisition rates than in laser scanning-based 2-photon imaging. Nonetheless, there have been recent efforts to build two-photon mesoscopes that allow to image larger portions of the brain (e.g. simultaneously imaging two cortical areas) on awake head-fixed behaving animals (Ota et al., 2021; Stirman et al., 2016; Terada et al., 2018; Sofroniew et al., 2016; Clough et al., 2021; Abdeladim et al., 2023).

In order to overcome the various trade-offs posed by different imaging techniques (e.g. the type of signal recorded, the spatiotemporal resolution and cell-type specificity), multimodal approaches have been implemented to bridge the gap between the different imaging modalities and synergise their strengths to investigate the organisation of the nervous system (Lake et al., 2022). For example, optoencephalography or widefield calcium imaging has been combined with electrophysiology (Xiao et al., 2017; Peters et al., 2021; Clancy et al., 2019; Clancy et al., 2021),

2-photon imaging (Barson et al., 2020) or fibre photometry (Ramandi et al., 2023), to enable the simultaneous recording of neocortex-wide activity and single-cell dynamics of a particular brain region or even a peripheral nerve (Xiao et al., 2023). In order to gain a better understanding of the BOLD signal, fMRI and optoencephalography have also been combined as complementary approaches to establish the neural basis for the observed macroscopic functional connectivity patterns (Lake et al., 2018; Vafaii et al., 2023). This enables the translation of cell-specific dynamics and activity patterns in rodents to the macroscopic observations in both human and non-human subjects.

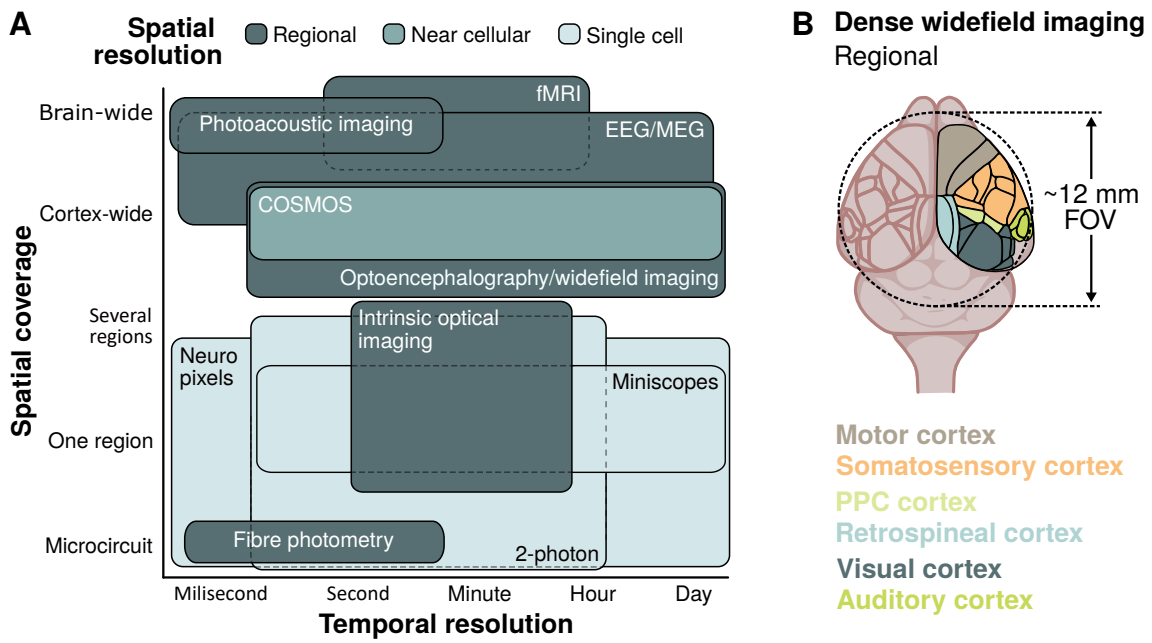


**Fig. 2.2 Schematic overview of the spatiotemporal resolution and spatial coverage spectra of techniques to monitor brain dynamics. A|** Different recording methods exhibit a set of trade-offs between spatial coverage (y-axis, ranging from just one region to the entire brain), temporal resolution (x-axis, sampling time for *in-vivo* chronic imaging, depending on their acquisition speed) and spatial resolution (shading, ranging from regional to single-cell resolution). **B|** Illustration of the spatial coverage of dense widefield imaging like optoencephalography. It allows complete coverage of the dorsal cortex without cellular resolution. COSMOS = Cortical Observation by Synchronous Multi-focal Optical Sampling, is a specific type of optoencephalography.

Whilst this ability to record multi-region neural activity has led to unexpected insights into the distributed nature of neural representations, analysing the vast amounts of data generated presents an ongoing challenge (Stevenson et al., 2011; Urai et al., 2022; Cunningham et al., 2014). Analysis techniques need to scale parallel to the amount of data available, leveraging the ability to provide insights into how networks of neurons represent and process information, while keeping the processing time computationally feasible. State-space models and multi-region network-models have emerged as promising tools for analysing large-scale neural recordings (Perich et al., 2020; Glaser et al., 2020; Capone et al., 2023; Karniol-Tambour et al., 2022). Typically, these models operate under the assumption that neural activity is intrinsically low-dimensional, and therefore, it can be characterised by a limited number of

factors that represent the interactions and correlated behaviour of groups of neurons recorded simultaneously (Stevenson et al., 2011; Urai et al., 2022).

It has been observed that neural activity variability, particularly that relevant to behaviour, can often be explained by a limited number of dimensions. For instance, a study has shown that a choice decoder based on the first principal component of neural activity in the higher visual cortex of monkeys performs similarly to a decoder built on the entire dataset (Ni et al., 2018). Similarly, in the premotor cortex of monkeys performing a reaching task, low-dimensional activity has been observed (Churchland et al., 2012). This is not limited to task-related activity but is also evident in cortex-wide spontaneous activity, which exhibits a restricted set of spatiotemporal patterns (MacDowell et al., 2020). However, the question remains whether neural codes are truly low-dimensional or if they only appear that way (Humphries, 2020). Theoretical work suggests that higher-dimensional responses can be crucial for computation and representation (Fusi et al., 2016). Supporting this notion, recent experimental findings demonstrated that the high dimensional structure of neural responses in V1 allows for a coding scheme that balances efficiency and robustness image perturbations (Stringer et al., 2019a). Although interpreting these low-dimensional factors might pose additional challenges, these approaches have already provided insights into how information is processed within and between different brain regions, demonstrating that neural representations are distributed and heavily influenced by cortical brain states (Urai et al., 2022). The development of novel analysis techniques and theoretical tools opens up exciting new pathways to investigating these questions. Ongoing advancements in these methods hold great potential for providing significant insights into the neural basis of behaviour.

### 2.1.3 Optoencephalography or widefield calcium imaging.

Alongside the increasing interest in multi-region recordings, there has been a remarkable surge in the use and development of optoencephalography or widefield calcium imaging (Ren et al., 2021; Couto et al., 2021; Cardin et al., 2020). Widefield calcium imaging is defined as an *in vivo*, mesoscopic, single photon, fluorescence-based imaging modality capable of monitoring brain activity across multiple regions and up to the entire superficial dorsal cortex (Cardin et al., 2020). It provides sufficient SNR as well as spatiotemporal resolution to record cortical activity in awake, head-fixed, behaving animals by balancing high spatiotemporal resolution with large fields of view (Figure 2.2, panel B, Table 2.1). This method has been successfully employed not only in mice, but also in rats and other mammals (Scott et al., 2018; Chen et al., 2022).

Although widefield calcium imaging provides a large field of view (FOV) with a theoretically high optical resolution (high numerical aperture), its spatial resolution is limited by absorption and light scattering of the tissue (Waters, 2020). Scattering occurs when light passes through the brain tissue, causing it to change direction, dispersing the emitted photons *en route* to the camera sensor. This leads to a loss of lateral spatial resolution, as the signal from one area

can overlap with adjacent regions (Waters, 2020; Silasi et al., 2016). The degree of scattering depends on the tissue properties, such as the density and composition of the tissue, as well as the wavelength of the light used for imaging (Johansson, 2010; Ugryumova et al., 2004). The use of longer wavelengths of light (e.g. green/red light) can improve the spatial resolution, since they are less prone to scattering (Ugryumova et al., 2004). Additionally, the wide illumination source used in widefield imaging leads to out-of-focus background fluorescence that adds noise to the signal measured at the single focal plane (Machado et al., 2022). Due to these features, and the fact that this technique generally employs dense labelling of the calcium indicator to maximise light collection, this method does not provide single-cell resolution. Efforts have been made to improve the spatial resolution using sparse expression of the indicators, which enables near single-cell/cluster resolution, as well as a dual-focus lens (Kauvar et al., 2020). Imaging is typically performed through a cranial window that can either be the intact or thinned skull, most times optically cleared to match the refraction index of air. Although these are the least invasive preparations, the presence of the skull affects the light scattering and make it difficult to gain sufficient optical access to the brain (Waters, 2020), so it is sometimes substituted by a large transparent window (Cramer et al., 2021).

As mentioned above, widefield imaging is generally combined with GECIs, which are the gold standard for chronic optical monitoring of neuronal activity *in vivo* (Kim et al., 2022). These GECIs are usually cytoplasmic sensors that can detect changes in intracellular calcium, which increases as a result of voltage-gated calcium channels that open in response to neuronal depolarisation. Therefore, it acts as a proxy for neuronal activity, enabling a relatively quick and indirect readout of the changes in neural activity (Knöpfel, 2012). One of the most commonly used GECIs is GCaMP, which is mainly comprised of a calcium buffer or calcium binding protein (calmodulin), and a fluorophore (circularly permuted GFP protein) that will fluoresce once the calcium is attached to the sensor in a concentration dependent manner (Zhao et al., 2011). Other widely used GECIs are the red-shifted sensors, which have been constructed by coupling the calcium binding protein with other fluorophores such as mRuby and mApple, which have less phototoxicity and allow for more tissue penetrance of the excitation and emitted light (Dana et al., 2016). Together, the separable spectral characteristics of GCaMP and red-shifted GECIs allow for dual imaging approaches, which in combination with intersectional genetics and/or promoter specific viruses, enable the selective expression of these indicators in particular cell populations or subpopulations, facilitating simultaneous imaging.

The combination of these sensitive and bright GECIs with transgenic mouse lines has emerged as a reliable way to obtain specific, dense and uniform expression of the indicator, in a stable and consistent manner across cells and animals, thus improving reproducibility (Kim et al., 2022; Dana et al., 2018; Wekselblatt et al., 2016). There is a huge repository of transgenic lines, with widely available reporter mouse lines and Cre lines that provide access to diverse cell types (Taniguchi et al., 2011; Daigle et al., 2018; Madisen et al., 2015. Alternatively, viral approaches allow for higher selectivity, since cell populations with specific projection patterns

can be targeted using viral serotypes that have shown to preferentially target anterograde or retrograde synaptic pathways (Haery et al., 2019). Furthermore, it has been suggested that relatively brief viral expression can bypass problems associated with prolonged, high expression levels typically associated with early embryonic expression in transgenic mice (Daigle et al., 2018). Nevertheless, transgenesis is still a powerful way to express these molecular tools early in development without the need for an intervention and a delay onset for robust systemic expression. This is particularly the case when studying mouse brain development, which requires early postnatal or embryonic expression of the indicators. There have been recent developments in whole-brain vector delivery techniques that allow for fast and effective delivery of the indicators a few days after injection (Hamodi et al., 2020). This approach enables dense labelling and targeting of specific cell populations to study neural activity during early developmental stages.

Widefield calcium imaging enables the recording of neural activity across the entire dorsal neocortex of head-fixed, awake and behaving animals placed under a stable microscope. However, a head-fixed assessment of behaviour can have disadvantages related to stress and helplessness (Juczewski et al., 2020). As a result, self-initiated head-fixation imaging approaches have been developed, allowing for flexible and chronic assessment of mesoscale cortical function (Murphy et al., 2016). Although other large-scale imaging techniques are available to record freely moving rodents (Table 2.1), unfortunately, these portable systems are too heavy for neonatal mice and thus unsuitable for studying multi-region activity during early development. Furthermore, neonatal mice cannot be trained to self-head-fix because they only exhibit uncoordinated movements and huddling behaviour during the first postnatal weeks of development (Alberts, 2007; Blumberg et al., 2015) and spend the majority of their time sleeping (Rensing et al., 2018).

### 2.1.4 Aims and outline.

This project developed a chronic, dual-colour widefield imaging approach that enabled the simultaneous observation of neuronal activity across most dorsal cortical areas of two distinct cell groups, pyramidal and GABAergic neuronal populations, and thus provided the means to study the coordination and dynamics of multiple and distributed brain regions and cell types across early postnatal development.

This chapter describes the setup of the main experimental approach used in the project to simultaneously image two neuronal populations across the developing mouse neocortex. The hardware and software setup, imaging acquisition protocols, post-acquisition image processing, and data analysis approaches are all described in the following sections. Controls are also provided for the validation of the dual-colour imaging approach and the chronic implantation on neonatal mice.

## 2.2 Methodological approach: technique development and preprocessing pipeline.

### 2.2.1 Custom-built macroscope for widefield imaging.

One photon, low magnification widefield optics have become very popular due to their potential for high sampling rates (>20 Hz) over large FOVs (∼10 mm) with genetic specificity, as well as their ease of implementation and affordability (Couto et al., 2021; Kauvar et al., 2020). This section outlines the protocol for assembling a dual-colour imaging widefield macroscope and how to adapt it to image neonatal mouse pups; as well as the surgical preparation required to image through the intact skull (detailed steps for similar setups can be found in Couto et al., 2021; Kauvar et al., 2020) and the preprocessing steps.

#### Macroscope setup.

The macroscope design was based on the original configuration from Ratzlaff et al. (1991), which makes use of a tandem lens configuration for efficient excitation and light collection. The system was divided into two main components: the illumination or excitation light path, which delivers light to the cortical surface, and the collection or emission pathway, which collects the light emitted by the indicator and projects it onto the camera sensor to create the image (Figure 2.3, spectra).

The excitation light path was optimised for simultaneous dual-colour imaging of green and red fluorophores, GCaMP6f and jRGECO1a, respectively. The illumination was mounted onto the macroscope column and provided through the objective lens, using a dichroic mirror (reflection band: 452–490 nm, transmission band: 505–800 nm, MD498 Thorlabs) to combine and direct the light from each of the LEDs used to excite the sample, blue (470/28 nm M470L4 Thorlabs mounted LED, filtered through 469/35 nm BrightLine basic Semrock filter) and lime (465/104 nm M565L3 Thorlabs filtered through 565/24 nm BrightLine basic Semrock filter). This epifluorescence configuration was chosen over external illumination, from beside the objective, to avoid unwanted visual stimulation of the subject and optimise the angle of light hitting the sample (Figure 2.3, vertical angle). However, this meant that the main excitation/emission dichroic had to be a wide dual band mirror (50.8 mm, reflection bands: 456–480, 541–565 nm, transmission bands: 500–529, 584–679 nm, FF493/574-Di01-50.8-D, Semrock).

Emitted fluorescence was collected using a face-to-face tandem configuration of two 50 mm single-lens reflex (SLR) camera lenses (50 mm, 1.4 f-stop, Nikon), the objective and camera lens (Figure 2.3). This configuration offered a long working distance (determined by the objective lens's focal distance) and high collection efficiency (high numerical aperture). As the objective lens is inverted, it can project a near-collimated (infinity focused) light into the camera lens,

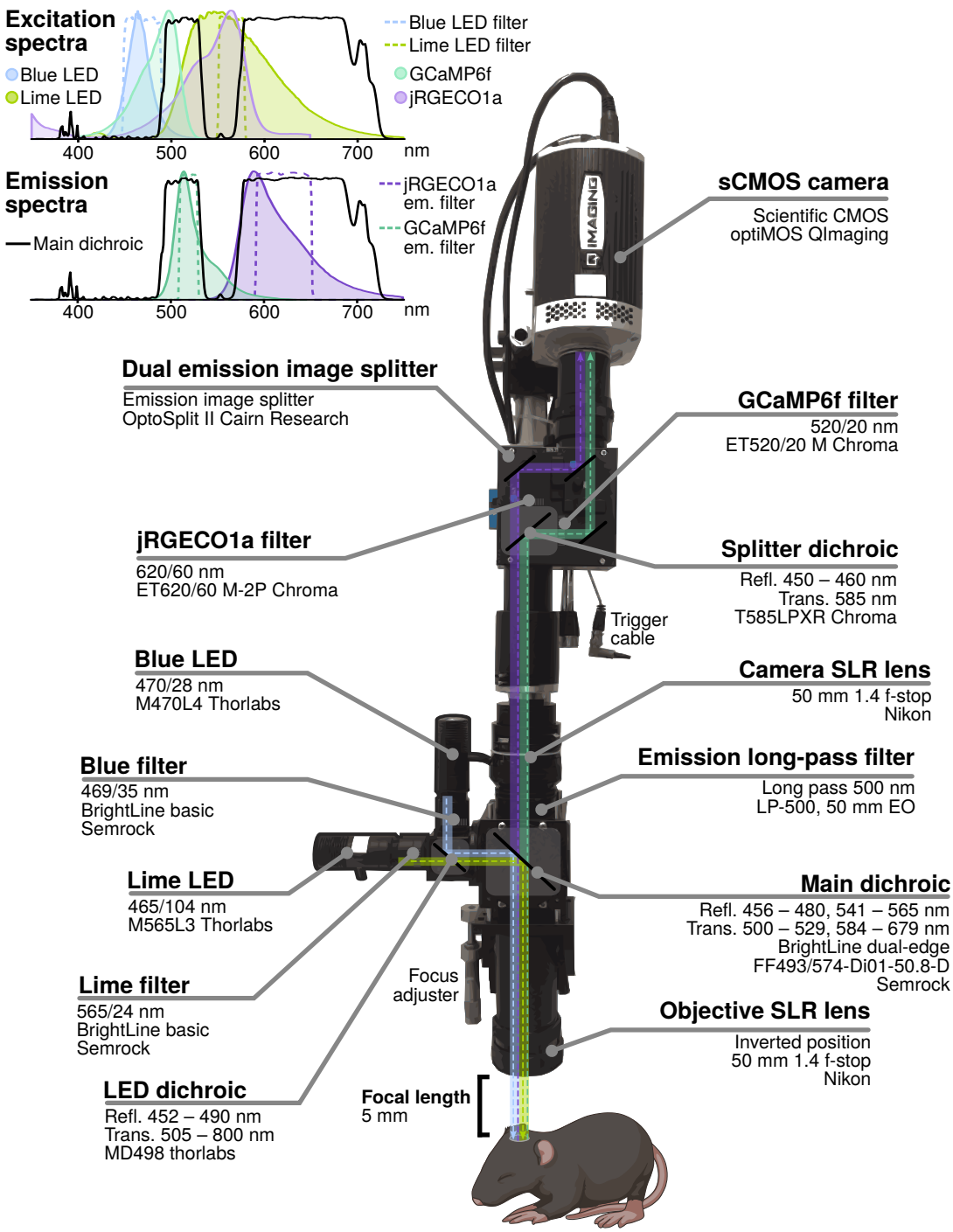


**Fig. 2.3 Overview of the components of the custom-built macroscope.** The illustration includes the main components required for constructing a dual-colour widefield imaging setup, along with the specifications for each component. Basic optomechanical components are not highlighted but were acquired from Thorlabs. The excitation and emission spectra along with the filters and light sources were created using FPbase Fluorescence spectra viewer.

which focuses the light onto the camera sensor. This allowed for a long working/focal distance (50 mm), a very wide aperture (f-stop = 1.4) to allow more light to pass through the lenses, and thus a shallow depth of field (depth of field = width of imaged object/numerical aperture (NA) x magnification, NA = 0.35). The magnification of the sample seen on the camera sensor is

determined by the focal length ratio of the lenses (camera/objective). Since the focal length of both lenses is identical, theoretically there was no magnification, resulting in a FOV equal to the size of the camera sensor, in this case 12.48 mm (1920 pixels) by 7.02 mm (1080 pixels). The sample could eventually be magnified on the sensor if its position is not at the focal distance of the objective lens or the camera sensor is not at the focal distance of the camera lens, which alters the effective FOV. Due to the positioning of the various components on the macroscope column, there was an effective FOV of 21 mm by 11.8 mm, and thus a magnification of 1.68 in this setup. This can vary slightly depending on how the sample is positioned under the scope, which had to be adjusted based on the age and size of the mouse. The FOV was optimised to fit the brain's longest axis (lateral to lateral) into the camera sensor's height (11.8 mm).

The effective aperture (diameter of the entrance pupil) of the lenses is the ratio of the focal length and the aperture (f-stop), with both lenses having an entrance pupil of 35.7 mm (50 mm/1.4). As a result, a 60 mm cage cube (LC6W Thorlabs) was used to connect them in order to maximise the amount of light collected by the imaging lens. The light that exits the objective lens will diverge slightly as it travels through the column; therefore, a camera lens with a larger entrance pupil is generally required to collect the majority of the diverged light. Since the entrance pupil of both lenses was identical to prevent further magnification of the sample, some divergent light may be lost. As the two tandem lenses were infinity focused, the space between them could accommodate the majority of the imaging optics (Figure 2.3). To collect and separate the photons emitted by the two different fluorophores, the emission light was first long-pass filtered (500 nm, LP-500, 50 mm Edmund Optics) to prevent most LED light from passing through the camera lens, and subsequently unmixed by using a dual emission image splitter (The Cairn OptoSplit II, Cairn research), which employed a rotating mirror cradle to display the images from each fluorophore simultaneously, side by side, on the camera sensor. This two-way image splitter accommodates a filter cube with a dichroic (reflection band: 450–460 nm, transmission band: 585 nm, T585LPXR Chroma) and two filters optimised to the peak emission fluorescence of each of the fluorophores, $\sim$520 nm (520/20 nm, ET520/20 M Chroma filter) and $>$590 nm (620/60 nm, ET620/60 M-2P Chroma filte) for GCaMP6f and jRGECO1a, respectively (Figure 2.3). As previously stated, this strategy allowed the optimisation of camera sensor space, fitting the entire dorsal cortical surface of the animals imaged at various ages, including the base of the cerebellum and the base of the olfactory bulbs.

Fluorescence from the calcium indicators was projected onto the sensor of a sCMOS (scientific Complementary Metal–Oxide–Semiconductor) camera (optiMOS, Qimaging) with high sensitivity and quantum efficiency (57% at 600 nm), low noise, large sensor (14.3 mm diagonal, 1920 x 1080 pixels), large dynamic rate (16 bit), fast pixel scan rates (283 MHz) and high frame rates (100 Hz at maximum resolution). The camera was used in a rolling shutter readout mode with "all rows out" behaviour, which exposes all pixels simultaneously for the indicated exposure time to avoid possible artefacts within one same frame due to fast changing dynamics of the fluorophores. It also prevented contamination of the signals with ambient lighting when

the excitation LED lights were turned off. Imaging was performed at 33.3 frames per second (FPS), with an exposure time of 20 milliseconds for each indicator, leaving approximately 10 milliseconds for the shutter to fully open. Higher imaging rates are possible; however, most temporal limitations arise from the calcium indicator dynamics. It has been previously shown that faster imaging rates, even above 10 FPS, do not resolve events better as they maximise with the indicator kinetics (Vanni et al., 2017).

Illumination was alternated between the blue and lime LEDs, resulting in an effective imaging rate per fluorophore of 16.6 FPS (Figure 2.4, panel A). This approach was necessary because, while the splitter allows for simultaneous recording of both indicators, the fluorophore jRGECO1a exhibits photoswitching behaviour under blue light (Dana et al., 2016), resulting in non-calcium dependent events that could confound ongoing neuronal activity (see section 2.3.2 for an investigation on this phenomenon). The signal channels for each of the transgenic animals, Gad2/GCaMP6f (blue-GCaMP6f, green dynamics), Thy1-jRGECO1a (lime-jRGECO1a, purple dynamics) and Thy1-jRGECO1a/Gad2/GCaMP6f (blue-GCaMP6f and lime-jRGECO1a, green and purple dynamics), showed large activity transients for the extracted region of interest (ROI) (Figure 2.4, panel B, black/white square). The GCaMP6f channel under lime light did not display any activity related transients for any of the transgenic mice, indicating proper filtering (Figure 2.4, panel B, lime dynamics). However, there were some non-activity-related artefacts that could suggest LED light leakage or slight mismatch with synchronisation between the LEDs and camera frame acquisition (Figure 2.4, panel B, waveforms). These artefacts appear as small and stereotyped step-like activations the ROI waveforms that do not present activity dynamics.

This same behaviour was observed on the Gad2/GCaMP6f mice under lime light for the jRGECO1a channel (Figure 2.4, panel B, left, purple dynamics). On the other hand, the jRGECO1a channel did not exhibit the same light artefacts when illuminated with blue light (Figure 2.4, panel B, left, blue dynamics). Instead, a slightly smoother signal was observed, which did not follow the calcium-dependent dynamics observed under the signal channel (blue-GCaMP6f, green dynamics). The fluorescence observed in this channel for the Gad2/GCaMP6f mice could be due to autofluorescence of brain tissue, which is higher when illuminated with shorter wavelengths (Moreno et al., 2020) and emits at longer wavelengths (>550 nm, Deliolanis et al., 2011). This signal could also originate from the long tail of GCaMP6f emission, which shows a very small but non-zero contribution (3%) that bled through the jRGECO1a emission filter (Figure 2.3, emission spectra), although it did not show the peaks observed for the GCaMP6f dynamics (green dynamics). In the case of the Thy1-jRGECO1a mice, while the excitation spectra of jRGECO1a overlapped with the blue LED filter and, therefore, could be excited by blue light (Figure 2.3, emission spectra), its fluorescence emission should not bleed through the GCaMP6f emission filter. Hence, the light detected in this channel could be attributed to either autofluorescence, mentioned previously, or hemodynamic signals (Figure 2.4, panel B, middle, green dynamics). Nevertheless, the emission of jRGECO1a when excited by blue light will be recorded on the jRGECO1a channel (blue dynamics), which showed fluorescence

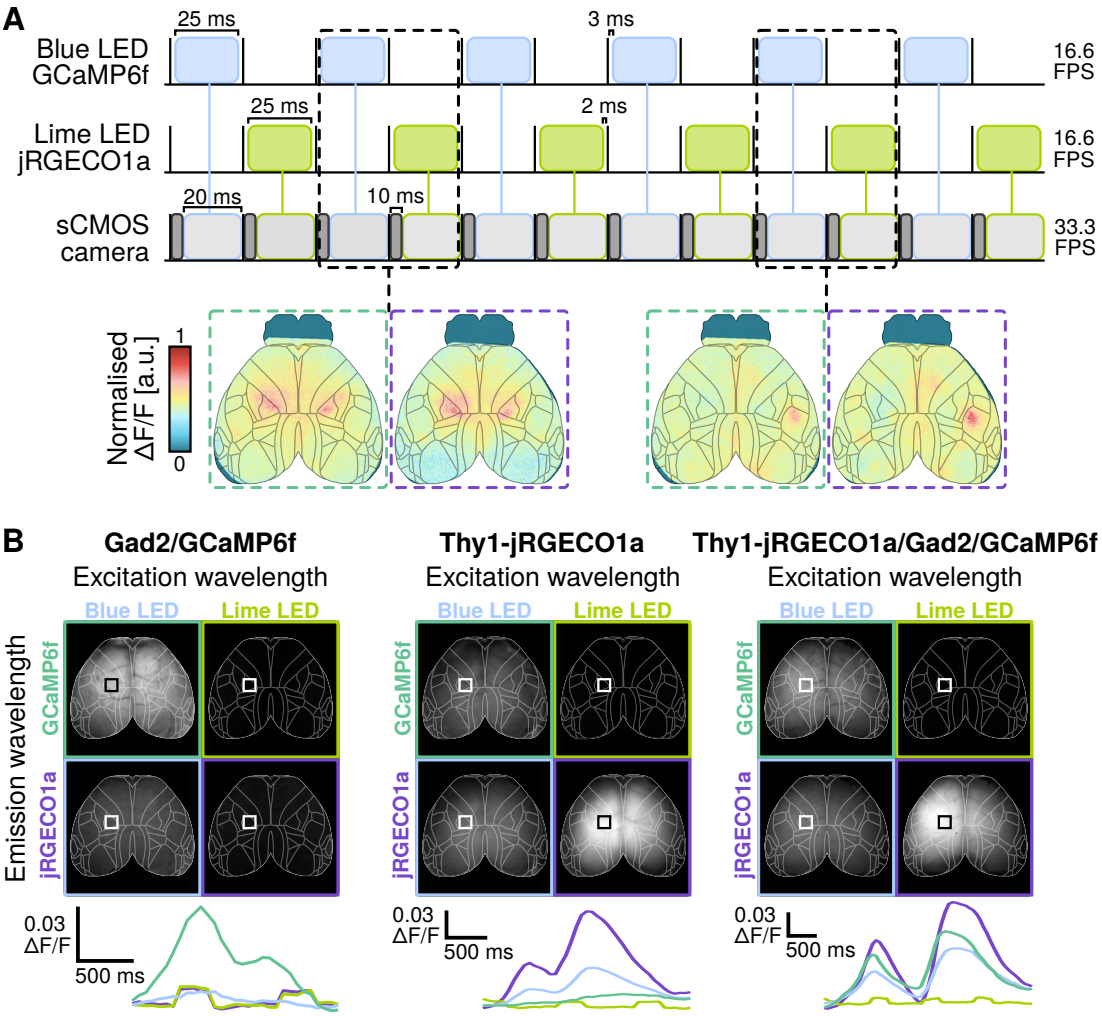


**Fig. 2.4** **Acquisition parameters for dual-colour light excitation and collection pathways. A|** Camera frame trigger and excitation light alternating sequence between the blue and line LEDs for GCaMP6f and jRGECO1a respectively. Camera is triggered at every frame at 33.3 FPS, with an exposure time of 20 ms, leaving ∼10 ms for the camera rolling shutter to open. Excitation light is restricted and centred around to the camera's exposure time period (25 ms), and alternating the 2 LEDs at 16.6 FPS. Two snapshots of the "simultaneously" imaged GCaMP6f and jRGEO1a normalised fluorescence (ΔF/F) are shown to illustrate the synchronous dynamics of the two fluorophores. The Allen Common Coordinate Framework (CCF) reference adult atlas is overlaid on top of the images. **B|** The efficacy of the excitation/emission filter combination for each transgenic animal was evaluated by assessing both emission channels, jRGECO1a and GCaMP6f, under the two excitation wavelengths. A black/white square outlines the region of interest (ROI), and its ∼2 s dynamics are displayed by the waveforms below, to assess the bleed through in the filter system. GCaMP6f channel under blue light is shown in green (GCaMP6f emission), GCaMP6f channel under lime light is shown in lime, jRGECO1a channel under blue light is shown in blue, and jRGECO1a channel under lime light is shown in purple (jRGECO1a emission).

changes that followed those observed in the signal channel (lime-jRGECO1a, purple dynamics), although with smaller amplitude due to the lower (20%) excitation efficacy (Figure 2.4, panel B, middle, green dynamics). The triple transgenic mice (Thy1-jRGECO1a/Gad2/GCaMP6f) thus resulted in a combination of the artefacts observed for the other transgenic mice (Figure 2.4, panel B, right). Therefore, alternating the illumination and image acquisition for each emission

channel allowed to separate the fluorophore detection and effectively eliminate any potential contamination across channels.

To avoid signal saturation on the sensor and allow for the detection of smaller events, the LED power was adjusted with an LED driver (LEDD1B, Thorlabs) so that the emitted fluorescence fell within the linear regime of the sensor detection range. The maximum power of the blue and lime LEDs were 27 mW and 4 mW, respectively; which was optimised to avoid excessive photobleaching during longer and/or repeated recordings. The required power depends on the brightness and expression profile of the indicator, and therefore, can vary slightly from mouse to mouse and across development. The camera trigger and the LED alternating sequence were synchronised and controlled through TTL pulses sent by a data acquisition unit (Micro1401-4 CED limited). The camera was controlled through Micromanager software (Micro-Manager 2.0), whereas the data acquisition unit was controlled through Spike2 software (CED limited). Data collection was performed in a dark, quiet room with minimal changes in ambient light or sound. Data per imaging session was written as a set of tiff stacks of 5000-12000 frames in total.

### Adaptation of the setup to neonatal imaging.

Neonatal mice have unique traits, therefore, care must be taken to customise the system to meet their requirements. Since the macroscope is too big to be portable and it's crucial to have a stable FOV while imaging, the animal needs to be physically restrained to minimise head movement. This is especially important in the z-plane (vertical axis), as it is a single plane imaging technique and so *post hoc* image correction cannot account for this type of motion artefact.

For the head fixation system, a 3D-printed headpost was custom-designed, with a shape that follows the curvature of the skull to ensure better contact and improved stability during attachment. Headposts were produced in a variety of sizes to accommodate the head growth during the first three postnatal weeks (Figure 2.5, top). The headposts can be easily printed on polylactic acid material (PLA) using commercial 3D printers to be both lightweight (<10 mg) and sturdy enough to withstand wear and tear as they age. The headpost was clamped by custom titanium holding bars that can be adjusted in height and proximity depending on the size of the animal. Despite the fact that the LEDs were collimated to ensure that the beam was narrow and centred on the dorsal surface of the brain, light could still potentially hit the animal's eyes, triggering unwanted visual responses, even with the eyelids closed (Caval-Holme et al., 2022). To prevent this from happening, a custom 3D-printed light shield cone in various sizes was designed, which could be clamped down alongside the headpost during the imaging session (Figure 2.5).

Since neonatal mice are pilothermic up until the second postnatal week (Lagerspetz, 1966), they must be kept warm when away from the dam. Therefore, a bespoke miniaturised heating

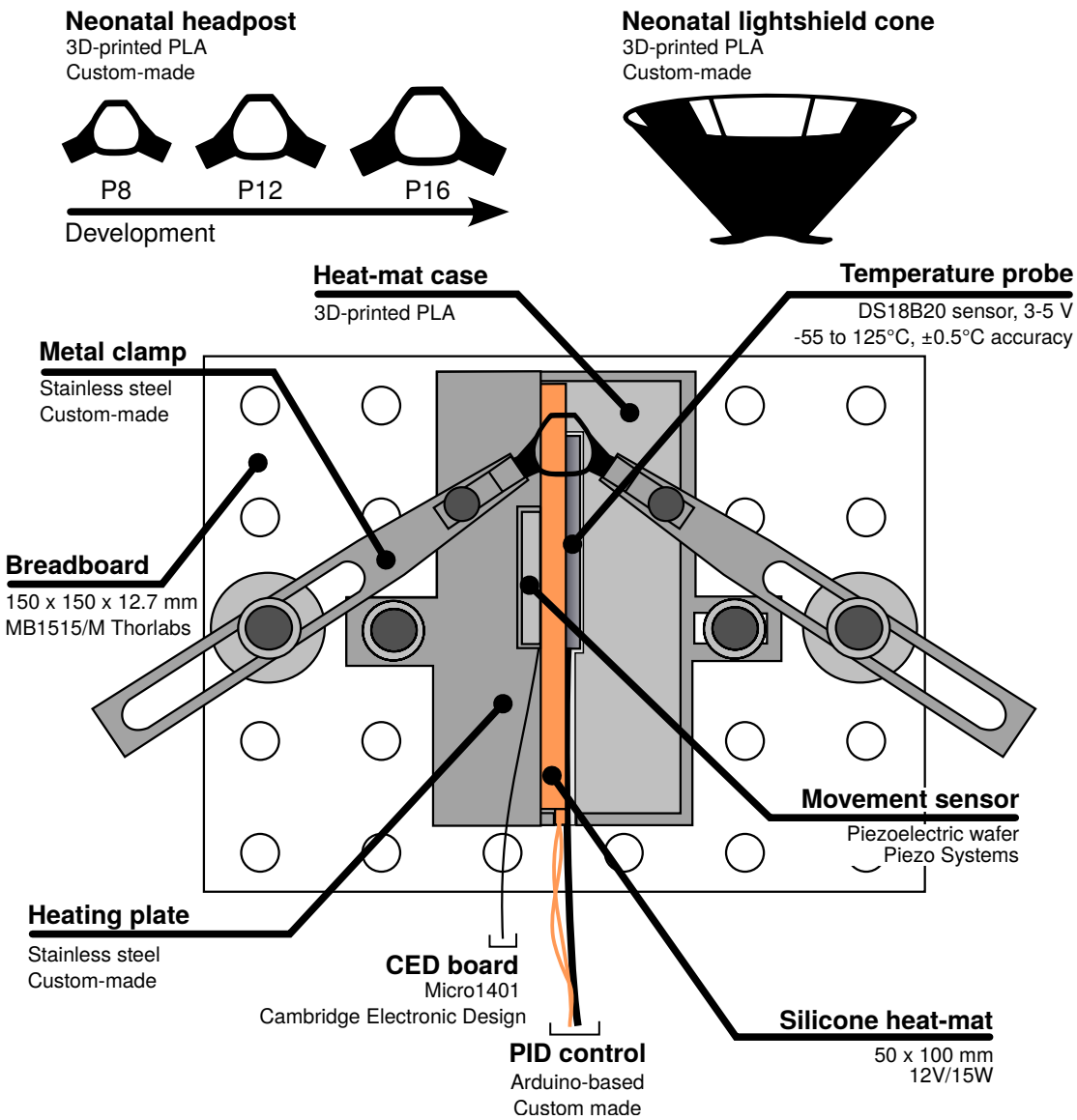


**Fig. 2.5** **Overview of the system requirements for neonatal mice head fixation.** Illustration of the setup designed to accommodate the growth of neonatal mice while ensuring their head was properly fixed and they remained warm during imaging. The entire system was portable, allowing the mice to be moved from the surgical area to the imaging setup. The custom-made components were either 3D printed or manufactured locally.

system was built using a custom PID controller to measure and regulate the temperature of a heating mat (Figure 2.5). A temperature probe (DS18B20 sensor, 3-5 V) is placed beneath the silicon heat-mat (50 x 100 mm 12V/15W), which warms up a stainless steel metal plate that is in contact with the animal's body. The heatmat is connected to an Arduino-based PID system (Arduino Uno), which allows for precise temperature control of the plate to 0.1 degrees. The PCB board and PID control code were custom designed to create a low-cost temperature control system for neonatal animals. The system takes 5 min to warm up to a stable temperature, and keeps it constant within 0.1 degrees. The Arduino PID control and the heatmat are enclosed in custom 3D moulds and attached to a portable breadboard (150 x 150 x 12.7 mm, MB1515/M Thorlabs, Thorlabs) that is used for both surgery and experiments.

A piezo wafer sensor was placed under the animal's torso and connected to the CED board to monitor the animal's body movement during the recording. This piezo records voltage deflections at 1kHz (30 times faster than the imaging frequency) that reflect the pressure on it caused by large animal movements, but is less sensitive to small movements like twitches. Electrical interference from the heatmat introduces high frequency noise and artefacts, which can be reduced by using a temporal filter to downsample the piezo sensor output to match the imaging frequency. This preserves movement-related voltage amplitude changes while reducing noise. To create a binary movement vector for the recording, a peak envelope was fitted over the downsampled movement voltage trace and manually and individually thresholded above the noise.

### 2.2.2 Surgical preparation to image through the intact skull.

Imaging cortical activity requires optical access to the cortex. Generally, the animal preparation requires a procedure for skull clearing to maintain optical clarity. Different techniques can be used, ranging from more invasive methods including removing large parts of the skull and implanting a clear window to less invasive methods such as skull thinning and chemical clearing, or sometimes nothing at all. Less invasive procedures have lower risk of tissue damage and make the surgical procedure much shorter and straight forward. Considering the thinness and transparency of the neonatal skull, it was not necessary to perform any additional procedures to create an optical window for imaging.

Mice can be surgically prepared for an acute imaging session as early as 1 day old (P1), whereas chronic implantation for longitudinal imaging is done in animals at least 6 days old (P6) (Cruz-Martin et al., 2014). The surgical protocol followed the procedures reported in Cross et al., 2021 with minimal modifications. Mice aged P6-P22 lied on a warm water recirculating blanket (37°C) and were deeply anaesthetised with isofluorane (2.3%, matched to the minimum alveolar concentration of P9-P10 pups (Loepke et al., 2006) in 100% oxygen administered through a custom nose piece (flow rate = 0.5 - 1 L/min). Local anaesthesia was applied by subcutaneous injection of (0.02 ml) 2% Xylocaine with adrenaline (10 mg/ml lidocaine, 0.02 mg/ml epinephrine, AstraZeneca), before the scalp was removed to expose the entire dorsal surface of the skull. The skull was then cleaned using cotton swabs with 70% ethanol. The periosteum was pushed to the edges of the skull, leaving a clean, exposed surface. The scalp incision was secured with Vetbond (Fisher, UK) and the custom head-post for imaging was fixed with optically clear cement (CB super bond kit - Prestige Dental UK, Bradford, UK) to the interparietal bone (over the cerebellum). This cement matches the refractive index of the skull, which has a higher refractive index, to that of the underlying tissue to improve the transparency. The whole surgical procedure took $\sim$10 minutes per pup. Pups were left to recover for 60 minutes, which was sufficient for cortical activity to recover from the anaesthesia (Cross et al., 2021). This surgical preparation allowed for optical access to most of the dorsal cortex.

For longitudinal experiments, mice were administered analgesia into the loose skin over the neck for anti-inflammatory effects at the beginning of the procedure (carprofen, 5 mg/kg - 0.01 mg / 2 g pup, Zoetis). Surgery for chronic experiments was carried out in batches, with all pups but one within a litter being implanted with the headpost, keeping the not implanted one as a littermate control. Litter sizes were limited to a maximum of 6 pups to avoid competition for food. Following a recovery period of at least 1.5 hours, all pups were returned to their home cage, and the behaviour of the dam towards them was closely monitored for the next 2 hours. The dam was gently pushed away if she showed any signs of aggression towards the pups. Dams have a tendency to overgroom and cannibalise pups with head implants, since they can carry strong scents (e.g. cement, glue). To minimise the incidence of cannibalism by the dam, it is important to ensure that pups have recovered completely from the anaesthesia and the dam's snout was dabbed with a cotton swab soaked with glue and ethanol periodically before and after the pup's surgery. Additionally, pups were rubbed with the cage bedding, ideally with the dam's urine on it, before returning them to the cage. Dams rarely showed any signs of cannibalism or rejection; however, they occasionally tried to remove the headpost, resulting in injury to the pups, with one of them out of all the experimental mice being unable to survive (1 out of 27, 3.7%).

### 2.2.3 Data preprocessing pipeline.

Widefield calcium imaging is a high-throughput technique that produces very large files (> 10 GB), therefore, it is necessary to preprocess the data in order to efficiently handle it during subsequent analysis. The following preprocessing pipeline was common to all analysis. The image tiff stacks consisted of a set of continuously collected images at 33.3 FPS, interleaving blue (GABAergic population) and lime (pyramidal population) excitation, for a maximum of 6 minutes per recording (Figure 2.6, top left). The image resolution was 960 by 540 pixels (13 by 13 $\mu$m per pixel), after performing 2 by 2 digital binning through the camera software to increase the SNR and reduce the size of the file. The total amount of recorded data per animal was at least 15 min, with 10 min of rest between each recording segment. Image stacks were first split into the GABAergic (GCaMP6f channel) and pyramidal (jRGECO1a channel) frames (Figure 2.6, step 1), rendering an effective imaging rate of 16.6 FPS, and manually square cropped to the brain size in the FOV to remove unwanted empty pixels. When imaging the single and double transgenic animals, Thy1-jRGECO1a and Gad2/GCaMP6f respectively, the LEDs were not interleaved. Therefore, the recording was decimated to 16.6 FPS by removing every other frame, to best match the effective frame rate of the triple transgenic recordings.

Once the data were separated into the different channels, motion artefacts of the skull in relation to the objective were corrected (Figure 2.6, step 2). These artefacts were corrected for each channel independently by aligning each frame to the reference image, the median frame across the recording. The motion correction algorithm was based on the NoRMCorre algorithm (Pnevmatikakis et al., 2017), using the rigid implementation. In short, motion correction was performed using a discrete Fourier transform subpixel registration approach. This approach

calculates the upsampled cross correlation between the image to be registered and the reference image in the frequency domain. It identifies the peak of the cross correlation and uses it to perform a rigid body registration that takes into account both translation and rotation artefacts (Guizar-Sicairos et al., 2008; Pnevmatikakis et al., 2017). Given that each fluorophore's fluorescence was acquired in each half of the camera sensor, both images had to be co-registered to make sure they were in the same space and perfectly overlapping (Figure 2.6, step 3). The use of the opto-split allowed an adjustable spatial separation of both channels, which ensured excellent registration results. Nonetheless, a time-averaged reference image from each of the channels was spatially filtered using a median filter of large radius (1/3 of the reference image size) and subtracted from the reference image to reveal the superficial vasculature. The jRGECO1a channel was registered to the GCaMP6f channel using this exposed vasculature pattern, which was identical in both channels. The registration parameters were estimated using an intensity-based technique and then applied to a geometric transformation. The accuracy of the registration was assessed through visual examination of the superimposed channels after registration. Each channel from the first recording of the session was used as the reference for further registration of all recordings from the same animal during a session.

Once the two channels are co-registered, both datasets were baselined by computing the relative fluorescence changes ($\Delta F/F$) for each pixel (Figure 2.6, step 4). It is critical to baseline the data in order to reveal small changes in fluorescence during the recording. The $\Delta F/F$ was computed by subtracting and dividing each frame by the baseline frame fluorescence, which was the pixel by pixel average of all frames in the recording. Given that neuronal dynamics are decoupled from hemodynamic signals in neonatal mice (Kozberg et al., 2016), hemodynamic correction of the GCaMP6f dynamics is generally unnecessary. Furthermore, it has been shown that the use of bright calcium indicators on densely labelled populations results in a strong enough neuronal signal that it is not confounded with non-neural signals (Vanni et al., 2014; Xiao et al., 2017; Valley et al., 2020). While jRGECO1a is a relatively new calcium indicator and has not been extensively used in widefield imaging studies (Saxena et al., 2020), it is worth noting that red light is less scattered and less absorbed by brain tissue compared to shorter wavelengths. Additionally, the vasculature provides little contrast when viewed through red filters (Dana et al., 2018). This suggests that hemodynamic artefacts may be minimal for the jRGECO1a channel, and neuronal signals may not be affected by them. Therefore, it could be argued that hemodynamic correction is not necessary for either of the channels.

The next step in the pipeline was to denoise and compress the data to further improve the SNR by isolating the neural signal from background fluorescence and artefacts, and to reduce the data dimensionality to a manageable size (Figure 2.6, step 5). The physiological signals are buried in this high-dimensional dataset containing $>2\text{x}10^5$ pixels and $\sim 10^4$ time frames. The factorisation of the recordings into its constituent spatial and temporal components (of reduced size) was critical for the computational efficiency of downstream analyses, since they could be performed on the spatial and temporal components instead of individual pixels. A recently

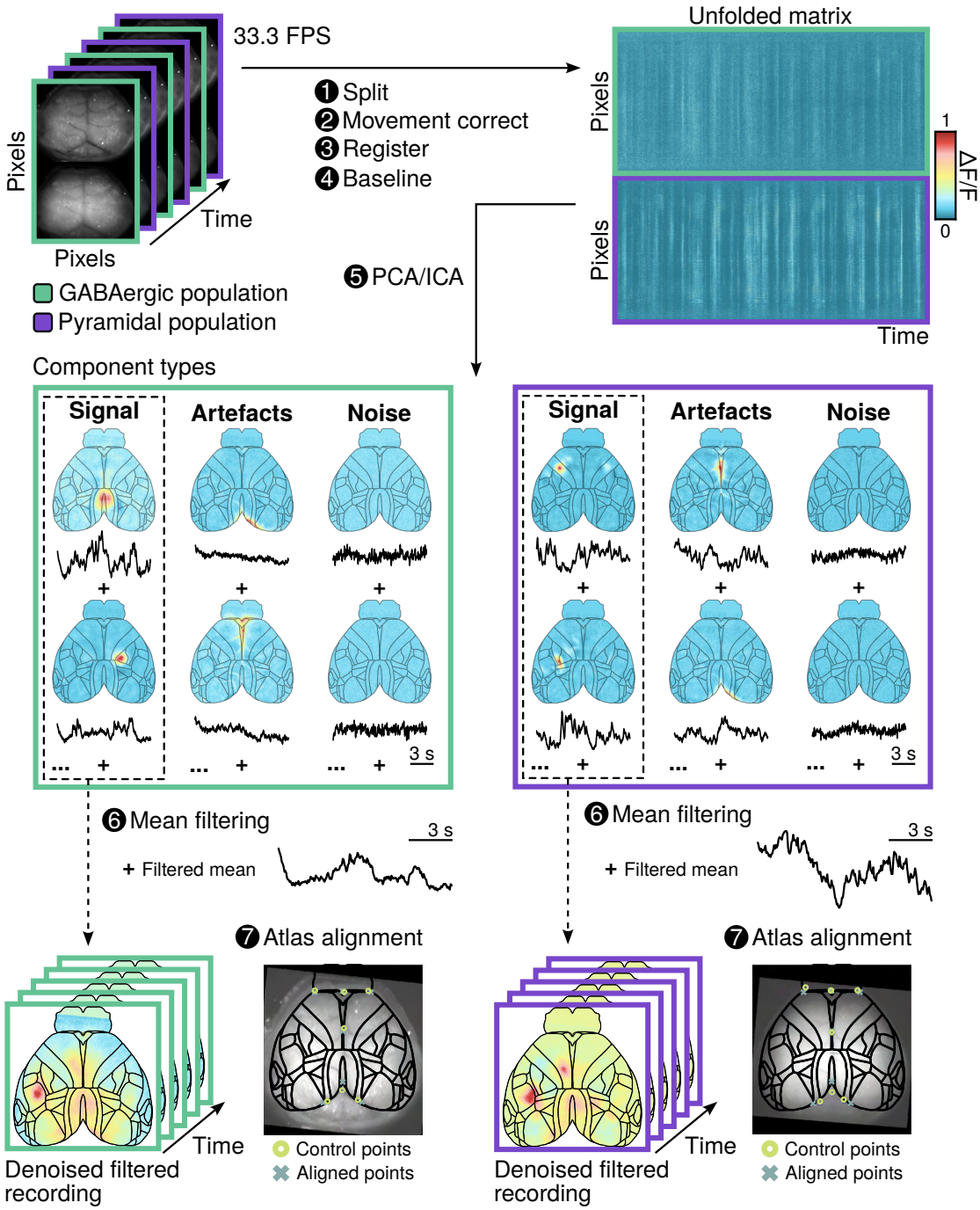


Fig. 2.6 **Diagram of the data processing pipeline.** Following data acquisition shown in Figure 2.4, all data from each session was preprocessed following the workflow outlined above (steps 1-7).

developed data-driven method allowed for the isolation of signals and artefacts from calcium activity patterns and the segmentation of these into independent functional units (Weiser et al., 2021). The baselined image series ($\Delta F/F$) was masked to capture just the cortex, and spatially flattened (pixels by time) to form a 2D representation of the recording (Figure 2.6). A spatial Independent Components Analysis (sICA) decomposition was performed on the flattened data to produce a series of spatial components (sources), and temporal weights (mixing matrix), that together represented the influence of each fluorescence source on each frame in the recording.

The sICA relies on the assumption that the signals of interest are spatially independent of one another and sparse (spatial skewness), i.e. each spatial motif is confined in a relatively small portion of the frame with a skewed intensity distribution. No assumptions are made on how the sources are temporally mixed, but requires these underlying source signals to be non-Gaussian (Hyvärinen et al., 2000). Prior to running sICA, the global mean, which represents the average activity level across the entire FOV, was subtracted from the baselined recording. The global mean includes synchronised or coordinated activity occurring across most brain regions, and therefore, by subtracting it from the recording, the focus shifts to local and relative changes in activity. This enables the detection of fine-scale activity patterns and reduces the impact of global fluctuations, enhancing the effectiveness of subsequent PCA/sICA analysis. This approach prioritises the identification of smaller and more local spatial motifs of activity, while the temporal information of these motifs can provide insights into the sequential activation of different patterns across the entire cortex, enabling the study of coordinated activity across the cortex. While the global mean is subtracted initially, it can be reintroduced later to incorporate the information about brain-wide changes in dynamics.

sICA was performed using the fast ICA algorithm (Hyvärinen et al., 2000), which finds a predefined number of independent components. If this predefined number of components underestimates the diversity of activity motifs, then information would be lost. However, requesting the full number of components, which is equal to the total number of pixels, would be extremely time-consuming and biologically implausible, as not every pixel is expected to be spatially independent from each other. Therefore, in order to determine the optimal number of components needed for sICA, the data was first run through singular value decomposition (SVD). The matrix of singular values was used to find the threshold between SVD signal and noise floor by calculating the integral of the eigenvalue 'influence' per component, fitting a second degree polynomial to this curve, which finds the point at which the integrated eigenvalues first overshoot the polynomial fit. As such, the target sICA motif number was predefined by multiplying this inflection point (noise cut-off value) by 3, in order to allow enough dimensions for the sICA that ensured no signal was lost while keeping the number low enough (Weiser et al., 2021). It is important to highlight that, in the case of insufficient sample size for the number of sources to recover (e.g. not enough pixels for the number of components), the sICA will produce overfitted estimates of source signals that will show a single spike or bump shape (Särelä et al., 2003; Deng et al., 2012). These artefacts result from the non-gaussianity and sparsity assumption, since, in the space of the source signal with unit variance, the non-gaussianity and sparsity constraints are usually maximised by spike or bump signals (Särelä et al., 2003). This highlights the importance of having an appropriate number of samples to accurately estimate the underlying sources. To decompose data with a large number of sources ($\sim$100 or more), it is advisable to use a number of samples at least 20 or more times the number of sources squared (Makeig et al., 2011), e.g. the theoretical number of pixels necessary to separate 100 sICA sources is 200,000 pixels. As the approximate number of pixels per recording was close

to this lower bound, no additional spatial downsampling was performed on the recordings prior to sICA factorisation.

Thus, the fast ICA algorithm was used on the full dataset with the SVD decomposition as a first guess for the sources mixing matrix, using a squared non-linearity and estimating all the independent components in parallel. Fast ICA uses an initial principal component analysis (PCA) decomposition to reduce the data's dimensionality, and whitening of the variance corresponding to the PCA components (variance becomes equal to 1 and its covariance matrix becomes the identity matrix), which eliminates correlations between the different pixels, normalises the scale of different features in the data and reduces the impact of noise on subsequent analyses. It then uses sICA to find a rotation in this PCA space that identifies the directions of largest non-gaussianity and maximal independence to find the drivers or sources of the information. As mentioned, sICA is rooted in the assumption of statistical independence, thus aiming to minimise the mutual information between the components and maximising the non-gaussianity of the source signals. Practically, this approach maximally separates the independent spatial activity patterns which can be combined with their temporal weights to reconstruct the entire recording of cortical dynamics. The benefit of this decomposition was the extraction of a practical number of spatiotemporal activity patterns, which were an optimal representation of the original high-dimensional recording, and could be easily included in subsequent analyses.

The resulting independent components obtained from the sICA can be categorised into three main groups based on their spatiotemporal characteristics: neural components, artefact components, and noise components (see Figure 2.6, middle panel). The neural components typically exhibit localised activity in specific regions of the cortical tissue, known as spatial motifs or cortical domains. In some cases, signal components may encompass multiple activity motifs, for which the activation patterns are similar enough (co-activation of cortical areas) to be identified as a single neural component. Artefact components could take many forms, including the vasculature, movement artefacts, optical surface artefacts, etc. As seen in the artefacts pool of motifs for each of the cell populations (Figure 2.6, step 5, middle panels), these motifs likely included a representation of hemodynamics or blood volume movement artefacts from the superior sagittal and transverse sinus veins, as well as the middle cerebral artery (Figure 2.6, step 5, artefact examples). The signal and artefact components per recording were visually inspected and manually separated into each category using their spatial and temporal properties. On the contrary, noise components lack a spatial domain, and have little to no temporal structure. Therefore, it is possible to sort out these different components by assessing their lag-1 autocorrelation values (Figure 2.7, panel A, left). Noise motifs, due to their absence of temporal structure, showed very low lag-1 autocorrelation values, whereas structured activity coming from calcium dynamics, as well as that coming from recording artefacts, presented higher values. Therefore, a noise cutoff was defined by determining the minima between the variance sorted lag-1 autocorrelation distribution using a two-peaked Kernel Density Estimation (KDE) fit (Figure 2.7, panel a, middle). The number of noise components obtained for a decom-

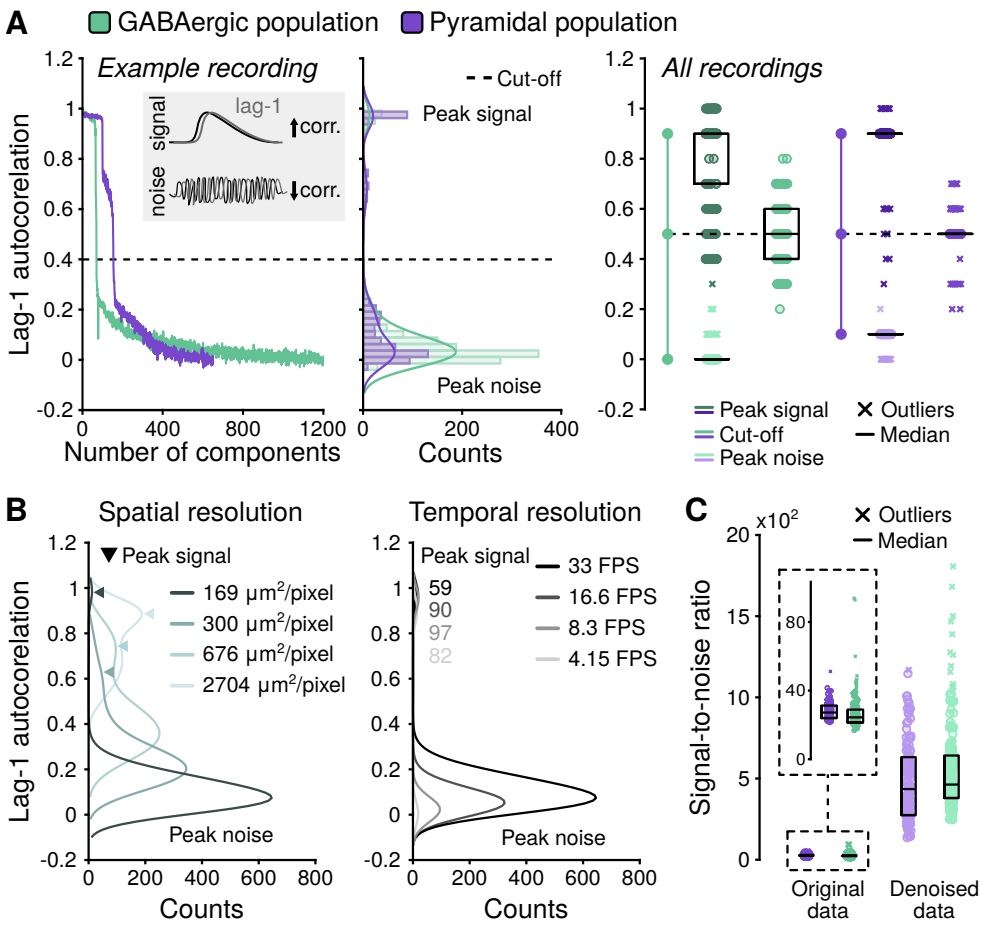


**Fig. 2.7** **sICA noise sorting and resolution analysis. A|** Example of the separation of noise components from signal by lag-1 autocorrelation. Schematic depicts the high lag-1 autocorrelation of signal (non-noise) components which correspond to waves of structured activity, compared to noise components, which have a low lag-1 autocorrelation. A two-peak kernel density estimator (KDE) was fit to the histogram of lag-1 autocorrelation for each neuronal population, obtaining two major peaks, signal and noise peaks, and the minima between them, defined as the noise cutoff. To the right, the locations of these peaks and the cutoff values are shown for all recordings for each of the populations. The black dashed line depicts the average cutoff value. **B|** Changes in the spatial and temporal resolution of an example recording for the GCaMP6f channel. The spatial resolution was sequentially reduced from the maximum (169 $um^2$/pixel) by bilinear interpolation. The temporal resolution was modified by decimation of the original frame rate (33 FPS). The number of signal motifs obtained for the 4 different temporal resolutions were shown next to the signal peak. **C|** The SNR is calculated for the original data and the denoised data, composed only by the signal components after sICA, for each of the neuronal populations. Box plots display the first quartile, median, and third quartile. Outliers are shown as crosses.

position needed to conform at least 25% of all components returned by the sICA to ensure signal components were sufficiently unmixed. If not enough noise components were returned after the sICA decomposition, the algorithm was re-run with a higher number of components (higher SVD cutoff) (Weiser et al., 2021). The locations of the KDE fit peaks varied slightly across recordings, being slightly less variable for the pyramidal cell population recordings (Figure 2.7, panel A, right). However, in both cases, the non-noise peaks (signal and artefacts) were centred at high autocorrelation values (∼0.9) for both populations, whereas the noise peaks were centred at low values (0-0.1) (Figure 2.7, panel A, right, barbell plots). In both cell populations, the noise

cut-off averaged to 0.5, indicating a high degree of separation between the peaks (Figure 2.7, panel A, right). This suggested that the signal sources and noise were successfully separated and distinguished for all recordings.

Identification of ICA components has been shown to be dependent on the spatiotemporal resolution of the recording (Weiser et al., 2021). Therefore, the effect of the recording resolution on the lag-1 autocorrelation distribution peak separation was explored to identify the best spatial and temporal parameters to use for the sICA decomposition. The spatial resolution of the images was gradually diminished through bilinear interpolation, which resulted in a consistent reduction in the separation between peaks. Already at a resolution of 300 $\mu m$/pixel, the signal peak merged with the noise one, with the lag-1 autocorrelation values of each component group becoming less distinguishable (Figure 2.7, panel B, left). This observation indicates that a reduction of spatial resolution by a factor of 2 leads to a suboptimal separation of the signal and noise sources. This is likely due to the fact that the number of pixels in the recording is already at a minimum required for proper sICA compression. Further reduction in spatial resolution led to the merging of both peaks, suggesting that there are not enough components (pixels) available for separating the sICA sources effectively (Figure 2.7, panel B). Thus, as sICA is very sensitive to the sample size to achieve accurate source unmixing (Särelä et al., 2003; Deng et al., 2012), the spatial resolution of the recordings was maintained at its maximum (169 $\mu$m/pixel) for optimal sICA decomposition. On the other hand, the modification of the sampling rate (temporal resolution) of the recordings had minimal effect on the peak separation (Figure 2.7, panel B, right). If anything, there was a slight increase in the peak separation at 16.6 FPS, which is the effective frame rate for the dual-colour recordings. Moreover, the number of signal motifs found was notably smaller for the highest temporal resolution compared to the rest (Figure 2.7, panel B, right). Previous studies have shown that sampling rates higher than 10 Hz had little effect on this phenomenon (Weiser et al., 2021) due to maximisation of the indicators' kinetics (Vanni et al., 2017).

To assess the effect of the sICA compression and unmixing on the image data, the SNR was calculated before and after the data was decomposed into neuronal signal components, removing the artefacts and noise. In widefield imaging systems, the sources of noise can be varied, from signal-dependent to signal-independent photon shot noise and read noise. Shot noise is random variation in the number of detected photons by each pixel on the camera sensor, and can be reduced by increasing light exposure or using post-processing techniques like image binning and denoising, which are implemented in the preprocessing pipeline. Read noise or thermal noise, caused by electronic components and circuitry, introduces a constant signal offset unrelated to light intensity. However, in sCMOS cameras, read noise is often negligible due to their high-performance sensor architectures (Kauvar et al., 2020), particularly when the signal of interest is relatively strong or when long exposure times are employed. In general, independent noise arises from background fluorescence at each pixel, which may consist of tissue autofluorescence and nonspecific neuropil fluorescence. The mean value and

variance of this noise are typically independent of the ongoing dynamics. Hence, to estimate the background noise, the median fluorescence of the difference between successive frames was computed. This approach is adopted because the dynamics between consecutive frames are expected to be highly similar, and the median value is resistant to outlier intensity values (Homma et al., 2009; Rupprecht et al., 2021). An average 12.5-fold increase in the SNR of the recordings for both cell populations was observed after sICA processing (Figure 2.7, panel D).

Image timeseries can be reconstructed using any combination of the identified sICA components. For all reconstructions, the mean signal, which was removed prior to sICA, was added back and filtered by a 0.1 Hz zero-phase, second-order Butterworth temporal high-pass filter (Figure 2.6, lower panel), to correct for any slow drift in the imaging data (Musall et al., 2023). A filtered video can be reconstructed excluding all artefact and noise components, leaving only the denoised neural signal (Figure 2.8, panel A, denoised signal). To assess the accuracy of the decomposition, a visual inspection of spatial topography of each component group was performed. This helped to determine if the decomposition effectively captured meaningful patterns from the original data, while making sure the artefacts and noise components did not show any neural-like patterns. In addition, the correlation between the recording reconstruction of each component group, as well as the global mean signal, and the original signal was calculated to quantify how much information was retained from the original recording. A higher correlation value indicated a stronger fidelity to the original data. The global mean signal and the denoised recording exhibited higher correlations with the original data compared to the artefacts and noise recordings, for both populations (Figure 2.8, panel B). Particularly, the global mean signal showed the highest average correlation compared to the other groups, emphasising the influence of global events and artefacts, such as slow fluctuations and bleaching, in the widefield calcium imaging signal. The denoised recording showed a significantly higher correlation than the artefacts (GABAergic $p = 0.6610e\text{-}24$; pyramidal $p = 2.390e\text{-}11$) and noise (GABAergic $p = 0.0043e\text{-}24$: pyramidal $p = 2.390e\text{-}11$), which suggested that the signal components effectively captured the ongoing dynamics without being obscured by unwanted artefacts or noise sources. Interestingly, the artefacts and noise recordings exhibited a small correlation with the original signal, with only the artefact components of the GABAergic population displaying a significantly higher correlation compared to the noise components ($p = 0.0049e\text{-}24$). This discrepancy may be attributed to the higher amount of blood-induced movement artefacts in the GCaMP6f channel (see section 2.3.2 for further details). These results confirmed that the sICA decomposition can successfully separate meaningful patterns in the data, while keeping an accurate representation of the original data.

As briefly mentioned in section 2.2.1, fluorescent indicators are susceptible to photobleaching, which causes a gradual loss of signal over time due to prolonged or repeated exposure to high-intensity illumination (Waters, 2007; Patterson et al., 2000). This can introduce spurious correlations in the data by reducing the apparent variability of the signals, resulting in increased

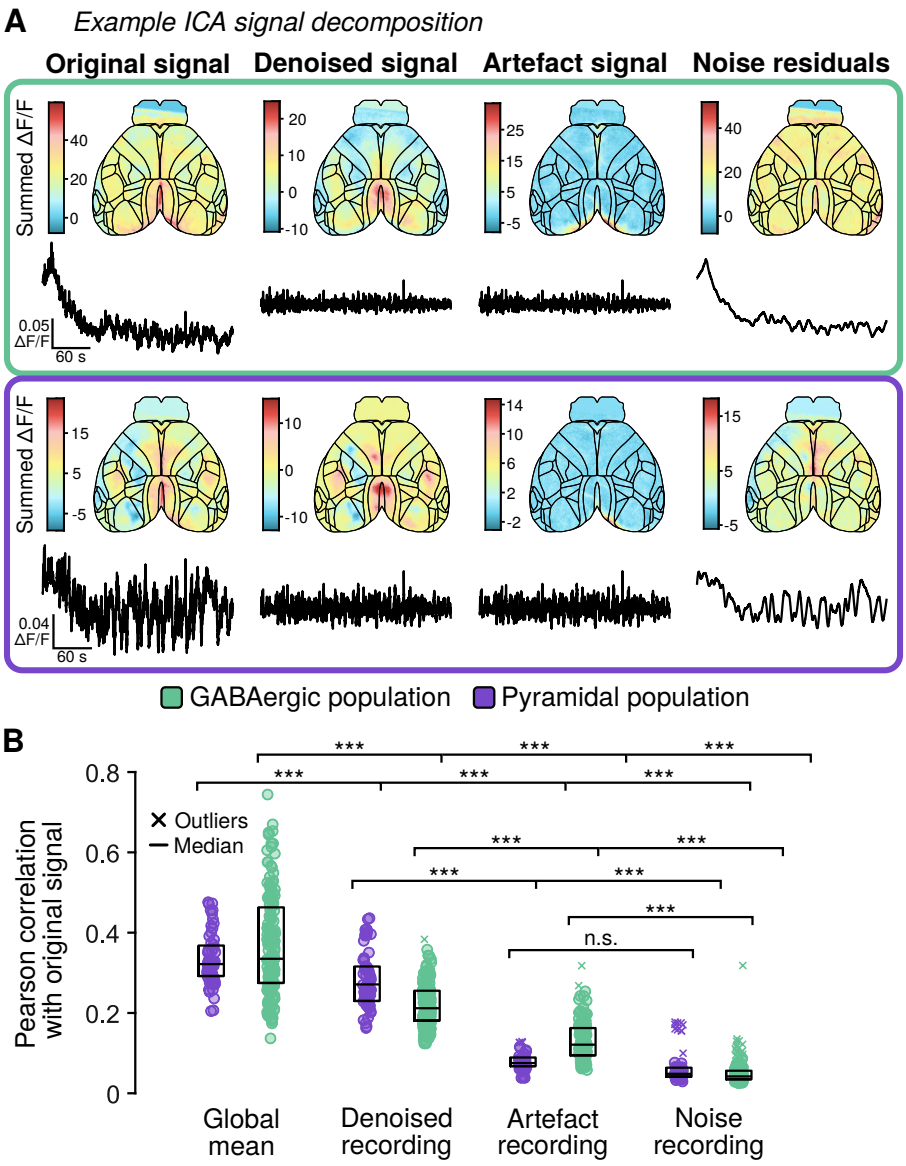


**Fig. 2.8 Comparison of spatial and temporal information content through sICA compression and filtering A|** The signal information is visualised by summing the $\Delta F/F$ values across all frames in a given recording and projecting them spatially (top) and temporally (bottom) for each neuronal population for one example recording. The original signal represents the data prior to sICA decomposition. The denoised and artefact signals correspond to the reconstructed recordings using only the signal or artefact sICA components, respectively. The noise residuals are obtained by calculating the difference between the original signal and the reconstructed recording using both the signal and artefact sICA components. **B|** The correlation between the original signal and the different recording reconstructions, as well as the global mean signal, is significantly different across groups for the GABAergic (Mean-Denoised p = 0.0057e-24; Mean-Artefact p = 0.0021e-24; Mean-Noise p = 0.0008e-24; Denoised-Artefact p = 0.6610e-24; Denoised-Noise p = 0.0043e-24; Artefact-Noise p = 0.0049e-24) population, and significant for all but the artefact-noise comparison for the pyramidal (Mean-Denoised p = 5.830e-07; Mean-Artefact p = 2.390e-11; Mean-Noise p = 2.390e-11; Denoised-Artefact p = 2.390e-11; Denoised-Noise p = 2.390e-11; Artefact-Noise p = 0.0644) population. First, a Friedman test for non-normally distributed paired data revealed significant differences among the four groups for the GABAergic ($\chi^2$ = 445.181 p = 3.609e-96) and pyramidal ($\chi^2$ = 153.325, p = 5.0508e-33) populations. Second, post-hoc Bonferroni-corrected Wilcoxon matched pairs signed ranks tests were performed to identify specific group differences for each population, significance level alpha = 0.0083 (0.05/6) for multiple comparisons. Significance is shown as *** for p < 0.001.

autocorrelation (Nolan, 2018). Moreover, weaker "bleached" signals may fail to capture true fluctuations in calcium dynamics. Additionally, photobleaching can introduce spatial correlations unrelated to underlying dynamics due to uneven fluorescence illumination across the sample, leading to asymmetrical decline in fluorescence. To address this issue, the fluorescence is often corrected using exponential fitting detrending (Patterson et al., 2000). However, this correction process can also introduce artefacts if there is a slow signal drift, resulting in overcorrection and introduction of more spurious correlations (Nolan, 2018).

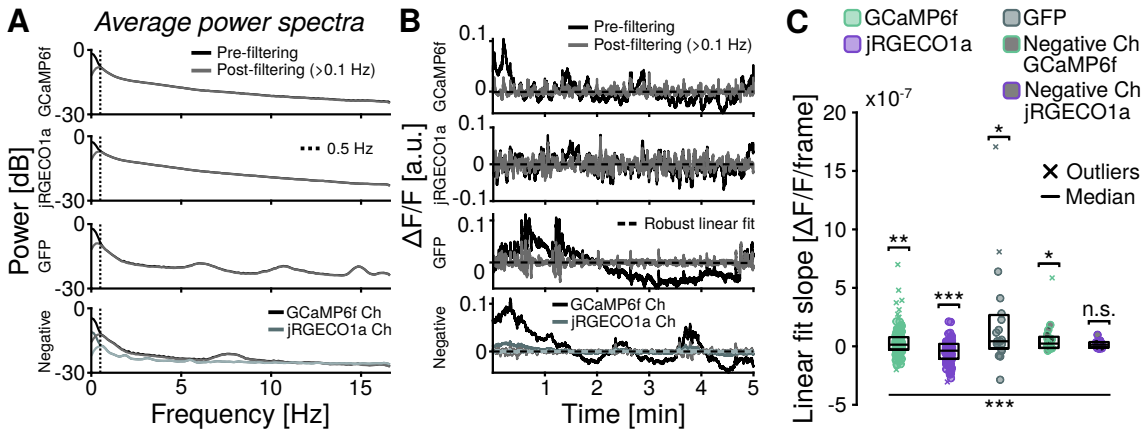


**Fig. 2.9** **Photobleaching and temporal filtering of fluorescent signals. A|** The average power spectra for each signal was calculated for the range of all possible frequencies (0-16.6 Hz). The recorded signals come from GCaMP6f (GCaMP6f channel), jREGCO1a (jREGCO1a channel) and GFP (GCaMP6f channel) fluorescence, as well as non-fluorophore-expressing (negative) signal (GCaMP6f and jREGCO1a channels). Dashed line indicates 0.5 Hz frequency. **B|** Example global mean of a 5 minute recording is shown before (dark) and after (light) filtering for each recorded signal. Dashed line indicates a robust linear fit to the filtered signal. **C|** The slope of the robust linear fit was used to quantify the rate of fluorescence change over time ($\Delta F/F$/frame). First, a Kruskal-Wallis test for non-normally distributed data revealed significant differences among the five groups ($H$ = 40.236, p = 3.868e-08). Second, post-hoc Wilcoxon signed rank tests for zero median were performed to identify specific group differences. Significant differences were observed for GCaMP6f ($Z$ = 3.149, p = 0.0016), jRGECO1a ($Z$ = -4.376, p = 1.207e-05), GFP ($Z$ = 2.093, p = 0.0364) and negative GCaMP6f channel ($Z$ = 2.017, p = 0.0437); and non significant differences the negative jRGECO1a channel ($Z$ = 1.913, p = 0.0557). Box plots display the first quartile, median, and third quartile. Outliers are shown as crosses. Significance is shown as * for p < 0.05, ** for p < 0.01, and *** for p < 0.001.

The frequency content and relative strength of fluorescence signals from different transgenic mice were analysed by calculating their average power spectra, with the aim of filtering out slow (<0.1 Hz) and continuous drift unrelated to neural activity. The global mean signals for GCaMP6f, jRGECO1a, GFP (see section 2.3.2 for context) were analysed, as well as a negative signal from non-fluorophore-expressing mice (Figure 2.9, panel A). High power was observed at slow frequencies, below 0.5 Hz, for all signals. In addition, other power peaks at higher frequencies were observed for the GFP and negative average signals, potentially due to predominance of respiration and heart rate artefacts. These peaks were not present in the GCaMP6f and jRGECO1a signals, which displayed smoother exponential decay of power with frequency (Figure 2.9, panel A). The slow frequency power band was reduced after filtering (high-pass filtered >0.1 Hz), removing slow temporal fluctuations in the signals, without affecting faster transients (Figure 2.9, panel B). A robust linear fit, which is less sensitive to outliers, was

performed on the filtered global average for each signal to determine the amount of bleaching, with the slope of the linear fit used to quantify the rate of fluorescence change over time. Although the linear fit slopes were significantly different between the signals ($p = 3.868e-08$) and significantly different from zero for the GCaMP6f ($p = 0.0016$), jRGECO1a ($p = 1.207e-05$), GFP ($p = 0.0364$), and negative in GCaMP6f channel signals ($p = 0.0437$), the rate of change was negligible, at 1 in 10 million frames (0.00001%) (Figure 2.9, panel C). Since photobleaching tends to occur at a low frequency, and high-pass filtering can effectively attenuate these signals and remove slow drift that can be caused not only by hemodynamics or motion artefacts but also by photobleaching. Previous studies have shown that the bleaching rate for one-photon excitation increases exponentially with power (Patterson et al., 2000), with light powers of >50 mW inducing photobleaching within 5-10 minutes of imaging (Couto et al., 2021). Although the required light power could vary across animals, the highest LED power (blue LED) never exceeded 30 mW, well below the 50 mW threshold.

The last step of the preprocessing pipeline was to align all the recordings into the same anatomical space using the Allen CFF as a reference atlas (Wang et al., 2020). This registration process facilitated the comparison of sICA activity patterns across different animals and sessions, and enabled the assignment of anatomical labels to these patterns (Saxena et al., 2020). However, given that the developing brain is not just an immature version of the adult brain, standardised mapping of brain regions may be difficult for brains at different developmental ages. This may result in imperfect atlas alignment. Thus, the alignment was only used as a reference for interpreting the location of spatial motifs obtained from sICA, rather than being used to establish a definitive association between neural activity and specific cortical regions.

All preprocessing of the recordings at full spatial resolution and duration (~6 min, 16.6 FPS) were run on a 24 CPU node of a computing cluster (Advanced Computing Research Centre, University of Bristol) having 100 GB of RAM per node. After sICA processing, most analysis were performed on local computers having 48 GB of RAM.

## 2.3 Results and validations.

### 2.3.1 Sources of widefield fluorescence.

Widefield calcium imaging, as previously mentioned, is a single focal plane technique with large spatial coverage but low spatial resolution. As such, fluorescence observed in each image pixel will likely have originated from thousands of nearby neurons from multiple cortical layers, making it challenging to assign the signal to a particular cellular or laminar population (Allen et al., 2017). This phenomenon is primarily due to photon scattering through the tissue and skull, which has a strong influence on both the collection and illumination pathways, and affects the lateral resolution of the superficial fluorescence (Silasi et al., 2016; Waters, 2020). As a

result, one of the most pressing unanswered questions when using this technique is determining what are the primary sources of widefield fluorescence collected on the dorsal cortical surface, whether they are dominated by somatic, neuropil, or passing-by axonal activity, and from what depth and volume of the cortex they originated from.

In a recent study (Waters, 2020), a Monte Carlo random-walk model was employed to simulate the propagation and scattering of photons through brain tissue (grey matter) to infer the primary sources of widefield fluorescence in various GCaMP mouse lines. The study revealed that tissue scattering influences both the illumination pathway, leading to an intensity bias around L2/3, approximately 300-400 $\mu m$ below the pia; and the fluorescence collection pathway by making sources deep within the cortex extend across a diameter of 3-4 mm at the brain's surface. As a result, the fluorescence observed at the brain surface represents a weighted average of multiple neurons and cortical layers.

Using this model, the simulations were extended to include red-shifted indicators in addition to the GFP-based ones to accommodate for the dual-colour imaging, given that absorption and light scattering by the tissue is wavelength-dependent. In brief, the Monte Carlo random-walk model is implemented in Python and simulates packets of photons moving stochastically through a spatially homogeneous 3-dimensional volume, while being subjected to absorption and scattering by tissue (for details see Waters, 2020). The model uses absorption and scattering coefficients and anisotropy parameters measured from human grey matter and skull from previous studies (Johansson, 2010; Ugryumova et al., 2004). The simulations were performed using the macroscope objective lens specifications employed in the project (Table 2.2), to evaluate the collection efficiency of the setup. This allowed them to theoretically compare how the widefield fluorescence sources from each of the fluorophores may differ when observed superficially due to their differences in absorption and scattering properties (Table 2.2, Johansson, 2010; Ugryumova et al., 2004). This is particularly important during early postnatal development given the changes in cell distribution across cortical layers as a result of ongoing neuronal migration (Marín et al., 2001), and potential differences in developmental expression of the promoters used to drive the fluorescence (Taniguchi et al., 2011; Porrero et al., 2010). Two major questions were investigated: How much does each cortical layer contribute to the total fluorescence observed from different cell populations? And, is this contribution affected by changes in the distribution of the cell populations across cortical layers during early development?

As the two promoters, Thy1 and Gad2, in the triple transgenic line used for this project label cells that span the entire cortical depth, excitation photons from the illumination source will need to travel varying distances to be absorbed by the fluorophore at different cortical layers. Consequently, emitted photons will need to propagate back to the pial surface, randomly through the tissue, to be detected, which will cause varying degrees of lateral scattering. This phenomenon results in differences in the intensity of illumination arriving at the sources located

**Tab. 2.2 Widefield macroscope specifications and optical parameters of grey matter at different wavelengths used for the simulations.**

| Numerical aperture | Effective focal length | Working distance | Magnification | Field number | Focal depth |
|---|---|---|---|---|---|
| 0.35 | 50 mm | 40 mm | 1 X | 35.7 mm | 0 mm |

| | GCaMP6f excitation 480 nm | GCaMP6f emission 520 nm | jRGECO1a excitation 575 nm | jRGECO1a emission 600 nm |
|---|---|---|---|---|
| Absorption coefficient | 0.37 | 0.32 | 0.2 | 0.09 |
| Scattering coefficient | 11 | 10.5 | 9.8 | 9.5 |

*units* $mm^{-1}$

at different cortical depths and the diameter of the sources observed at the brain surface (Figure 2.10, panel A). In order to consider the spread of excitation photons into the brain tissue, two incoherent illumination sources focused onto the brain surface were simulated, using 480 nm and 565 nm excitation wavelength for the GCaMP6f and jRGECO1a indicators, respectively. The fluorescence intensity was estimated as a function of cortical depth, observing a gradual decline in illumination intensity for both fluorophores due to absorption and tissue scattering (Figure 2.10, panel B). In the absence of skull, an initial increase in intensity was observed over the first $\sim$250 $\mu m$ for both indicators, producing a superficial illumination bias. This accumulation of photons was due to tissue scattering, since setting the scattering coefficient to zero removes this bias (Waters, 2020). Since the tissue scattering coefficient for the excitation wavelengths of jRGECO1a is smaller than that of GCaMP6f, illumination of jRGECO1a is subject to similar initial bias but with a less pronounced decline in intensity with cortical depth (Figure 2.10, panel B, no skull).

The concentrating effect of photons around L2/3 disappears when the influence of the skull is taken into account, as it helps randomising the angles of the photons at the brain surface, counteracting the initial tissue scattering (Waters, 2007). As a result, the intensity over the depth of the cortex decreases more exponentially as a function of skull thickness (Figure 2.10, panel B, skull thickness). On average, the adult mouse skull is $\sim$245 $\mu m$ thick (Ghanbari et al., 2019), however, the skull is much thinner during early development (Vora et al., 2016). This suggests that there may be a greater bias towards photon concentration in the superficial layers in neonatal mice compared to adults. The effect of changes in skull thickness during the first postnatal weeks on the intensity profile was modelled by simulating several skull thicknesses ranging from 100 $\mu m$ up to 300 $\mu m$. The intensity decay as a function of depth became steeper with increasing skull thickness (Figure 2.10, panel B). This suggests that large changes in skull thickness during the first three postnatal weeks may affect the layer bias of the widefield sources. The intensity of the illumination was halved at $\sim$800 $\mu m$ and 1 mm for GCaMP6f and jRGECO1a respectively, and starts to relax towards zero at around >2 mm. Despite potential slight variations in *in vivo* light intensity profiles caused by changes in the scattering properties as a result of

developmental processes, such as myelination and blood vessel growth, photons should be able to reach deep cortical layers at all postnatal ages since the cortex is ∼1.2 mm thick at weaning time (Hammelrath et al., 2016). Furthermore, subcortical structures located within 4 mm from the pial surface could theoretically receive some residual illumination, potentially contributing to the observed signal.

Regarding the fluorescence collection pathway, photons emitted by the two GECIs will also be scattered by the tissue *en route* to the cortex surface. The percentage of collected photons showed a slight increase with source depth for both fluorophores up to ∼300 $\mu m$, but decreased thereafter, remaining relatively constant for the first millimetre of depth for the jRGECO1a indicator and slightly decreasing for the GCaMP6f one, due to their differences in light scattering (Figure 2.10 panel C, top). The emitted photons from different sources deep in the brain will appear as fluorescence patches on the surface of the brain, which appeared larger the further the source was from the pial surface (Waters, 2020). For example, the diameter of the

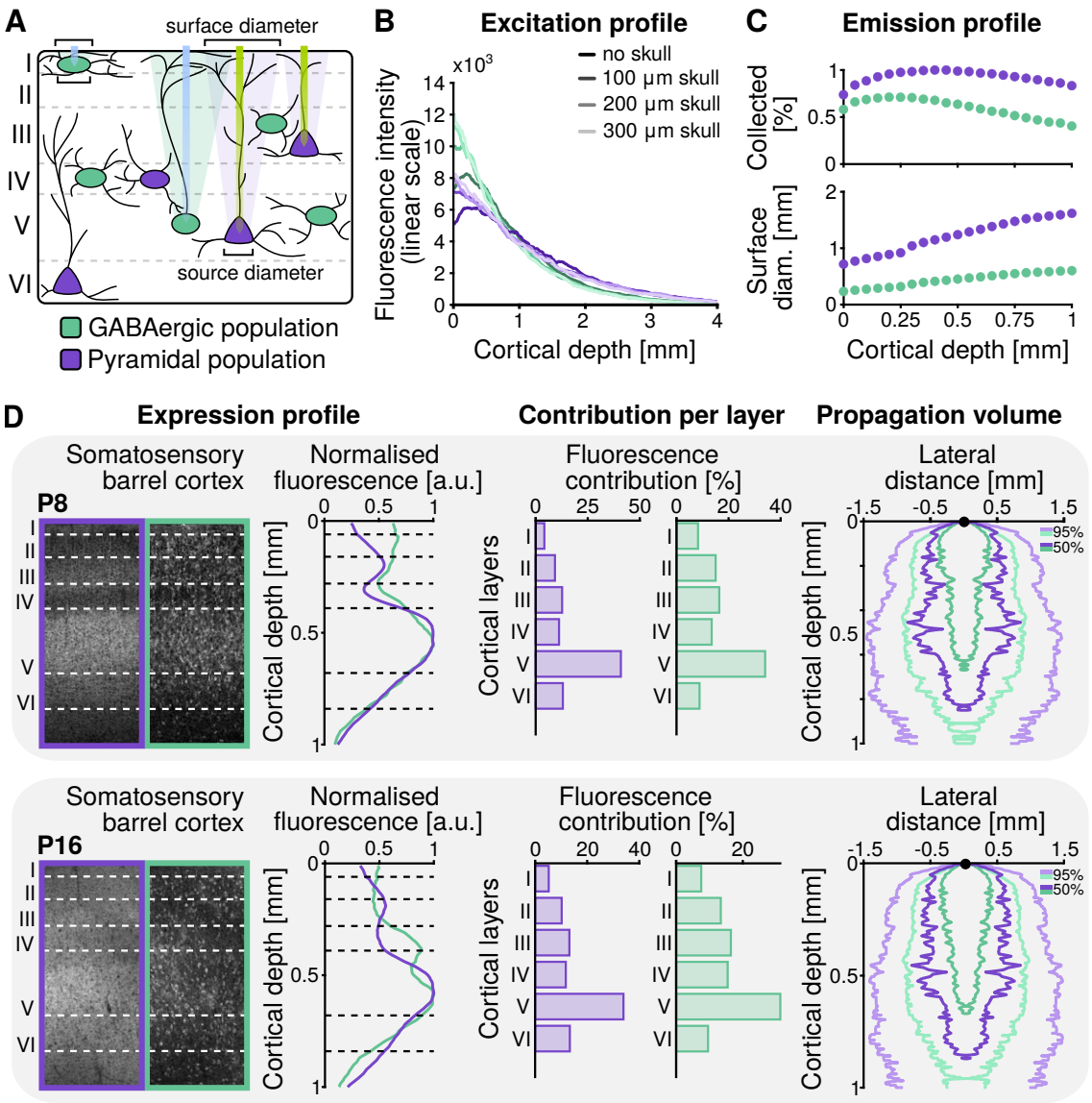

**Fig. 2.10 Contribution of the Thy1-jRGECO1a;Gad2;GCaMP6f transgenic mouse line to widefield fluorescence. A|** Illustration of the cortical distribution of the cell types labelled by the Thy1-jRGECO1a (pyramidal) and Gad2-GCaMP6f (GABAergic) promoters and their location in different cortical layers. Excitation photons for GCaMP6f (blue) and jRGECO1a (lime) are shown as graded arrows. The emitted photons from source cells are shown as shaded patches with gradually increasing diameter as a function of distance form the source. Cortical layers are labelled from I to VI. **B|** Illumination intensity per fluorophore as a function of cortical depth with and without skull, normalised to the total intensity in brain tissue. Skull widths: 100 $\mu m$, 200 $\mu m$ and 300 $\mu m$, dark to light shades. **C|** Percentage of photons collected per fluorophore, as a function of source depth (top panel), and diameter of the patch of fluorescence at the surface for 95% of collected photons from sources at different depths (bottom panel). **D|** Laminar fluorescence for each fluorophore at P8 and P16. Left panel shows the expression profile from coronal sections of mouse primary somatosensory cortex as a function of depth and normalised to the maximum fluorescence of each fluorophore. Middle panel shows the contribution to the widefield fluorescence per cortical layer, as a percentage of total fluorescence from the *pia* to the base of white matter. Calculated as the product of the expression profile (left panel), the excitation intensity through a 100 $\mu m$ skull (panel B), and the percentage of fluorescence photons collected (panel C, top). Right panel shows 2-dimensional illustrations of the volume of tissue from which photons propagate to a single location on the brain surface. Black circle represents zero depth and zero lateral distance. Lines encircle the voxels contributing 50% and 95% of collected photons.

fluorescence patch containing 95% of the photons emitted by a point source at the surface of the brain was $\sim$200 $\mu m$ for GCaMP6f and $\sim$700 $\mu$m for jRGECO1a, increasing to $\sim$400 $\mu m$ and 1.1 mm respectively at 500 $\mu m$ below the surface (Figure 2.10 panel C, bottom). Therefore, nearby sources in any cortical layer will produce overlapping distributions, making it unfeasible to resolve individual sources. Nonetheless, optical parameters such as the focal plane depth, numerical aperture or FOV had very modest effects on the illumination and collection pathways, as well as on the distribution of fluorescence at the tissue surface (Waters, 2020).

The laminar fluorescence and volume from which the emitted photons are collected were simulated to determine which layer the widefield signal might originate from and thus what percentage of that fluorescence comes from the layers where the somata of the two different cell populations are located. Making use of the expression profile of P8 and P16 coronal sections from the somatosensory cortex for each of the two cell populations (Figure 2.10 panel D, left), the theoretical amount of *in vivo* widefield fluorescence was estimated by multiplying their expression pattern by the modelled illumination intensity (Figure 2.10 panel B) and collection efficiency (Figure 2.10 panel C, top) profiles for a skull of 100 $\mu m$ thick (Vora et al., 2016; Ghanbari et al., 2019). These estimates revealed the theoretical relative contributions of different layers to the collected superficial widefield fluorescence (Figure 2.10, panel D, middle). The different layers are broadly defined by distance from the pial surface; 100 $\mu m$, 300 $\mu m$, 130 $\mu m$, 270 $\mu m$, 200 $\mu m$ and 100 $\mu m$ for layer I (L1), II (L2), III (L3), IV (L4), V (L5) and VI (L6) respectively, using a normalised cortical depth of 1 mm to facilitate the comparison and the delineation of cortical layer boundaries (the brain surface and L6-white matter border were at 0 and 1 mm depth). Notably, the size variability across developmental stages was minimal, measuring approximately 1.2 mm and 1.3 mm for P8 and P16 ages, respectively. The percentages of fluorescence arising from the different cortical layers followed a similar pattern for both fluorophores and ages explored, with a bias towards L5 and a relatively stronger contribution from the pyramidal

population (Figure 2.10, panel D, middle). Despite being the surface layer, the model predicted that L1 contributes only $\sim$10% to the total fluorescence for the GABAergic population, and $<$10% for the pyramidal population, likely due to the fact that dendrites and axons passing through this layer are the only structures present for this population. This observation was consistent with a previous study on a GCaMP mouse line with homogeneous cortical layer expression (Waters, 2020), where L1 showed a relatively small contribution compared to L2/3. With age, the relative difference between L5 and the rest of the layers decreased, observing greater contributions from L2, L3 and L4. The emitted photons that propagated to the brain surface could have originated from a large volume of underlying tissue (Figure 2.10 panel D, right). This phenomenon underlined the sensitivity of widefield imaging to light scattering, with only fluorescence from pixels $\sim$ 500 $\mu$m apart coming from non-overlapping volumes, for 50% of collected photons arriving at each 10 $\mu$m surface pixel (>1 mm for 95% of collected photons) (Waters, 2020). The volume from which emitted photons could theoretically have originated for each cell population was very similar between both developmental ages, but differed between the two fluorophores, with the pyramidal cell population (jRGECO1a) presenting a fairly constant radius across all layers of >500 $\mu m$, and up to 1.5 mm for 95% of collected photons; compared to a maximum of 900 $\mu$m for the GABAergic population (GCaMP6f).

In summary, the random walk model has provided theoretical estimates of the contributions of the Thy1-jRGECO1a (pyramidal population) and Gad2-GCaMP6f (GABAergic population) expression patterns to the widefield fluorescence that would theoretically be observed through the macroscope setup. The intensity of illumination and the collection of fluorescence gradually decayed as a function of cortical depth, and were affected by tissue scattering and skull thickness. The observed widefield fluorescence was biased towards L5, as both populations' expression profiles peaked at this layer, and originated from a volume of tissue as large as $\sim$7 mm$^2$, resulting in a surface resolution on the millimetre scale.

### 2.3.2 Controls for dual-colour widefield calcium imaging.

To ensure that any observed changes in fluorescence in widefield calcium imaging were due to neural activity and not confounding factors, it was essential to conduct control experiments. The experiments outlined in these sections aimed to assess the stability of the preparation, the effects of motion and hemodynamics, and the behaviour of calcium indicators *in vivo*. Identifying and correcting potential sources of artefacts was critical to enhance the validity and reliability of subsequent results.

#### Photoswitching behaviour of jRGECO1a.

Similarly to other mApple-based (red-shifted) calcium indicators, jRGECO1a exhibits blue-light-activated photoswitching behaviour, meaning it is transiently activated by blue light in a

calcium-independent manner (Dana et al., 2016). This effect could pose a challenge in its use for dual-colour imaging, as these transient events could potentially confound ongoing activity signals. Photoswitching assays on the purified protein have shown that the frequency of the blue light pulses differentially affects photoswitching behaviour, with higher frequency pulses (>1.8 Hz) resulting in an effective increase in baseline fluorescence (Dana et al., 2016). This appears to be true because the photoswitching response has fixed and stereotypical dynamics, which means that high-frequency pulses would not allow enough time for the transient pulse to revert to its initial state or baseline. As a result, the baseline jRGECO1a fluorescence increases caused by blue light exposure, could potentially interfere with the jRGECO1a calcium-dependent events under green light. To ensure that the increase in baseline fluorescence does not affect the detection of calcium-dependent events, a control experiment was conducted to assess the effect of the alternation of blue-lime LEDs used in the imaging setup on the jRGECO1a dynamics.

Single transgenic Thy1-jRGECO1a animals were imaged under continuous lime illumination (spontaneous baseline) and exposed to 50 ms long blue light pulses of varying frequencies (Figure 2.11, panel A). The frequencies employed were matched to those from the original assay (Dana et al., 2016), with an additional frequency that corresponded to the imaging frequency used for the dual-colour imaging experiments. Each imaging sweep consisted of an initial spontaneous baseline block lasting approximately 18 seconds, followed by a pulse train consisting of 6-10 pulses of blue light, and a second baseline block that lasted up to 60 seconds. This imaging procedure was repeated 30 times aiming to quantify the photoswitching behaviour by analysing changes in fluorescence between the blue light pulses and to evaluate any effects on the *in vivo* dynamic range of jRGECO1a.

At the lowest frequency (0.2 Hz), there was a clear photoswitching effect, characterised by transient increases in jRGECO1a fluorescence that were time-locked to the blue light pulses and recovered to pre-pulse levels over 2-3 seconds after the pulse (Figure 2.11, panel B, top, black average trace). However, at higher frequencies, although transient increases in fluorescence were observed, they were less clearly time-locked to individual light pulses (Figure 2.11). This confirmed that jRGECO1a exhibits photoswitching *in vivo*, but the dynamics of this behaviour during high frequency exposure are unclear. Given the importance of understanding the impact of photoswitching on recordings made with strobing illumination, the effect of high frequency blue light exposure on jRGECO1a was investigated. At a frequency of 33.3 Hz, although it was not possible to observe pulse-by-pulse effects, as the strobing frequency equalled the imaging rate, there was an increase in fluorescence that slowly decayed back to baseline after the end of the pulse train, with similar time course of that observed for lower frequency photoswitching events (Figure 2.11, panel B, bottom, black average trace). This suggests that the high frequency LED strobing used for imaging likely leads to an increase in fluorescence that is calcium-independent but, importantly, this increase is stable as long as strobing continues (i.e. during the imaging sessions). This increase would only return to baseline once the blue light was switched off.

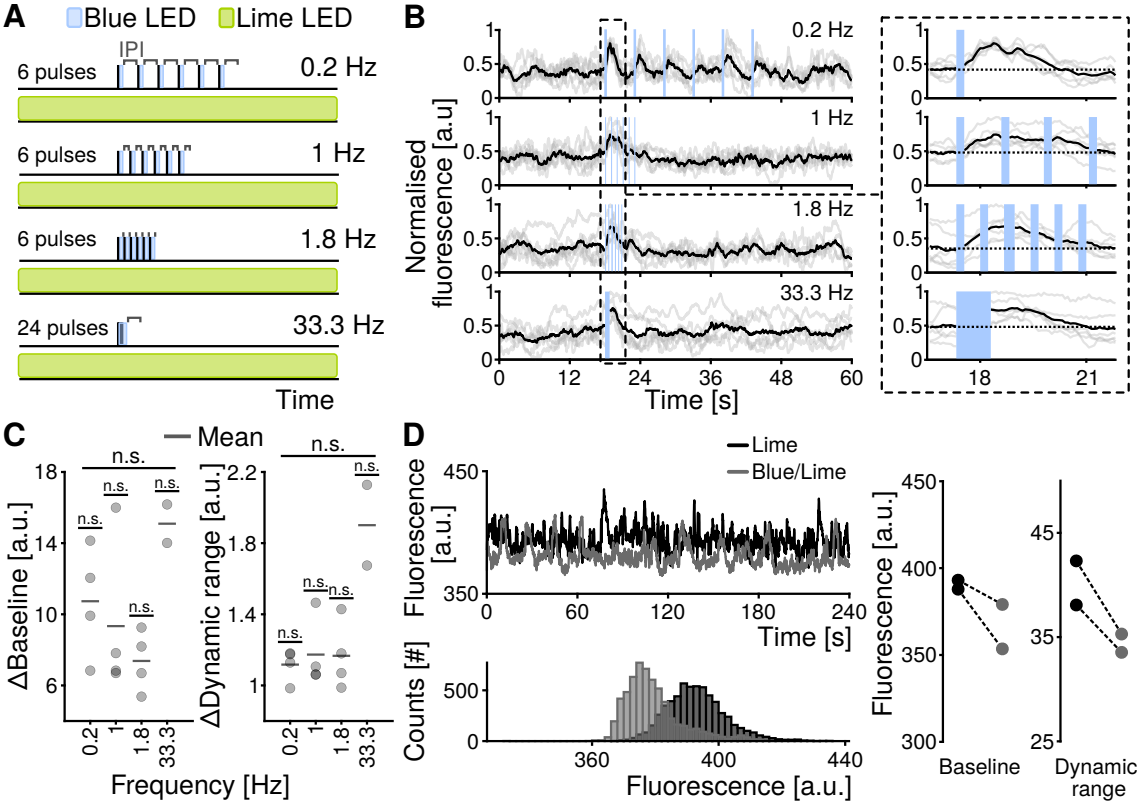


**Fig. 2.11 Photoswitching effect of jRGECO1a at different blue-light frequency pulses. A|** Schematic of the experimental layout per recording sweep. The lime LED was continuously on, while blue light pulses were turned on for 50 ms at different frequencies. The Inter-Pulse-Interval (IPI) segments are used to analyse the effect of blue light on the dynamics. **B|** Representative example of the jRGECO1a fluorescence dynamics under 4 different blue light pulse frequencies. Average of all the sweeps is shown in black, individual sweeps are shown in light grey. The right inset provides a close-up look at the IPI dynamics. Dashed line indicates the average baseline prior to the blue light pulse train. **C|** A Kruskal-Wallis test for non-normally distributed data revealed no significant differences among the four frequency groups for both, the change in baseline fluorescence ($H$ = 5.657, p = 0.130) and the change in dynamic range ($H$ = 4.829, p = 0.185). Post-hoc Wilcoxon signed rank tests for zero median (one median) were performed to identify specific group differences in baseline (dynamic range) change. No significant differences were observed for 0.2 Hz (Baseline: $Z$ = 10, p = 0.125; Dynamic range: $Z$ = 9, p = 0.250), 1 Hz (Baseline: $Z$ = 10, p = 0.125; Dynamic range: $Z$ = 10, p = 0.125), 1.8 Hz (Baseline: $Z$ = 10, p = 0.125; Dynamic range: $Z$ = 9, p = 0.250) and 33.3 Hz (Baseline: $Z$ = 5, p = 0.500; Dynamic range: $Z$ = 3, p = 0.500) frequencies. **D|** Representative example of global mean jRGECO1a fluorescence dynamics with continuous lime light or alternating blue-lime lights at 33.3 Hz (top left). Histogram of the global mean fluorescence values for each condition (bottom left). Baseline and dynamic range values for each condition (right panel) was not statistically tested due to sample size (n = 2). Dashed line indicated paired recordings.

The change in baseline was calculated as the difference between the average baseline prior to the blue light pulse train and the maximum value of fluorescence for the average inter-pulse-interval trace. The dynamic range was calculated as the difference between the peak fluorescence observed across all individual sweeps, and the baseline value, calculated as previously stated. Therefore, the change in dynamic range was calculated by dividing the dynamic range prior to the blue-light pulse trains by the dynamic range in the inter-pulse-interval. A value of 1 indicates no change in the dynamic range due to blue light strobing, whereas a

value greater than 1 indicates a decrease in the dynamic range caused by the strobing. There were no significant differences in the baseline or dynamic range observed across frequencies (Figure 2.11, panel C). Additionally, the median distributions for the baseline and dynamic range were not significantly different from zero and one, respectively. However, it is important to interpret these results with caution given the small sample size.

This photoswitching behaviour has been shown to be more pronounced when exposed to continuous widefield illumination, but could be greatly mitigated by employing alternating excitation wavelengths or intermittent illumination (Shaner et al., 2008). Therefore, a similar analysis was conducted on a full 6-minute recording in which the lime LED was either continuously on or interleaved with blue light at 16.6 Hz, to examine whether the baseline or dynamic range changed in these recordings. The dynamics of the global mean fluorescence of a representative example recording showed a decrease in baseline, causing the entire trace to shift to smaller fluorescence values when blue and lime LEDs were alternated compared to only having lime light (Figure 2.11, panel D, top left). This reduction in baseline was observed in the shift of the fluorescence value distributions towards a lower fluorescence average (Figure 2.11, panel D, bottom left). This change was also apparent when calculating the baseline and dynamic range between the two light configurations (Figure 2.11, panel D, right). Although the sample size is very small, these results were consistent with previous findings using R-GECO1 indicators, for which blue light pulses resulted in a red-shift in absorbance, leading to a temporary decrease ( 40%) in fluorescence when subsequently illuminated with lime light (Akerboom et al., 2013).

Taken together, these results have shown that the photoswitching behaviour of jRGECO1a indicator is complex. Brief low frequency blue light pulse trains seem to allow the protein to recover to its original conformational state, leading to a slight increase in the baseline fluorescence. However, under continuous high-frequency blue light pulses, the protein was unable to fully recover, resulting in a decrease in baseline fluorescence, possibly due to the red-shift in absorbance. Despite the reduction in baseline fluorescence caused by blue-lime alternating wavelengths, the calcium dynamics of the jRGECO1a molecule could still be detected and measured with sufficient dynamic range.

### Assessment of head fixation system stability during awake imaging.

Stability of the sample under the macroscope is crucial to ensure that the recorded signals accurately reflect the underlying neural activity, minimising head motion artefacts that can cause changes in the focus and FOV. Although post hoc motion correction can fix lateral (XY) movement, axial (Z) movement cannot be corrected due to the lack of optical sectioning. To quantify lateral displacement during recordings, a frequency-based, subpixel (1/10 of a pixel) registration approach was used (see section 2.2.3) to calculate the amount of pixel displacement in both the pyramidal (jRGECO1a channel) and GABAergic (GCaMP6f channel) neuronal populations. A representative example of the pixel displacement traces in the X and Y directions

over 30 seconds of a recording detected by the motion correction algorithm is shown in Figure 2.12, panel A. The median value of pixel displacement distributions for both directions was centred around zero, with the largest displacement rarely exceeding 1 pixel (13 $\mu$m, Figure 2.12, panel B). The GABAergic population exhibited a wider distribution of pixel displacement values compared to the pyramidal population, especially in the Y direction, which corresponds to the animal's forward and backward movement. This difference across populations may be due to the higher vasculature contrast observed in the GCaMP6f channel, which facilitates the registration process.

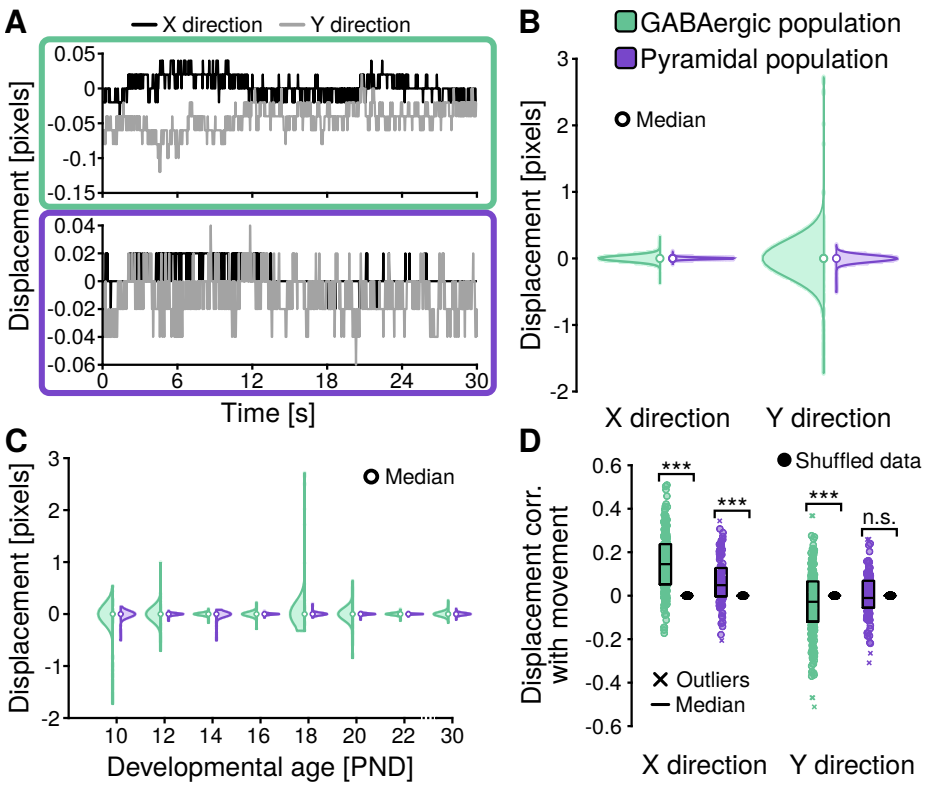


**Fig. 2.12** **Assessment of lateral brain movement during awake imaging. A|** Representative example of lateral pixel displacement values in X and Y directions during a recording for each of the population. **B|** Half violin plots of the distribution of pixel displacement values in each direction across all recordings, for each population. **C|** Distribution of pixel displacement values both directions across development, for each population. **D|** A Kruskal-Wallis test showed a significant correlation between the pixel displacement values in both directions and the binary movement vector for the GABAergic population (X: $H$ = 151.032, p = 1.031e-34; Y: $H$ = 18.322, p = 1.866e-05), whereas the pyramidal population only showed a significant correlation in the X direction (X: $H$ = 42.246, p = 8.047e-11; Y: $H$ = 0.736, p = 0.391). Box plots display the first quartile, median, and third quartile. Outliers are shown as crosses. Significance is shown as *** for pval < 0.001.

To account for any changes in the head fixation system stability over time, the distributions of pixel displacement were plotted as a function of developmental age (Figure 2.12, panel C). The observed distributions of pixel displacement values did not exhibit any consistent changes as the animals aged, suggesting that headpost stability remained constant even as the animals develop more coordinated movements. The pixel displacement traces in each direction were correlated with the binary movement vector obtained from the piezo wafer recording the animal's

body movement. Results showed that pixel displacement on the GCaMP6f channel (GABAergic population) displayed a significant positive correlation with movement in both the X (p = 1.031e-34) and Y (p = 1.866e-05) directions, as compared to their shuffled versions. On the other hand, displacement recorded on the jRGECO1a channel (pyramidal population) displayed a significant correlation only in the X direction of displacement (p = 8.047e-11). Shuffled surrogate data for each direction and population were generated by randomly shuffling the binary movement vector 100 times, computing the correlation with the pixel displacement trace, and averaging it across all repetitions.

Taken together, the observed pixel displacements in all recordings were relatively small, typically less than the size of a single pixel (169 $\mu m^2$) or the focal volume of conventional macroscope setups (1 mm in diameter and 200 $\mu m$ in depth, Ratzlaff et al., 1991). This suggested that the head fixation system remained stable during recordings and across development. Consequently, post hoc motion correction should be able to correct for these small spatial shifts, which were correlated with the animal's movements, without introducing any significant artefacts that may bias data interpretation.

### Contribution of hemodynamics and movement-induced blood volume artefacts to widefield sources.

Hemodynamic artefacts are fluctuations in the fluorescence signal which can be collected by widefield imaging and arise from changes in blood flow and oxygenation in the vasculature surrounding the imaged tissue (Valley et al., 2020). These artefacts generally manifest as slow, low-frequency fluctuations in the signal, which can obscure or mask true underlying neural activity. On the other hand, movement-induced blood volume artefacts refer to the changes in the overall light absorption and scattering of the vasculature, as well as the reflection of the illuminating light, due to motion during the imaging session (Silasi et al., 2016). It is important to correct for these type of artefacts as they can introduce spatial correlations in the data and transient changes in fluorescence, which can obscure or mimic true neural signals, leading to misinterpretations of the data.

In most adult mouse widefield calcium imaging studies using GFP-based calcium indicators, hemodynamic correction is commonly performed through techniques like green diffuse reflectance (Ma et al., 2016), UV-light correction (Couto et al., 2021), and blind source separation methods such as ICA (Weiser et al., 2021; Ma et al., 2016). However, some studies simply exclude vasculature pixels by masking to eliminate the hemodynamic contamination (MacDowell et al., 2020; Makino et al., 2017; Pinto et al., 2019). It is crucial to note that various vascular compartments have distinct hemodynamic artifacts, with capillary contributions exhibiting different time courses from arteries or veins (Ma et al., 2016). Large vessels are more superficial, allowing for easier separation of changes in fluorescence in the neural tissue from those associated with these larger arterial and venous vessels (Waters, 2020). Despite robust neural activity during

the first two postnatal weeks, it has been shown that neonatal hemodynamics are uncoupled from neuronal ones, exhibiting minimal local hyperemia (Kozberg et al., 2016).

Therefore, to evaluate the potential contamination by hemodynamics and movement-induced blood volume artefacts across developmental age, especially in the GCaMP6f channel, the widefield fluorescence signal from CAG-GFP mice, which express the calcium-independent GFP fluorophore instead of the GCaMP6f calcium indicator under the ubiquitous CAG promoter, was recorded. A total of five animals at different developmental ages were recorded, with each animal undergoing four recordings, two spontaneous and two whisker stimulation recordings, except for the P22 mice, which had only one whisker stimulation recording. This group of mice was subjected to the same imaging setup and preprocessing pipeline as the experimental transgenic mice.

The sICA components obtained were visually assessed for the presence of neural-like motifs to determine whether they represent calcium-independent hemodynamic signals or blood volume artefacts resembling superficial vasculature patterns. As the CAG-GFP mice do not exhibit calcium-dependent dynamics, any fluctuations in fluorescence can be attributed to changes in blood flow or motion artefacts. The head fixation system provided a stable preparation throughout the recordings (see section 2.3.2), thus any motion artefacts are likely to be caused by movement of the brain within the skull. The sICA components were categorised into three groups: blood volume artefacts, other artefacts, and noise. Blood volume artefacts included any signal-like spatial pattern within the brain mask, while other artefacts included reflections from the cement rugosities or the edge of the headpost. The normalised sum of the spatial weights of all blood volume artefacts components, for each developmental age, showed a clear vasculature pattern, including the superior sagittal and transverse sinus veins, and left and right middle cerebral artery (Figure 2.13, panel A). These components could potentially be used to create a relatively high-resolution map of the dorsal cortical vessel patterns. The time courses of these spatial patterns were compared across each group of sICA components per age, and overlaid with the movement binary trace to look at any potential temporal structure (Figure 2.13, panel B). The blood volume artefacts group displayed more clear temporal patterns, which seemed to align with the movement bouts, while the other artefacts were slightly less structured.

The correlation between the animal movement trace and the temporal weights of the different component groups was calculated to determine whether the motifs represented movement-induced artefacts. The surrogate data was created by circularly shifting the movement binary trace 5 seconds to the right, to decouple the temporal dynamics of the sICA components, while keeping the overall structure of the movement patterns. The dynamics of the blood volume artefacts ($p = 3.981e-04$), as well as the combination of all groups' components (whole recording, $p = 4.634e-04$), showed the highest significant correlation with movement (Figure 2.13, panel C). There was also a slight, but significant correlation with movement observed in other artefacts ($p = 0.0218$), since the nature of these artefacts could also be affected by

the animal's movement, such as changes in light reflection or hair obstructing the FOV. The noise artefacts also showed a significant correlation with movement (p = 5.385e-04), which could be attributed to small, random movements or fluctuations in the background fluorescence that are related to the animal's movement. Alternatively, the noise motifs could be picking up on other sources of noise, such as electrical or thermal noise, which may be correlated with movement. This suggested that some of the fluorescence artefacts observed in the recordings can be attributed to movement-induced changes in the fluorescence. The correlation of each component group with movement did not change across development (Figure 2.13, panel D), indicating no significant changes in the correlation as the animals aged and presented more coordinated movements.

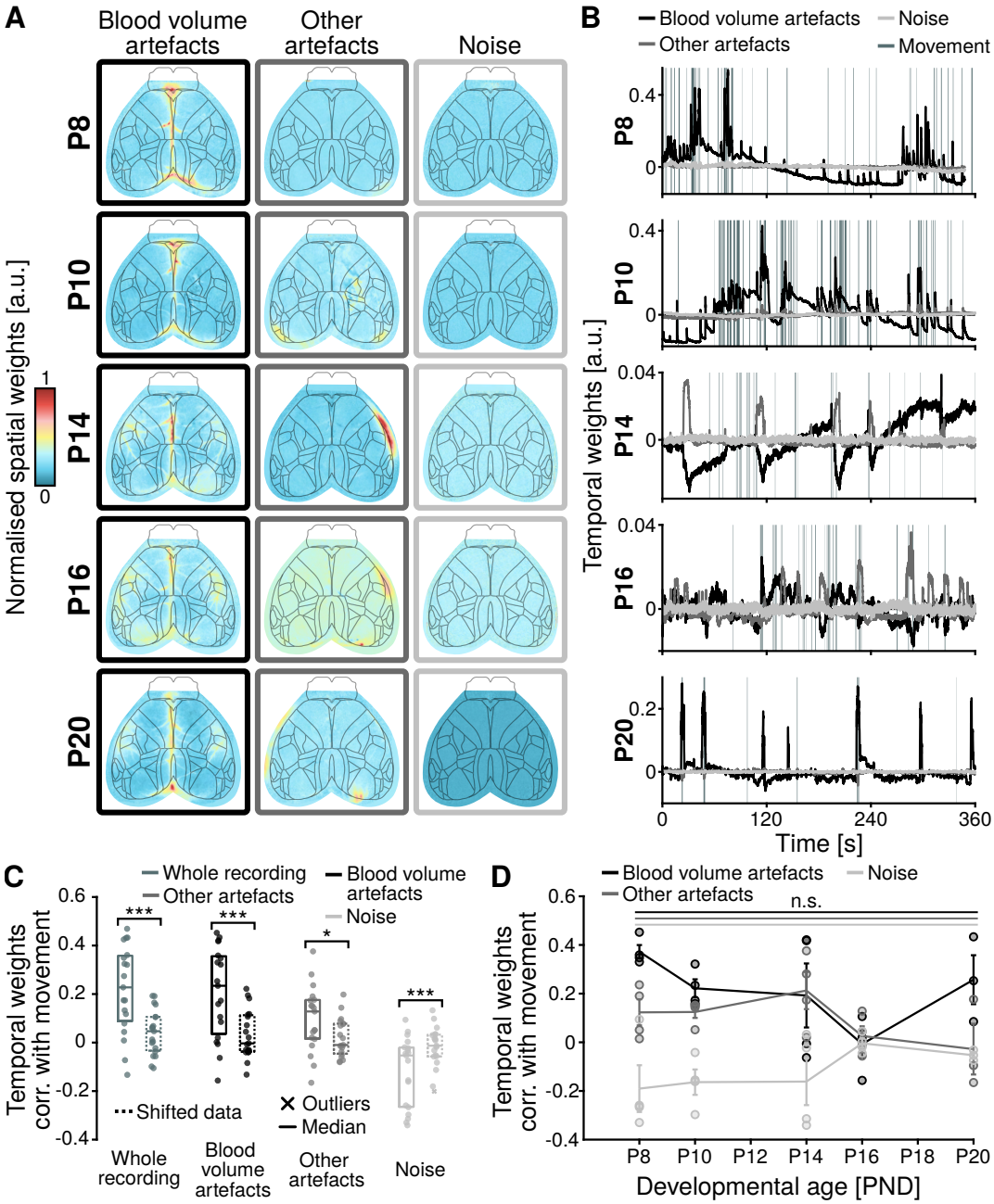

**Fig. 2.13 Movement-induced blood volume artefacts in CAG-GFP mice across early postnatal development. A|** Representative example of the spatial patterns of sICA motif groups at different developmental ages. Spatial weights are summed across all motifs within a group and normalised. **B|** Temporal dynamics associated with the spatial patterns displayed in A. Temporal weights are summed across all motifs within a group and overlaid with the binary movement trace. **C|** A significant correlation of the temporal weights with the movement binary trace (n = 19 recordings) was observed for the whole recording ($Z$ = 3.501, p = 4.634e-04), blood volume artefacts ($Z$ = 3.541, p = 3.981e-04), other artefacts ($Z$ = 2.294, p = 0.0218) and noise ($Z$ = -3.461, p = 5.385e-04). Wilcoxon matched pairs signed ranks tests were performed to identify the group differences. **D|** No significant correlation of the temporal weights with the movement binary trace was observed across development (n = 4 recordings per age, 3 for P20) for the blood volume artefacts (p = 0.0914), other artefacts (p = 0.0909) and noise (p = 0.0588). Significance tested by LMM. Further statistical information in Annex 4.2. Box plots display the first quartile, median, and third quartile. Outliers are shown as crosses. Significance is shown as * for pval < 0.05 and *** for pval < 0.001.

The mean global signal per recording of the CAG-GFP expressing mice was analysed to create a spectrogram and visualise the changes in the frequency spectrum at different developmental ages. Figure 2.14, panel A shows two representative examples at different ages, each with three main power bands: a very slow frequency band between 0-0.5Hz, a middle band between 5-6 Hz (respiratory rate, RR), and a higher frequency band (heart rate, HR) that shifts its position across ages, moving from being centred at 15 Hz to ∼10 Hz. While the fluorescence observed in this mouse line is not related to brain activity, the presence of these bands can still provide valuable information about underlying processes that produced the signal. For example, the middle band present across all ages may relate to RR, which has been measured at around 5 Hz (300 RPM) in P7 neonatal mice. Additionally, the higher band could represent HR, which has been measured at around 10 Hz (600 BPM) for P7 mice (Zehendner et al., 2013). The average power density spectra across the different developmental ages imaged showed a shift in the heart rate frequency peak towards lower frequencies, whereas the respiratory rate remained relatively constant at around 5 Hz (Figure 2.14, panel B).

To investigate the possible contribution of hemodynamics to the changes in fluorescence detected through the sICA, an external sensory stimulus was used to align and time-lock the fluorescence with an event. This allowed for the detection of any changes in blood flow, and therefore fluorescence, that were driven by the stimulus. The sensory stimulation involved the deflection of multiple whiskers using a custom paddle. The stimulation device consisted of a plastic paddle, measuring 15 x 8 mm, attached to a 9V micro servo motor (SG92R - Tower Pro). This motor was controlled via an Arduino Uno board connected to the Micro1401 data acquisition box, enabling precise timing synchronisation with image acquisition. Positioned caudal to the right whisker field, the paddle was angled to make contact with the whiskers during its arched movement. Each stimulation lasted 30 ms, allowing the paddle to traverse the entire whisker field to the snout and return to its resting position. A 500 ms rest period preceded the first stimulation, with a 9 s inter-stimulus interval (ISI) between stimulations. A total of 40 stimulations were administered per recording block. Seed-pixel correlation maps were created for two example recordings to identify the regions functionally connected to the

seed region in the primary somatosensory cortex (S1) of the contralateral hemisphere to the whisker stimulation. These representative maps showed no spatial structure, suggesting that there was not a clear pattern of fluorescence change in S1 in response to the stimulation, and therefore no hemodynamic signal was successfully detected (Figure 2.14, panel C). The temporal dynamics of the contralateral S1 average fluorescence trace were overlaid with the time of whisker stimulations to visually examine whether any fluorescence peaks that aligned with the stimulus delivery (Figure 2.14, panel C). The correlation between the contralateral S1 temporal trace and the whisker stimulation times fluctuated around zero, showing no significant changes across development (Figure 2.14, panel D). However, the surrogate data, generated by circularly shifting the whisker stimulation times 5 seconds to the right, exhibited a significant change across development ($p = 1.597e\text{-}04$), possibly due to alterations in the noise structure. Taken together, the use of bright fluorescence indicators and dense labelling resulted in a strong background signal that hindered the detection of hemodynamic changes (Vanni et al., 2014; Xiao et al., 2017; Valley et al., 2020), suggesting that this setup might not be sensitive to potential hemodynamic contamination.

### Assessment of epileptiform events associated with high-levels of transgene expression.

Strong expression of genetically encoded indicators, particularly during the early stages of brain development, has the potential to disrupt calcium dynamics and contribute to pathological brain activity. These pathological events have shown to resemble synchronised interictal discharges, which are generally observed in the context of epilepsy, characterised by repetitive ($\sim$0.5 Hz), large amplitude (>10% increase) and short duration (<200 ms in GCaMP6f) events (Daigle et al., 2018; Steinmetz et al., 2017). This aberrant activity has been observed in transgenic strains with dense and widespread expression of the calcium indicator, including the Emx1-IRES-Cre line (Steinmetz et al., 2017). However, this phenomenon was not detected in a Emx1-IRES-Cre/GCaMP6f cross during the first two postnatal weeks of development (Cross, 2018). This activity was most prominent in mice that expressed the calcium indicator under the TIGRE locus, which is more susceptible to germline recombination events (Steinmetz et al., 2017). Despite the fact that the genetic lines used in this study were not among those that exhibited epileptiform events (Steinmetz et al., 2017, Table 2), the incidence of such events during spontaneous activity was screened, given that the promoters in these genetic lines express early in development and could be contributing to some of these deficits.

A similar approach as Steinmetz et al., 2017 was used to investigate the occurrence of these epileptiform events during early postnatal development in the triple transgenic line employed in this study, which labelled the GABAergic (Gad2/GCaMP6f) and pyramidal (Thy1-jRGECO1a) populations. These events were originally identified by analysing calcium events with large amplitudes and brief durations, which corresponded to >1 mV events observed in LFP recordings (Steinmetz et al., 2017). In order to define the characteristics of the potential epileptiform

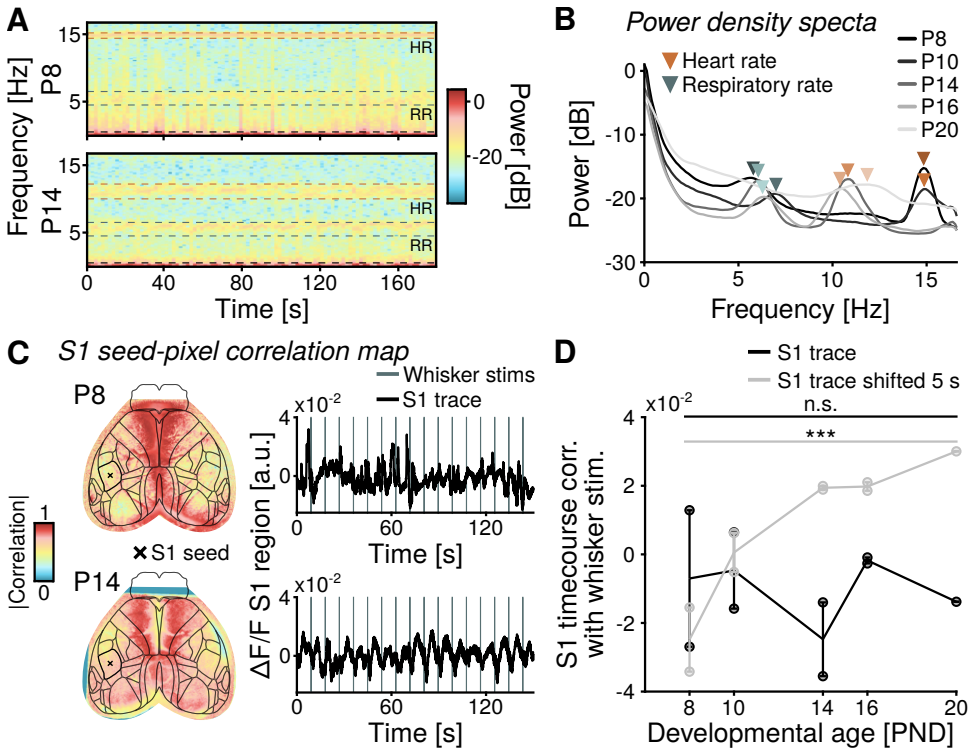


**Fig. 2.14 Evaluation of signals contributing to the spectrogram and hemodynamics in CAG-GFP mice. A|** Representative example of the spectrogram of the global mean signal at two different developmental ages. HR band (orange) corresponds to heart rate, RR band (dark teal) corresponds to the respiratory rate. Black dashed line indicates 0.5 Hz. **B|** Average power density spectra across all CAG-GFP recordings per developmental age. Triangle indicates power peaks. **C|** Seed-pixel absolute correlation maps for two representative whisker stimulation recordings. Seed positioned on the centroid of the contralateral S1 barrel. Average contralateral S1 trace (black) is overlaid with the whisker stimulation times (teal). **D|** A significant correlation of the temporal weights with the movement binary trace was observed across development (n = 2 recordings per age, 1 for P20) for the circularly shifted contralateral S1 trace (p = 1.597e-04), whereas the contralateral S1 trace was not significant (p = 0.699). Significance tested by LMM. Further statistical information in Annex 4.2. Box plots display the first quartile, median, and third quartile. Outliers are shown as crosses. Significance is shown as *** for pval < 0.001.

events for the two different calcium indicators used, picrotoxin (PTX), a non-competitive GABA antagonist, was unilaterally and intracortically injected in S1 in order to increase the local neuronal excitability and induce potential seizures (see section 3.2.4 for more details). A S1 barrel area sICA activity motif and a control motif in the primary visual cortex (V1) were visualised to investigate the properties of the calcium events under PTX (Figure 2.15, panel A). The S1 barrel trace showed high-frequency and high-amplitude events that were highly correlated across both populations, displaying a skewed prominence distribution in relation to the event widths (Figure 2.15, panel A, right). This indicated the presence of very stereotypical events with prominences higher than 20% and event widths smaller than 600 ms. These epileptiform events were not present in the V1 motif, although the tight balance and high correlation between both population dynamics was still observed (Figure 2.15, panel A, bottom). For the chronic experimental recordings, a representative example showed that the sICA activity patterns in both S1 and V1 did not display these epileptiform events, nor the tightly balanced and correlated population dynamics observed under the influence of PTX (Figure 2.15, panel B).

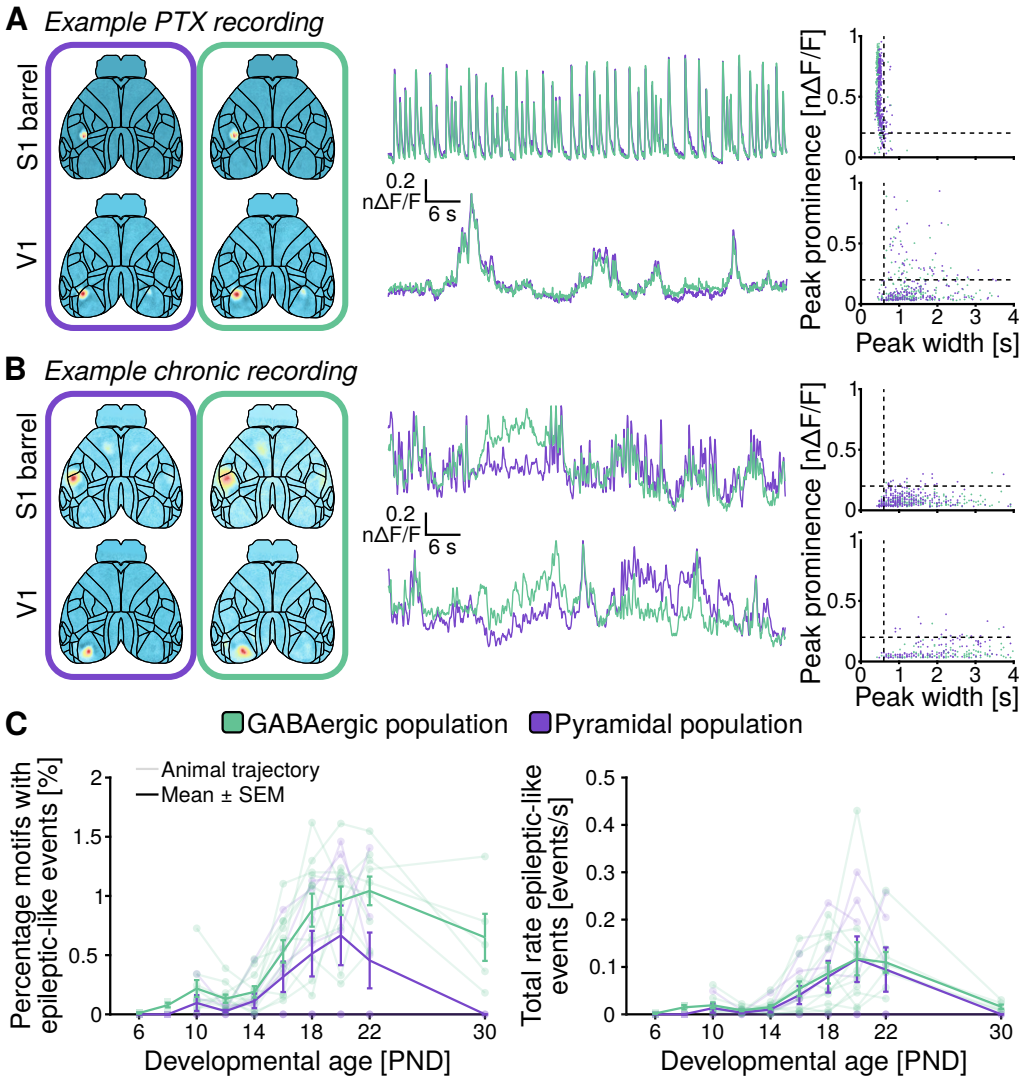


**Fig. 2.15** **Incidence of epileptiform events observed in longitudinal widefield calcium imaging A|** Representative example of spatial patterns (left panel) and temporal weights (middle panel) of S1 and V1 sICA motif activity after injection of PTX in the left S1 barrel region. The prominence versus width (right panel) is shown for all peaks per sICA motif (n = peaks/motif). **B|** Same as in A but for a representative control recording (no PTX injection). Dashed lines indicate 0.2 n$\Delta F/F$ prominence, and 600 ms width. **C|** The percentage of motifs per animal that present at least one event within the epileptic-like category (left panel) and the rate of the total number of epileptic-like events per animal (right panel) increase over development.

In order to determine the prevalence and potential late onset of epileptiform events during early postnatal development, all chronically imaged mice were searched for events that matched the characteristic prominence and width observed in the S1 motifs under PTX (prominence > 20% and width <600 ms). The percentage of motifs per recording that showed one or more of these events was consistently below 1% at all ages for both the GABAergic and pyramidal populations, but increased as animals got older (Figure 2.15, panel C), likely due to the general increase in event frequency during early postnatal development (Colonnese et al., 2010; Colonnese, 2014). However, no events faster than 200 ms were recorded in this project's dataset, which is the characteristic width for the epileptiform events observed in juvenile mice (Steinmetz et al., 2017).

The total rate of epileptiform events also showed a developmental increase, peaking at an average rate of 0.1 events per second for both populations (Figure 2.15, panel D). Nonetheless, these results should be interpreted with caution because the classification of these events is not very strict, and the potential changes in these event properties during development, similarly to the typical increase in event frequency (Colonnese et al., 2010; Colonnese, 2014), could be confounding the findings. It is worth noting that germline recombination was prevented during the breeding of the transgenic line by avoiding the use of homozygous male GCaMP6f (Ai95D) mice, as mice carrying both transgenes may have the recombined Ai95D allele in some sperm (Cross, 2018). Moreover, no behavioural phenotype was observed.

### 2.3.3 Validation of the long-term headpost implant on neonatal mice for chronic imaging.

Longitudinal studies involving chronic imaging of the same animal over development can reveal individual differences and changes in neural activity over time, providing a more comprehensive understanding of the underlying mechanisms of neural development. However, implanting a lightweight headpost in neonatal mice for this purpose could potentially influence their typical development by restricting brain growth. Therefore, to validate this approach, the growth of implanted pups was monitored daily by measuring their body weight up to weaning time, which was approximately two weeks after the implant surgery. Pups that were kept until early adulthood still had their weight measured, but less frequently. Other measures of normal development, including age at eye opening (not shown), fur growth (not shown), open field behaviour at weaning, brain size and weight after extraction, and cortical layer size were also assessed to compare the post-surgery development of the implanted pups with that of non-surgery littermates (Figure 2.16, panel A).

For each imaging session, the implanted pups were temporarily removed from the nest, but when returned, they were quickly taken back and fed by the dam. The weight of the implanted pups across all developmental ages did not differ significantly from their non-implanted littermates ($p = 0.195$), increasing across development (Figure 2.16, panel B, $p = 4.387e\text{-}34$), and was similar to previously reported C57BL/6 mice pre-weaning weights (Castelhano-Carlos et al., 2010). Additionally, the brain weight after extraction did not show a significant difference between the two groups (Figure 2.16, panel C). To evaluate potential growth restriction caused by the implant, the anterior-to-posterior (AP) by lateral-to-lateral (LL) ratio of the whole brain was calculated by fitting a rectangular box from the base of the olfactory bulbs to the end of the cortex, without including the cerebellum. This revealed a significant increase in the ratio for the implanted pups ($p = 0.0151$), indicating that their brains were slightly longer (AP) and less wide (LL) than the controls (Figure 2.16, panel D). The brains were collected at the time of weaning ($\sim$P22) using cervical dislocation (UK Home Office Schedule 1 procedure). Subsequently, brains were fixed in 4% paraformaldehyde at 4°C for 12 hours. After fixation, the brains were transferred to PBS and embedded in a block of low melting point agarose (3% in distilled water) to facilitate sectioning.

Coronal sections of the regions of interest (ROIs), including the M1, S1, A1, and V1, were sliced at a thickness of 50 µm using a vibratome (VT1200 Leica Microsystems). The sections were mounted directly onto slides (Thermo Scientific), air-dried for 30 minutes, and cover-slipped (No.1 VWR) using Fluoromount-G with DAPI (Invitrogen, Thermo Fisher Scientific).

Visual inspection of the coronal brain slices for each ROI already revealed longer and narrower shapes for the implanted group (Figure 2.16, panel E). This difference was quantified by calculating the dorsal-to-ventral (DV) by lateral-to-lateral (LL) ratio, fitting a rectangular box

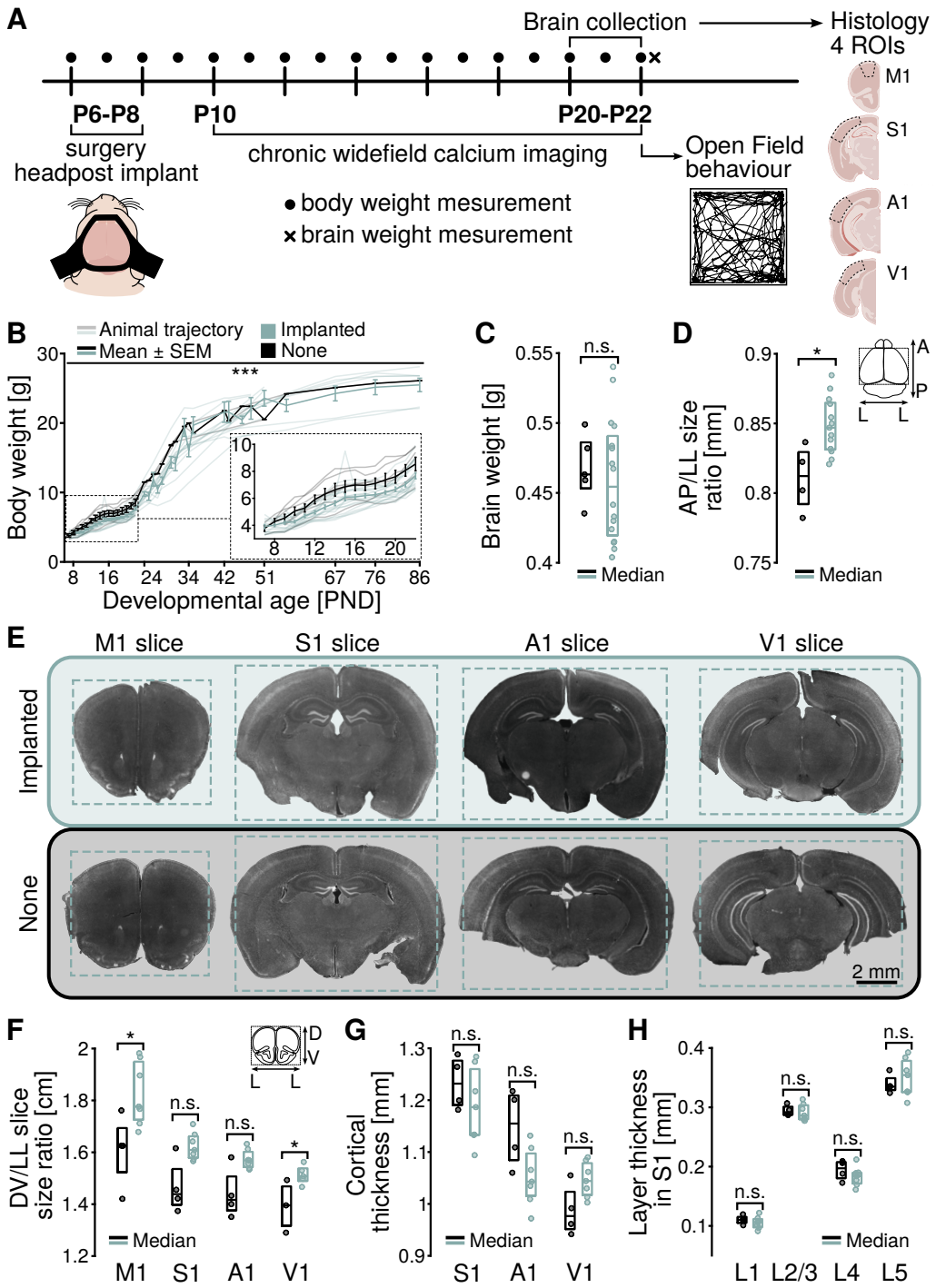

**Fig. 2.16 Assessment of the effect of the chronic implant on developmental growth A|** Schematic of the data collection timeline. **B|** There were significant differences in body weight (n = 25 animals) during development (p = 4.387e-34), but no significant differences were observed across protocols (p = 0.195), for implanted (n = 19 animals) and not implanted (n = 6 animals) groups, or the combined effect of age and protocol (p = 0.913). Significance tested by LMM. **C|** The brain weight after extraction at ∼P22 showed no significant difference between the implanted (n = 16 animals) and not implanted (n = 5 animals) groups (p = 0.620). Significance tested by a Wilcoxon rank sum test for equal medians ($Z$ = -0.4956). **D|** The anterior-to-posterior (AP) and lateral-to-lateral (LL) ratio, from the dorsal view of the brain showed a significant difference between the implanted (n = 13 animals) and not implanted (n = 4 animals) groups (p = 0.0151). Significance tested by a Wilcoxon rank sum test for equal medians. **E|** Representative coronal slices of the increase in AP/LL ratio seen as an elongation in the dorsal-to-ventral (DV) direction in the implanted mice. **F|** The DV and LL ratio of the coronal slices for all the different mice showed a significant increase for the implanted mice (n = 7 animals) in M1 (p = 0.0242) and V1 (p = 0.0242), but not in S1 (p = 0.0727) and A1 (p = 0.109), compared to the not implanted (n = 4 animals) group. Significance tested by a Wilcoxon rank sum test for equal medians. **G|** The cortical thickness showed no significant differences between the implanted (n = 7 animals) and not implanted (n = 4 animals) groups, for S1 (p = 0.412), A1 (p = 0.0727) and V1 (p = 0.0727). Significance tested by a Wilcoxon rank sum test for equal medians. **H|** The cortical layer thickness for the S1 region showed no significant differences between the implanted (n = 7 animals) and not implanted (n = 4 animals) groups, for L1 (p = 0.412), L2/3 (p = 0.527), L4 (p = 0.527) and L5 (p = 0.788). Significance tested by a Wilcoxon rank sum test for equal medians. Further statistical information in Annex 4.2. Box plots display the first quartile, median, and third quartile. Significance is shown for age as * for pval < 0.05, *** for pval < 0.001.

around each slice. These results showed a slight significant difference in this ratio (Figure 2.16, panel E) only for the M1 (p = 0.0242) and V1 (p = 0.0242) regions. The cortical and layer thickness was evaluated by examining the DAPI staining on ImageJ (Fiji). L1, was defined as adjacent to the pial surface with a scarce presence of cell bodies, followed by L2/3, which was between L1 and L4. L4 was recognisable by an increase in the number of cell bodies, while L5 was just below L4, displaying a higher density of cell bodies compared to L6. Neither the cortical nor the layer thickness showed any significant differences between the implanted and non-implanted pups (Figure 2.16, panels F and G). This suggested that, despite the possibility of slight changes in the growth direction, as indicated by changes in the ratios, the layers were able to develop similarly in both groups.

To examine the impact of the implant on behavioural development, the open field behaviour of chronically implanted mice at weaning age was tested. A square open field measuring 50 cm along each side was used, with the inner arena representing a 30 cm square in the centre. Animals were placed individually in the central area, and the area was recorded from a top-down view for 20 minutes. DeepLabCut (DLC version 2.2, Mathis et al., 2018) was employed for automated video tracking and analysis of the open field behaviour. To train the DLC network, frames from three different open field recordings were automatically extracted for labelling using k-means clustering to ensure a diverse and representative sample. The head, body, and tail base were labelled for each mouse. The labelled data was then augmented by flipping and rotating frames to increase the size and variability of the training set and to prevent overfitting. The network was trained using the default ResNet-50 architecture with 50 hidden layers and approximately 200,000 training iterations, while setting the learning rate to

0.0003. Cross-validation was performed to test the accuracy of the network, which correctly labelled the positions of the body parts with an average error of 3.94 pixels. This trained network was used to determine the positions of the body parts in the remaining recordings and then to extract the X and Y coordinates of the body marker. This allowed for the analysis of parameters such as the total distance travelled, the distance and speed ratio between the outer and inner arena, and the number of entries into the inner arena, which were used to evaluate anxiety and thigmotaxis, a behaviour that emerges before eye opening (Choleris et al., 2001; Bass et al., 2020). The results showed that none of the measured parameters were significantly affected by the implant, indicating no differences in anxiety and thigmotaxis between the implanted mice and their non-implanted littermates (Figure 2.17).

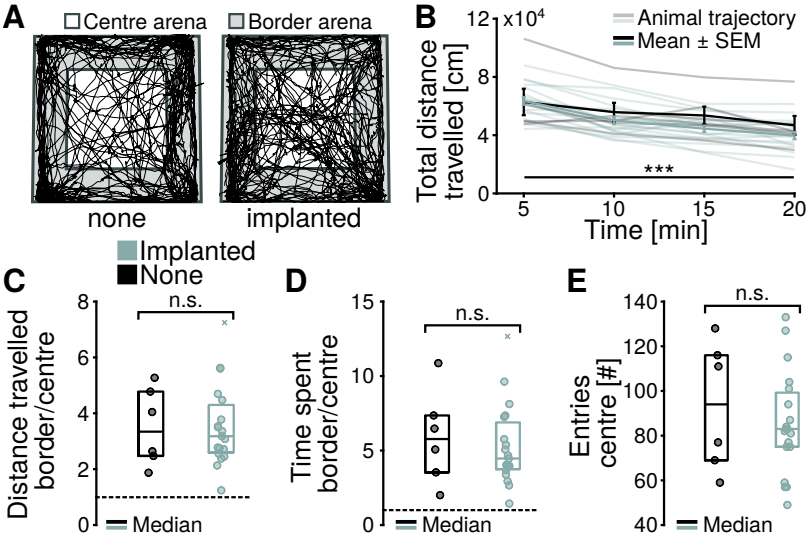


**Fig. 2.17 Open field behaviour of the chronic implanted animals after longitudinal recordings A|** Representative examples of open field trajectories for an implanted mouse and not implanted littermate. **B|** A significant difference was observed in the distance travelled during the recording (p = 1.222e-21), but no significant differences were observed across protocols (p = 0.259), for implanted (n = 19 animals) and not implanted (n = 6 animals) groups. Significance tested by LMM. **C|** The ratio between the distance travelled along the border compared to the centre (thigmotaxis ratio) was not significantly different between the implanted and not implanted groups (p = 0.824). Significance tested by a Wilcoxon rank sum test for equal medians ($Z$ = -0.223). **D|** The ratio between the time spent in the border compared to the centre was not significantly different between the implanted and not implanted groups (p = 0.874). Significance tested by a Wilcoxon rank sum test for equal medians ($Z$ = -0.159). **E|** The number of entries to the centre arena was not significantly different between the implanted and not implanted groups (p = 0.874). Significance tested by a Wilcoxon rank sum test for equal medians ($Z$ = -0.159). Further statistical information in Annex 4.2. Box plots display the first quartile, median, and third quartile. Significance is shown for recording time as *** for pval < 0.001.

## 2.4 Discussion.

This chapter presented a detailed protocol for chronic dual-colour neocortex-wide calcium imaging, including the adaptation of the setup for neonatal imaging, the protocol for surgical preparation, the data acquisition parameters and preprocessing pipeline. Using this protocol, transgenic animals expressing two different calcium indicators, GCaMP6f (green) and jRGECO1a (red), can

be longitudinally imaged across most of the dorsal neocortex. Imaging large-scale population dynamics using this approach has become increasingly popular in recent years due to its technical simplicity, affordability, and compatibility with genetically encoded sensors (Cardin et al., 2020; Machado et al., 2022). Additionally, this method has demonstrated high compatibility for early postnatal imaging, not only because it is minimally invasive and permits longitudinal recordings, but also because head fixation may not be as restrictive or stressful in early postnatal mice to record *in vivo* neural dynamics. This is due to the fact that neonatal mice spend a large portion of the time sleeping (Rensing et al., 2018), and will habituate naturally to the head fixation due to the repeated recordings, making within session habituation unnecessary.

### 2.4.1 Possible sources of the widefield fluorescence signals across early postnatal development.

Widefield calcium imaging is a single focal plane technique that provides a large spatial coverage at the expense of spatial resolution. As such, the fluorescence observed in each image pixel originates from thousands of nearby neurons from multiple cortical layers, making it challenging to identify the nature (soma, neuropil or passing-by axons) and specific laminar origin of the signal (Allen et al., 2017; Silasi et al., 2016; Waters, 2020).

Widefield imaging during early postnatal development poses additional challenges. Firstly, principal pyramidal and GABAergic neurons are still migrating and adopting their laminar position during the first postnatal week (Marín et al., 2003), especially the GABAergic population which experiences a protracted period of migration before reaching their final location within the cortex (Marín et al., 2001; Lim et al., 2018). The extended migration and ongoing growth and maturation processes indicate that the characteristics and the composition of the neuronal populations may be changing during the imaging period examined in this study. While most migration processes should be finished at the beginning of the second postnatal week (Lim et al., 2018; Luhmann, 2022), processes such as dendritic arborisation for both pyramidal (Petit et al., 1988) and GABAergic (Lim et al., 2018) neurons will continue and will be modified by sensory experience (Richards et al., 2020; Maravall et al., 2004), potentially altering their contributions to the signal. Consequently, the exact contribution to the widefield fluorescence of these different cell populations at each developmental stage is complex and completely unknown. One way to investigate this could be through the use of cell subtype and layer specific transgenic lines or viral approaches, which will allow to restrict the fluorescence expression to investigate population or layer specific changes in widefield fluorescence. However, this is a challenging approach, especially during development, due to the limited time for viral expression and lack of expression at early developmental stages of certain molecular markers used to identify neuronal classes (Hanson et al., 2022). A simpler way to tackle this issue would be to utilise computational modelling, akin to the one employed in this chapter, along with further information about the laminar organisation and expression profiles of the cell types of interest. This would allow a

detailed investigation of potential changes in widefield sources due to morphological and layer reorganisation during early postnatal development.

Secondly, the expression and stability of different promoters during development may affect the recorded signal. In this project, two different promoters, Gad2 and Thy1, were used to label distinct neuronal populations, GABAergic and pyramidal neurons respectively. The Gad2 promoter, which encodes the glutamic acid decarboxylase (GAD65), is expressed embryonically and presents a stable expression throughout postnatal development (Taniguchi et al., 2011). On the other hand, the Thy1 promoter, encoding for a cell surface glycoprotein, has shown to be developmentally regulated. The timing of this transgene expression in various neuronal populations is unclear, as the developmental expression profile of this promoter is mixed, going through spatial and temporal developmental waves of maturation (Wang et al., 2006). Some studies have observed postnatal labelling (Feng et al., 2000; Holtmaat et al., 2006), while others observed no expression during the first postnatal week (Wang et al., 2006). It is known that in Thy1 transgenic mice, expression patterns are strongly dependent on the transgene cassette integration site in the genome (Dana et al., 2018; Chen et al., 2012). Therefore expression time and patterns can differ greatly across lines. The Thy1-jRGECO1a mouse line came from the GP8.20 line, which showed highest density of cortical labelling (60%) with homogeneous labelling across all cortical layers in adult mouse brains (Dana et al., 2018). Although the developmental expression pattern of this mouse line has not been previously investigated, the line showed strong labelling across all cortical layers by the end of the first postnatal week (Figure 2.10, panel D), displaying widefield activity as early as P3 (data not shown).

The widefield fluorescent signal captured in the adult neocortex has revealed functional cortical patterns that are related to the activity of individual cortical and subcortical thalamic neurons (Xiao et al., 2017). This fluorescence signal captured is not limited to cell bodies of neurons, but also extends to their dendritic (Siegel et al., 2013) and axonal projections (Broussard et al., 2018), and these projections can represent activity correlates that may differ from the neuron's spiking activity, such as presynaptic activity, neuromodulator release or backpropagating action potentials (Ali et al., 2020). Moreover, while neuronal cell bodies are located in specific cortical layers and regions, their projections can traverse across layers and reach distant cortical areas not just in pyramidal neurons (Gerfen et al., 2018), but also in GABAergic ones (Urrutia-Piñones et al., 2022). A previous study showed that widefield fluorescence collected from pyramidal neurons located throughout all cortical layers primarily reflected the activity of the superficial L1 neuropil (Allen et al., 2017). The widefield signal was more correlated with L1 fluorescence, which comprises both potentially distal axonal inputs and local dendritic dynamics, than with that of L2/3, where the cell somatas lie. However, a recent modelling study challenged this conclusion (Waters, 2020). Specifically, the modelling of the widefield fluorescence of a mouse line expressing the fluorescence indicator only in superficial layers, showed that L1 contributed only <10% to the superficially observed fluorescence. Similarly, using a similar modelling

approach, this study found that the contribution of L1 to the total fluorescence signal was relatively small, with deep layers (L5) having the highest contribution (Figure 2.10, panel D).

In Waters, 2020, several potential explanations are discussed to explain the discrepancy between their model and the study by Allen et al., 2017. The model used the steady-state fluorescence of histological brain slices, whereas the study by Allen et al., 2017 used fractional changes in fluorescence ($\Delta F/F$), as it was *in vivo* fluorescence. This difference could have led to a bias towards relatively higher fluorescence in axons and distal dendrites, as they often display larger fractional changes than the somata (Xu et al., 2012; Larkum et al., 2007), and are major contributors to fluorescence signals in L1. However, to substantially change the contribution of L1 to the total fluorescence in the model, the steady-state fluorescence would need to increase 10 times in L1 to contribute approximately $\sim$40% to the signal (Waters, 2020), which is unlikely. Therefore, the model still predicts that L1 contributed a minority to the resting fluorescence and likely also of the fractional change in fluorescence in most mouse lines (Waters, 2020). As a result, the observed discrepancy could be due to differences in the expression pattern or the behavioural task monitored, which could be specifically involving L1 dendrites compared to L2/3 (Allen et al., 2017).

According to the model simulations, it is difficult to achieve finer spatial precision by changing hardware properties, given the nature of the technique. Higher magnification results in smaller FOV and vignetting, while illuminating a smaller region will not limit the excitation volume (Waters, 2020). The model predicted that a volume of $\sim$0.1 mm$^3$ and $\sim$1.5 mm$^3$ of tissue contributes to the observed widefield fluorescence for the GABAergic and pyramidal population respectively, resulting in resolution on the millimetre scale. To achieve higher spatial precision, the expression of the fluorescent indicator will need to be restricted to sparse cellular clusters (Kauvar et al., 2020), as well as the somatic compartment (Shemesh et al., 2020), to eliminate the contribution of dendritic or axonal processes to the emitted fluorescence. However, while the model does not account for temporal dynamics, such information can be leveraged to pinpoint active regions of the cortex using widefield fluorescence (Figure 2.18). Examples of high spatial resolution achieved using widefield fluorescence imaging include the localisation of the border between visual areas within tens of micrometers by driving converging waves of activity with visual stimuli (Zhuang et al., 2017), the precise tonotopic gradient in the auditory cortex with auditory stimuli at different frequencies (Romero et al., 2020), and the spontaneous patchwork activation of single barrels in early postnatal development with structures of <300 $\mu m$ (Ackman et al., 2014b; Mizuno et al., 2018).

The depth of imaging through the intact cleared skull using a macroscope is constrained by the scattering of light (refer to section 2.3.1 for further information) and the characteristics of the optics (refer to section 2.2.1 for further details). While positioning the focal plane deeper within the cortex can result in image blurring, it allows for greater fluorescence detection from deeper cortical layers. Consequently, the macroscope was adjusted to focus the z-plane just below the

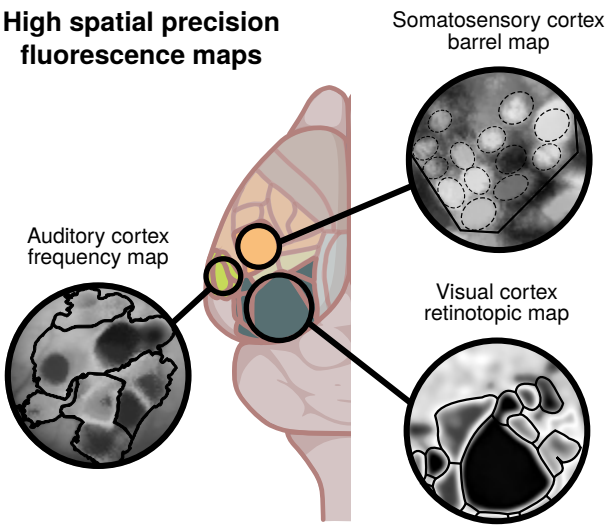


**Fig. 2.18 Examples of high spatial precision maps obtained with widefield calcium imaging.** A high resolution fluorescence-based retinotopic map derived from azimuth mapping in the visual cortex (Zhuang et al., 2017), a sound frequency map in primary and higher order fields of the auditory cortex (Romero et al., 2020), and a time projection map of spontaneous activity in the developing barrel cortex (Ackman et al., 2014b). Dashed line outlines single barrels.

surface of the skull. Given that the depth of focus of these type of setups is $\sim$200 $\mu m$ (Ratzlaff et al., 1991), the fluorescence captured should be primarily coming from this volume, which should include L1 and L2/3, and maybe part of L4, and will change slightly as the animals age. Moreover, given the curvature of the skull within the FOV, the focus might be differently centred in different regions across the dorsal cortex. Furthermore, as observed with the modelling, the highest contribution to the widefield fluorescence came form L5, followed by L2/3 and L4 (Figure 2.10, panel D); and therefore, developmental changes in the connection patterns of these layers could reflect the changes in the *in vivo* fluorescent dynamics (see section 3.4.4).

Taken together, widefield calcium imaging is capable of capturing the largest mode of ongoing brain activity, effectively representing the overall pattern of activity in a particular brain region or small patch of the cortex. This can act as a first step towards reducing the dimensionality of the data, which can reveal meaningful patterns of activity related to behaviour. Although there are trade-offs associated with this approach, as the signal will be generated from a large volume of tissue covering several millimetres and can come from multiple cortical layers; widefield imaging would be suitable for capturing the large events of synchronised activity that characterise early postnatal dynamics, particularly those cortico-cortically generated (Leighton et al., 2021; Siegel et al., 2012). Determining the relevant spatiotemporal scale for the dynamics of interest remains a challenge, as there is a debate on whether to focus on single-neuron dynamics or larger populations, and if the latter, whether cellular resolution or collective population dynamics are sufficient to understand behaviour. Ultimately, the choice of approach depends on the specific research question; however, it is still unclear whether single-cell resolution whole-brain recordings will be necessary to understand all known aspects of brain computation and behaviour. The example of *C. elegans*, where the entire nervous system has been mapped

but the understanding of its behaviour is still limited, highlights the need to explore different research questions and data modalities.

### 2.4.2 Validity of the preprocessing method.

The widefield imaging technique is challenged by a significant bottleneck, as it generates very large datasets that are difficult to preprocess, analyse, store and share. This not only leads to reproducibility issues but also causes the data to be underutilised, as it cannot be easily shared for further analysis. Recent computational advances in techniques such as dimensionality reduction and statistical modelling offer new opportunities for compressing, denoising and exploring the rich dynamics provided by widefield data (Urai et al., 2022; Cunningham et al., 2014; Weiser et al., 2021).

Although there is no consensus or standardised approach to analysing this type of data yet, the first step typically involves reducing the dimensionality (factorisation) of the data, since single pixel activity is not independent and is generally clustered in functional modules. These dimensionality reduction methods can also help with denoising the data. Factorisation methods generally attempt to represent the data as a collection of spatial and temporal components that can be used to reconstruct the original data. Popular methods include singular value decomposition (Musall et al., 2019) and non-negative matrix factorisation (Mojtahedi et al., 2021; Musall et al., 2023), while more traditional segmentation methods include seed-based correlations (Vanni et al., 2017), and functional clustering (Ackman et al., 2014b). While a direct comparison between these methods has not been made, they likely provide complementary information which needs to be interpreted based on the assumptions of the method employed.

For this project, a linear demixing method that combined PCA and ICA was employed (Weiser et al., 2021; Ren et al., 2021). The validity of this approach is based on three main assumptions: 1) Widefield signals can be separated into paired spatial and temporal components, supported by the organisation of the neocortex non-overlapping functional modules. 2) Signals from different motifs are statistically independent, supported by the fact that different neural motifs have distinct activity patterns, while mixed signals are caused by shared inputs or temporal dependencies. 3) Cortical motifs' spatial filters and temporal signals have skewed distributions, based on the fact that activity patterns of neural populations tend to be sparse and localised. PCA alone is not suitable for separating individual activity motifs as it relies on variance differences, which can lead to multiple motifs being combined into the same component due to similar amplitude variations in fluorescence across different cortical motifs. In contrast, ICA is capable of identifying motifs with significant signal correlations and separating them into independent sources of fluorescence. In this particular study, the sICA components were determined independently of the Allen CFF atlas (Wang et al., 2020), but they were later aligned to it for comparison purposes. While some other factorisation methods utilise the anatomical atlas to demix the data into components that correspond to specific brain regions (Saxena et al., 2020), this study

opted for independent determination of components with posterior alignment, to accommodate the brain's substantial growth during early postnatal development.

### 2.4.3 Control experiments to assess the longitudinal dual-colour imaging approach.

To perform dual-colour calcium imaging, two different calcium indicators with distinct emission spectra needed to be used, and which could be selectively expressed in two different neuronal populations. Typically, one of the indicators would emit in the green range while the other would emit in the red range. Using transgenic mouse breeding approaches, reporter mouse lines for green indicators, such as GCaMP6f, can be used in conjunction with cre-dependent driver mouse lines to express the indicator in a specific cell type of neurons (Daigle et al., 2018), while a second transgenic mouse line will be required to express the other indicator in a different population of neurons. This second line will need to use a different recombination mechanism, such as flp-dependent system (Ng et al., 2001), or would need to be a transgenic mouse line that already carries the calcium indicator under the promoter of choice, driving its expression in a specific cell population. The Thy1-jRGECO1a transgenic mouse line was the most readily available option with a red-shifted calcium indicator (jRGECO1a) expressed in cortical pyramidal cells (Thy1 promoter) (Dana et al., 2018), which had already demonstrated good performance in *in vivo* widefield studies (Montagni et al., 2018; Saxena et al., 2020).

The jRGECO1a indicator exhibits fast and bright dynamics, similar to GCaMP6f (Park et al., 2021), making it suitable for widefield imaging. However, it shows photoswitching behaviour when exposed to blue light (Akerboom et al., 2013; Dana et al., 2016), which can interfere with dual-colour imaging. The assessment of different blue light pulse frequencies on Thy1-jRGECO1a dynamics *in vivo* demonstrated a more pronounced photoswitching effect at low frequencies compared to higher frequencies(Figure 2.11, panel B). Short trains of high-frequency pulses caused an increase in the baseline (Figure 2.11, panel B, 33 Hz, Dana et al., 2016), while continuous blue light strobing resulted in a reduction of the baseline(Figure 2.11, panel D, Akerboom et al., 2013). Despite the seemingly contradictory effects observed, possibly due to the complex dynamics of the photoswitching conformational change, the results confirm the feasibility of using the Thy1-jRGECO1a line for dual-colour imaging.

Hemodynamic and movement-induced blood volume artefacts can distort neural signals, necessitating correction methods that utilise the hemoglobin absorption spectra (Ma et al., 2016; Valley et al., 2020; Ma et al., 2014). However, these methods often require additional light sources, which was not feasible for current imaging setup. As an alternative, blind source separation methods like sICA were explored. By applying sICA to widefield fluorescence data from GFP-expressing mice, vasculature-like motifs were identified and removed from the analysis (Figure 2.13, panel A), as they represented movement-induced fluorescence vasculature changes (Figure 2.13, panel C). While some fluorescence changes resulting from hemodynamics may

still remain, the influence of hemodynamics on the fluorescence signal was found to be limited. Stimulation of the whisker field did not elicit a clear hemodynamic response in the contralateral S1 barrel area (Figure 2.13, panel C), supporting previous findings of minimal hemodynamic effects on the fluorescence signal (Allen et al., 2017; Makino et al., 2017; Musall et al., 2019; Vanni et al., 2014). Moreover, a recent study determined the influence of hemodynamics on sICA components using the UV-light approach to remove calcium-independent changes of fluorescence in the data, observing that the blood flow changes have minimal effect on the segmentation and network connectivity of sICA (West et al., 2022). Although simultaneous widefield calcium and fMRI studies have shown similarities and divergent responses between the two types of responses (Vafaii et al., 2023), for the purpose of this project, and given the uncoupling of these two dynamical components in neonatal mice (Kozberg et al., 2016), the contribution of blood flow to the fluorescence signal is minimised by removing components that show a vasculature-like pattern.

The strong expression of GECIs in certain cell types or brain regions, perhaps specifically during early development, has shown to contribute to aberrant activity in the brain, which can complicate the interpretation of the data (Steinmetz et al., 2017). Therefore, the occurrence of abnormal activity in the brain using the Thy1-jRGECO1a/Gad2/GCaMP6f mouse line, which labelled pyramidal and GABAergic cell populations. Acute epileptiform events were induced in the S1 barrel area, and their properties were analysed to understand their prevalence in longitudinally recorded mice. During early postnatal development, the prevalence of these events was consistently less than 1% for both populations (Figure 2.15, panel C), and no events with durations faster than 200 ms were detected, which is the characteristic length of this abnormal activity according to its original definition (Steinmetz et al., 2017). While some events seen in the Thy1-jRGECO1aGad2/GCaMP6f line were identified as resembling epileptic activity, caution should be taken in interpreting these results, as the classification of events is not strict and changes in their properties during development could confound the findings, especially considering the general increase in event frequency during this period (Colonnese et al., 2010; Colonnese, 2014).

Longitudinal recordings can increase the statistical power of observations and reduce the number of animals required for research. Therefore, validating the chronic implantation of the headpost for longitudinal studies was crucial. The surgical procedure for implantation was optimised to ensure proper recovery of the pups and their return to the nest for care by the dam. The implantation of the lightweight headpost did not significantly impact pup development, as measured by weight gain and cortical layer distribution for proper brain growth (Figure 2.16). However, it had a minor effect on the direction of brain growth, which was slightly restricted laterally due to the large window and implant on the dorsal surface of the skull. This was compensated by an increased AP and DV length (Figure 2.16, panel D, E). Additionally, the implant had no impact on pup behaviour, as measured by the open field test (Figure 2.17). Thus, this demonstrated the efficacy of this approach for repetitive recordings during early

postnatal development, and even into early adulthood. A similar method has been developed for longitudinal two-photon imaging (Che et al., 2021). The ability to record activity dynamics reliably and longitudinally in neonatal mice without disrupting their growth and behaviour opens up a wide range of research opportunities to study this crucial period of intense brain reorganisation.

### 2.4.4 Limitations of dense labelling widefield calcium imaging.

Multi-region, widefield fluorescence imaging techniques offer a powerful means of studying large-scale brain dynamics, which are thought to provide the basis for behaviour and cognition, with high spatial coverage and temporal resolution (Cardin et al., 2020). However, this technique has several limitations, particularly regarding its spatial resolution and imaging depth, which should be taken into account when considering the research question and interpreting the findings. Nevertheless, recent attempts have been made to integrate this method with other techniques, such as 2-photon microscopy or electrophysiology, which allow to simultaneously study both micro- and macroscale networks (Lake et al., 2022).

The spatial resolution is limited by light scattering through the tissue. As a result, it can be challenging to differentiate signals from individual neurons in large brain regions, which restricts the ability to study fine-scale neural activity patterns. Although it provides a large spatial coverage, capturing a significant portion of the dorsal cortex, more lateral regions like the auditory cortex, or regions deep along the midline, generally remain unobserved. Additionally, the penetration depth of the excitation light is typically limited to around 200 $\mu m$, and while the light collected on the surface can come from a large underlying tissue volume, this further limits the ability to study deeper structures, like the hippocampus and thalamus. Although genetically-encoded calcium indicators provide high sensitivity and SNR, they only provide an indirect measure of neural activity, and the relationship between changes in calcium levels and action potential firing is not well understood (Huang et al., 2021). Some studies show qualitative agreement in static and relatively coarse measures (Stringer et al., 2019a; Chen et al., 2013), while more refined measurements can reveal diverging results (Wei et al., 2020). The technique's temporal resolution is also limited due to the indicators' temporal dynamics. Although the high sensitivity of calcium indicators used in this project, GCaMP6f and jRGECO1a, allows the detection of high frequency events and fast dynamic response (Dana et al., 2016; Helassa et al., 2016), they can only capture changes in dynamics in the order of 100 milliseconds, which limits their ability to resolve sub-millisecond changes in neural activity that may be important for understanding certain aspects of brain function.

Furthermore, fluorescent indicators can introduce other technical challenges such as phototoxicity and photobleaching, which can limit the length of experiments as well as the accuracy of the data. Since calcium indicators sequester the intracellular calcium, they can alter calcium dynamics and prevent normal interaction with the cellular machinery (Helassa et al., 2016). Some transgenic lines have shown aberrant cortical activity due to the expression of these

calcium indicators (Steinmetz et al., 2017), so it is crucial to verify that the GECIs are not affecting the mouse lines' normal development. Another main technical drawbacks of this technique is the limited control of the illumination size. The reason for this is that a large illumination area is necessary to cover the entire exposed dorsal cortex. However, due to the curved shape of the skull, not all areas of the imaging surface will be in the same focal plane. This results in a blurred image for fluorescence that is out of focus, generally on edges of the skull, as it is not possible to have the entire FOV simultaneously in focus. To address this issue, a recent approach has been developed that employs a dual lens system (Kauvar et al., 2020). This system allows for two focal planes, one centred on the sagittal sinus and another on the most lateral areas in FOV, which improves the quality of the images. A further limitation is that the imaging is limited to head-fixed animals, which may result in behavioural alterations due to stress and helplessness (Juczewski et al., 2020). Although, there are automated systems available for task training and longitudinal monitoring of mesoscale cortical circuits using home cages, which could reduce such alterations (Murphy et al., 2020; Murphy et al., 2016), they are not suitable for neonatal mice.

Although there are limitations to widefield calcium imaging, it still offers important advantages such as high spatial coverage, specificity, and easy manipulation of recorded neuronal populations, making it suitable for evaluating large-scale brain dynamics.

### 2.4.5 Closing remarks.

Understanding brain function and behaviour requires the investigation of multi-region dynamics. Several techniques, such as multi-electrode arrays and mesoscale fluorescence imaging, have been developed to explore these dynamics, each with its advantages and limitations.Therefore, it is essential to consider these factors when choosing the appropriate method to address specific research questions. Widefield calcium imaging is a minimally invasive technique that allows for the evaluation of large-scale activity patterns longitudinally, providing a means for identifying functional networks and their evolution during early development. Furthermore, it allows for cell specificity and easy manipulation of neuronal populations, making it suitable for evaluating the contribution of different populations to the neocortex-wide dynamics. By characterising the typical developmental trajectory of these dynamics, further insights can be gained into how neurodevelopmental disorders arise and identify potential targets for intervention.

# 3

# Characterisation of developmental neocortex-wide spontaneous activity patterns

Although molecular cues guide the initial formation of cortical architecture, patterned spontaneous activity has been shown to play a crucial role in the formation and refinement of neural circuits during early development (Kirkby et al., 2013; Nakazawa et al., 2021). Disruptions of the activity patterns can have long-term consequences (Zhang et al., 2011a). Given the importance of this period, it is key to understand the *in vivo* developmental trajectories of spontaneous activity across brain structures to gain a more comprehensive understanding of the formation of these highly recurrent and interconnected networks. One way to achieve this is through the use of chronic imaging of brain activity in awake mice across the entire neocortex during early postnatal development. This approach allows for a comprehensive description of the spatiotemporal activity patterns in the developing neocortex, effectively bridging the gap between traditional physiological and functional neuroimaging techniques, and thereby offering a broader scope that can encompass both, microscopic and macroscopic resolutions.

## 3.1 Introduction.

The mammalian cortex exhibits spontaneous activity patterns during early postnatal development that play a crucial role in shaping the structural and functional organisation of the brain (Ackman et al., 2012; Leighton et al., 2016; Tritsch et al., 2007). Before the onset of sensory experience, developing circuits spontaneously generate synchronised activity that will not only influence and guide its wiring (Kirkby et al., 2013; Leighton et al., 2016; Triplett et al., 2018), but ultimately contribute to behaviour (Luczak et al., 2013). These complex functions are thought to rely on widely distributed cortical networks that simultaneously operate in multiple spatial and temporal scales to process sensory inputs and perform motor and cognitive tasks (Panzeri et al., 2015; Quairiaux et al., 2011; Wekselblatt et al., 2016. Although numerous studies have assessed the morphological and functional development of local connectivity in cortical microcircuits (Che et al., 2018; Duan et al., 2020; Griguoli et al., 2017; Modol et al., 2020), the dynamics of the functional maturation of cortical networks at the large-scale level have rarely been investigated (Ackman et al., 2014b; McVea et al., 2017; Mojtahedi et al., 2021; Linden et al., 2021).

### 3.1.1 Spontaneous activity during early brain development.

Spontaneous activity, or ongoing activity, is generally referred to as activity that occurs in the absence of an active external sensory input. In other words, it is the activity that occurs when the brain is at rest or during spontaneous behaviours. Given this definition, the majority of the activity in the brain is spontaneous, and this type of activity has been observed in virtually every region of the brain (neocortex, thalamus, spinal cord, cerebellum, and hippocampus, etc.) in every species studied (Yamada et al., 2010). However, given its nature, spontaneous activity has been difficult to study experimentally *in vivo* since it cannot be time-locked to a specific stimulus or easily manipulated in a controlled manner, so its functional role remains largely unknown. Nonetheless, this non-random activity has unique spatiotemporal patterns that have shown to have a strong influence on a wide range of processes, including those involved in brain development (Thivierge, 2009; Colonnese et al., 2012; Luhmann et al., 2016). In fact, the structure of spontaneous activity during development is critical for the proper establishment of neuronal circuits (Leighton et al., 2016; Kirkby et al., 2013; Yamamoto et al., 2012). For example, the attenuation of spontaneous oscillatory activity after ablation of subplate neurons prevents the development of the barrel-like appearance in the primary somatosensory cortex (Tolner et al., 2012). Thus, changes and aspects of this type of activity will provide essential information on how the neuronal circuits are established, making the study of spontaneous activity a crucial area of research.

There is a growing appreciation of the intricate spatiotemporal dynamics of spontaneous neuronal activity observed in the *in vivo* perinatal brain (Figure 3.1), from the propagation of spontaneous retinal waves all the way to the visual cortex (Ackman et al., 2012; Gribizis et al., 2019), to the somatotopic activation of somatosensory cortex in neonatal rodents in response to the spontaneous twitching of individual whiskers (Tiriac et al., 2012). These activity patterns are related to the functional organisation of the cortex and show spatial diversity, both laminar (Sakata et al., 2009) and regional (Martini et al., 2021), which dynamically changes over time as the cortex matures (Nakazawa et al., 2021). During early postnatal development, there are distinct phase transitions that lead to the sparsification of spontaneous activity patterns (Golshani et al., 2009; Luhmann et al., 2018; Modol et al., 2020; Colonnese et al., 2010). These transitions are associated with critical periods of plasticity in sensory circuit development, particularly in the primary somatosensory cortex of rodents (Nakazawa et al., 2021). In this cortex, the spatial organisation of spontaneous activity undergoes two notable transitions (Nakazawa et al., 2021). Initially, cortical spontaneous activity exhibits a patchwork-like spatial pattern corresponding to the barrels, which is driven by thalamocortical inputs (Mizuno et al., 2018). As development progresses, spontaneous activity becomes less dependent on thalamocortical inputs and transitions into synchronised activity across all barrels (Nakazawa et al., 2020), eventually reaching adult-like sparse firing patterns (Mizuno et al., 2018; Nakazawa et al., 2020; Golshani et al., 2009).

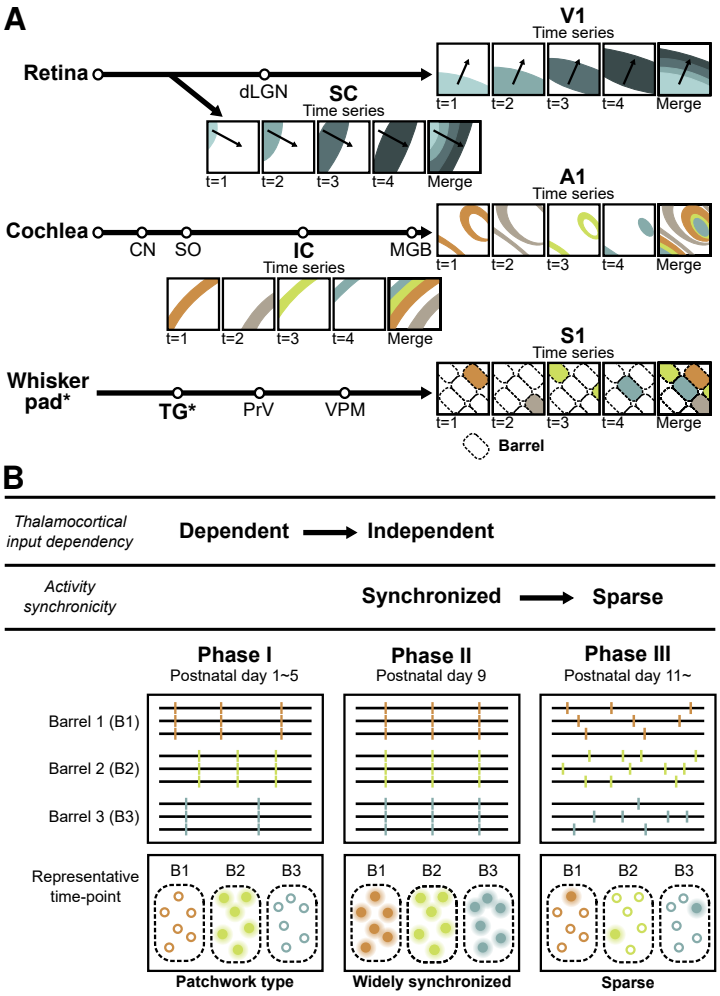


**Fig. 3.1** **Modality-specific spatial organisation of spontaneous neuronal activity in the sensory systems during early developmental stages**. **A|** During early developmental stages, sensory systems exhibit spontaneous activity that is derived from the periphery and transmitted to the brain, and displays modality-specific spatial organisation. In the visual system, spontaneous activity arises from the retina and is transmitted to the superior colliculus (SC) and primary visual cortex (V1), propagating tangentially like a wave. In the auditory system, spontaneous activity arises from the cochlea and is transmitted to the primary auditory cortex (A1), where neuronal activity is confined to bands aligned along the same tonotopic axis, before hearing onset. In the barrel region of the primary somatosensory cortex (S1), spontaneous activity displays "patchwork-type" firing which corresponds to the underlying barrel map, and that originates from the whisker pads and trigeminal ganglia, transmitting via trigeminal principal nucleus (Prv) and ventral posteromedial nucleus (VPM). **B|** The organisation of spontaneous activity in the rodent S1, particularly that of L4 glutamatergic neurons, changes during postnatal development, with two distinct mechanisms: termination or reduction of thalamocortical input-dependency and sparsification. Phase I (P1-P5) exhibits barrel map firing driven by thalamocortical inputs. Phase II (P5-P9) exhibits synchronised activity across the barrels independent of thalamocortical inputs. Phase III (P9-P11) exhibits sparse firing with loss of synchronisation across the barrel field. Adapted from Nakazawa et al., 2021.

Therefore, spontaneous activity in the brain can be indicative of its underlying connectivity, whether it is anatomical or functional. The structured patterns of spontaneous activity observed in various sensory cortices, such as the visual, somatosensory, and auditory cortex, correspond to the presence of functional sensory maps, even before the onset of active sensing. There-

fore, investigating spontaneous activity provides a means to gain insight into the underlying connectivity of the developing brain and the formation of functional sensory circuits.

### 3.1.2 GABAergic interneurons shape the functional maturation of the cortex.

Activity associated with specific brain functions tends to emerge within spatially discrete cortical domains, but these patterns increasingly integrate with activity in other cortical areas as the brain develops (Tritsch et al., 2007; Ackman et al., 2014b). As mentioned above, postnatal cortical activity patterns vary with age and cortical region (Ackman et al., 2014b), reflecting different developmental trajectories of the neural circuitry within them (Dehorter et al., 2012). The maturation of GABAergic signalling has been shown to play a key role in the functional development within individual cortical areas (Modol et al., 2020; Duan et al., 2020; Le Magueresse et al., 2013; Luccioli et al., 2018; Hensch, 2005; Fagiolini et al., 2000). Many of the mechanisms involved in this process, including the switch from excitatory to inhibitory GABA and formation of cell-specific GABAergic synapses, are common across cortical regions so far studied (Le Magueresse et al., 2013; Frye et al., 2016). However, the timing of GABAergic maturation seems to be aligned to the different developmental trajectories of each region (Murata et al., 2019). Changes in the inhibitory circuit function seem to be essential for the optimal inhibitory-excitatory balance during the critical period plasticity (Lo et al., 2017; Deidda et al., 2015a; Maffei et al., 2010), hence fundamentally modulating local cortical circuit refinement. Still, this leaves open the question of how and when maturation of GABA signalling contributes to the inter-regional interactions that form the basis of cortex-wide functional networks.

GABAergic neurons are very diverse and they originate from a different source than the excitatory projection neurons that make up the majority of the neurons on the brain (Lim et al., 2018; Kepecs et al., 2014). These interneurons exhibit early structured population dynamics, primarily driven by the activity of prospective PV+ interneurons, which leads to the coordination of local cortical networks with sensory signals (Modol et al., 2020; Duan et al., 2020; Kastli et al., 2020). Given the importance of GABA maturation on local circuit function, one can hypothesise that it will also shape development of cortex-wide network activity. Furthermore, a small but important population of GABAergic neurons are long-range, making synaptic connections in distant target areas (Zurita et al., 2018; Tomioka et al., 2005; Urrutia-Piñones et al., 2022; Tamamaki et al., 2010; Caputi et al., 2013). Such neurons have potential for great influence in the development of coordinated activity across regions within large networks (Bonifazi et al., 2009). Very interestingly, some GABAergic cells form transient, non-static circuits during development, that are fundamental for the sensory awakening of the neocortex (Marques-Smith et al., 2016; Anastasiades et al., 2016; Tuncdemir et al., 2016). This transient circuit comprises deep SST+ interneurons that receive input from the thalamus and relay the information to the L4 pyramidal cell, being key for sensory integration. These inhibitory motifs could be modality specific, meeting the processing needs of different brain regions (Kätzel et al., 2011). This is critical to understand the origin of neurodevelomental disorders because the manipulation of

the GABAergic activity can have a different impact across distinct brain areas (Hanganu-Opatz et al., 2021). Therefore, it is key to understand how GABAergic dynamics affect the brain-wide communication and how is the information integrated across brain regions.

### 3.1.3 Aims and research questions.

As reviewed above, the functional development of individual regions of the cortex have been extensively investigated (Khazipov et al., 2004; Kirischuk et al., 2017; Duan et al., 2020; Modol et al., 2020), while the development of regional interactions and global cortical activity is underexplored, particularly, the influence of GABAergic interneurons on the development of the neocortex-wide (mesoscale) functional networks. No single region develops in isolation, therefore, this chapter aims to shed light on the dynamic and spatiotemporally organised nature of spontaneous activity in the developing neocortex of the two main groups of cortical neurons, glutamatergic pyramidal neurons and GABAergic interneurons, and its potential role in shaping the formation of sensory circuits.

An important technical challenge is to provide high spatial and temporal resolution simultaneously, together with genetic specificity to be able to ask specific questions about large-scale development of diverse neuronal populations and how those trajectories interact. The use of dual-colour widefield calcium imaging offers an opportunity to explore the development of neocortical networks in awake neonatal mice with high spatial and temporal resolution.

Three principle research questions will be addressed:

- Does maturation of the mesoscale spontaneous GABAergic activity mirror that of neocortex-wide pyramidal functional networks?
- How does the engagement of specific specific cortical regions in large-scale functional networks change across development?
- How does the interplay between activity of pyramidal and GABAergic neurons change across brain regions as the brain develops?

## 3.2 Methods.

All data analysis and calculations presented in this thesis were performed using MATLAB (MathWorks).

### 3.2.1 Database summary.

The imaging data comprises chronic recordings of 14 animals throughout early postnatal development, ranging from P10 until P22, with one litter recorded until early adulthood. The animals' genotypes include single transgenic (Thy1-jRGECO1a, n = 4), double transgenic (Gad2-GCaMP6f, n = 8), and triple transgenic (Thy1-jRGECO1a:Gad2-GCaMP6f, n = 3) mice. Younger animals (P6 - P8) were also acutely recorded, all of them being triple transgenic mice (Thy1-jRGECO1a:Gad2-GCaMP6f, n = 6, 3 per age). The imaging sessions were conducted on even ages (postnatal days), with one session per day. Each session consisted of at least 3 recordings of approximately 6 minutes each, including 2 spontaneous recordings and 1 whisker stimulation recording (not used in the current project), with at least 5 minutes of rest between each recording. To allow the animals to habituate to the LED light flickering sequence, a "sham" recording was conducted without collecting any data in each recording session. The sessions were kept as short as possible to reduce the time the mice were away from the dam. Mice were taken from its home cage for approximately 1 hour, including both the "habituation" and the recording period.

### 3.2.2 Breeding the triple transgenic mice.

Animal care and use was performed in compliance with the Animals Scientfic Procedures Act (ASPA) 1986 and Amendment Regulations 2012 as outlined in UK law and approved by the University of Bristol Animal Welfare and Ethics Review Board (AWERB). All mice were housed in breeding pairs on a 12-hour light/dark cycle with food and water available *ad-libitum*. Experimental animals were both male and female neonatal mice ranged in age generally from 6 to 22 days (P6-P22, P = postnatal day), which corresponds to a period of profound cortical maturation, with some of them living into adulthood. Pregnant dams were checked daily for pups before 12 pm and the day of birth was considered as P0.

In order to perform the dual-colour imaging experiments, a genetic strategy was followed to label two different neuronal populations. Mice expressing simultaneously the jRGECO1a indicator (derived from mApple, Dana et al., 2016) and GCaMP6f, in pyramidal and GABAergic cortical neurons, respectively, were generated by crossing three transgenic lines (Figure 3.2, panel A). First, heterozygous Thy1-jRGECO1a mice (JAX stock #030525, Dana et al., 2018), expressing the red-shifted calcium indicator in pyramidal neurons, were bred with homozygous Ai95D floxed GCaMP6f reported mice (RCL-GCaMP6f, JAX stock #024105, Madisen et al., 2015), containing the green calcium indicator. Half of the offspring of this first crossing will carry both transgenes, Thy1-jRGECO1a:loxP-GCaMP6f-loxP, and was subsequently bred with the homozygous cre-dependent GAD2-IRES-cre mice (JAX stock #028867, Hwang et al., 2017), with 1/4 of the offspring being the triple transgenic, Thy1-jRGECO1a:loxP-GCaMP6f-loxP:GAD2-IRES-cre. The background of all transgenic lines was C57BL/6J. This approach allowed to simultaneously image the activity dynamics of pyramidal and GABAergic cell populations, without singling any

specific cell subtype. The experimental yield for the triple transgenic breeding strategy was very close to the theoretical one (Figure 3.2, panel B), although it varied slightly per litter (Figure 3.2, panel C). Breeding was devised and monitored to ensure a steady supply of neonatal mice, including both genders as the experimental cohort.

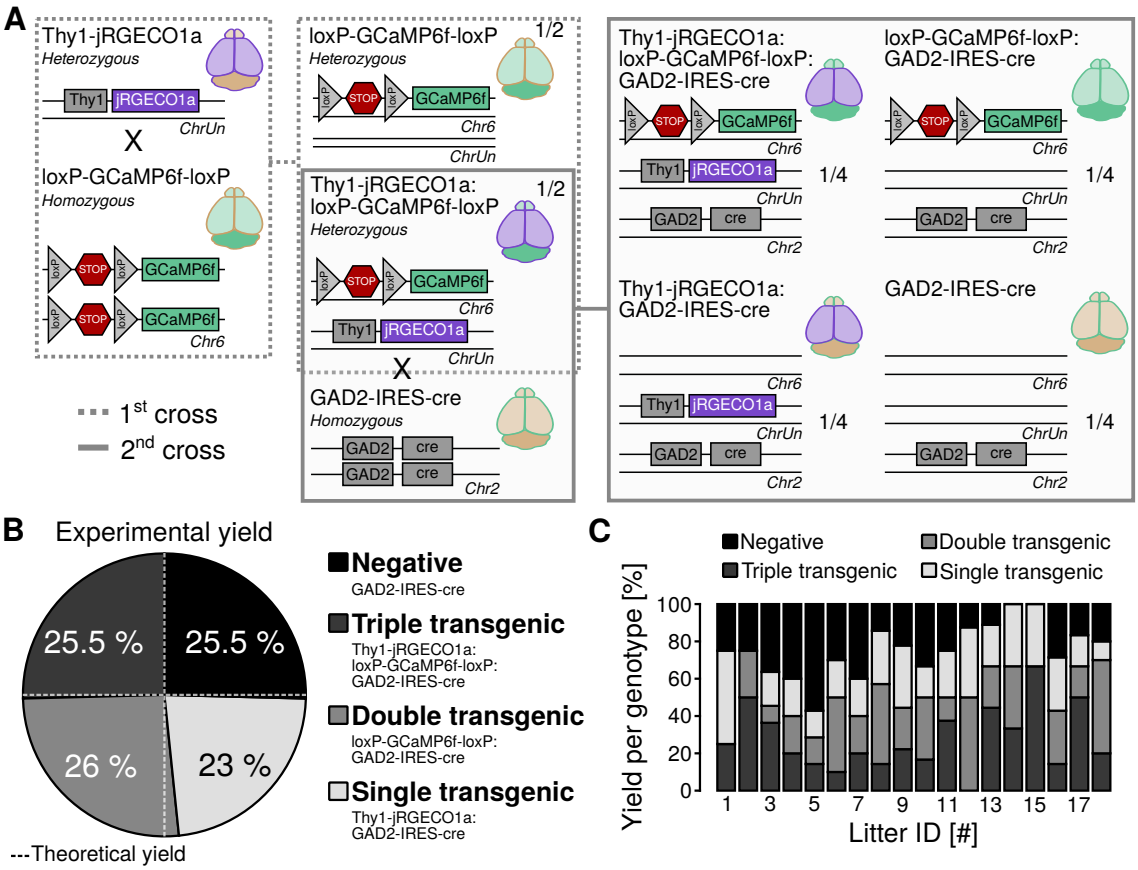


**Fig. 3.2** **Breeding of the triple transgenic mouse line and experimental yield. A|** Illustration of the first and second mouse line crossings performed for the triple transgenic breeding. It displays all possible combinations of offspring and their corresponding theoretical yields, which are 1/2 for the first crossing and 1/4 for the second crossing. **B|** Average experimental yield for the triple transgenic breeding (second crossing, n = 130 animals from 18 different litters). **C|** The yield of triple transgenic genotypes per litter is presented to demonstrate the variability of genotypes within each litter.

Genotyping was performed by Transnetyx using real-time PCR in tissue samples obtained when mice were ear tagged before weaning at $\sim$ P14-16 or by collecting tail tip samples at the end of an experiment, in accordance with Home Office (HO) regulations. Alternatively, the genotype of experimental animals was initially checked at birth by using a dual LED flashlight and matching barrier filter glasses (Nightsea, USA) shining through the skin and skull to visualise the emitted fluorescence, or after removing the scalp before an experiment. The fluorophores were bright enough to be detected through the skull and/or dissected brain after P6.

In addition to the genetic mouse lines involved in the breeding of the triple transgenic, a fourth line, TCA-RFP, was used to examine the patterns of thalamocortical axon terminals on the dorsal cortex that allow to outline and define the primary sensory cortical areas during mouse

postnatal development. The parcellations from this reference map are aligned and scaled to the adult Allen brain atlas (Wang et al., 2020) to obtain the reference coordinates for each cortical area. The TCA-RFP line was kindly provided by Iwasato's lab and was created as described in Arakawa et al., 2014; Mizuno et al., 2014; Mizuno et al., 2018.

### 3.2.3 Surgical preparation to image through the intact skull.

A detailed explanation of the surgical procedure can be found in section 2.2.2. To summarise, all chronic surgeries were performed in batches, with the exception of one animal per litter, which was kept as a developmental control. The maximum number of pups per litter was limited to a maximum of 6 pups to prevent food competition. The pups were briefly anaesthetised with isoflurane to remove the sterilised scalp and expose the skull's surface, creating the imaging "window". A custom head-post was then fixed with optically clear cement. Pups were allowed to recover for 5 minutes under 100% oxygen. The entire surgical procedure took $\sim$ 10 minutes per animal. After surgery, the pups were left to recover while the rest of the litter underwent the same procedure. The recovery period lasted approximately 1.5 hours in total. The control pup was removed from the home cage before returning the implanted pups back to the dam, and it was kept away from the dam ($<$ 1.5 hours) during the re-homing process, to prevent the dam from favouring the non-implanted pup and equalise the stress associated with food deprivation. The dam's behaviour towards the pups was closely monitored for at least the next 2 hours and during the following day to ensure proper feeding. Surgery for acutely imaged pups followed the same protocol, but the pups were not returned to the home cage and were terminated at the end of the imaging session. Pups were chronically implanted not earlier than P6-P7 and they were allowed to recover for at least 2 days before the first imaging session.

### 3.2.4 Picrotoxin injections.

For intracortical injections, additional surgical steps were taken following the acute widefield imaging preparation. Firstly, once the optically clear dental cement dried, a small craniotomy (<2mm) was made above the theoretical location of the left/right barrel cortex using a fine stab knife. Gelfoam soaked in cortex buffer was then used to cover the craniotomy and keep the brain moist. A glass micropipette, pulled using a horizontal puller (P-87, Sutter Instrument Co.), was used for the injections. The micropipette was primed with double distilled water, a 300 nL air bubble to monitor the injected volume, and backfilled with the appropriate drug or vehicle. The injection was performed at a rate of 50 $\mu L$/min, approximately 200 $\mu m$ below the pial surface, injecting a volume of 250 nL. Before, the injections, a control recording without vehicle or drug was conducted, followed by the vehicle, saline (0.9% sodium chloride) and then the drug, 200 $\mu M$ picrotoxin (PTX) in cortex buffer, injections on the same animal.

### 3.2.5 Protocol for widefield calcium imaging of spontaneous activity.

The imaging session generally consisted of 3 imaging blocks, 2 of those being recordings of 12,000 continuous frames, acquiring a total of 12 min of spontaneous data per animal. Across all 14 chronic mice and 6 acute mice and all ages, a total of 1,680 min of spontaneous activity were recorded. The order and timing of the blocks was kept consistent across subjects, following the sequence spontaneous-(whisker)-spontaneous. For all recordings, the mouse was "habituated" to the recording setup and head fixation system, as well as the experimenter, to avoid stress while imaging. Initially, the mouse was allowed to explore the setup area for around 10 minutes to become familiar with the smells. Next, the mouse was headfixed on the clamping system and given a 2-minute period to adapt. This process was repeated at least twice. If the mouse exhibited any signs of distress while being clamped, it was immediately removed from the fixation system and the habituation process was restarted. As the mice were imaged longitudinally, they became increasingly accustomed to the setup, thus reducing the required habituation time. All recordings were done under the heated blanket (37°C) and a piezoelectric wafer was placed under the pup's torso to record gross body movements. The imaging setup and acquisition parameters are explained in detail in section 2.2.1. All image stacks were captured using Micromanager software at 16-bit 960x540 pixels (2 x 2 digital binning) at 33.3 Hz frame rate.

### 3.2.6 Preprocessing of widefield calcium imaging data.

The preprocessing pipeline, described in detail in section 2.2.3, was applied to image data from all recordings. Highlighted below are some additional information on preprocessing steps relevant to this chapter.

#### Spatial registration and image alignment.

The preprocessed images from the different days and animals were spatially registered across channels and to a common framework to ensure the intra- and inter-indvidual correspondence of the ICA motifs. For dual-colour recordings, channels were aligned to one another, having the green channel as the reference, due to higher vasculature contrast, and the red channel as the moving image. Within each recording session, recordings for each channel are aligned to the first recording of that session. The process involved an automated geometric similarity transformation with a multimodal optimiser. The registration was done by means of the vasculature, which was exposed by subtracting the median filtered image. The different recordings across animals and ages are aligned to the Allen CCF adult reference atlas (Wang et al., 2020) employing user-defined anatomical landmarks (sagittal suture, base of the olfactory bulbs, bregma and the cerebellar suture). This allows the spatial registration of all animals to the same space to aid their comparison.

### Exposed cortical surface and brain masks.

A brain mask was defined by drawing the outline of the visible exposed skull on the average frame of one of the channels, preferably GCaMP6f, from the first recording of the session. Since every recording per session was registered to this first recording, the same brain mask was applied to all recordings for each animal within one session. Brain masks were drawn for each animal and age group individually, even though the exposed area (the "window") within the same animal was fixed across ages. Although the size of the exposed cortical surface may vary slightly due to surgical variability at opening the window, it generally exposes the base of the olfactory bulb and the cerebellar sutures, which are required for atlas alignment.

### Baseline fluorescence and PCA/sICA.

The procedure for fluorescence baselining and PCA/sICA is explained in detail in the previous section 2.2.3. A few key points will be highlighted here. The global temporal mean, which is the average fluorescence intensity across all pixels over time, was subtracted from the baselined recording ($\Delta F/F$) prior to PCA/sCA decomposition. The components identified by the PCA/sICA were manually classified into the three different categories: neural signal, artefact and noise, by assessing both the spatial pattern and the temporal dynamics. The spatial pattern of each activity motif was filtered using a 2-D Gaussian smoothing kernel with standard deviation of 1, and thresholded to create a mask of the spatial activation of the motif.

The threshold was calculated individually per motif using Otsu's method, iterates through a range of possible threshold values and calculates a measure of dispersion for the pixel intensities on both sides of the threshold, corresponding to foreground and background regions. It computes an optimised threshold value where the sum of foreground and background measures is minimised. Pixels above the threshold are considered active and therefore included in the mask, while the remaining areas are excluded or masked out. This binary mask can divide the image into distinct active regions or blobs, which represent areas of neuronal activity that have been detected based on their intensity levels surpassing the threshold. The masked image was analysed for each motif to determine the number of distinct blobs present. In cases where there were multiple blobs, indicating multiple active areas, individual masks were generated for each blob to ensure that each mask represented a single activity motif. Masking was done independently per motif and across genotypes.

Using the PCA/sICA method, the activity was decomposed into spatial motifs, with their corresponding spatial weights, as well as the time courses (temporal weights) associated with each motif. The units of these weights are arbitrary, but they can be converted back to fluorescence values by calculating the dot product between the spatial and temporal motifs, which allows for the reconstruction of the original signal.

### Photobleaching and temporal filtering.

In section 2.2.3, the effect of bleaching was explored, showing that any differences between the two indicators disappeared after filtering the mean (Figure 2.9). The filter used was a 0.1 Hz zero-phase, second-order Butterworth temporal high-pass filter. Filtering was only applied to the global mean of fluorescence signal that was initially subtracted from the data prior to the PCA/sICA decomposition. The global mean is removed to allow the decomposition algorithms better capture the underlying structure and variations in the data, removing any global average effects. This global mean contains information about baseline fluctuations and fluorescence decay, which is not present in the temporal weights of the extracted sICA motifs. Adding the global mean back after the decomposition serves the purpose of maintaining the original intensity scale of the data. Therefore, this step was just performed when reconstructing the full recording, while most analyses were conducted directly on the temporal weights of the sICA motifs.

### 3.2.7 Spatiotemporal properties and metrics to describe spontaneous motifs.

Total spatial coverage of all the identified motifs was calculated by summing all the motif masks per animal within a session and calculated as the percentage coverage of the entire exposed cortical area (brain mask outline). Each hemisphere was defined relative to the midline. Motif size was calculated as the number of pixels within each single motif mask. Motif frequency was calculated by detecting the peaks of activity across the temporal weights per motif and dividing by the length of the recording. Peaks of activity were located by first, normalising the temporal weights between [0, 1] and finding peaks with a vertical drop of more than 0.02 (2%) from the peak on both sides without encountering either the end of the signal or a larger intervening peak.

The probability density functions (PDFs) of the spatiotemporal properties were compared across development by the Kullback–Leibler (KL) divergence. PDFs provide information about the likelihood of the variable taking on different values; and the KL divergence measures the information gain when one probability distribution is used to approximate another. It quantifies the difference between two PDFs by calculating the relative entropy or divergence. KL divergence emphasises the dissimilarities between the shapes and magnitudes of the probability distributions and provides information on the specific areas where the distributions differ. On the other hand, the cumulative density functions (CDFs), calculated for the pyramidal-GABAergic (EI) motif correlation, are compared across ages by the Wasserstein distance. When applied to CDFs, the Wasserstein distance captures the discrepancy between the two distributions in terms of their shapes and positions. It considers the entire distribution and provides a measure of how much mass needs to be transported from one distribution to match the other. Wasserstein distance is suitable for comparing CDFs because it takes into account both the location and magnitude of differences between distributions, providing a meaningful measure of similarity or dissimilarity. The maximum Wasserstein distance between two distributions is equal to the distance between

their support, which is the range of values that each distribution takes. In this case, the support of all CDFs was the interval [-0.5,1]. Therefore, the maximum possible Wasserstein distance between them is 1.5, which will indicate each the distribution was at either end of the possible correlation values.

### 3.2.8 sICA motif identity assignment.

Each sICA motif mask was assigned to an Allen CCF atlas region. The Allen CCF Atlas regions included: primary (M1) and secondary (M2) motor cortex; frontal pole (FRP); primary somatosensory barrel field (S1b), nose (S1n), mouth (S1m), lower limbs (S1ll), upper limbs (S1ul), trunk (S1t), unassigned (S1u); secondary somatosensory cortex (S2); primary auditory cortex (A1) and dorsal (AUDd), ventral (AUDv), posterior (AUDpo) auditory areas; primary visual cortex (V1) and anterolateral (VISal), anteromedial (VISam), lateral (VISl), posterolateral (VISpl), posteromedial (VISpm), laterointermediate (VISli), postrhinal (VISpor) visual areas; anterior cingulate area dorsal (ACAd); prelimbinc area (PL); retrosplenial lateral agranular (RSPagl), dorsal (RSPd), ventral (RSPv); anterior area (VISa); rostrolateral visual area (VISrl), temporal association area (TEa). This map was simplified into M1, M2. S1b, S1t (combines S1t, S1up, S1ll), S1f (combines S1m, S1n, S1u), S2, AUD (combines A1, AUDd, AUDv, AUDpo), PCC (combines VISrl, VISa), V1, VISm (combines VISpm, VISam), VISl (combines VISal, VISl, VISpl, VISlo, VISpor), and RS (combines RSPagl, RSPd, RSPv).

To assess the distribution of motif masks across regional boundaries, the proportion of spread of each motif mask into neighbouring regions was determined. If the spread of a motif mask into a region accounted for less than 10% of its total size, that region was not considered as one of the regions where the motif significantly spread. Additionally, if more than 80% of a motif's mask size was confined within a single region, it was considered that the motif was present solely within that region. That way motifs were classified as single or multi region (2 or more) spread. The motif was assigned a region identity based on the region where it exhibited the highest extent of spread.

### 3.2.9 Reduction of the SNR for the recordings.

The SNR from the recordings was calculated making use of the fact that, due to the slow dynamics of the calcium signal, fluorescence will typically be very similar between adjacent frames, particularly for fast imaging rates like the one used in the current study. The SNR was computed as the median of the difference across consecutive frames (Rupprecht et al., 2021). Median was chosen instead of mean to mitigate the impact of outliers caused by the rapid onset dynamics of calcium signals. To equalise the SNR of all recordings across different developmental stages and neuronal populations, Gaussian noise was introduced to the $\Delta F/F$ values of each recording. The amount of noise was adjusted iteratively until the SNR reached

a target value of 19.5 $\pm$ 0.15, which corresponded to the lowest SNR observed among all recordings. This approach ensured that the SNR was standardised across animals, populations, and age groups.

### 3.2.10 Jaccard index for EI partners and instantaneous correlation.

Spatial pairwise comparisons of the pyramidal and GABAergic sICA motifs were performed using the Jaccard index (JI) in order to assign pyramidal-GABAergic (EI) partners based on their similarity of spatial location acros the dorsal cortex. The JI is a common and robust statistic to determine similarity between data sets, including images and segmentations (Weiser et al., 2021; Nietz et al., 2022), and it is calculated by dividing the size of the intersection between the motif masks of each EI partner by the size of their union. In this context, the JI can be applied to assess the overlap or similarity between the spatial patterns represented by the motifs. The spatial masks corresponding to each motif can be treated as sets, so the JI can then be calculated by dividing the number of pixels that are common to both motif masks by the total number of pixels encompassed by both masks. This provides a quantitative measure of the spatial similarity between the motifs, indicating how much they overlap or share common regions of activity. A higher JI indicates a greater overlap or similarity between the motifs, while a lower index suggests more distinct or dissimilar spatial patterns. For two pyramidal and GABAergic sICA motifs to be considered an EI partner, a minimum overlap of 30% (Jaccard Index value = 0.30) was set. A partner was identified for each pyramidal motif by finding the GABAergic motif with the highest similarity above the threshold. In cases where multiple GABAergic motifs exceeded the threshold, the temporal dynamics of those GABAergic motifs were combined to create a new temporal motif, which served as a partner for the pyramidal one. If no GABAergic motifs met the threshold, the pyramidal motif remained unpartnered.

The instantaneous correlation between EI partners was calculated as a moving Pearson correlation, which computes the correlation coefficients for subsets of data within a specified window or time interval. This approach provided a more dynamic view of the correlation between the two populations and allows for the detection of temporal patterns or changes in their relationship. The choice of window size should be carefully considered as different window sizes may highlight different aspects of the relationship between the dynamics of both populations. While smaller window sizes may be more sensitive to local variations and noise, leading to higher variability and potentially capture more short-term changes; larger window sizes can smooth out shorter-term fluctuations, being better suited for capturing longer-term trends or patterns in the data. Hence, a total of 33 distinct window sizes were employed to determine the correlation between the EI partners. These window sizes were evenly distributed in a logarithmic manner, ranging from 180 milliseconds to 60 seconds. The logarithmic spacing was selected to optimise computational efficiency while ensuring a denser distribution of window sizes, particularly in finer time resolutions. For the instantaneous correlation analysis, a window size of 1.5 milliseconds

was selected as it effectively captured short-term changes in the signal without excessive noise fluctuations or overly smoothing the data.

### 3.2.11 Statistical analysis.

The distribution of the data was assessed for normality using Shapiro-Wilk test, used for data with < 50 samples, or Kolmogorov–Smirnov test, for data with > 50 samples. Unless otherwise stated, none of the data showed a normal distribution. Therefore, non-parametric statistical tests were employed for the analysis. For comparisons involving two groups (pyramidal vs. GABAergic), the Wilcoxon rank-sum test (Mann-Whitney U test) was used. This test is suitable for non-normally distributed data and compares the medians between two independent groups. Wilcoxon rank-sum test are presented as the test statistic ($Z$ value) and the statistical significance (p value).

For the analysis across developmental age (P6-P30) and between neuronal populations (pyramidal and GABAergic), linear mixed-effects models (LMM) or generalised linear mixed-effects models (GLMM) were employed to account for other potential confounding factors. LMM and GLMM are robust statistical models that can handle non-normal and non-independent data, allowing for the inclusion of random effects and fixed effects in the analysis. The fixed effects on the models were developmental age and population (or region or drug/vehicle), while the Age-Animal identity interaction, litter size, sex, and genotype (either single/double or triple transgenic) were included as random effects for the full model. The statistical significance of the fixed effects is reported on the figure caption, while the model formula, estimates and model fit are included in the Annex 4.2. None of the random effects had a significant effect on the model, unless otherwise stated.

After fitting the full model using LMM/GLMM, the random effects were dropped to fit the reduced model version. The likelihoods of both models were then compared to evaluate which model offered a better fit and to assess the impact of the random effects. Comparing the likelihoods of two models with and without random effects can determine whether the inclusion of random effects significantly improves the model fit. The likelihood ratio test (LRT) is commonly used for this purpose. The LRT statistic is computed as the difference between the log-likelihoods of the two models, and tests whether this difference is statistically significant using a chi-squared distribution. If the p-value of the LRT is less than the specified significance level, then the model with random effects is considered to provide a significantly better fit to the data than the model without random effects. If the models are significantly different, LRT can determine which random effects are significant. This involves comparing the full model, which includes all the random effects, with a reduced model that systematically drops one or more of the random effects.

Although GLMMs are more flexible than LMMs, as they allow for non-normal error distributions and non-constant variance, if the sample size is large enough and the departures from normality are not too extreme, LMMs can often still used with non-normally distributed data (Schielzeth et al., 2020). Hence, both models were initially employed to fit the data, and a visual examination of the residuals was conducted along with assessing the goodness of fit to determine which model provides a more accurate representation of the data.

### 3.2.12 Data visualisation.

All spatiotemporal properties are shown as an average of all motifs obtained in both of the spontaneous recordings in each imaging session, unless otherwise stated. Distributions are computed for the collection of motifs from both recordings. In figures, the data for each animal average developmental trajectory are shown as circle markers connected by a solid shaded line, with an example trajectory for a triple transgenic mouse highlighted by a dashed line for each cell population. Data from acutely recorded animals is shown as unconnected squares markers. Solid lines with error bars represent the average across all animals per developmental age, plus-minus the standard error of the mean.

## 3.3 Results.

Spontaneous neuronal activity, which occurs in the absence of active sensory input, plays an important role in the development of brain circuits. While previous studies have extensively investigated the spatial and temporal organisation of spontaneous activity in individual brain regions during development, particularly for primary sensory regions (somatosensory, visual and auditory cortices), the interaction across them and their engagement with cortex-wide activity remains understudied. Moreover, the simultaneous recording of the *in vivo* large-scale activity dynamics of pyramidal and GABAergic populations across development has rarely been performed (Mulholland et al., 2021), even for single region studies.

This project used neocortex-wide calcium imaging to simultaneously and chronically record the activity of GABAergic and pyramidal neuron populations in head-fixed, behaving early postnatal mice, from P10 to P22, with one litter of animals imaged into early adulthood (P87 - data not shown due to limited optical access). The results in this chapter focus on the characterisation of the spatiotemporal properties of the signal components obtained after the sICA decomposition of the data for each of the two neuronal populations imaged. The data was compared across neuronal populations and developmental age, given that other attributes such as sex, animal ID, litter size, or genotype generally did not significantly affect the developmental trajectories.

### 3.3.1 Spatiotemporal development of spontaneous neocortex-wide activity.

Spontaneous activity exhibits spatiotemporal properties and dynamics that become increasingly complex during development. These activity motifs were explored simultaneously in both GABAergic and pyramidal cell populations within the same mouse and across ages. Examples of activity motifs associated with sensory areas, specifically primary somatosensory (S1) and visual (V1) cortices, matched across neuronal populations, GABAergic (green) and pyramidal (purple), and developmental age, are shown in Figure 3.3. There was broad coherence between activity in pyramidal and GABAergic neuronal populations, which is reflected in the overall similarity of spatial activity motifs that emerge from the PCA/sICA analysis of the data from each recording period (Figure 3.3). However, the spatial patterns of these activity motifs change during development, with the motifs broadening and occupying a larger portion of the cortex, particularly in the GABAergic population (Figure 3.3, top panel, green). The early emergence of a functional sensorimotor network involving co-activation of whisker-related somatosensory cortex and motor cortex, which has been previously reported in pyramidal cell populations (Cross et al., 2021; McVea et al., 2017), is also apparent here, not only in the pyramidal population, but also in the GABAergic activity patterns (Figure 3.3, S1 activity spatial motifs). Moreover, these spatial patterns also show spontaneous homotopic regions co-activation at older ages in both neuronal populations and sensory regions, which indicates the co-activation of the contralateral region (Figure 3.3). This could be due to the maturation of L2/3 callosal projection neurons by the end of the second postnatal week in mice (Mizuno et al., 2007; Wang et al., 2007).

#### The developmental broadening of spatial activity maps diverges between pyramidal and GABAergic populations.

Given that the imaging happens chronically at a time of extensive brain growth, it is important to investigate whether the spatial coverage of detected activity changes with age. This can reveal any potential loss of access to certain regions due to brain growth and an increase in skull curvature. Additionally, it can provide insights into changes in the spread and overlap of the spatial motifs that could reflect a transition from spatially discontinuous and small motifs, with large portions of the cortex being silent, to a more distributed and continuous activity. To assess this spatial coverage, the total area covered by all the spatial activity motifs was compared to the area of the cortex that was exposed for imaging. While the size of the exposed cortex (size of the "window") could vary slightly across animals due to variability in opening the window during surgery, it should stay fixed within the same animal across the imaged ages. However, since brain masks were drawn independently for each animal at each different age, the size of the exposed cortex, defined by the outline of the brain masks (Figure 3.4, panel A, examples exposed cortex), may exhibit slight variations, even for the same animal, due to manual masking (Figure 3.4, panel A, example brain masks for same animal across development). All brain masks outlining the exposed cortex were individually registered to the reference coordinate system (based on the Allen Atlas), to compare change in exposed cortex across the different

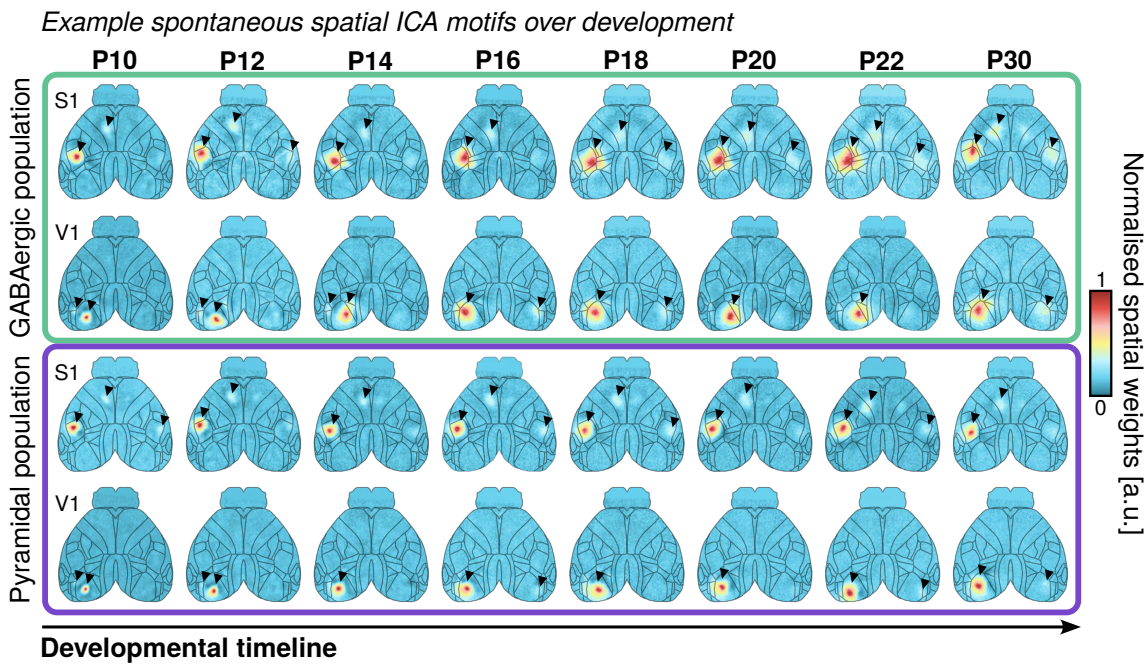


**Fig. 3.3 Illustration of spontaneously occurring spatial activity motifs across early postnatal development**. The spatial weights of two example motifs from a triple transgenic mouse imaged chronically are shown to illustrate the changes in the spatial sensory maps during early postnatal development (from P10 to P30). To highlight the relative spatial pattern and compare across ages and populations, the spatial weights are normalised between 0 (minimum spatial weight value) and 1 (maximum spatial weight value). The location of the activity motifs is indicated by the black arrows.

animals. Although variable, on average, the size of the exposed cortex was consistent across ages and animals, showing no significant differences to the size of the exposed cortex on the imaging session (Figure 3.4, panel B; $p = 0.304$). Variability was not significantly affected by sex, litter size, genotype or individual animal variation over time (Figure 3.4, panel B; $p = 0.475$).

The spatial coverage refers to the amount of space covered by all the spatial motif masks obtained during each recording session per animal and neuronal population, in reference to the size of the exposed cortex (Figure 3.4, panel C, right inset). Despite some individual variability, the spatial coverage remained consistent across all chronically recorded animals (Figure 3.4, panel C, circle markers), with no significant differences across neuronal populations ($p = 0.870$) and developmental ages ($p = 0.323$). In this case, the the animal identity across age, the genotype, the sex and the litter size had a collective effect on the spatial coverage (GLMM full model vs reduced model, $p = 0.00525$); however, the standard deviations of these effects are so small (see Annex 4.2) that although statistically significant, it is probably negligible. On average, the spatial coverage fluctuated around 70% for both population, with most lateral and frontal cortical areas not being accessible for imaging due to skull curvature and out-of-focus restrictions on the edges of the FOV (Figure 3.4, panel C, right inset), which can lead to a loss of signal (Kauvar et al., 2020). At earlier ages (P6-P8), for acutely imaged animals, the spatial coverage was slightly reduced (between 50-60% of the exposed cortex), with a tendency of a

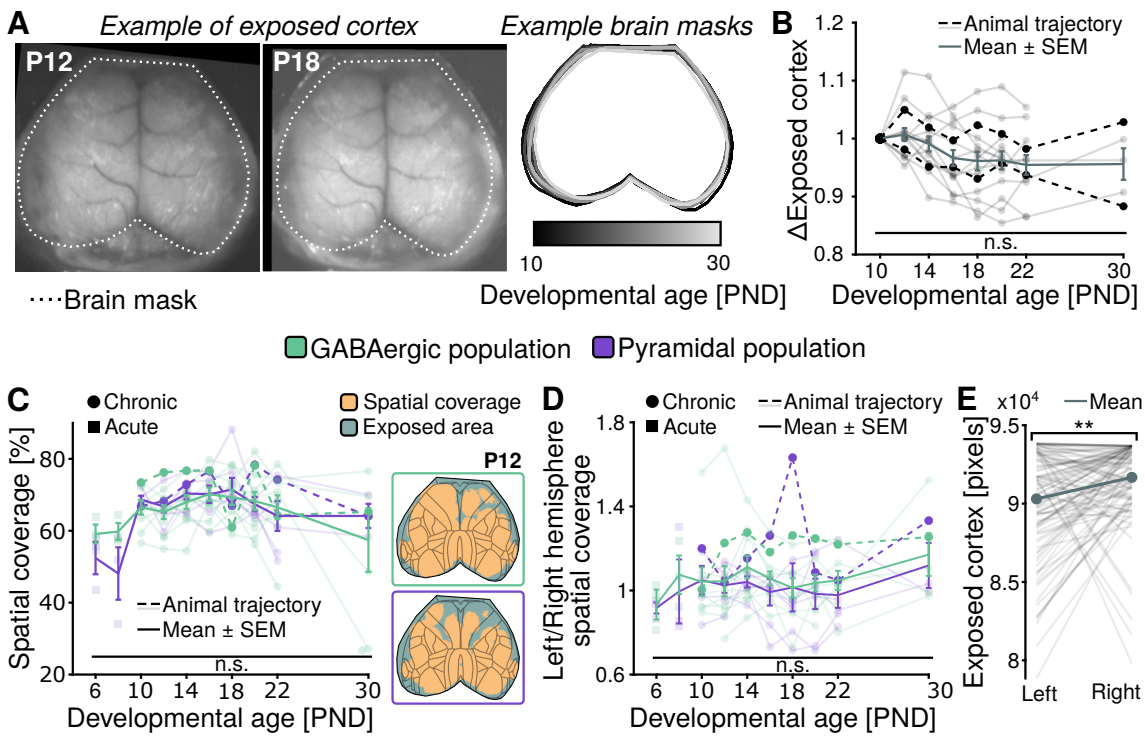


**Fig. 3.4** **Stable coverage of the exposed cortex by spatial activity motifs during early postnatal development**. **A|** Example of the user-drawn brain masks outlining the exposed cortex ("window" size) on the same mouse at two different developmental ages, P12 and P18 (left panel). Overlaid brain masks of the same mouse at all imaged ages from P10 to P30 (right panel). **B|** No significant change in the area of exposed cortex (n = 10 animals), relative to the first imaging day, across ages (p = 0.304). Significance tested by LMM. **C|** The percentage of spatial coverage of activity motifs (n = 21 animals) is not significantly different across developmental ages (p = 0.323) and between neuronal populations (p = 0.870). To the right is an example of the difference between the exposed area and the motif spatial coverage for each neuronal population. Significance tested by GLMM. **D|** The proportion of spatial coverage between the left and right hemisphere (n = 21 animals) is not significantly different across developmental ages (p = 0.642) and between neuronal populations (p = 0.902). Significance tested by GLMM. **E|** Total amount of exposed cortex in pixels per hemisphere in each recording (n = 109 recordings, from 21 animals), showing a small, significant bias towards the right hemisphere (p = 0.0099). Wilcoxon rank sum test for equal medians: $Z$ = -2.5795. Further statistical information in Annex 4.2. Significance is shown for age (population) as **($^{++}$) for p < 0.01.

larger coverage of the GABAergic population compared to the pyramidal one (Figure 3.4, panel C, square markers).

The spatial coverage between the left and right hemispheres also remained stable on average (Figure 3.4, panel D). Although individual animal trajectories varied and differed to some degree between populations within the same animal (Figure 3.4, panel C, dashed lines), these fluctuations were not significant across ages (p = 0.642) and between populations (p = 0.902). However, the animal identity across age showed a significant effect on the left/right coverage (GLMM full model vs reduced model, p = 4.441e-16), indicating that some individual animals presented significantly different ratios between each other across development, even though overall age did not show a significant difference overall. Across mice, there was a very small (∼1%) bias towards a larger right hemisphere (p = 0.00986), possibly due to the surgical

procedure, performed by a right-handed surgeon (Figure 3.4, panel E). Overall, these data suggest that imaging captures most, but not all, of the cortex similarly across different animals and that there are no systematic changes in the area that is imaged at different ages.

Cortical spatial activity maps have been key to understanding the topographical organisation of the brain, providing a general understanding of the development of the functional connectivity patterns across different brain areas (Cang et al., 2013; Nakazawa et al., 2020). The progression of map refinement across early development, from diffuse and overlapping representations to refined patterns, has shown similarities across many brain areas, from sensory regions like visual cortex (Ackman et al., 2012) and somatosensory cortex (Mizuno et al., 2018; Arakawa et al., 2014), to the cerebellum (White et al., 2014). Traditional mapping has primarily focused on characterising glutamatergic pyramidal or mixed neuronal population responses. However, a recent study has shown that, contrary to the refinement observed in these excitatory maps, inhibitory sensory maps broaden during maturation and are influenced by sensory experiences (Quast et al., 2017). Therefore, understanding the development of inhibitory spatial activity maps as well as the more broadly studied excitatory maps, and highlight their differences, is key to understand how different cell populations and their functional connectivity patterns contribute to brain function, and uncover potential general mechanisms of network development.

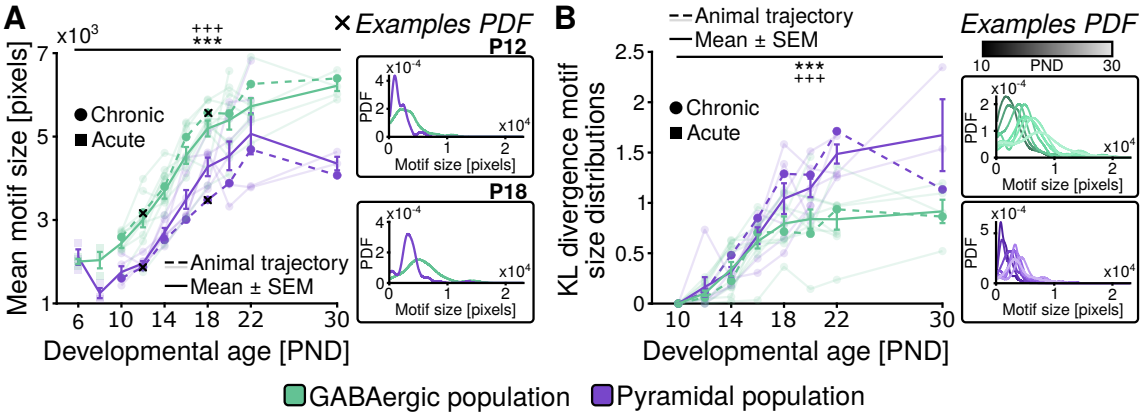


**Fig. 3.5 Developmental trajectory of activity motif size in pyramidal and GABAergic populations during early postnatal development**. **A|** The average sICA motif size (n = 21 animals) is significantly different across developmental ages (p = 2.239e-29) and between neuronal populations (p = 6.443e-08). To the right is an example of the probability distribution function (PDF) of motif sizes for each population at P12 and P18. Black crosses indicate the data points chosen for each population and age. Significance tested by GLMM. **B|** The KL divergence of the sICA motif size distributions (n = 21 animals) is significantly different across developmental ages (p = 4.351e-20) and between neuronal populations (p = 0.00974). To the right is an example of the PDFs of motif sizes for each population across development, from P10 (lighter colour) to P30 (darker colour). Significance tested by LMM. Further statistical information in Annex 4.2. Significance is shown for age (population) as ***(+++) for p < 0.001.

The neocortex-wide fluorescence of cortical pyramidal and GABAergic cell populations was subjected to PCA/sICA-based deconvolution to establish the individual patterns of cortical activation that combine to produce overall cortical activity dynamics. The term "map" and "motifs" in this context are interchangeable and refer to the discrete cortical activity spatial domains (spatial weights) that are obtained through sICA decomposition. As development

progresses, the average size of the active parts of the motifs, in both pyramidal and GABAergic populations, significantly increases at a similar rate and slows down at around P18 (Figure 3.5, panel A, solid lines). This means that, on average, patches of coordinated activity get larger relative to the anatomical atlas, as they mature. Individual animal trajectories are very similar within populations, with the GABAergic population showing significantly larger motif sizes across all ages but P6 (Figure 3.5, panel A, shaded solid lines, p = 6.443e-08). This larger domain size for the GABAergic population compared to the pyramidal one has been previously described in the visual cortex of ferrets (Mulholland et al., 2021).

Motif sizes can also be represented as a probability distribution for the different populations and across ages, which represents the likelihood of observing different sizes of the spatial motifs that occur in the different populations at different ages. These distributions were different between pyramidal and GABAergic activity motifs, which indicated that the relative frequencies of motif sizes in the pyramidal population were not the same as those in the GABAergic population, suggesting that two populations of neurons present different patterns of activity as seen in the different sizes of activity motifs that they produce (Figure 3.5, panel A, examples PDF). Similarly, the shape of the probability distribution of motif sizes also changed with development age, which suggested that these patterns of activity across populations are changing over time (Figure 3.5, panel A, examples PDF, P12 to P8 comparison).

The Kullback-Leibler (KL) divergence can be used to quantify changes in probability distributions, measuring how much one distribution differs from another in terms of the amount of information needed to encode the two distributions. In other words, the KL divergence indicates how much information is lost if one attempts to use one distribution to approximate another. Intuitively, if the KL divergence is high, it means that the two distributions are very different and cannot be well approximated by one another. When it is low, the distributions are similar and can be approximated fairly well. This can provide insights into how the sizes of the pyramidal and GABAergic spatial motifs evolve over time when compared across ages, and whether there are critical developmental time points at which the trajectories of the two population deviate. In this case, the KL divergence for both cell populations, when compared to their P10 distribution of motif sizes, steadily increased over development, until their trajectories bifurcated at around P16, point at which the distribution of GABAergic motif sizes stabilises (KL divergence plateaus), while the pyramidal distribution continues to increase until around P22 (Figure 3.5, panel B, Age p = 4.351e-20, Population p = 0.00974). This indicated that, at an earlier age, the size distribution of GABAergic motifs becomes more uniform, suggesting that the motifs become more consistent in their spatial organisation. Specifically, the proportion of smaller motifs to larger motifs in the GABAergic distribution remained relatively constant (Figure 3.5, panel B, example PDFs across ages) as the average size of the motifs continued increasing (Figure 3.5, panel A).

These findings suggest that there are fundamental differences in the underlying dynamics and spatial organisation of the two populations, even though both experience an increase in motif size over development, reflecting potential distinct roles in cortical network function development.

### Dynamic changes in motif event frequencies reveal unique developmental trajectories for pyramidal and GABAergic populations.

Activity motifs not only drastically change their spatial properties during early postnatal development, but also transition in their spontaneous temporal dynamics, switching from discontinuous (often silent and intermittently bursting) to continuous activity, generally happening just before the start of active sensing (Colonnese et al., 2010). This switch in the patterning of ongoing in activity happens concurrently to an increase in neural firing rates, reflecting the termination of immature activity and the onset of a mature "active" state (Colonnese, 2014). A time projection map of 10 seconds of neocortical activity showed that, in a relatively short period of time, activity cycled throughout most of the regions of the dorsal cortex (Figure 3.6, panel A). The pyramidal and GABAergic populations generally displayed similar spatiotemporal patterns, with activity evolving from more distinct and isolated bouts of activity at younger ages, to more diffuse and continuous ones as the cortex matures (Figure 3.6, panel A). Each activity motif has a spatial pattern associated to a temporal weight vector, which describes the dynamics of that particular patch of the cortex. Spatially matched motif patterns of each neuronal population within the same animal displayed similar temporal dynamics, although they were not perfectly matched (Figure 3.6, panel B). The peaks of activity per motif were automatically detected for both populations and across ages to explore changes in temporal dynamics and motifs frequency, to infer the global transition from discrete events to more frequent and continuous activity that occurs as the cortex matures (Figure 3.6, panel B, peaks indicated with the triangles).

The frequency of motif events showed a significant increase across early postnatal development for both neuronal populations ($p = 1.723e-09$), but their behaviour seemed to start to diverge around P14, to converge again at P30 (Figure 3.7, panel A). This window of different frequencies between the pyramidal and GABAergic populations coincides with the onset of active sensing and the transition to more continuous activity (Colonnese et al., 2010). The average motif event frequency for the GABAergic population remained below that of the pyramidal population (Figure 3.7, panel A,$p = 2.040e-05$). It has been previously shown that sensory experience, at the beginning of the second postnatal week, increases the connectivity across the glutamatergic pyramidal cell population (Ashby et al., 2011), leading to a highly recurrent network state that could be driving the continued increase in event frequency of the pyramidal population. The motif event frequency between the right and left hemispheres showed no significant differences across ages (Figure 3.7, panel B).

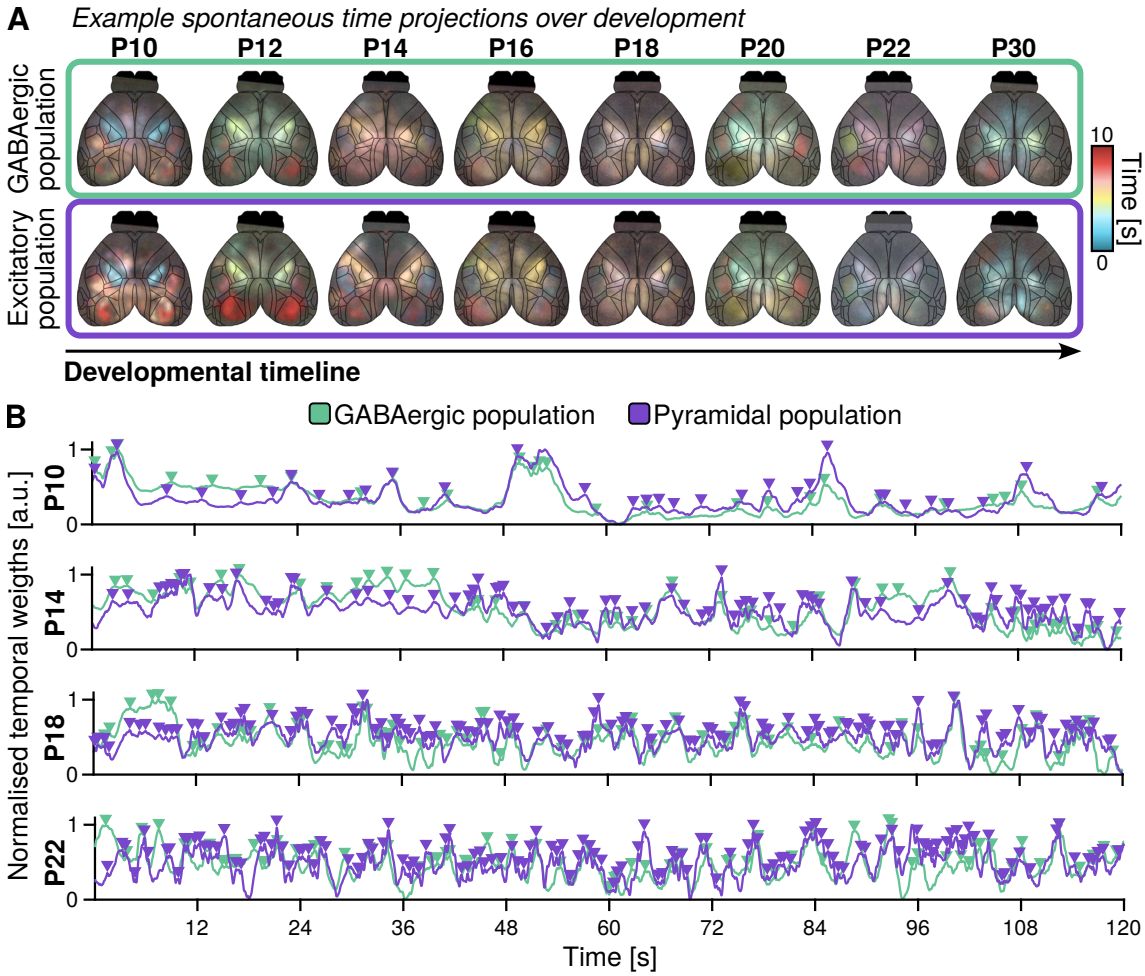


**Fig. 3.6** **Temporal dynamics of activity motifs across early postnatal development**. **A|** Example of spontaneous activity projected in space over a 10-second recording period for each population and developmental age. **B|** Illustration of the normalised temporal weights of an example sICA motif at four different developmental ages for each neuronal population. Triangles depict the peaks detected on each trace.

The event frequency, similarly to the motif size, can be represented as a probability distribution of the frequencies across ages, from each of the neuronal populations. In this context, the event frequency distribution of the pyramidal population stabilises at an earlier age, as evidenced by the plateauing of the KL divergence measure across ages prior to that of the GABAergic population (Figure 3.7, panel C, $p = 0.0393$). The bifurcation between the evolution of each population distribution across age occurs around P14, coinciding with the opening of the window between their average event frequencies (Figure 3.7, panel A). The overall increase in average event frequency for both neuronal populations indicates a global change in neural activity during this developmental period. The continued increase in the average pyramidal event frequency throughout the third postnatal week compared to the GABAergic population, indicates still ongoing developmental changes in the former, while its distribution of motif frequencies stabilised and was less variable at earlier ages, around the period when active sensory processing begins, compared to the GABAergic population.

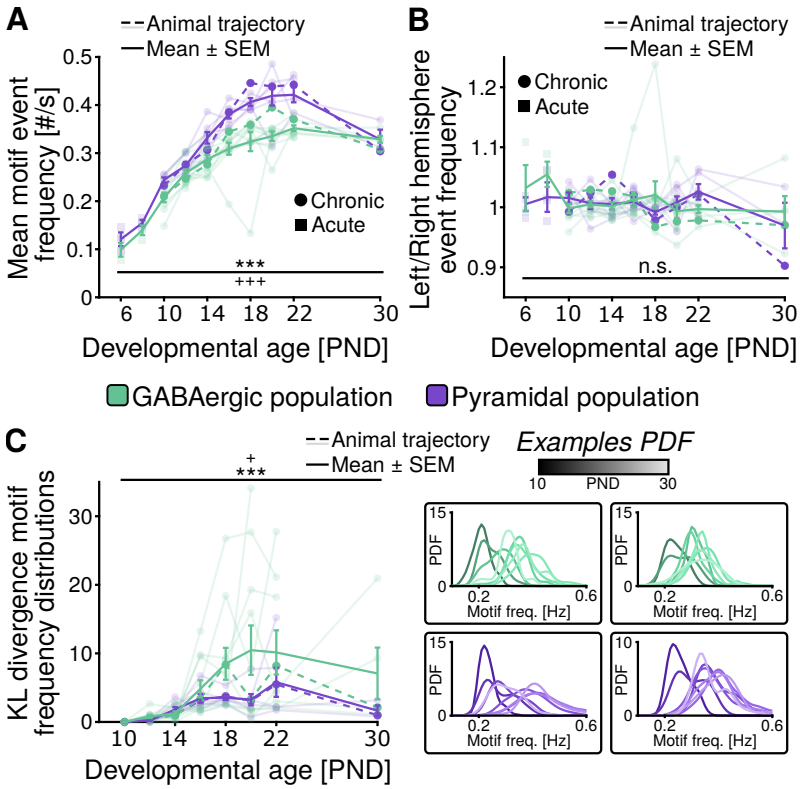


Fig. 3.7 **Developmental trajectory of activity motif frequency in pyramidal and GABAergic populations during early postnatal development**. **A|** The average sICA motif frequency (n = 21 animals) is significantly different across developmental ages (p = 1.723e-09) and between neuronal populations (p = 2.040e-05). Significance tested by GLMM. **B|** The proportion of average motif frequency between the left and right hemisphere (n = 21 animals) is not significantly different across developmental ages (p = 0.161) and between neuronal populations (p = 0.910). Significance tested by LMM. **C|** The KL divergence of the sICA motif size distributions (n = 21 animals) is significantly different across developmental ages (p = 1.673e-11) and between neuronal populations (p = 0.0393). To the right are two examples of the PDFs of motif frequency for each population across development, from P10 (lighter colour) to P30 (darker colour). Significance tested by GLMM. Significance tested by LMM. Further statistical information in Annex 4.2. Significance is shown for age (population) as *($^{+}$) for $p < 0.05$ and ***($^{+++}$) for $p < 0.001$.

As a result, there are significant developmental differences between the pyramidal and GABAergic populations, not only in terms of changes in their spatial maps (section 3.3.1) but also in their temporal dynamics, which suggests distinct functional roles in neural processing during early postnatal development.

### 3.3.2 Regionalisation of spatiotemporal activity motifs across the dorsal cortex.

In order to examine and compare the spatiotemporal dynamics of each neuronal population in different brain areas, the dorsal surface of the brain needs to be parcellated into distinct anatomical regions using reference coordinates from standardised brain atlases. Generally, the reference atlas of choice is the CCF atlas (Wang et al., 2020), which is based on an adult brain (P56). This atlas can be scaled down to accommodate the neonatal brain size; however, if we

assume that the developing brain is not just an immature version of the adult brain, the standard adult organisation of brain structures will likely not fit the developing brain. Systematically mapping these changes is necessary to obtain standardised coordinates for the developing brain, as postnatal development involves daily changes in the brain structure. In this project, by using a line that expresses the RFP reporter in thalamocortical afferents (Mizuno et al., 2014; Mizuno et al., 2018), the pattern changes in the position and size of the primary sensory cortical areas on the dorsal cortex during postnatal development was defined (Figure 3.8, panel A).

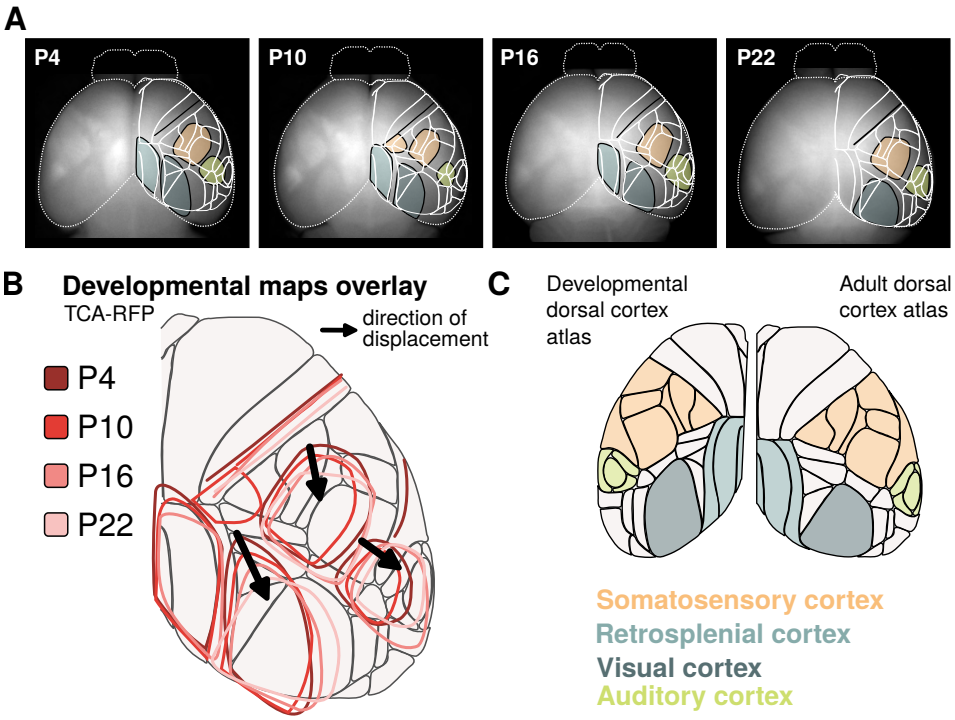


**Fig. 3.8 Functional parcellation of developing neocortex using the TCA-RFP mouse line. A|** Widefield snapshots of a dorsal view of TCA-RFP brains at different developmental ages. The adult CCF atlas is overlaid in white and solid lines. The outline of the sensory areas is outlined in black and colour-coded by region. The dashed white line outlines the edge of the cortex and olfactory bulbs. **B|** Overlay of the different developmental maps outlining the visible sensory regions and boundaries in reference to the adult CCF atlas. The direction of displacement of the three main sensory regions is indicated by a black arrow. **C|** Illustration of the adult CCF atlas and the average developmental dorsal cortex atlas.

The thalamocortical axon terminals outline the primary sensory cortical areas during mouse postnatal development (Mizuno et al., 2014; Mizuno et al., 2018; Ackman et al., 2014b), which can be subsequently aligned and scaled to the CCF adult atlas to obtain the reference coordinates for each cortical area. Most RFP dorsal cortical expression lies within primary sensory areas (primary somatosensory - S1, visual - V1, and auditory cortex - A1), as well as some association areas (retrosplenial cortex - RS) (Figure 3.8, panel A). To investigate the direction of displacement of the sensory regions across ages, the outline of the thalamocortical axon terminals at each developmental age was scaled and aligned to the CCF adult atlas (Figure 3.8, panel B). While the RS and motor cortex division lines remained in similar location, the primary sensory regions moved to a more posterior and lateral position, while changing

their outline shape, particularly V1 (Figure 3.8, panel B). This allowed to create an average developmental dorsal cortex atlas, which could be compared to the adult version (Figure 3.8, panel C). Given that the location of the rest of the dorsal cortical regions is unknown, and the primary sensory cortices change location throughout development, it is possible that an average developmental dorsal cortex atlas is as inaccurate as the adult one. Moreover, the chronic implantation of the head-post for longitudinal imaging significantly changed the AP/LL ratio, changing the brain shape slightly (Figure 2.16). Therefore, the adult dorsal cortex atlas was still used to align the recording, while factoring in the possible misclassification of sensory motifs.

The spatial weights from the sICA motifs provide a catalogue of activity patterns that can be associated with functionally relevant cortical regions. The sICA approach does not rely on any assumptions regarding the underlying neuroanatomy of the developmental mouse neocortex; instead, it is a data-driven technique that minimises the mutual information between spatial functional regions to ensure maximum independence. Each of this sICA motifs can be assigned to region of interest based on the registration of the recording to the common coordinate system (Musall et al., 2023; Saxena et al., 2020). This allows the motifs to be labelled, which can provide information about the early development of various cortical regions. Despite the potential inaccuracies of parcellating an immature cortex, the labelling approach still preserves the information and pattern of each sICA motif. The spatial patterns (spatial masks) of the motifs can be located at various positions within and between region boundaries, with different degrees of spread across neighbouring regions (Figure 3.9, panel A). The pie charts show the distribution of the corresponding motif mask, displayed above, across the specific brain regions where it is localised. The spread ranges from being perfectly contained within one region to being split evenly between two regions, or even distributed across four or more regions. This highlights both the possibility of imperfect alignment of the recording to the common coordinate atlas, as well as the limitations of rigid anatomical boundaries, especially during development.

The extent to which motif masks spread across different anatomical regions varies widely, with many motifs spreading a small proportion of their size (<10%) in different regions, while a smaller number of motifs spread a larger proportion of their size within the same region, being more confined within a region's anatomical boundaries (Figure 3.9, panel B). The distribution of motif spread across regions for all sICA motif masks was asymmetrical, indicating that most motif masks cross anatomical boundaries only slightly between neighbouring regions, while a smaller number of motifs displayed a large spread within a single region (Figure 3.9, panel A, example pie charts). However, the observed peak at the further end of the distribution suggested that there was a high number of motifs that were entirely within the boundaries of one anatomical region (Figure 3.9, panel B). To consider a motif to be part of a region, it had to spread at least a 10% of its area inside that region (minimum cut-off), whereas motifs with over 80% of their size within the same region were considered single region motifs (Figure 3.9, panel B, cut-off dashed line).

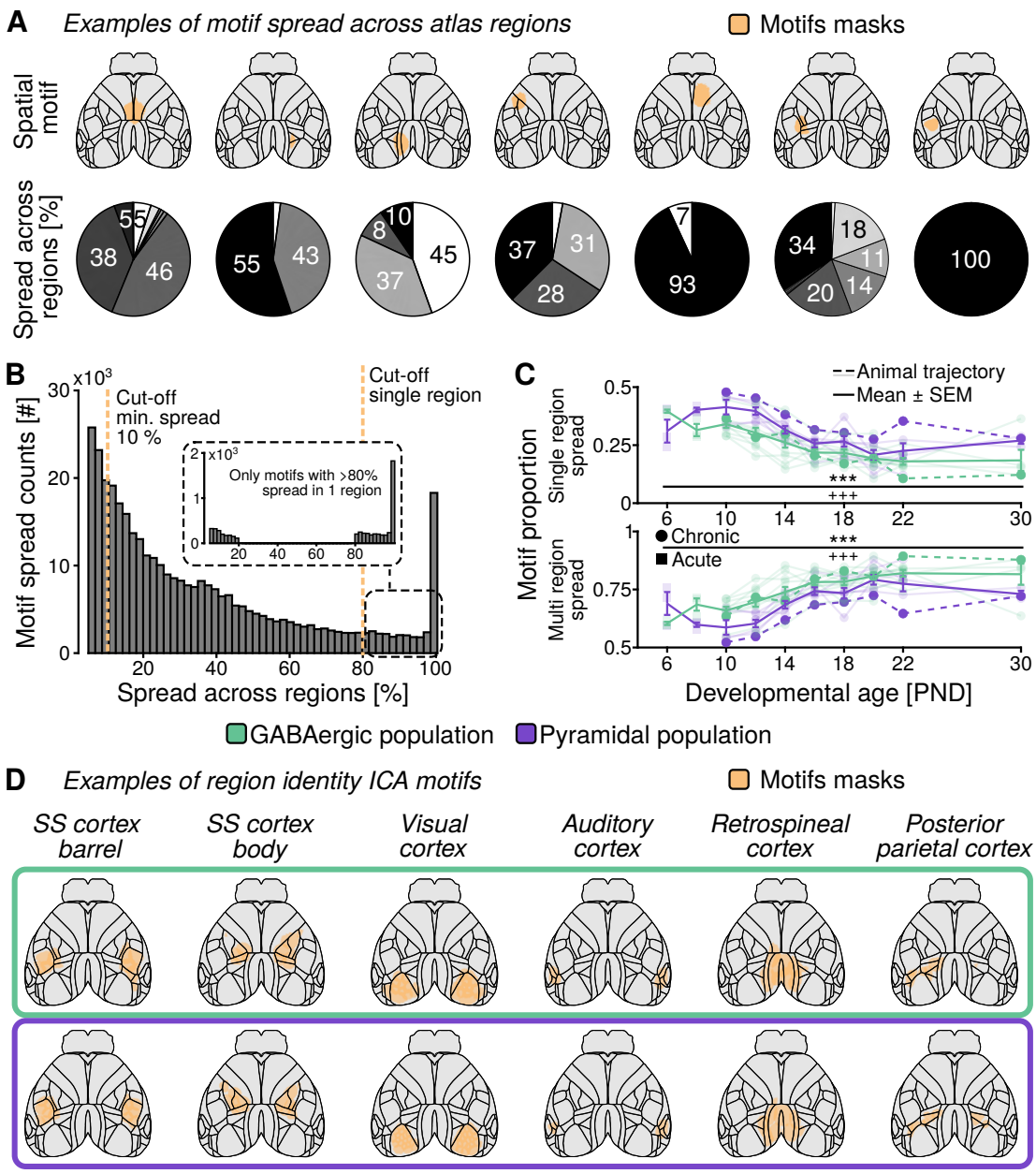


**Fig. 3.9** **Spread of the sICA motif spatial masks across cortical region boundaries. A|** Examples of single sICA motif masks and the percentage of their spread across the different region boundaries. **B|** Histogram showing the spread across region boundaries of all sICA motif masks, with a lower threshold of 10% considered as not significantly spreading in that one region, and a higher cut-off of 80% indicating a significant single region spread. The inset displays the spread histogram only for motifs that spread above 80% in a single region (single region spread). **C|** The proportion of single (upper panel) and multi (lower panel) region spread motifs (n = 21 animals) is significantly different across developmental ages (p = 1.475e-11 single, p = 3.323e-13 multi) and between neuronal populations (p = 1.695e-05 single, p = 8.854e-07 multi). Significance tested by GLMMs. **D|** Example of the region identity assigned to the different sICA motifs for one example recording. Further statistical information in Annex 4.2. Significance is shown for age (population) as ***($^{+++}$) for $p < 0.001$.

Using these criteria, the relative appearance of single and multi-region motifs across development was assessed. The proportion of single region spread motifs significantly decreases over development (Figure 3.9, panel C, top panel, p = 1.475e-11), with fewer motifs observed for the

GABAergic population at all ages but P6, compared to the pyramidal population (p = 1.695e-05). In contrast, multi-region motifs follow the opposite behaviour (Figure 3.9, panel C, bottom panel; Age p = 3.323e-13, Population p = 8.854e-07). These trends could be a reflection of the changes in average motif size across development (Figure 3.5, panel A), where the GABAergic population showed on average larger motifs than pyramidal one (at every age but P6), making them more likely to cross multi-region boundaries. To investigate the developmental activity patterns of various brain areas, motifs were categorised by anatomical region based on where they are most heavily represented, assigning them to the region where they had the highest proportion of area spread. An illustration of the spatial motifs masks assigned to each brain region for both populations imaged simultaneously for a P10 example recording is presented in Figure 3.9, panel D. Given that the exposed cortex showed limited spatial coverage (around 70%, as shown in Figure 3.4, panel B) and the brain undergoes extensive growth during early postnatal development, the proportion of motifs assigned to different brain regions may vary across ages.

To simplify the CCF reference atlas, the regions were combined into 12 different areas, which included primary sensory regions and association areas, such as PPC and RS (Figure 3.10, panel A). The relative proportion of motifs assigned to the motor cortex (M1 and M2) exhibited a significant developmental change (M1 p = 1.565e-05, M2 p = 1.199e-05), with a fluctuating trajectory for the M2 around an average proportion of 7% and a gradual increase for M1 up to $\sim$ 12%, which could be reflecting the developmental "awakening" of M1 region that takes place during the second and third postnatal weeks (Dooley et al., 2018). Moreover, the GABAergic population had a relatively higher proportion of motifs assigned to M1 region when compared to the pyramidal population (p = 0.00145) (Figure 3.10, panel B, M1 and M2), potentially due to the key role of inhibition in motor learning (Donato et al., 2013). Sensory feedback, including passive touch and spontaneous movements, assigned to the primary somatosensory cortex, trunk and limb regions (S1t), showed a relatively high proportion of motifs (20%) with no significant developmental changes (Figure 3.10, panel B, S1t). On the contrary, the proportion of motifs in the somatosensory face-related cortex (S1f) was smaller (2.5%) and much more variable, showing both an age (p = 1.976e-04) and population difference (p = 1.764e-05). The large variability and small proportion could be attributed to its lateral position on the dorsal cortex (Figure 3.10, panel A, dorsal map), which showed limited spatial coverage (Figure 3.4, panel B). These motifs were combined with the S1t region into the S1bod region for subsequent regional analysis. The primary somatosensory cortex barrel field (S1b) presented a high (>20%) and gradually increasing proportion of motifs across ages (p = 1.536e-13), with a significant difference between genotypes (p = 2.262e-05), presenting a larger proportion of GABAergic motifs (Figure 3.10, panel B, S1b).

Similarly to the S1f region, the secondary somatosensory (S2) and auditory cortex (AUD) had a variable and low proportion of motifs due to their lateral position, and were not included in further analysis. Nonetheless, it is important to mention that the proportion of motifs assigned to

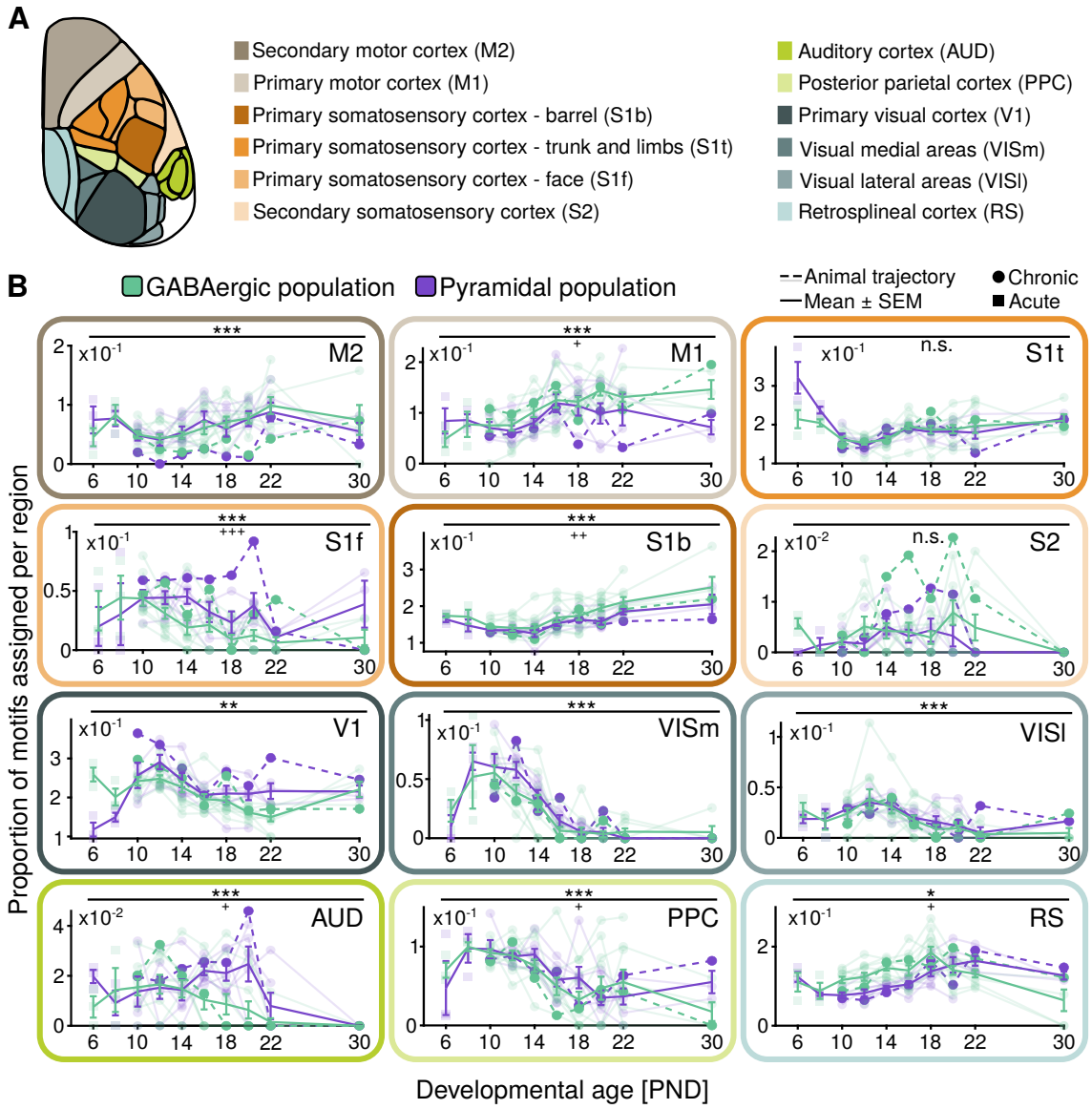


**Fig. 3.10** **Proportion of sICA motifs assigned to each region of interest across development. A|** Schematic of the cortical regions of interest. **B|** The proportion of motifs (n = 21 animals) is significantly different across developmental ages for most regions (M2 p = 1.199e-05; M1 p = 1.565e-05; S1t p = 1.0947e-07; S1f p = 1.976e-04; S1b p = 1.536e-13; S2 p = 0.653; V1 p = 0.00377; VISm = 1.442e-10; VISl p = 1.267e-07; AUD p = 7.208e-05: PPC p = 1.618e-04: RS p = 0.0274), while only significant across neuronal populations for a few regions (M2 p = 0.806; M1 p = 0.00145; S1t p = 0.0232; S1f p = 1.764e-05; S1b p = 2.262e-05; S2 p = 0.0506; V1 p = 0.0618; VISm = 0.198; VISl p = 0.967; AUD p = 0.0190; PPC p = 0.0282: RS p = 0.0295). Significance tested by LMM/GLMM. Further statistical information in Annex 4.2. Significance is shown for age (population) as *(+) for p < 0.05, **(++) for p < 0.01, ***(+++) for p < 0.001.

the AUD showed significant changes across development age (p = 7.208e-05) and populations (p = 0.0190). Specifically, the proportion of pyramidal motifs exhibited an increase following the termination of the critical period plasticity of pure tones (Nakamura et al., 2020). The proportion of primary visual cortex motifs (V1) significantly changed across development (p = 0.00377), with a steep increase in pyramidal motifs that peaked just before eye opening at P12 (Figure 3.10, panel B, V1). The visual medial areas (VISm) showed a bell-shaped trajectory

across ages (p = 1.442e-10), with a sharp increase in their proportion and a subsequently gradual decrease between P12 and P18, with no population differences (Figure 3.10, panel B, VISm). On the other hand, the lateral visual areas (VISl) showed a smaller proportion of motifs, likely due to their lateral position, with significant developmental changes (p = 1.267e-07) but no population differences. The proportion of motifs assigned to each association areas, the posterior parietal cortex (PPC) and the retrosplenial cortex (RS), exhibited significant changes over development (Figure 3.10, panel B, PPC p = 1.618e-04; RS p = 0.0274). Between P10 and P18, the RS showed a larger proportion of GABAergic motifs, which shifted to a higher proportion of pyramidal motifs thereafter. Taken together, throughout development, the proportion of motifs per cortical region exhibited significant changes, indicating that the relative representation of activity patterns in different brain regions and neuronal populations varies as the brain matures. This implies that certain regions may become more or less involved in the broader network during development, reflecting changes in spontaneous behaviour (Dooley et al., 2019) and how information is processed and transmitted, as well as in the connections between different brain regions.

### Consistent developmental trajectories of motif size and event frequency across cortical regions.

As the involvement of various brain regions differed across development, it was essential to examine whether any of the spatiotemporal motif characteristics presented in the previous sections exhibited any regional differences, given that it has been suggested that development of different brain regions appear to follow a similar pattern but occur at slightly different time (Dehorter et al., 2012). The average motif size varied with age in all cortical areas (Figure 3.11, panel A), with all regions showing a significant difference between pyramidal and GABAergic populations (MC p = 5.787e-05; S1bod p = 3.211e-14; S1b p = 4.0398e-12; PPC p = 0.0235; VC = 5.339e-09; RS p = 2.843e-06). In the motor cortex (MC, consisting of M1 and M2), the GABAergic population had generally a larger average motif size than the pyramidal population (Figure 3.11, panel A, MC). In the somatosensory body area (S1bod, consisting of S1t and S1f), both populations showed a steady and gradual increase in size, with the GABAergic motif sizes being larger than the pyramidal ones (Figure 3.11, panel A, S1bod). The somatosensory cortex barrel field (S1b) showed a similar trajectory to the one observed when all regions were analysed together (Figure 3.5, panel A). The PPC and RS showed a steady increase in size, with only a small but significant difference between populations (Figure 3.11, panel A, PPC and RS).

The visual cortex (VC, consisting of V1, VISm, and VISl) showed a steep increase in the average size of motifs from P8 until P22, where it plateaued. At P6, the pyramidal cells had a larger size than the GABAergic ones, which is consistent with the fact that there were fewer pyramidal motifs assigned to this region (Figure 3.10, panel B). The sizes of GABAergic and pyramidal motifs seemed to start diverging at around P12, age at which the eyes open, and appeared

to maintain their size differences throughout (Figure 3.11, panel A, VC). The pattern of the regional event frequency trajectories was highly similar across all areas (Figure 3.11, panel B), aligning with the average trajectory observed for all motifs (Figure 3.7, panel A), which exhibited both a significant population and age effect. Specifically, between P14 and P22, the differences between the pyramidal and GABAergic populations seemed to be accentuated, before converging again at P30 (Figure 3.11, panel B).

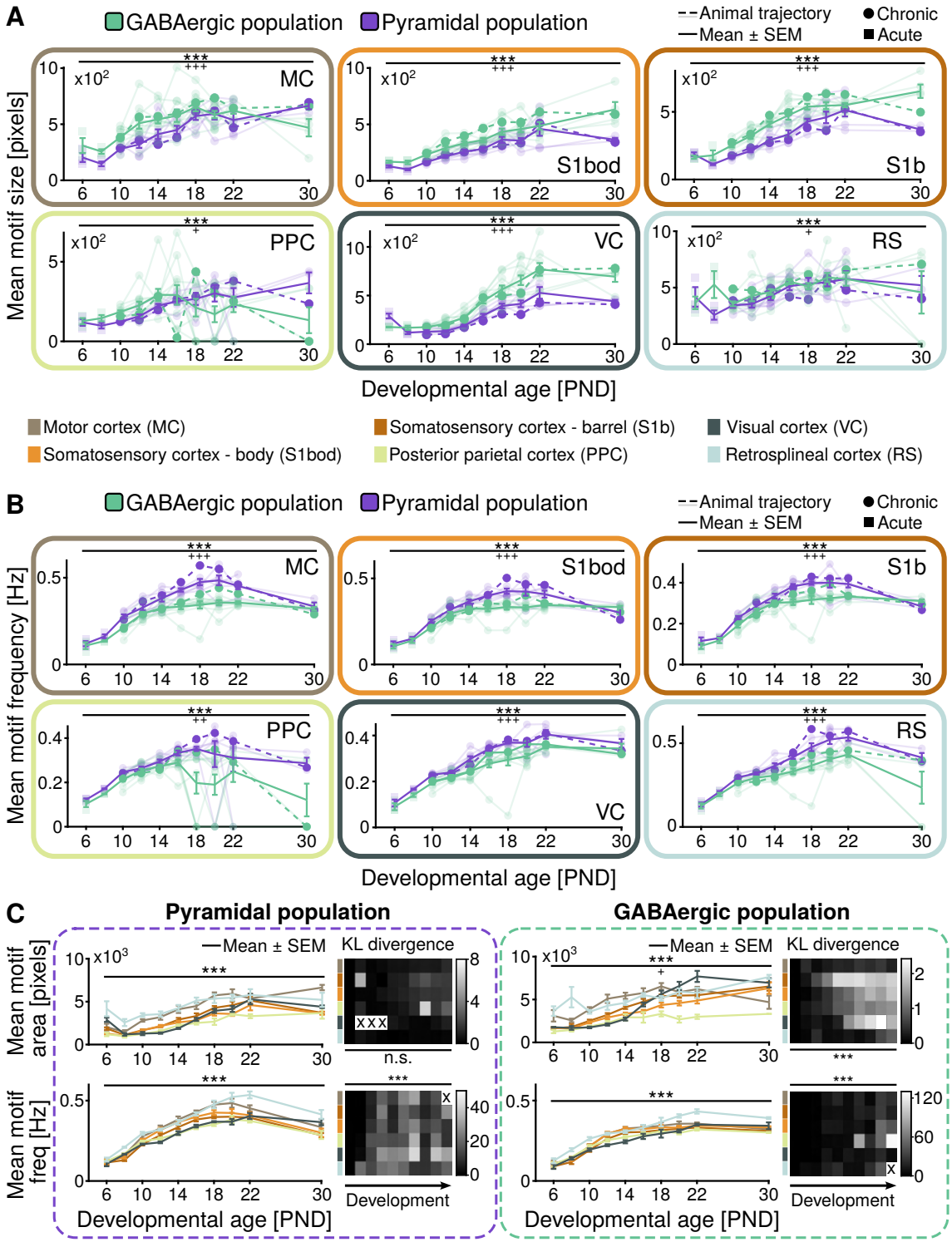

**Fig. 3.11 Motif size and frequency per region across development. A|** The mean motif size (n = 21 animals) per region is significantly different across developmental ages (MC p = 7.680e-09; S1bod p = 2.0075e-21; S1b p = 3.950e-23; PPC p = 1.402e-10; VC = 4.358e-13; RS p = 1.176e-07), and between neuronal populations (MC p = 5.787e-05; S1bod p = 3.211e-14; S1b p = 4.0398e-12; PPC p = 0.0235; VC = 5.339e-09; RS p = 2.843e-06). Significance tested by LMMs. **B|** The mean motif frequency (n = 21 animals) per region is significantly different across developmental ages (MC p = 3.135e-10; S1bod p = 2.0511e-10; S1b p = 8.211e-12; PPC p = 5.180e-13; VC = 2.329e-16; RS p = 2.329e-16), and between neuronal populations (MC p = 2.0217e-13; S1bod p = 6.1524e-05; S1b p = 8.689e-04; PPC p = 0.00128; VC = 7.414e-05; RS p = 7.414e-05). Significance tested by LMMs. **C|** The mean motif size and frequency (n = 21 animals) of all regions is significantly different across developmental ages for the pyramidal (Size p = 4.981e-10; Frequency p = 3.0418e-12) and GABAergic population (Size p = 8.263e-12; Frequency p = 2.441e-09), while it is only significant between regions for the GABAergic mean motif size (Size p = 0.0487; Frequency p = 0.724), and not for the pyramidal ones (Size p = 0.909; Frequency p = 0.953). The KL divergence of the mean motif frequency in all regions exhibited significant differences across developmental ages for both the pyramidal (p = 1.517e-05) and GABAergic populations (p = 8.383e-08). Similarly, the mean motif size showed significant differences across developmental ages for the GABAergic population (p = 3.0565e-08), but not for the pyramidal population (p = 0.748). On the other hand, the KL divergence of the mean motif size and frequency across regions is not significant for either neuronal population, pyramidal (Size p = 0.430; Frequency p = 0.784) and GABAergic (Size p = 0.323; Frequency p = 0.0965). Significance tested by LMMs. The black crosses displayed on the heatmap indicate the values that reached over the the maximum limit of KL divergence shown on the colour-bar, and were capped at that maximum value for visualisation purposes. Significance tested by LMM. Further statistical information in Annex 4.2. Significance is shown for age (population/region) as *($^{+}$) for $p < 0.05$, **($^{++}$) for $p < 0.01$, ***($^{+++}$) for $p < 0.001$.

The average trajectories of event frequency and average motif size for different brain regions were compared separately for each neuronal population (Figure 3.11, panel C). A significant difference across regions was only observed for the mean motif size in the GABAergic population (p = 0.0487), while the frequency showed no differences across regions (GABAergic p = 0.724; Excitatory p = 0.953), displaying only a significant developmental change (Figure 3.11, panel C; Excitatory: Size p = 4.981e-10, Frequency p = 3.0418e-12; GABAergic: Size p = 8.263e-12, Frequency p = 2.441e-09). Furthermore, the KL divergence measurements of the changes in the probability distributions of motif size and frequency during development did not exhibit any regional differences but showed a significant change over time, except for the motif size distributions of the pyramidal population (Figure 3.11, panel C, top left). This implies that, despite the increasing average pyramidal motif size in different brain regions during development, the shape of the distribution of motif sizes remains relatively stable over time for the pyramidal population.

### 3.3.3 Complexity of cortical population dynamics across early development.

The intricate interaction between GABAergic and excitatory neurons during early postnatal development is essential for comprehending the maturation of cortical circuitry. Therefore, understanding the functional interactions and divergence between these populations is crucial for unravelling the establishment of cortical microcircuits.

### Age and region-specific changes in variance highlight the developmental diversity of cortical activity patterns.

Clear differences were apparent in the variance of the neocortex-wide activity of each neuronal population, which can provide insights into the modulation of spontaneous activity across development and between cortical regions (Figure 3.12, panel A). While the previous spatiotemporal properties explored focused on spatial characteristics and frequency of the activity, the variance can capture degree of fluctuation or stability in the activity levels, offering insights into the dynamic nature of the activity motif. This temporal dimension of variance allows to explore the temporal dynamics and heterogeneity of activity patterns, offering additional information about the underlying neural processes and their modulation. As the cortex matures, the total variance of cortex-wide activity varied across regions, showing a high modulation of a large portion of the cortex at early ages (P10-P12), compared to more matures stages, which showed higher modulation in more discrete areas (Figure 3.12, panel A). For example, at older ages, the total variance of cortex-wide activity was largest in the somatosensory body cortical regions and association areas like RS, for both the GABAergic and pyramidal populations. In contrast, at younger ages, the variance was highest in the visual cortex for the pyramidal population, but not for the GABAergic population (Figure 3.12, panel A).

A comparison of the total variance in each region was conducted across neuronal populations to assess developmental and population effects. In the MC, significant age dependent changes in variance were observed, with a fast increase in variance for both populations up to P12, and a gradual decrease after (Figure 3.12, panel B, MC), which showed significant population differences. In contrast, the S1bod area exhibited no age-dependent changes in variance, while showing a significant difference between populations, with the GABAergic population generally showing a higher variability than the pyramidal population (Figure 3.12, panel B, S1bod). The S1b showed no population differences with a strong developmental dependence, displaying two peaks in variability,one between P6 and P14 and a second peak at P20 (Figure 3.12, panel B, S1b). The PPC exhibited both age and population effects, with a gradual decrease in total variance across ages and fluctuation of dominance across populations (Figure 3.12, panel B, PPC). Surprisingly, the VC did not display significant age-dependent and population changes in variance (Figure 3.12, panel B, VC). RS did not show a difference between populations but exhibited a change over development, similar to the PPC, with a gradual decrease in total variance across ages (Figure 3.12, panel B).

Comparing developmental trajectory of different regions is crucial in order to investigate whether the maturation of the spontaneous activity follows a common course across brain areas. The pyramidal population displayed significant changes in the total average variance not only across ages, but also between regions (Figure 3.12, panel C, left; Age $p = 0.00491$; Regions $p = 4.666e-05$). However, the distribution of motif variance across regions did not show a significant change over time, which suggests that while the average motif variance changed across development,

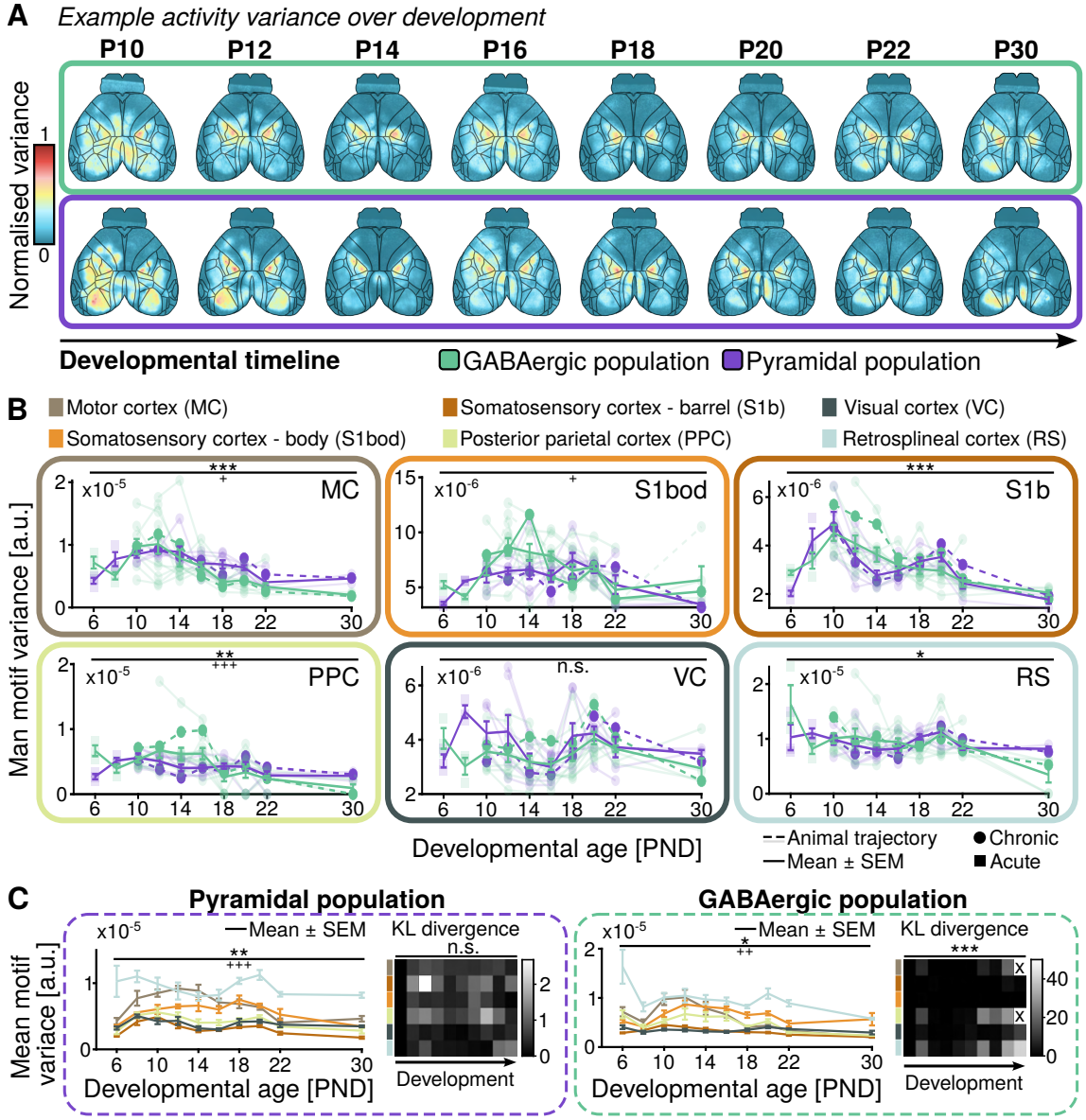


**Fig. 3.12 Developmental changes in population and region-specific variance of cortical activity.** **A|** Example of total variance maps across development for each neuronal population. **B|** The mean motif variance (n = 21 animals) per region is significantly different across developmental ages for the MC, S1b, PPC and RS (MC p = 3.0331e-09; S1bod p = 0.490; S1b p = 2.910e-13; PPC p = 0.00189; VC = 0.517; RS p = 0.0457), and between neuronal populations for all regions but the S1b and RS (MC p = 0.0287; S1bod p = 0.0114; S1b p = 0.121; PPC p = 2.250e-04; VC = 0.830; RS p = 0.239). Significance tested by LMMs. **C|** The mean motif variance (n = 21 animals) of all regions is significantly different across both developmental ages (Excitatory p = 0.00491; GABAergic p = 0.0114) and regions (Excitatory p = 4.666e-05; GABAergic p = 0.00117) for both populations. The KL divergence of the mean motif variance of all regions is significantly different across developmental ages for the GABAergic population (p = 7.647e-05), and not the pyramidal one (p = 0.428), while the mean motif variance is not significantly different between regions for either neuronal population, pyramidal (p = 0.0794) and GABAergic (p = 0.738). Significance tested by LMMs. The black crosses displayed on the heatmap indicate the values that reached over the the maximum limit of KL divergence shown on the colour-bar, and were capped at that maximum value for visualisation purposes. Further statistical information in Annex 4.2. Significance is shown for age (population/region) as *($^{+}$) for $p < 0.05$, **($^{++}$) for $p < 0.01$, ***($^{+++}$) for $p < 0.001$.

the spread or shape of the motif variance distribution remains relatively consistent over time. In other words, the overall amount of variability of the motif variance changes over time, but the way in which this variability is distributed within a region across development does not change significantly. For example, if a group of neurons becomes desynchronised in their firing, the total average variance of the signal would increase, since the activity of those neurons is now less tightly linked, without having to change the shape of the variance distribution. Similarly, the GABAergic population showed a significant regional ($p = 0.00117$) and developmental ($p = 0.0114$) changes in the total average variance, but also displayed a significant age-dependence change in the shape of variance distributions across development (Figure 3.12, panel C, right, $p = 7.647e-05$). This suggests that, for the GABAergic population, there were still ongoing changes in the activity patterns that affected the shape of the variance distribution. Changes in the proportion of firing rate types across neurons could affect the shape of the distribution. For example, if the contribution of fast-spiking neurons to the overall signal increases, highlighting the ongoing maturation of feed-forward (fast-spiking neurons) inhibition that is taking place throughout the second and third postnatal weeks (Daw et al., 2007).

### Developmental differences in the number of activity motifs between populations reflects unique changes in the complexity of cortical dynamics.

The differences observed in the motif variance suggest that there are distinct spatiotemporal patterns of cortex-wide activity for each neuronal population that change across development. The overall complexity of cortical dynamics can be captured by the number of sICA activity motifs, and changes in these can point to population-specific activity differences. The number of motifs required to describe the cortical dynamics across development for each population was found to differ significantly (Figure 3.13, panel A, Age $p = 1.584e-34$; Population $p = 1.193e-07$). Moreover, the animal identity across ages, showed a significant effect on the statistical model fitting ($p = 5.971e-06$), indicating that the variation in the number of motifs per animal across ages is important for accurately capturing the underlying patterns in the data. This implies that the effect of age on the response is not constant across all individuals, but rather there are individual-specific variations. The pyramidal population showed a sharp increase in the number of motifs from P6 to P10, gradually decreasing over time. In contrast, the GABAergic population had a higher number of motifs at P6, which remained constant until around P10, before decreasing at a similar rate as the pyramidal population, ultimately resulting in a significantly smaller number of GABAergic motifs (Figure 3.12, panel A). This finding is consistent with the fact that GABAergic motifs tend to be larger in size (Figure 3.5, panel B).

These changes were primarily driven by the number of motifs exhibiting a single activity motif (Figure 3.13, panel B), as multi activity motifs appeared in a much smaller proportion and did not show a significant difference across populations (Figure 3.13, panel B, example motif masks). However, multi activity motifs were the ones which showed the significant effect of the animal identity across ages on the statistical model fitting ($p = 8.53e-12$); therefore, indicating that the

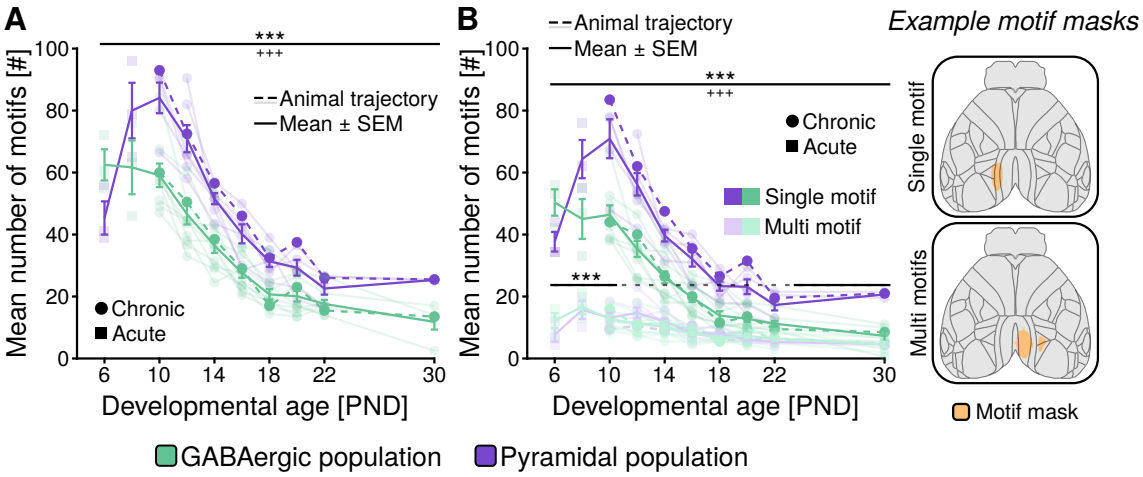


**Fig. 3.13 Distinct developmental trajectories of activity motifs in pyramidal and GABAergic neuronal populations. A|** The mean sICA motif number (n = 21 animals) is significantly different across developmental ages (p = 1.584e-34) and between neuronal populations (p = 1.193e-07). To the right is an example of the probability distribution function (PDF) of motif sizes for each population at P12 and P18. Black crosses indicate the data points chosen for each population and age. Significance tested by GLMM. **B|** The mean sICA single and multi motif number (n = 21 animals) is significantly different across developmental ages (Single p = 3.737e-13; Multi p = 2.185e-17) and between neuronal populations for the single (p = 1.190e-11) and not the multi (p = 0.262) motif numbers. To the right is an example of the probability distribution function (PDF) of motif sizes for each population at P12 and P18. Black crosses indicate the data points chosen for each population and age. Significance tested by GLMMs. Further statistical information in Annex 4.2. Significance is shown for age (population) as *($^{+}$) for $p < 0.05$, **($^{++}$) for $p < 0.01$, ***($^{+++}$) for $p < 0.001$.

heterogeneity in the individual animal trajectories across ages comes from differences in the multi activity motifs. Multi activity motif components happen when there are multiple regions which share common statistical features which make them hard to separate, such as similar temporal dynamics or overlapping spatial patterns. The overall reduction in the number of motifs over development suggests that cortical dynamics become less complex over time. This may be because as the brain matures, the neural activity becomes more specialised and less variable. It is often assumed that the complexity of cortical dynamics should increase with development, as the brain becomes more structurally and functionally mature. However, there are other different factors that can lead to changes in the complexity of cortical dynamics over development. For example, changes in the sensory input statistics due to the start of the active sensing period. Although, the number of multi activity motifs showed a significant developmental decrease, the proportion of single to multi activity motifs increases. This switch from single to multi region activity might reflect a higher weight on complex patterns of activity that involve multiple regions, which seems to follow animal-specific trajectories. As such, the developmental decrease in the number of motifs required to explain the activity may actually represent an increased functional coordination between regions rather than a decrease in complexity.

The study employed two different calcium indicators, GCaMP6f and jRGECO1a, to image the GABAergic and pyramidal neuronal populations, respectively. Although both indicators have similar kinetics, their different emission wavelengths can affect the amount of signal detected

by the imaging system, as well as the amount of background noise. Consequently, this would impact the SNR of the data collected, which can in turn affect how the sICA performs the decomposition. A low SNR can make it harder for the sICA algorithm to accurately separate the different components, resulting in a greater likelihood of mixing or misidentification of the components. Therefore, if the SNR varies across populations and developmental ages, observations could have been confounded by the changes in SNR and not necessarily by the underlying biological factors studied. The SNR (peak signal to background ratio) for both populations showed significant age-dependent changes, as well as a significant difference across populations (Figure 3.14, panel A; Age p = 1.301e-09; Populations p = 4.730e-08). The background fluorescence was estimated by calculating the median of the difference between consecutive imaging frames, as the imaging rate was much higher than the dynamics of the calcium indicator and therefore, consecutive frames could be used to approximate of the background fluorescence. This decrease in the SNR could be due to changes in indicator expression and background fluorescence, as well as skull thickening during early development. To assess the potential impact of these changes, the relationship between SNR and performance of PCA/sICA in detecting activity motifs was assessed. Although the SNR showed a weak positive correlation with the number of sICA motifs (Figure 3.14, panel B), suggesting a mild inter-dependency, both populations followed the same tendency.

To directly test the effect of the SNR on the number of motifs, the SNR values from all recordings were adjusted to a target value. This involved equalising the SNR across all recordings by adding noise to achieve the same SNR value. This target SNR was set to the minimum SNR value observed in the entire dataset, ensuring consistency across all imaging datasets obtained from chronically imaged animals. After equalising the SNR, the sICA decomposition was rerun to assess its effect on the resulting motifs (Figure 3.14, panel C). Similar results were found when comparing the equalised SNR dataset to the number of sICA motifs obtained, specifically in the observation of a significant reduction in the number of motifs across development, with a highly significant population effect (Figure 3.14, panel D; Age p = 2.122e-12; Populations p = 7.796e-24). However, the rate of decrease in the number of motifs was slightly different across populations, with the GABAergic motifs reducing at a slower rate. The reduction in the average number of sICA motifs found before and after equalising the SNR across the dataset showed a slightly more significant decrease in the GABAergic population compared to the pyramidal one (Figure 3.14, panel E). This could indicate a higher sensitivity of the GCaMP6f signal to changes in SNR. The proportion of motifs lost between the original dataset and the reduced SNR version exhibited a highly significant age-dependent effect (p = 1.362e-05), with no population differences (Figure 3.14, panel F). However, there was a tendency to observe a proportionally greater loss of GABAergic motifs from the original dataset in the reduced SNR dataset compared to the pyramidal motifs, particularly at younger ages, which disappeared at older ages. Taken together, these results showed that the decline in the number of motifs observed across early development (Figure 3.13, panel A) could not be attributed to a decrease

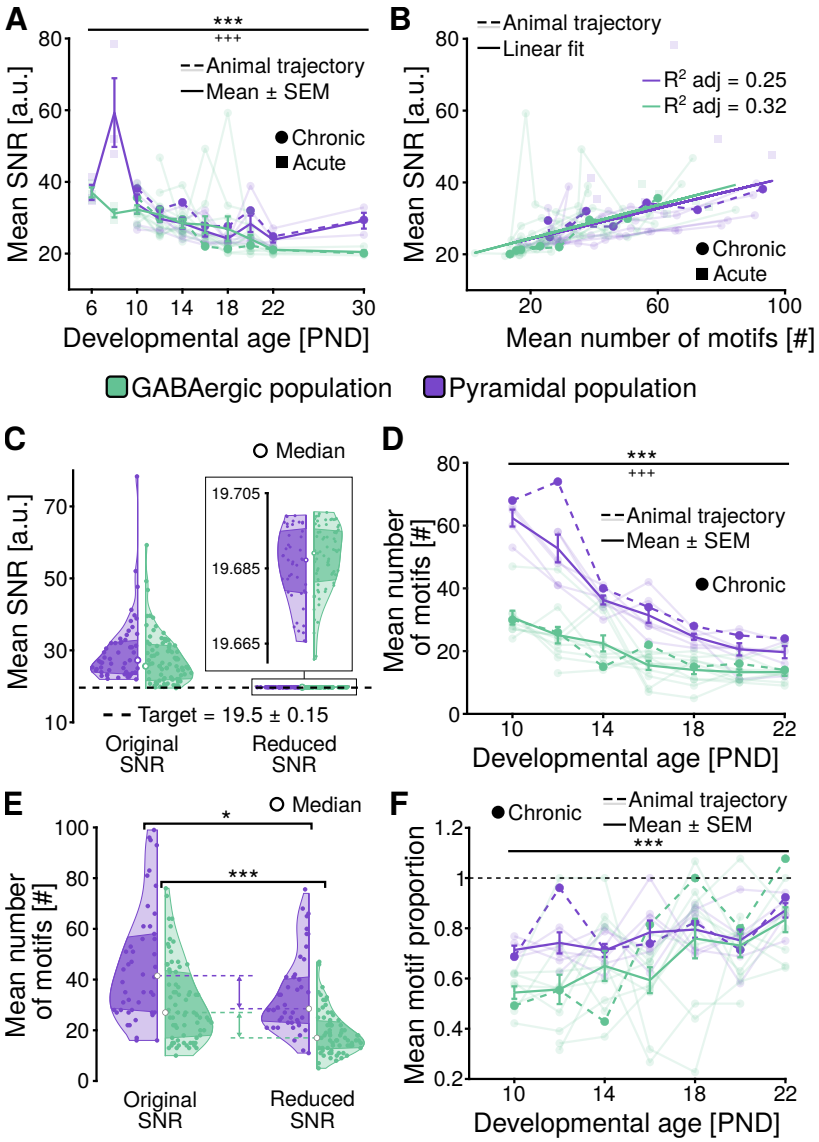


**Fig. 3.14** **Influence of SNR on the sICA decomposition of GCaMP6f and jRGECO1a dynamics. A|** The mean SNR (n = 21 animals) is significantly different across developmental ages (p = 1.301e-09) and between neuronal populations (p = 4.730e-08). Significance tested by GLMMs. **B|** The mean SNR is weakly correlated with the mean number of motifs (n = 21 animals) for both the pyramidal ($R^2$ adjusted = 0.25) and GABAergic ($R^2$ adjusted = 0.32). Solid dark lines indicate the fit of a robust linear regression for each neuronal population across all recordings. **C|** The mean SNR distribution for the pyramidal and GABAergic populations for the original recordings and the reduced SNR ones (n = 15 animals, 98 recordings). The reduced SNR distributions fluctuate around the target SNR = 19.5 + 0.15. **D|** The mean number of motifs (n = 15 animals) is significantly different across age (p = 2.122e-12) and between populations (p = 7.796e-24). Significance tested by GLMMs. **E|** The distributions of the mean number of motifs before (Excitatory n = 49; GABAergic n = 78 recordings) and after (Excitatory n = 46; GABAergic n = 73 recordings) SNR reduction significantly differ for the pyramidal (p = 0.0123) and GABAergic populations (p = 1.993e-07). Wilcoxon rank sum test for equal medians: Excitatory $Z$ = 2.503; GABAergic: $Z$ = 5.200. **F|** The mean number proportion (n = 15 animals) is significantly different across age (p = 1.362e-05), but not between populations (p = 0.14493). Significance tested by LMMs. Further statistical information in Annex 4.2. Significance is shown for age (population) as *($^+$) for p < 0.05, ***($^{+++}$) for p < 0.001.

in the SNR. Instead, it may indicate genuine variations in dynamics across development and between the two populations.

### 3.3.4 Developmental maturation of excitation and inhibition balanced temporal dynamics.

Understanding the relationship between the temporal dynamics of pyramidal and GABAergic (inhibitory) neurons is crucial for the study of brain dynamics. However, there is a debate about the degree of correlation between these two populations and whether inhibition just merely follows excitation or plays an active role in orchestrating activity dynamics. Recent studies involving simultaneous single-cell recordings of pyramidal and inhibitory inputs *in vivo* have shown that both populations are continuously synchronised, exhibiting a tight instantaneous correlation and highly correlated strength during spontaneous and sensory-evoked activities in the rat somatosensory cortex (Okun et al., 2008). Furthermore, the level of balance between excitation and inhibition depends on the time scale of the correlation between them, with a global balance for slow correlations (long time scales) and a fine-scale balance for strong correlations with a fast time scale (Zhou et al., 2018). Understanding this interplay is especially important during development, as a tight EI balance has not yet formed (Dorrn et al., 2010), strengthening rapidly during the second and third postnatal weeks due to a rapid increase in inhibition (Zhang et al., 2011b; Chini et al., 2022). This balance is generally assessed at the level of synapses (Zhang et al., 2011b), and the level of single cell spikes (Chini et al., 2022); or even at the level of feature representations like tuning curves (Dorrn et al., 2010), but most times is only assessed in an specific cortical region, and not brain-wide.

Simultaneous recordings of pyramidal and GABAergic inputs allowed the investigation of their temporal relationship and its changes during early postnatal development. Since the sICA motifs were independently found for each population, it was necessary to match each pyramidal motif with its GABAergic partner. This can be challenging since the number and size of the motifs differed between the populations, and therefore, some motifs may not have a exact matching spatial partner. GABAergic motifs were larger but less abundant, while pyramidal motifs were smaller but more numerous; both decreasing in number during development (Figure 3.15, panel A, example sICA motif masks for simultaneously recorded GABAergic and pyramidal populations). To identify the matching partners between pyramidal (E) and GABAergic (I) motifs, the Jaccard index (JI) was calculated to determine the percentage of overlap between motif masks of the two populations (Figure 3.15, panel B). The JI overlap matrices were sorted based on the EI partners with the highest JI value, thereby pairing each pyramidal motif with its best matching GABAergic partner. These matrices demonstrated a broad spectrum of overlap values, with the maximum overlap value between any given motif partners varying widely, with some motifs not having a partner match at all (Figure 3.15, panel B, maximum overlap values per motif projected on each side of the matrix). The distribution of all JI values was skewed with most motifs sharing near zero overlap, and just a few motifs having higher JI values (Figure 3.15,

panel B, pyramidal distributions). Three examples of the spatial overlap between EI partners with different maximum JI values are shown in Figure 3.15, panel B, from a high overlap (0.85, 85% of motif masks overlapping) to a very small overlap (0.02, 2% of pyramidal mask overlapping). Each motif mask is outlined by population, with the overlap between the masks of the two motifs shown in orange (Figure 3.15, panel B, spatial overlap).

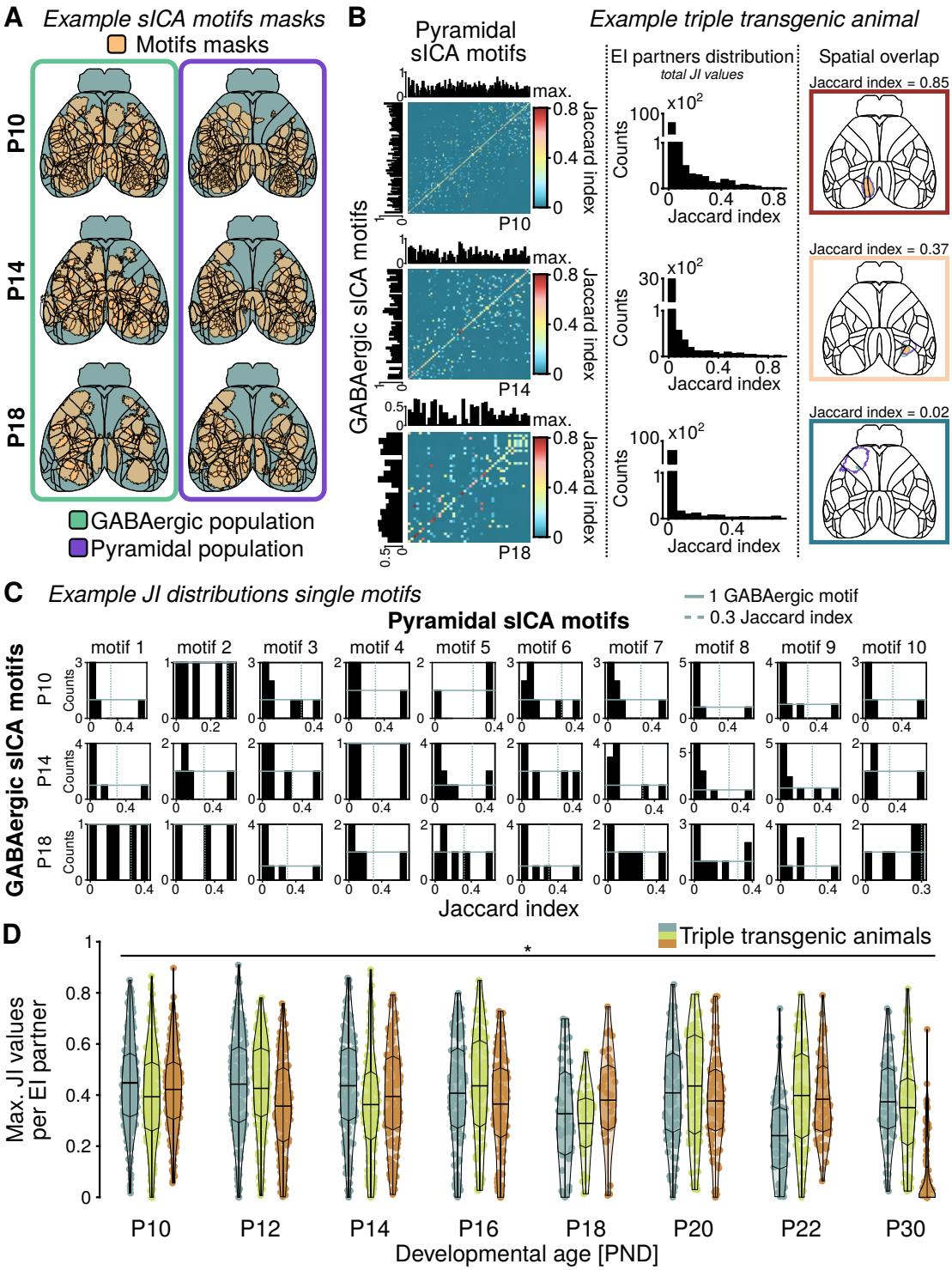

**Fig. 3.15 Overlap distributions between pyramidal and GABAergic sICA motifs across development. A|** Representative example of all sICA motif masks obtained at different developmental ages for both neuronal populations. **B|** Matrix of JI of the examples in A, comparing the GABAergic motif masks with the pyramidal ones (left panels). Side histograms represent the maximum JI values of EI and IE partners. Matrices are non-symmetrical. Zero values are shown as dark teal indicating no overlap. Histogram counts of the JI values fo the all EI partners of the examples in A (middle panels). Examples illustrating the spatial overlap of three different EI partner motifs, each with distinct JI values (right panels). **C|** Histogram counts of the overlap (JI values) between 10 representative pyramidal motifs, and all the GABAergic motifs per age. GABAergic motifs with zero overlap (the majority) are not included in the counts. Dashed lines indicated the JI threshold for minimum similarity (JI = 0.3). Solid lines indicates one GABAergic motif. **D|** The distributions of maximum JI values per EI partner for the triple transgenic animals (n = 3 animals) did not significantly changed across developmental age ($p = 0.133$) or across animals ($p = 0.689$) individually, but the combined influence of age and animal led to a significant change in the distributions ($p = 0.0482$). Significance tested by LMMs. Further statistical information in Annex 4.2. Significance is shown for age *** for $p < 0.001$.

To select the best matching GABAergic partner for a given pyramidal motif, a minimum amount of overlap with them was required. A single pyramidal motif could have multiple GABAergic partners if the overlap was above 0.3 JI. The histograms of JI overlap values with all possible GABAergic motifs for 10 example pyramidal motifs are displayed in Figure 3.15, panel C. Most pyramidal motifs had only one matching GABAergic motif above the threshold, but some had more (e.g., pyramidal motif 5 at P10, or pyramidal motif 6 at P14). Thus, all GABAergic motifs with a JI greater than 0.3 were chosen as partners for that same pyramidal motif, and their temporal weights were summed up to create a new signal representing the combined dynamics of those GABAergic motifs. This way the EI partners were generated for future analysis. The distributions of maximum JI values across development showed a slight but significant decrease in average, that resulted from the combined influence of developmental age and animal identity (Figure 3.15, panel D; $p = 0.0482$), due to the smaller number of motifs obtained at older ages (Figure 3.13, panel A), which might worsen the EI matching across motifs. This result suggested that the relationship between the JI distributions and the age and animal identity was not simply additive but depended on the interaction between them. This interaction effect indicates that the effect of age may differ depending on the specific animal identity.

To assess their temporal dynamics, it is important to examine instantaneous changes in the relationship between EI partners, rather than relying on average correlations. This is because, over prolonged temporal scales, excitatory and inhibitory dynamics are usually tightly coupled and highly correlated, even during development (Mulholland et al., 2021). Therefore, to explore the ongoing temporal relationship between the two populations during development, the temporal weights of each EI paired motif were used to calculate the instantaneous correlation using a non-overlapping rolling window. An example of the temporal activity traces from 10 EI matched motifs, and their instantaneous correlation over a 1.5 second rolling window for a full 6 minute recording is shown in Figure 3.16, panel A. Generally, the correlation between activity in E and I was very high, but the correlation traces displayed dynamic fluctuations, with peaks of low correlation indicating times when the relative activation of the pyramidal and GABAergic

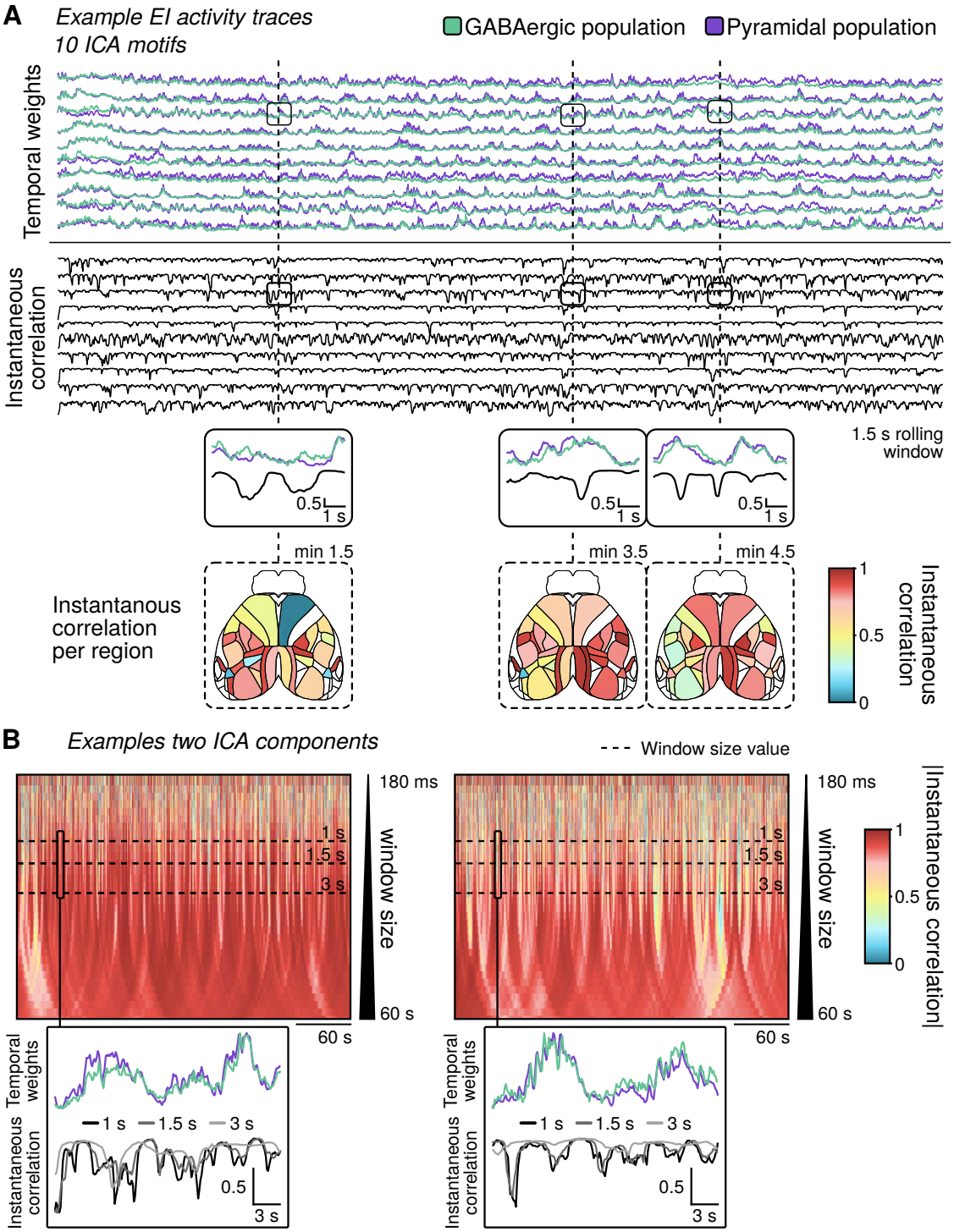


**Fig. 3.16** **Instantaneous correlation between GABAergic and pyramidal dynamics across different temporal scales. A|** Representative examples of the temporal weights and instantaneous correlation of 10 EI partners pairs. Instantaneous correlation was calculated using a 1.5 s rolling window. The lower section illustrates magnified insets showing the dynamics and correlation of an example EI partner, along with spatially projected correlation values for each region at that given temporal snapshot. **B|** Each example heatmap shows the instantaneous correlation for an example EI partner pair for a given rolling window size. Rolling indows sizes are logarithmically increased from 180 ms to 60 s. The lower section shows the activity dynamics of the EI partner pair and the instantaneous correlation values for three different representative rolling window sizes of 1, 1.5 and 3 s.

populations changed during bouts of spontaneous cortical activity. For example, an instance where the correlation between the two populations was reduced can be observed at minute 1.5, which was due to an increase in the GABAergic activity relative to the pyramidal one (Figure 3.16, panel A, zoomed in inset). In contrast, at minute 3.5, the reduced correlation was due to an increase in the pyramidal activity relative to the GABAergic one. Examining snapshots of the correlation state of all EI partners at different time points by projecting them to the dorsal cortex, can reveal the correlation state of the brain across different regions (Figure 3.16, panel A, instantaneous correlation per region). For instance, there were time points when frontal areas were less correlated than posterior areas (minute 1.5), or when most of the cortex was highly correlated (minute 3.5), as well as times when one hemisphere was highly correlated while the other was not (minute 4.5), all within the same recording.

The rolling window chosen to calculate the correlation between the two populations is important, as it determines the timescale of the correlation. If the rolling window is too small, the correlation will appear noisy, whereas if the rolling window is too large, the correlation will be smoothed out. Therefore, it is crucial to define the optimal rolling window for this correlation, given that excitation and inhibition have been shown to be correlated at very different timescales (Zhou et al., 2018; Delaney et al., 2023). Different rolling time windows were used to calculate the instantaneous correlation for two example EI partners (Figure 3.16, panel B). Large rolling windows led to a smooth and continuous correlation across time, losing the dynamic information between the pyramidal and GABAergic populations; while small rolling windows lead to noisy fluctuations in correlation values (Figure 3.16, panel B; Dehghani et al., 2016). The effect of the rolling window length on correlation smoothing is displayed in Figure 3.16, panel B bottom insets, with a 3-second rolling window showing excessive smoothing of the correlation, while the 1 and 1.5-second rolling windows were able to keep better track of the population behaviour. The rolling window of 1.5 seconds was chosen for future analysis of instantaneous correlation.

### Regional differences in the developmental tightening of the correlation between the GABAergic and pyramidal populations.

To assess changes in the relationship between EI pairs across development, the instantaneous correlation ($R_{1.5}$) was calculated for all three triple transgenic animals at each different developmental age. The mean $R_{1.5}$ displayed a significant change over development, gradually increasing until P20, to decrease thereafter (Figure 3.17, panel A). This indicates that the pyramidal and GABAergic population become more correlated during development between P10-P20. The average correlation was reduced and became much more variable between animals at older ages, possibly due to the smaller number of motifs and resulting overall weaker overlap of spatial alignment between EI partners. The increase in correlation through earlier stages was due to a reduction in the time spent in a low correlation mode (correlations below 0.7, Figure 3.17, panel B).

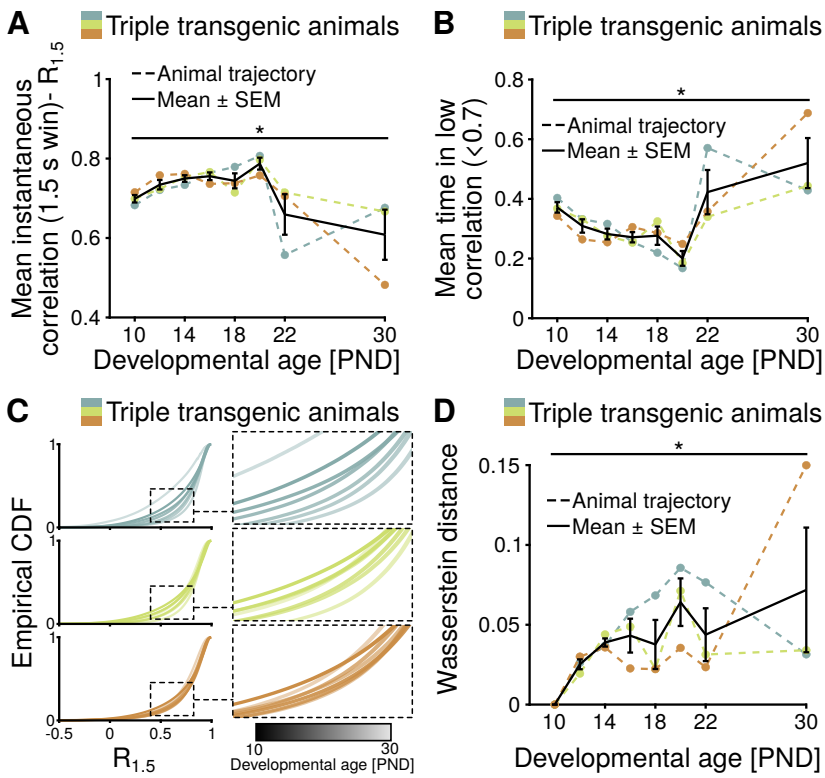


**Fig. 3.17** **Strengthening correlation between GABAergic and pyramidal dynamics during development. A|** The mean $R_{1.5}$ (n = 3 animals) significantly changes across development (p = 0.0463). Significance tested by LMMs. **B|** The mean time spent in low $R_{1.5}$ (n = 3 animals) significantly changes across development (p = 0.0257). Significance tested by LMMs. **C|** The empirical CDFs of all $R_{1.5}$ values for all motifs per age show a gradual shift towards higher correlation values. **D|** The Wasserstein distance between the eCDFs (n = 3 animals) significantly increases across ages (p = 0.0122). Significance tested by GLMMs. Further statistical information in Annex 4.2. Significance is shown for age *** for p < 0.001

The distribution of $R_{1.5}$ values from any given recording was highly skewed towards a tail of infrequent low correlation values. Therefore, instead of just considering the average $R_{1.5}$, the distribution of $R_{1.5}$ values per recording was analysed and compared across the different ages. The cumulative distributions of $R_{1.5}$ values shifted towards higher correlation (to the right) as the animals became older (Figure 3.16, panel C). The shift between these cumulative distributions across age for each animal was measured by the Wasserstein distance. This reveals a significant increase in the distance between distributions across development (Figure 3.16, panel D), driven by a significant shift of the cumulative distributions towards higher correlated values. The Wasserstein distance is better suited to calculate differences across cumulative distributions because it takes into account the structure and geometry of the distributions, and therefore, it is more sensitive to changes in its shape; while the KL divergence is a measure of dissimilarity that is based on the relative proportions of samples in each distribution, it is a measure of information loss. Although the change in the distribution is significant over development, the distance between the distributions seems to plateau at around 0.05 distance value, which corresponds to a 3.3% change in the distance, indicating that the distributions presented a relatively similar structure. This suggested that the dynamic fluctuations between

the pyramidal and GABAergic populations became tighter and more highly correlated between P10-P20.

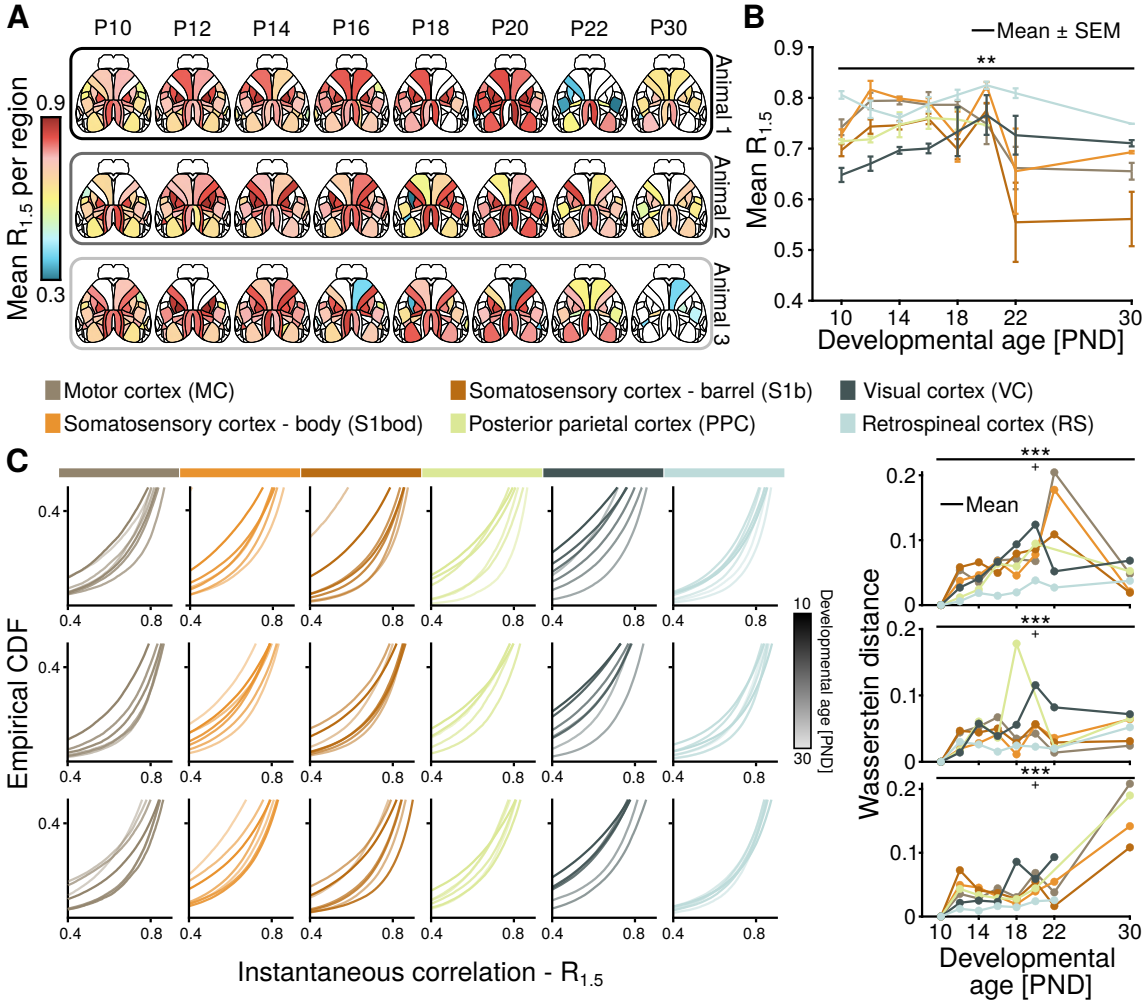


**Fig. 3.18 Region-specific tightening of correlation between GABAergic and pyramidal dynamics.** **A|** Visualisation of the mean $R_{1.5}$ per region throughout development, mapped onto the Allen CCF atlas, for each individual triple transgenic animal. **B|** The mean instantaneous correlation (n = 3 animals) significantly changes across development (p = 0.00327), but not between regions (p = 0.0913). Significance tested by LMMs. **C|** The empirical CDFs of all $R_{1.5}$ values for all motifs per region and age show a gradual shift towards higher correlation values (left panels). The Wasserstein distance between the eCDFs (n = 3 animals) is significantly different across ages (p = 0.00172) and regions (p = 0.0402). Significance tested by GLMMs. Further statistical information in Annex 4.2. Significance is shown for age *** for p < 0.001

Do these changes occur uniformly across different brain regions? The $R_{1.5}$ values showed varied regional patterns across development (Figure 3.18, panel A). However, the average $R_{1.5}$ trajectories did not show significant differences across regions (p = 0.0913), while they varied significantly across age (Figure 3.18, panel B; p = 0.00327). Yet, when examining the distribution of $R_{1.5}$ values across regions and their changes over development (Figure 3.18, panel C), there was a significant effect of both age (p = 0.00172) and region identity (p = p = 0.0402). For instance, the RS exhibited a stable average correlation throughout the developmental ages examined (Figure 3.18, panel B; light blue), with minimal changes in its cumulative distribution

across ages (Figure 3.18, panel C; light blue). In contrast, the VC displayed a pronounced increase in the distance between cumulative distributions from P10 to P20 (Figure 3.18, panel C; dark blue). This suggests that tightening of the GABAergic and pyramidal dynamics follow different developmental trajectories in distinct brain regions, which could indicate specific regional maturation patterns, despite following the similar average behaviour.

### Blocking GABAergic transmission drives correlation between the pyramidal and GABAergic population to higher values.

In order to test whether the instantaneous correlation between GABAergic and pyramidal activity dynamics can reflect changes in their interplay, the effect of acute perturbation of the link between pyramidal and GABAergic populations on $R_{1.5}$ was tested. To achieve this, GABAergic signalling was blocked by injecting picrotoxin (PTX), a non-selective antagonist of GABA$_A$ receptors, to inhibit of the synaptic effects of GABA neurotransmitter. This manipulation was performed unilaterally in the primary somatosensory cortex barrel area (Figure 3.19, panel A). The session consisted of an initial control recording, saline injection followed by two recordings within a 15-minute window, then PTX injection followed by repeated PTX recordings over a 40-minute period (Figure 3.19, panel A, bottom). In this way, the effects of inhibiting GABAergic signalling on spontaneous neuronal activity and EI correlation could be assessed within the same animal. Control and saline (vehicle) conditions showed sparse and discontinuous activity events, while the PTX injection led to a rapid increase in event frequency, exhibiting epileptic-like activity in the ipsilateral injection site, but not the contralateral (Figure 3.19, panel B). This high-frequency event activity relaxed by 40 minutes after injection time, but still showed some remnants of higher event correlation compared to the control conditions (Figure 3.19, panel B). This change in local activity confirms that the pharmacological perturbation of GABAergic signalling dramatically shifts the profile of activity in pyramidal and GABAergic neuronal populations. The spatial coverage of the motifs obtained for each of the conditions did not change, but there was a significantly larger spatial coverage of the GABAergic population compared to the pyramidal one (Figure 3.19, panel C, p = 2.308e-09). The PTX injected mice were aged between P8 and P12, and those early ages previously showed a tendency towards a larger coverage of the cortex by the GABAergic population compared to the pyramidal one (Figure 3.4, panel B), which could explain this difference. Importantly, after the PTX injection, there was a slight bias towards larger coverage of the injected site compared to the contralateral hemisphere (p = 0.0350), while no such difference was observed for the saline condition or between neuronal populations (Figure 3.19, panel D). These findings indicate that the drug had an impact on the patterns of spontaneous activity around the injected area, providing evidence of its effectiveness compared to the control conditions.

The number of sICA motifs did not vary significantly across different conditions, but there was a difference between the two populations (Figure 3.20, panel A). As it was previously shown, the pyramidal population displayed a higher number of motifs, particularly in control

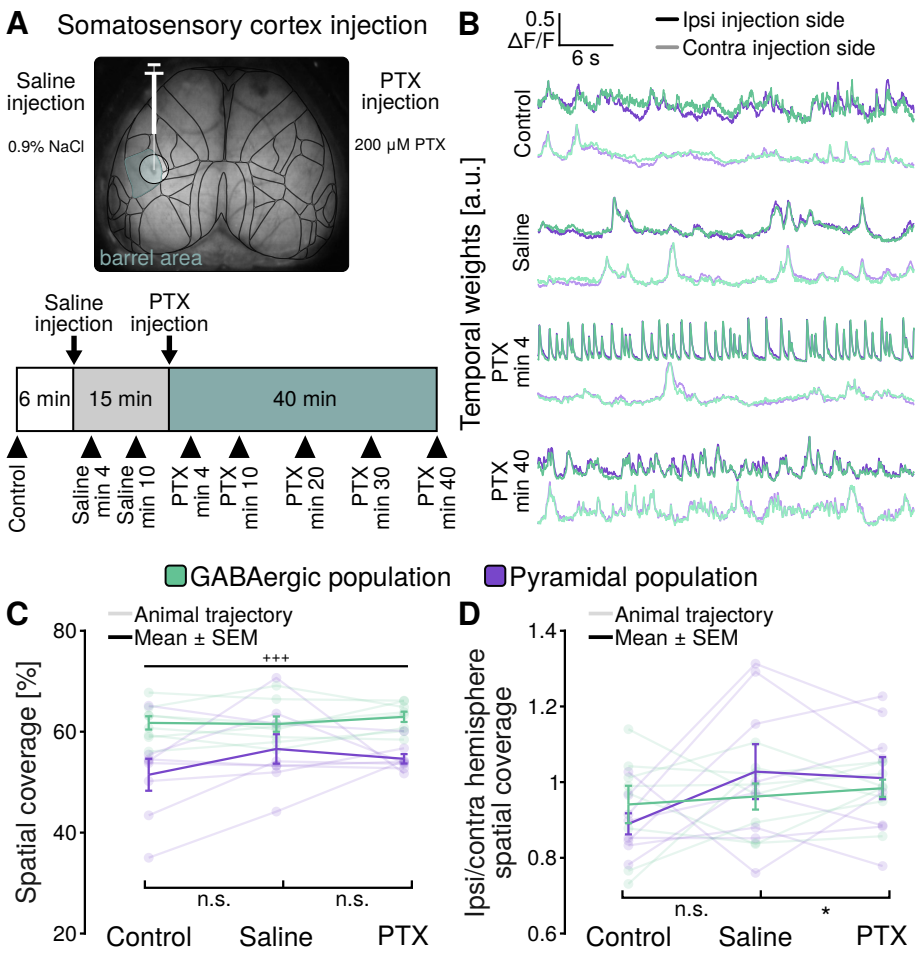


**Fig. 3.19** **Epileptic-like activity induced by blockade of GABAergic signalling. A|** Schematic depicting the experimental setup for drug/vehicle injection experiments. The S1 barrel area is highlighted in light teal. A window is surgically opened on the left hemisphere, specifically targeting the S1 barrel area. Below the diagram, a timeline illustrates the injection time points (black arrows), along with the times of the recordings (black triangles). **B|** Representative activity traces of example motifs, both ipsilateral and contralateral to the injection site. The conditions depicted include control (no injection), saline injection, and recordings taken at 4 and 40 minutes after PTX injections. **C|** The spatial coverage (n = 8 animals) observed in the control condition is not significantly different from the saline ($p = 0.112$) and PTX injections ($p = 0.245$), only being different between neuronal populations ($p = 2.308e-09$). Significance tested by LMMs. **D|** The ratio of ipsilateral to contralateral spatial coverage (n = 8 animals) in the control condition does not show a significant difference compared to the saline condition ($p = 0.0643$). However, a significant difference is observed after the PTX injection ($p = 0.0350$). There is no significant difference in this ratio between neuronal populations ($p = 0.648$). Significance tested by LMMs. Further statistical information in Annex 4.2. Significance is shown for age *** for $p < 0.001$

and saline conditions, while the number of motifs tended to become more similar between the two populations when influenced by the PTX. To examine whether the PTX increased synchronisation between cortical motifs and regions, the number of single and multi motif masks was analysed (Figure 3.20, panel B). Single motifs were more prevalent in the pyramidal population (Figure 3.20, panel B), reflecting the general trend on the number of motifs between conditions (Figure 3.20, panel A), while multi motifs were slightly more common in the GABAergic population, particularly for the PTX conditions (Figure 3.20, panel B). Notably, there was no

significant difference in the number of EI partners across the different conditions (Figure 3.20, panel C).

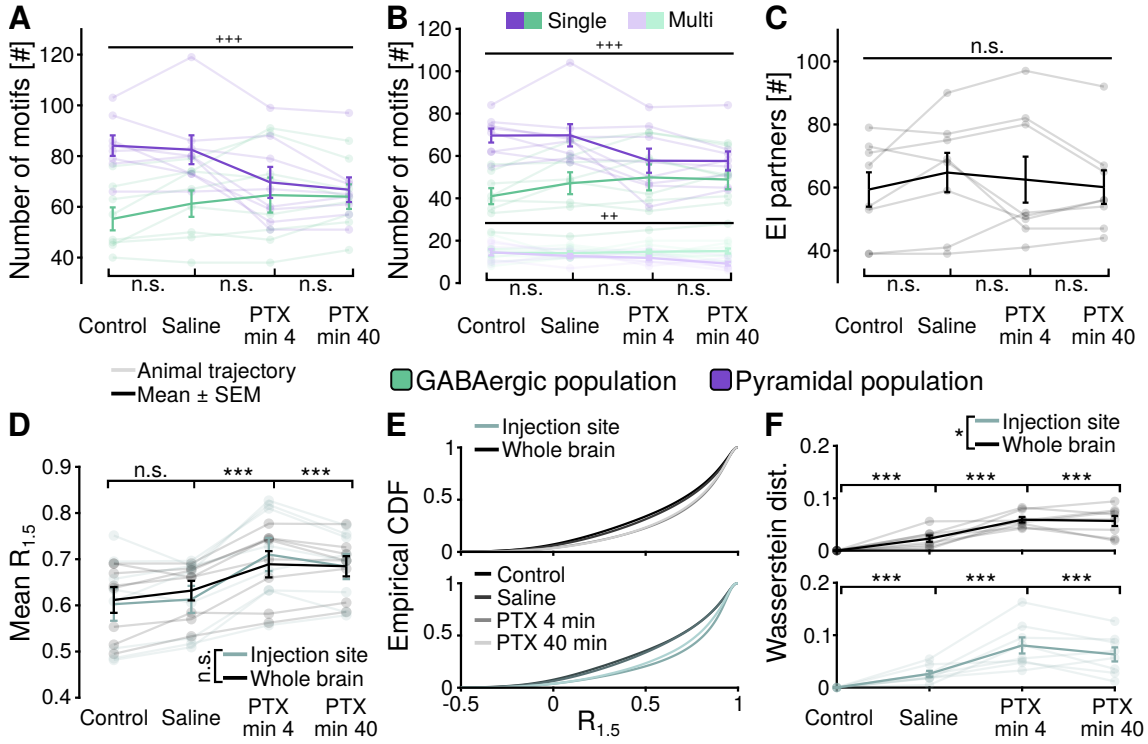


**Fig. 3.20 Shift towards higher GABAergic-pyramidal correlation after blockage of GABAergic signalling. A|** The number of motifs (n = 8 animals) observed in the control condition is not significantly different from the saline (p = 0.550), PTX 4 min (p = 0.920) and PTX 40 min (p = 0.316) conditions, only being different between neuronal populations (p = 1.307e-08). Significance tested by LMMs. **B|** The number of single mask motifs (n = 8 animals) observed in the control condition is not significantly different from the saline (p = 0.389), PTX 4 min (p = 0.588) and PTX 40 min (p = 0.582) conditions, only being different between neuronal populations (p = 1.590e-11). The number of multi mask motifs (n = 8 animals) observed in the control condition is not significantly different from the saline (p = 0.502), PTX 4 min (p = 0.0876) and PTX 40 min conditions (p = 0.334), only being different between neuronal populations (p = 1.0177e-04). Significance tested by LMMs. **C|** The number of EI partners (n = 8 animals) observed in the control condition is not significantly different from the saline (p = 0.121), PTX 4 min (p = 0.196) and PTX 40 min (p = 0.776) conditions. Significance tested by LMMs. **D|** The mean $R_{1.5}$ (n = 8 animals) in the control condition does not show a significant difference compared to the saline condition (p = 0.189), but it exhibits significant differences compared to the PTX 4 min (p = 7.13e-10) and PTX 40 min (p = 7.0188e-07) conditions. However, when comparing the mean $R_{1.5}$ around the injection site to the entire brain, no significant differences are observed (p = 0.746). Significance tested by LMMs. **E|** The empirical CDFs of all $R_{1.5}$ values for all motifs per condition show a gradual shift towards higher correlation values for both, the motifs around the injection site and the whole brain. **F|** The Wasserstein distance between the eCDFs (n = 8 animals) in the control condition shows a significant difference compared to the saline (p = 1.0618e-04), PTX 4 min (p = 2.594e-09) and PTX 40 min (p = 6.0021e-07) conditions. Moreover, a significant difference was observed between the injection site and the entire brain (p = 0.0276). Significance tested by LMMs. Further statistical information in Annex 4.2. Significance is shown for condition (population) **($^{++}$) for p < 0.01, ***($^{+++}$) for p < 0.001.

When examining the average increase in $R_{1.5}$ between all motifs and those found at the injection site (defined as a circular patch around the injection window), across all conditions, there was no change in the correlation between the control and saline conditions, but a rapid increase in

the correlation was observed following PTX injection, which was sustained over the 40-minute recording period (Figure 3.20, panel D). No significant difference was observed between the behaviour of the motifs closest to the injection site compared to all motifs. The cumulative distribution of $R_{1.5}$ values for each condition showed a shift towards higher correlation values (Figure 3.20, panel E), with a significant difference in distance between the control distribution and the PTX distributions for both, whole brain motifs and the ones close to the injection site (Figure 3.20, panel F). Interestingly, the distance was greater for motifs close to the injection site compared to whole-brain motifs, although not significantly different between the two types of motifs. Although the control and saline conditions exhibited a significant difference, resulting in a change in the correlation, it could potentially be attributed to tissue damage caused by the injection (Figure 3.20, panel F). This shows that acute disruption of a key pathway coupling GABAergic and pyramidal neuronal activity drives a change in coordination between the populations that is effectively detected by measuring changes in their instantaneous correlation.

## 3.4 Discussion.

This chapter has presented one of the first accounts of simultaneous dual-colour neocortex-wide calcium imaging in early postnatal development. This technique was employed to chronically investigate large-scale developmental trajectories of the activity patterns of pyramidal and GABAergic cell populations during the second and third postnatal weeks. Studying these changes in spontaneous activity during early development is crucial to understand the process of brain maturation as it undergoes significant structural and functional changes during this period, which can have long-term consequences on cognitive and behavioural outcomes later in life. Specifically, the interplay between GABAergic and pyramidal neuronal populations plays a critical role in shaping activity patterns, making it essential to understand the underlying mechanisms involved in their development. This knowledge can be valuable in understanding the pathophysiology of neurodevelopmental disorders that involve disruptions in the communication between these two cell populations.

### 3.4.1 Defining cortical domains based on spontaneous activity patterns in early postnatal development.

It is believed that the cortex has a modular structure consisting of clusters or domains of functionally similar neurons that allow for both integration and segregation among different brain areas (Puxeddu et al., 2020). These functional domains can capture specific spatiotemporal patterns of neural activity that can be largely predicted by the underlying corticocortical monosynaptic axonal projections across regions (Mohajerani et al., 2013), and may reflect distinct behavioural computations (MacDowell et al., 2020). To uncover these modules, the PCA/ICA decomposition approach was used to perform blind source separation, a technique widely used for other recording modalities such as EEG (Makeig et al., 2011). In this project, spatial ICA was

performed to uncover spatial sources of widefield fluorescence. This allowed for the data to be described as a set of low-dimensional dynamics, represented by independent spatial sources of fluorescence and their associated temporal weights (Weiser et al., 2021).

Previous studies using this segmentation approach for adult data observed between 16-31 different pyramidal motifs (Makino et al., 2017; West et al., 2022), which is similar to the number of motifs found in this study for the pyramidal population at older ages (Figure 3.13, panel A). However, a recent study found a larger number of motifs, with an average of approximately 230 detected motifs (Weiser et al., 2021). However, it is essential to take into account that the spatiotemporal resolution and duration of the recording can affect the number of motifs obtained, as it affects the quality of the signal separation from the noise (Weiser et al., 2021). Particularly, a reduction in the spatial resolution led to a steady decrease in signal and noise peak separation (Figure 2.7, panel B, Weiser et al., 2021), while an increase in the video duration will affect the number of components identified until reaching a stable number for a 20 minute recording (Weiser et al., 2021). Data in this project were recorded for 6 minutes at $\sim$170$\mu m^2$/pixel resolution, which is comparable to the specifications used by previous studies that found similar number of motifs (West et al., 2022; Makino et al., 2017); whereas the study by Weiser et al., 2021 recorded for 3 times longer and at a spatial resolution 3.5 times higher. However, this could suggest that 6 minutes might not be enough to cycle through all the possible activity motifs and stabilise the number of them identified. Moreover, if the recording duration to sample all motifs changes across development, e.g. older mice needing longer recording duration to cycle thorough all the possible activity patterns, it could confound the observed reduction in the number of motifs across development (Figure 3.13). It has been previously shown that individual differences in functional connectivity can be explained by differences sampling variability (MacDowell et al., 2022), and therefore, could suggest an undersampling of the activity motifs at older ages. Recording for longer at a higher spatial resolution may need to be considered for future recordings, although this can be computationally expensive.

On the other hand, it is possible that the decrease in the number of motifs observed during development was influenced by the significant changes in the SNR (Figure 3.14, panel A). However, even after adjusting the SNR to be consistent across the dataset (Figure 3.14, panel D), the reduction in motif numbers persisted. Another factor that could contribute to this developmental reduction in the number of motifs was a potential decline in the optical access to certain regions of the dorsal cortex, particularly those in the frontal and lateral areas. Although the spatial coverage of the dorsal cortex by the activity motifs did not significantly change during development (Figure 3.4, panel C), the skull thickening and skull curvature, as well as the window stability, could be affecting the type and number of motifs observed. One potential solution to this problem could be the use of a dual-lens macroscope to avoid the out-of-focus effect on the edges of the FOV and collect those lateral activity motifs (Kauvar et al., 2020), in combination with the use of a flexible and transparent polymer window which will both improve the optical access and allow better the growth of the cortex (Heo et al., 2016). This transparent polymer

window would also allow intracortical drug injections for cortical activity manipulation without requiring a cranial window. These polymer windows have been successfully used in pregnant dams for *in vivo* imaging of embryos (Jacquemin et al., 2021), and they can be combined with integrated electrode arrays for simultaneous opto-electrophysiological recordings (Donaldson et al., 2022; Driscoll et al., 2021).

The segmented activity domains were assigned to specific anatomical regions for regional comparisons of spatiotemporal activity properties during development. However, delineating the boundaries of cortical areas during early brain development is difficult due to extensive cortical growth and circuit refinement. A standardised dorsal brain atlas for early postnatal development does not yet exist due to the lack of systematic mapping of the regional changes that occur during early postnatal development. Previous studies used transgenic mice with fluorescent reporters on the thalamocortical projections to visualise the position of the primary sensory regions, which have a high density of these terminals (Ackman et al., 2012; Mizuno et al., 2014). However, this approach proved to be challenging when attempting to identify the these regions during development given that the size and position of the primary sensory cortices change significantly over a short period of time, making it difficult to construct a single developmental atlas that is applicable to the entire early postnatal period (Figure 3.8). Additionally, the genetic background of mice used for the calcium imaging differed from that of the transgenic mice used to map primary sensory regions, making the developmental trajectories of the two strains potentially hard to compare (Detmar et al., 2019). To simplify comparisons with other studies, an adult reference cortical atlas was used (Wang et al., 2020), providing good alignment with regions such as the visual and somatosensory body cortex, as shown by the variability maps (Figure 3.12, panel A). Nonetheless, the use of anatomical maps should be done cautiously because, even in the adult brain, functional motifs might not perfectly align to anatomical boundaries (Vanni et al., 2017). The absence of comprehensive behavioural tracking prevented the correlation of regional activations with specific behaviours. In future experiments, it is important to carefully monitor animal behaviour to enable accurate analysis of the relationship between regional activations and behavioural patterns, which will aid map alignment.

### 3.4.2 Excitatory and GABAergic populations exhibited divergent trajectories of their spatiotemporal dynamics across regions and developmental age.

During early postnatal development, neocortex-wide spontaneous activity exhibited discrete activity domains reflecting the modular organisation of the dorsal cortical surface. This spontaneous activity was present across the whole dorsal cortex and in both neuronal populations, even before the start of active sensing (Figure 3.3). This activity displayed complex spatiotemporal dynamics that varied not only across age but also among brain regions and populations, yielding heterogeneous developmental trajectories. These changes during early development have also been observed across cortical layers (Griffen et al., 2013). While changes in neocortex-wide glutamatergic pyramidal patterns have been previously documented (Ackman et al., 2014b;

Gribizis et al., 2019; Mojtahedi et al., 2021; Cross et al., 2021), there is currently no report on the large-scale developmental patterns of GABAergic spontaneous activity.

During the second and third postnatal weeks, the size of the spatial activity motifs increased by a factor of 3 for the GABAergic population and a factor of 2.5 for the pyramidal populations (Figure 3.5 panel A), consistent with previous reports (Ackman et al., 2012; Mulholland et al., 2021). The larger domain size observed in the GABAergic population compared to the pyramidal population has been previously reported in the visual cortex of ferrets (Mulholland et al., 2021), agreeing with the increased broadening of inhibitory sensory maps across development, in contrast with pyramidal maps (Quast et al., 2017). The progression of spatial map refinement, from diffuse and overlapping representations to refined patterns, showed similarities across many brain areas (Figure 3.12, panel A, Ackman et al., 2012; Mizuno et al., 2018; Arakawa et al., 2014; White et al., 2014). However, although both populations experienced an increase in the average motif size over development, the changes in the distributions of motif sizes followed divergent trajectories, with the distribution of GABAergic motif sizes stabilising between P16-P18 and remaining relatively constant, while the distribution of the pyramidal population continued changing until P22. Earlier studies have demonstrated the crucial role of inhibitory connectivity in regulating and shaping pyramidal plasticity (Mongillo et al., 2018). Thus, stabilising the spatial organisation and connectivity of GABAergic networks would facilitate this control mechanism. These findings suggest that there are fundamental differences in the underlying spatial organisation of the two populations, reflecting potential distinct roles in cortical network function development. Particularly when spatial properties of spontaneous activity have shown to have a larger effect on sensory map refinement than activity frequency (Xu et al., 2015).

Similarly to the changes in motif size, motif event frequency significantly changed across development for both populations (Figure 3.7), reflecting the termination of immature discontinuous activity and the onset of mature and continuous dynamics (Colonnese, 2014; Colonnese et al., 2010). The distribution of event frequencies across ages stabilised earlier for the pyramidal population, while the GABAergic population continues changing the shape of the distribution, potentially accommodating for the development of fast-spiking interneurons, which begin to exhibit this property by P18 (Cardin, 2018). Moreover, prior to the development of feed-forward inhibition, the delay between excitation and inhibition can result in the broadening of neuronal integration times, leading to reduced spike-time accuracy and an increase in firing frequency (Puzerey et al., 2014). Therefore, the maturation of PV basket cells and of feed-forward inhibition (Cardin, 2018; Lu et al., 2014), may potentially narrow the integration window (Puzerey et al., 2014), resulting in a tighter correlation between the dynamics of pyramidal and GABAergic neuronal populations (Figure 3.17, panel A). The continued changes in the event frequency distribution of the GABAergic population could indicate a less tight regulation and higher susceptibility to external influences, consistent with a period of progressive, experience-dependent refinement of intracortical inhibition (Dorrn et al., 2010). This increase in firing frequency across

development has previously been reported in both visual (Golshani et al., 2009) and barrel (Rochefort et al., 2009) cortex.

There were significant changes in variability across development and between regions for both neuronal populations (Figure 3.12, panel B). The total average variance in a region reflects the degree of variability or fluctuations in the region's dynamics over time, providing insight into the temporal properties of the signal. Different cortical regions exhibited distinct patterns of variability as the brain developed, suggesting changes in the functional and structural properties of the regions and providing insights into their timeline of functional specialisation. The pyramidal population showed significant changes in total variance across ages and regions, while the variance distributions did not show these modifications.This could be due to, for example, changes in the strength or synchronisation of synaptic inputs to a particular region, which could affect the average motif variance, but not necessarily the distribution across ages, as the variance may still be distributed similarly across the population. The GABAergic population, on the other hand, showed a significant change in both the average and the distribution shape across development.

These findings indicate that the ongoing activity observed in the developing cortex is not random, but rather exhibits coordination both spatially and temporally across the entire neocortex. These structures neocortex-wide patterns of activity may therefore have significant implications for the activity-dependent development of local and global circuit connections across the cortex.

### 3.4.3 Correlation patterns between GABAergic and pyramidal neuronal populations reveal developmental regional changes in cortical function.

Simultaneously imaging the activity of GABAergic and pyramidal neuronal populations across the dorsal neocortex allowed to asses the dynamic interplay between these two populations and across different brain regions during early postnatal development. Excitation and inhibition activity dynamics have shown to maintain tightly correlated levels of activity *in vivo*, displaying systematic macroscopic gradients of synaptic excitation and inhibition across the entire cortex, which provide a background for the generation of functional diversity among cortical areas (Wang, 2020; Haider et al., 2006). This is thought to be a general principle for large-scale cortical organisation in which cortical function operates in a dynamic balanced regime (Haider et al., 2006).

Despite maintaining a high correlation, the co-fluctuation of pyramidal (E) and GABAergic (I) dynamics exhibited brief instantaneous deviations from perfect timing (Figure 3.16, panel B). These deviations in correlation structure were evident at various time scales (Figure 3.16, panel B, Delaney et al., 2023). Analysis of EI paired activity motifs showed significant changes in correlation patterns across development, with the two populations becoming gradually more correlated as the cortex matured (Figure 3.17, panel A). Interneurons and synaptic inhibition

have been found to modulate network activity on a slower timescale during development, with interneurons acting as organisers of correlated population activity (Cardin, 2018). Therefore, this increase in correlation could be suggestive of the maturation of feed-forward inhibition and cortico-cortico connections across different regions, as balanced activity has shown to be generated by recurrent activity in the local network (Dehghani et al., 2016; Giannakakis et al., 2023; Pouchelon et al., 2021). Additionally, developmental sensory experience has been shown to balance cortical excitation and inhibition in the auditory cortex, leading to high correlation across both populations during the third week of postnatal development (Dorrn et al., 2010).

These changes in average correlation provided an overall idea of how the relationship between excitation and inhibition changed across development. On the other hand, the changes observed in the cumulative distributions of those correlation values revealed differences in the variability of this correlation across ages. The distance between the distributions at different developmental ages showed a reduction in the variability of correlation values, which narrowed the distribution, shifting towards higher correlation values during development (Figure 3.16, panel C). These changes in the distribution were also different across brain regions (Figure 3.18, panel B), suggesting that the mechanisms and/or timings that drive these changes in correlation patterns might be different across regions. These different patterns of correlation between excitation and inhibition have shown to depend on the cortical state. For example, during spontaneous activity, "up-and-down" states are highly correlated, while in the absence of these states, both inputs showed weak correlations (Tan et al., 2013). Furthermore, studies have shown that these correlations differ between spontaneous and evoked activity (Chew et al., 2022). Excitatory and inhibitory neurons are likely to have distinct contributions to sensory information processing. Alterations in the EI balance within local circuits, as well as changes in long-range synaptic inputs across cortical regions, have been associated with the behavioural performance, suggesting that learning-related modifications occur in the dynamic interplay between excitation and inhibition, impacting the processing of sensory information (Esmaeili et al., 2022).

While the balance between GABAergic and pyramidal populations is disrupted in pathological states like seizures (Dehghani et al., 2016), the manipulation of GABA signalling in this study appeared to modify correlation patterns throughout the cortex, not solely in the regions where epileptic-like activity was observed (Figure 3.19, panel B). The manipulation of GABAergic dynamics through blocking GABA signalling resulted in changes in correlation patterns between the GABAergic and pyramidal populations (Figure 3.20, panel F), highlighting the role of inhibition in shaping activity patterns (Isaacson et al., 2011). A recent study has demonstrated that excitatory networks in the rodent visual cortex maintain a balance between excitation and inhibition by forming subnetworks consisting of both types of neurons (Znamenskiy et al., 2018). This suggests the existence of excitatory-inhibitory subnetworks alongside excitatory-only subnetworks. In this context, when GABA signalling is blocked, inhibitory input onto excitatory neurons is disrupted, leading to reduced inhibitory influence. Consequently, the activity of excitatory neurons may become less regulated and exhibit increased excitability,

dominating over inhibition. This heightened excitability can result in a higher correlation between excitatory and inhibitory dynamics as interneurons become entrained. Therefore, in the absence of inhibitory control, excitatory activity becomes dominant and exhibits stronger correlations with inhibitory activity. This paradoxical effect has been observed in computational models of interneuron-stabilised networks, where the excitation of inhibitory neurons within a subnetwork leads to a decrease in their activity, particularly in networks with high levels of recurrent inhibition (Sadeh et al., 2020). Such a network regime has been proposed to emerge during later developmental phases (Rahmati et al., 2017). This observation has recently been shown *in vivo*, where optogenetic inhibition of interneurons in the mPFC led to an increase in their firing rate (Chini et al., 2022).

### 3.4.4 Limitations.

#### The dynamic flow of activity across regions might not be fully captured by static motifs.

In this study, the widefield data was denoised and compressed using spatial ICA to extract spatially independent patterns of activity and their temporal time courses. However, these static patterns of activity, with their corresponding fixed temporal signature, may not fully capture the dynamics of the activity when spatial travelling waves are present (e.g. retinal waves). To account for any remaining temporal dependencies not captured by the spatial components, temporal ICA could have been applied to the residual data (Figure 2.8, residual "noise") after subtracting the contribution of the spatial ICA components. Alternatively, the temporal weights of the spatial ICA components could be decomposed to extract sequences of activation or waves of activity.

Additionally, other approaches have been developed to extract spatiotemporal patterns of activity simultaneously by decomposing the activity into tensors (convolutional approach) that identify dynamic motifs which can capture unique spatiotemporal patterns of neural activity (Mackevicius et al., 2019; MacDowell et al., 2020; MacDowell et al., 2023). These type of motifs have shown to explain cortex-wide neural activity better than static decomposition methods (MacDowell et al., 2020). Given the shift of activity from discrete events to more continuous activity (Colonnese et al., 2010; Golshani et al., 2009; Modol et al., 2020) during the the second and third postnatal weeks, it would be worthwhile to perform this spatiotemporal analysis to explore the development of distributed activity patterns for the pyramidal and GABAergic neuronal populations.

In addition, the identity of the activity motifs as well as the contributions of their spatiotemporal dynamics to the overall neural activity can be influenced by the nature of the widefield calcium imaging approach. Although relatively fast calcium indicators were employed, GCaMP6f (Helassa et al., 2016) and jRGECO1a (Dana et al., 2016) still provide a slow time course that may not capture the fast transients of electrical activity, and can exhibit non-linearities in their

response that might vary by cell type, sensor, etc., potentially obscuring subtle differences between the pyramidal and GABAergic dynamics. Furthermore, the widefield calcium signals are biased in what the underlying activity reflects (Allen et al., 2017; Makino et al., 2017), which can result in decreased spatial resolution and slowed temporal dynamics, affecting the types of activity patterns that can be observed (Waters, 2020). However, it should be noted that the spatial resolution of the imaging system was higher than the size of the activity motifs observed, being high enough to capture multiple patterns within the same anatomical region.

### Functional mapping of brain regions to aid map alignment.

As previously mentioned, assigning activity motifs to specific anatomical regions is a challenging task. The approach followed in this project could lead to inaccurate region assignment due to inadequate map alignment, as well as an underestimation of motifs that belong to smaller regions. This is due to the reliance on the largest spread proportion for assigning the region identity. Given that the region assignment was in part done to aid the comparison across animals and ages, a potential solution would be to perform group ICA (Esposito et al., 2005), which can identify commonalities across animals and ages while preserving inter-individual differences.

Alternatively, instead of relying solely on anatomical landmarks, sensory mapping prior to the imaging experiment could improve the accuracy of region assignment. This involves presenting different stimulus modalities such as auditory, tactile whisker field, and stimulation of the forelimb and hindlimb paws. This approach would result in the identification of functional spots which, along with the anatomical landmarks, can serve as anchoring points for registering each individual brain to the reference atlas (Gallero-Salas et al., 2021).

### Cortical dynamics are behavioural state-specific.

The high correlation of neural activity across the cortical networks is not only due to similar input pathways but also global internal brain states that depend on factors such as behaviour, attention, and sleep (Kohn et al., 2009; Harris et al., 2011; McCormick et al., 2020). Importantly, the sensory processing during early development has been shown to be modulated by behavioural states such as sleep and awake states, which dynamically shift in the gating of sensory inputs (Ackman et al., 2012; Mojtahedi et al., 2021; Dooley et al., 2019). Transitions between cortical activity states and the associated gain control of sensory responses by behavioural state have shown to be gated by inhibition (Zucca et al., 2017; Pakan et al., 2016). Furthermore, different cell types have also shown distinct network properties dependent on the brain state (O'Connor et al., 2022). Thus, since circuits undergo extensive maturation during early postnatal development, it would be interesting to explore how these changes influence and control the information flow across large scale networks during the establishment of inter-regional connections.

Recent work has proposed that the processing of spatial and temporal information results from the interplay between external stimuli and the intrinsic dynamic state of neural networks (Buonomano et al., 2009; Andalman et al., 2019). Therefore, to understand the dynamics during development, it is essential to consider the context of brain state. Monitoring the behavioural state during development is challenging, as some approaches used for adult recordings may not be suitable for neonatal mice (e.g. pupillometry, as their eyes are closed until the end of the second postnatal week). Considering that neonatal mice tend to spend much of their time sleeping (Rensing et al., 2018), it would be useful to monitor their sleep states in order to understand behavioural state transitions during early postnatal development. To achieve this, improved monitoring of brain states could be accomplished by recording nuchal muscle electromyogram (EMG) to detect sleep and wake states (Gómez et al., 2021; Dong et al., 2022; Zhang et al., 2022). In addition, videography can be used to capture larger body movements, whisker twitches and spontaneous face movements, which have been shown to be the dominant factors in driving ongoing cortical dynamics (Musall et al., 2019).

### Specificity of the observed cortical dynamics.

The Gad2 promoter is a pan-GABAergic marker which is almost exclusively restricted to GABAergic neurons (high efficiency), and includes most interneuron subtypes (Taniguchi et al., 2011). Therefore, using this promoter to label the GABAergic population results in a loss of interneuron subtype specificity. This could be important given their distinct roles during early postnatal development, from their participation in transient circuits that regulate the afferent thalamic input (Tuncdemir et al., 2016; Marques-Smith et al., 2016), to differences in sensory processing (Baruchin et al., 2022; Leighton et al., 2021). Furthermore, the density of specific interneuron types varies across cortical areas (He et al., 2016), suggesting that the contribution of each subtype to the global pan-GABAergic signal could be changing across regions and during development, since the signal collected reflects a combination of the fluorescence emitted from different layers (Figure 2.10). Given that the focal depth of these type of setups is $\sim$200 $\mu m$ (Ratzlaff et al., 1991), the fluorescence captured should be primarily coming from this volume, which should include L1 and L2/3, and maybe part of L4, and will change slightly as the animals age. However, as observed with the modelling shown in the previous chapter, the highest contribution to the widefield fluorescence came form L5, followed by L2/3 and L4 (Figure 2.10, panel D); and therefore, developmental changes in the connection patterns of these layers could reflect the changes in the *in vivo* fluorescent dynamics. For example, there are differences in the layer contributions between S1 and V1 regions. Deep-layer GABAergic projections onto L4 neurons in the adult V1 are absent in S1 (Kätzel et al., 2011), only transiently appearing in S1 during early development (Marques-Smith et al., 2016). Nevertheless, the rationale for using this marker was to label as many cells as possible because the density of GABAergic neurons is lower than that of pyramidal cells, and the goal was to collect the widefield signal. Moreover, the pyramidal cell population was also generically labelled, although pyramidal neurons subtypes have also displayed broadly different cortex-wide spatiotemporal patterns (Musall et al., 2023).

It would be interesting to investigate whether different subtypes of neurons, particularly GABAergic ones, contribute distinctively at various developmental stages and in different cortical regions. Additionally, exploring their potentially correlation with ongoing pyramidal activity and examining their spatiotemporal properties could provide insights into their roles in orchestrating cortical dynamics (Kepecs et al., 2014; Cardin, 2018). While the expression of PV typically emerges towards the end of the second postnatal week (Taniguchi et al., 2011; Seto-Ohshima et al., 1990), SST is highly expressed in embryonic cortical GABAergic neurons (Batista-Brito et al., 2008). Moreover, SST neurons have been observed to possess extended axons in L1 postnatally (Taniguchi et al., 2011). Although these neurons' cell bodies are primarily located in layer 5 (Lim et al., 2018; Martinotti cells), previous studies have successfully imaged this population in adult mice using widefield calcium imaging (Allen et al., 2017). Hence, it should be feasible to image their dynamics during early postnatal development, ideally during the first postnatal week to potentially observe their transient participation in different circuits (Tuncdemir et al., 2016; Marques-Smith et al., 2016), using a transgenic breeding approach. If SST expression levels during development are low, a viral approach could be employed to enhance the signals, as demonstrated in the successful labelling and imaging of VIP interneurons using viral injection at P10 (Hamodi et al., 2020). Consequently, a similar strategy could be employed in this study.

### 3.4.5 Closing remarks.

The study aimed to investigate whether the GABAergic and pyramidal neuronal populations exhibit similar neocortex-wide dynamics during early postnatal development, focusing on regional differences and the interplay between both populations. The activity patterns observed were specific to each population, indicating the presence of divergent behaviours in the maturation of their spatiotemporal properties across multiple scales. These differences were observed not only across brain regions but also in the change of the correlation dynamics between the two populations. This highlights the power of dual-colour neocortex-wide calcium imaging, a minimally invasive technique that allowed to chronically image cell type-specific dynamics throughout early postnatal development. This technique shares similarities to fMRI, which is routinely used in human studies, offers a valuable translational tool for investigating typical and atypical cortical development.

# 4 General discussion and next steps

This study has provided the first broad description of GABAergic population activity across the developing cortex, and its cross-talk with pyramidal cell dynamics during early postnatal development. The spatiotemporal activity patterns of both populations varied with age and cortical region, exhibiting an overall increase in activity motif size and frequency across ages, while their distributions diverged. In addition, there were clear differences in the spontaneous modulation of cortical regions by each population, suggesting changes in the functional and structural properties of the regions and offering insights into the timeline of their functional specialisation. Finally, the correlation patterns between GABAergic and excitatory neuronal populations revealed developmental regional changes in their interaction. Therefore, these findings suggest that there are fundamental differences in the underlying spatiotemporal organisation of the two populations, reflecting potential distinct roles in the development of cortical network function.

During development, neural circuits spontaneously generate correlated activity that is crucial for the proper refinement of cortical connectivity and the formation of sensory maps (Kirkby et al., 2013; Leighton et al., 2016). However, a recent study has also emphasised the importance of activity-independent developmental mechanisms, revealing that neural circuits can achieve complete functionality and perform complex sensory-guided behaviours without relying on activity-dependent plasticity mechanisms (Barabási et al., 2022). Nevertheless, disrupting the patterns of spontaneous activity, particularly through regional perturbations, as well as disturbing the EI balance, can interfere with circuit refinement and have long-term consequences (Markicevic et al., 2020; Iannone et al., 2021; Luhmann et al., 2016; Zhang et al., 2011a). These spontaneous activity patterns have been observed in all sensory systems and across various species, and their characteristics can exhibit significant variations among them (Leighton et al., 2016). Furthermore, it is possible that the diverse spatiotemporal characteristics of spontaneous activity carry out distinct roles during development, underscoring the importance of investigating changes in this activity to understand the establishment of neural circuits necessary for mature processing. The brain is a complex network of interconnected regions, both structurally and functionally, and therefore, to gain a comprehensive understanding of its development, it is essential to examine the changes in inter-regional interactions.

Developmental cortical dynamics have been shown to differ not only with age, but also across cortical regions (Ackman et al., 2014b; Cross et al., 2021). Although the timing of the developmental trajectories varies across brain structures, the sequence of events seems to be conserved

across all of them (Dehorter et al., 2012). Across the different brain structures, the development of activity appears to follow a gradient, with "older" structures like the brain stem or spinal cord developing earlier than "younger" structures such as the cortex. Additionally, this stereotyped refinement of spontaneous activity has been shown to unfold along a sensorimotor-association axis within the cortex, providing evidence for a cortical gradient of neurodevelopmental change (Sydnor et al., 2023). Furthermore, the intrinsic developmental trajectories, particularly those of sensory cortices, have been found to be independent of sensory input, generalising across primary sensory areas (Frye et al., 2016). Furthermore, the development of sensory pathways has been observed to occur in an 'outside-in' manner, wherein the more peripheral regions of the pathway mature before the more central ones (Nakazawa et al., 2021).

The primary objective of the project was to investigate the simultaneous development of pyramidal and GABAergic activity dynamics across multiple regions during the early postnatal period. Therefore, a significant emphasis was placed on developing an appropriate technique for studying this phenomenon during early postnatal development (Chapter 2). Multiple imaging modalities exist, which enable the simultaneous recording of multiple brain regions (Table 2.1, Machado et al., 2022). However, when choosing the optimal technique for multi-region longitudinal neonatal imaging, several factors need to be taken into account. Early postnatal development is characterised by rapid growth (Baloch et al., 2009), necessitating an approach that can accommodate for these changes. Therefore, is crucial to optimise the weight of the implant to prevent discomfort or hindrance to the natural movements of the pups, which could otherwise impact its development. Longitudinal recordings in neonatal mice using portable systems such as electrophysiology probes (e.g., tetrodes, neuropixels, Steinmetz et al., 2021) or miniscopes (Rynes et al., 2021) presented challenges due to the size and weight of the probe or lens base.

These systems are generally not suitable for long-term recordings in neonatal mice unless a custom miniaturised system is specifically designed and implemented (Rensing et al., 2018). Furthermore, these systems typically have limited targeting capabilities, making it challenging to study several specific regions simultaneously. While these approaches have been utilised neonatally in larger rodents like rats (Dooley et al., 2018; Gómez et al., 2021), the availability of transgenic rat lines is limited, restricting the ability to achieve genetic specificity in targeting and visualising specific neuronal populations. The technique should allow for awake and behaving recordings, as spontaneous behaviours play a crucial role in the maturation and acquisition of internal models (Dooley et al., 2021). Unlike fMRI, which restricts body movement, widefield optical imaging (Cardin et al., 2020) offers a favourable compromise in terms of invasiveness, spatiotemporal resolution, and coverage. Overall, selecting an appropriate imaging technique for longitudinal neonatal imaging involves considering the specific demands of early postnatal development, the need for genetic specificity, the ability to record awake and behaving animals, and the compromise between invasiveness, resolution, and coverage. The developed custom

system and breeding strategy address these considerations, providing a suitable approach for studying early postnatal brain development.

The study focused on the second and third postnatal weeks of development and explored the neocortex-wide spontaneous activity of pyramidal and GABAergic neuronal populations, which exhibited distinct patterns, reflecting the modular organisation of the dorsal cortical surface (Chapter 3). The spatiotemporal dynamics of this activity varied across age, brain regions, and populations, leading to heterogeneous developmental trajectories. While changes in pyramidal activity patterns have been previously studied, there is limited knowledge about the developmental neocortex-wide patterns of GABAergic spontaneous activity.

Spontaneous events in the brain can vary in size, ranging from small local events that influence cortical columns (Yuste et al., 1992) to large-scale events that involve the recruitment of numerous cells across extensive cortical areas (Adelsberger et al., 2005; Kirmse et al., 2015). During this late stage of postnatal development, the average size of spatial activity motifs increased across ages for both pyramidal and GABAergic populations (Figure 3.5); however, the GABAergic motifs systematically presented larger domain sizes compared to the pyramidal population, suggesting the presence of broader inhibitory activity motifs during development. This broadening of inhibitory activity maps had already been observed in the olfactory bulb (Quast et al., 2017), indicating that it may be a generalised principle of inhibitory network development. This supports the notion that inhibitory neurons present broad tuning and can respond to a wide range of stimuli, resulting in the generation of a broader sensory map compared to the pyramidal population. Moreover, it has been shown that layer I interneurons play a crucial role in coordinating the formation of topographic sensory maps in the developing barrel cortex (Che et al., 2018), emphasising the significant contribution of GABAergic neurons in the refinement of receptive fields (Foeller et al., 2005) and the gating of critical period plasticity (Takesian et al., 2018; Hensch, 2005). The distributions of motif sizes showed divergent trajectories between the populations, with the GABAergic population stabilising earlier and remaining relatively constant at the start of active sensing, while the pyramidal population continued to change (Figure 3.5). This suggests that the spatial organisation and functional properties of inhibitory neurons reach a relatively stable state earlier in development compared to pyramidal neurons. The earlier stabilisation of inhibitory motifs can provide a stable foundation for the subsequent development of pyramidal circuits, where the latter can fine-tune their connections and receptive fields within the existing inhibitory framework. These findings suggest fundamental differences in the spatial organisation of the two populations, potentially reflecting distinct roles in cortical network function development.

The spontaneous activity observed in the developing cortex during the early neonatal period is non-random and exhibits coordinated patterns both in time and space (Thivierge, 2009). This activity becomes more frequent over time for both populations, indicating the transition from immature discontinuous activity to mature and continuous dynamics. This increase in

the frequency of spontaneous activity aligns with findings from electrical activity observed in animals and humans (Colonnese et al., 2010), observing a simultaneous increase across all cortical regions. The distribution of event frequencies stabilised earlier for the pyramidal population, while the GABAergic population continued to change (Figure 3.7). The emergence of refined intracortical inhibition (Lee et al., 2007) and the delayed maturation of fast-spiking interneurons, specifically PV basket cells, which acquire mature firing properties by the end of the second postnatal week (Daw et al., 2007), could explain this phenomenon. This will lead to a shift in the distribution of GABAergic motif frequencies towards higher frequencies until the fast-spiking properties of these cells have fully matured. Variability in neuronal activity also exhibited significant changes across development and between regions for both populations, providing insights into the temporal properties of the signal and functional specialisation of cortical regions. Moreover, the activity dynamics of the GABAergic and pyramidal populations maintain tightly correlated levels of activity, exhibiting brief instantaneous deviations from perfect timing, but gradually becoming more correlated as the cortex matures. Task performance has been associated with alterations in the EI balance within local circuits, as well as modifications in long-range synaptic inputs across distant cortical regions (Esmaeili et al., 2022), suggesting the occurrence of learning-related changes in the interplay between excitation and inhibition. Moreover, a recent study has suggested that the changes in activity flow across the cortical hierarchy during development are separate from the changes in functional connectivity (Pines et al., 2023). This highlights the importance of examining dynamic measures of activity rather than static ones. This suggested that the mechanisms and/or timings that drive these changes in correlation patterns might be different across regions. Therefore, these region-specific maturation trajectories, which have previously been observed (Dehorter et al., 2012), could be affecting the activity propagation across the cortical hierarchy, and GABAergic dynamics could be playing an important role in sculpting these complex spatiotemporal functional dynamics in cortex (Dehorter et al., 2017).

A reduction in the EI ratio is a hallmark of the critical period development (Hensch, 2005), which has shown to progress in a hierarchical manner from primary sensory to higher-order cortical areas (Takesian et al., 2013a; Reh et al., 2020). While EI ratio generally represents the relative strengths or magnitudes of excitatory and inhibitory influences, either at the level of synaptic inputs or postsynaptic potentials, the EI correlation (as measured in this study) reflects the statistical relationship or association between excitatory and inhibitory neuron activities. However, the EI ratio could be influencing the EI correlation in several ways. For instance, an imbalance in the EI ratio can affect the overall level of neural activity. If there is an excess of excitatory inputs relative to inhibitory ones, it can lead to increased neural activity, which can entrain interneuron activity, resulting in higher EI correlation. This effect was shown by blocking GABA signalling with PTX, which effectively pushed the synaptic EI ratio in favour to excitation and led to a higher EI correlation (Figure 3.19). Therefore, changes in the EI ratio can shift the balance within neural circuits, pushing the network toward a state of excessive excitation or inhibition. This modulation can affect the strength and dynamics of neural interactions

and subsequently impact the correlation between excitatory and inhibitory activity patterns (Chini et al., 2022). Therefore, decrease in the EI ratio observed during development (Hensch, 2005), which is believed to be linked to an increase in inhibition (Chini et al., 2022), could contribute to an elevated EI correlation, as inhibitory neurons play a crucial role in regulating the timing and synchronisation of excitatory neuronal activity (Dehorter et al., 2017; Warm et al., 2022b). Moreover, increased inhibition could be influencing the connectivity through plasticity mechanisms, promoting the formation of specific functional subnetworks, which can enhance the correlation between excitatory and inhibitory populations (Takesian et al., 2018; Butt et al., 2017; Hellyer et al., 2016).

Inhibition can also modulate the gain and signal-to-noise ratio of neural responses, amplifying or attenuating the excitatory signals (Mitchell et al., 2003; Ayaz et al., 2009), which can in turn affect the EI correlation. For instance, noisy synaptic input has shown to produce a multiplicative gain modulation of tuning curves, which can be controlled by local inhibitory interactions (Ayaz et al., 2009). The increase in EI correlation observed during development could have several functional advantages. It enhances the processing and integration of neural information by facilitating the integration of excitatory inputs with inhibitory regulation, allowing for precise control of strength and timing of neural activity and, thereby, information flow within a circuit (Puzerey et al., 2014; Sherrill et al., 2020). Moreover, it enhances the selectivity for the transmission of synchronised activity through a feedforward network, thereby improving its stability to background activity (Kremkow et al., 2010). This creates an optimal foundation for the propagation of signals and supports efficient signal transmission.

The manipulation of GABAergic dynamics by local blocking GABA signalling led to changes in the distribution of correlations between the GABAergic and pyramidal populations, highlighting the role of GABAergic dynamics in shaping the correlation patterns. Previous studies have shown that the inhibition of $GABA_A$ receptors can cause epileptiform discharges in immature brain, suggesting that GABA may mediate a net inhibitory effect (Richter et al., 2010; Vickers, 2017). However, depolarising GABAergic responses have also been suggested to contribute to epilepsy (Nardou et al., 2009; Khalilov et al., 2005). This discrepancy highlights the intricate functional implications of depolarising GABAergic responses. Importantly, *in vitro* experiments have demonstrated that mild GABAergic stimulation can induce excitation, whereas stronger GABAergic currents elicit inhibition (Khalilov et al., 1999; Winkler et al., 2019). Therefore, this suggests that the net effect of this neurotransmitter is determined by the balance between GABAergic depolarisation and shunting inhibition. More recent studies have shown that the *in vivo* optogenetic activation of GABAergic neocortical and hippocampal interneurons reduced the frequency of excitatory postsynaptic currents (Valeeva et al., 2016); while GABAergic antagonist (bicuculline and/or gabazine) have been shown to induce epileptiform activity (Isaev et al., 2005). Therefore, while the GABA blocking experiments suggested an inhibitory action of GABA in the primary somatosensory cortex, the functional consequences of GABA may be more nuanced and will require a more detailed optogenetic probing across the dorsal cortex, similar to the

approach taken by Allen et al., 2017, in order to identify potential regions where the switch has not yet occurred. Given that the GABA switch in the neocortex, although can vary across different brain regions (Dehorter et al., 2012), is typically completed around P7-10 in mice (Peerboom et al., 2021), and the longitudinal recordings are performed from the second to the third postnatal weeks, GABAergic signalling in the imaged period will predominantly be inhibitory. Moreover, a recent study has shown that even at P3, the visual cortex already exhibits inhibitory actions of GABA (Murata et al., 2020). This indicates that GABAergic inhibition is present and functional in the visual cortex at an early developmental stage, which might apply to the other cortical sensory regions.

Additionally, it is important to note that not all cortical GABAergic neurons are locally projecting cells. Around 10% of cortical GABAergic neurons are known to project over long distances, both within and outside the cortex (Urrutia-Piñones et al., 2022; Caputi et al., 2013), but little is understood about their development and functions in the neocortex. It has been recently shown that a small population of GABAergic subplate cells can form long-range axonal projections to the internal capsule, towards the thalamus and other subcortical structures (corticofugal), or the corpus callosum (Boon et al., 2019). These two different projection groups showed opposite expression patterns. While the corticofugal projection neurons were most abundant during the perinatal period, decreasing in number postnatally; the contralateral projecting GABAergic neurons showed an increase in numbers during the first postnatal week. Moreover, long-range GABAergic neurons in the hippocampus have been shown to originate during embryonic development (Christenson Wick et al., 2019). This population could be related to the hub neurons found in the hippocampus, which are responsible for coordinating and synchronising neuronal assemblies (Bonifazi et al., 2009; Picardo et al., 2011). A possible way to investigate the function of long-range GABAergic neurons in development is to selectively label them in one hemisphere and using optogenetics to stimulate their contralateral projections, while observing the pyramidal cell responses. Understanding the role of these projections is important due to their potential contribution to cortical feedback processing and synchrony across brain regions (Mazo et al., 2022; Tamamaki et al., 2010).

### Insights gained from the current dataset.

- The developmental trajectory of spontaneous GABAergic activity at the mesoscale level broadly aligns with that of functional networks formed by neocortex-wide pyramidal cells. However, the spatiotemporal dynamics of both populations exhibited fundamental differences in the spatiotemporal organisation and activity modulation, suggesting distinct and potentially important roles in the development of cortical network function.
- The relationship between the activity of pyramidal and GABAergic neurons displayed unique changes across regions, which were reflected in the trajectories of their correlation patterns.

### Open questions to explore with the current dataset.

The wealth of data collected in this study provides ample opportunity to delve deeper into the understanding of the development of multi-region interactions and the interaction between sensory and spontaneous activity. Below are a few examples of the questions that can be addressed through further analysis of the data.

- The reorganisation of functional connectivity (FC) within and across populations during early development: recent studies have shown that FC decreases across subcortical circuits while increasing between intra-cortical regions. This phenomenon is accompanied by hemispheric functional specialisation, as indicated by decreased FC between homotopic regions and lower similarity of the FC patterns between regions in each hemisphere (Ma et al., 2018; Rahn et al., 2022). Furthermore, the brain-wide network shows reduced clustering (local communication) but increased integration (distant communication). Therefore, this longitudinal dataset can be used to identify periods of dynamic change across ages in the context of inter-regional GABAergic and pyramidal population dynamics interplay.
- Neocortex-wide spatiotemporal patterns and communication subspaces: following a similar approach to MacDowell et al., 2023, it will be possible to infer the route of information flow across brain-wide networks to investigate how a population in a particular region is functionally connected with different cortex-wide 'subspace networks' of regions. By doing so, it will be possible to explore how the brain can interact with multiple independent networks and how these networks develop and change over time. Particularly, determining whether the GABAergic population plays a significant role in routing information using the dataset in which GABA transmission was locally disrupted. This type of dynamical functional connectivity has demonstrated a better correlation with behaviour compared to static measures (Benisty et al., 2021).
- Trajectories of spontaneous and sensory-evoked activity: how do spontaneous and sensory-evoked activities interact has been a topic of discussion in the literature (Afrashteh et al., 2020; Ferezou et al., 2017; Luczak et al., 2013). Two hypotheses have been proposed: the first suggests that spontaneous activity provides the basis for possible cortical sensory responses, with evoked patterns representing a subset of this space (Luczak et al., 2009; Cross et al., 2021), while the second proposes that spontaneous and evoked activity patterns are orthogonal to each other (Stringer et al., 2019b; Avitan et al., 2021). Using a similar methodology to Avitan et al., 2021, it would be possible to investigate whether spontaneous and evoked activity patterns converge or diverge during development.

## 4.1 Future experiments.

### Developmental apoptosis: how do changes in the GABAergic neuron proportion affect network activity in the developing cortex?

During development, a surplus of GABAergic interneurons is generated, which undergoes programmed cell death by the end of the second postnatal week, eliminating more than 30% of the interneurons generated embryonically (Southwell et al., 2012; Lim et al., 2018). This process affects all interneuron classes (Wong et al., 2018), however it has shown to present regional and cortical layer differences (Blanquie et al., 2017b). The proper integration of interneurons into the nascent circuits depends on neuronal activity (Wong et al., 2018; Priya et al., 2018; Duan et al., 2020). Glutamatergic pyramidal cells have shown to regulate interneuron survival through the negative modulation of PTEN (Phosphatase and Tensin Homolog, Wong et al., 2018). Moreover, the injection the PTEN inhibitor bpV(pic) systemically during the period of the interneuron programmed cell death (P7-8, Lim et al., 2018) dramatically increased the density of MGE interneurons compared to control mice (Wong et al., 2018).

If GABAergic cells are prevented from dying, do they correctly integrate in the developing circuits? Does it lead to a change in the activity dynamics? If apoptosis is inhibited in a specific brain region, does this manipulation spread to other regions? Does the potential change in circuit dynamics affect the wider network? How does it affect the balance between excitatory and inhibitory activity dynamics? Does it lead to any future behavioural deficits? It has been previously shown that neuronal circuits in cell cultures can adjust connection numbers to overcome imbalances in excitation and inhibition (Sukenik et al., 2021); however, transient imbalances in cell numbers have shown to lead to long-term changes in behaviour (Magno et al., 2021). Therefore, can this imbalance be homeostatically regulated given that the cortex is still developing? It remains unclear whether the excessive production of GABAergic interneurons has any functional relevance during the development, and what implications this has for the circuit's composition and activity dynamics.

Similarly to the proposal above, given the critical role of immature MGE interneurons in shaping activity patterns driven by GABA, which regulate the integration of interneurons into developing networks (Duan et al., 2020), and the observed reduction in GABAergic calcium events following whisker plucking (Modol et al., 2020), resulting in impaired sensory processing in adulthood (Sieben et al., 2015), it would be interesting to investigate the modulation of apoptosis by sensory deprivation and how this impacts the cortex-wide activity patterns that may underlie future sensory deficits.

### Multisensory integration and early engagement of association areas.

The integration of inputs across multiple senses through intricate interactions within neocortical networks is crucial for achieving optimal behaviour. This process of multisensory interplay gradually emerges and continues to mature even after the individual senses have developed (Xu et al., 2020b). A recent study has shown the importance of neonatal unimodal experience for proper cross-modal responses in the adult cortex (Sieben et al., 2015). Moreover, in the zebrafish developing tectum, it has been shown that multisensory integration is constrained by the balance of excitation and inhibition, observing a key developmental period in which the temporal window for multisensory integration narrows, correlating with developmental increases in evoked synaptic inhibition (Felch et al., 2016). However, recent studies in humans have revealed that early exposure to multisensory signals is not a prerequisite for the development of multisensory integration. Surprisingly, individuals who have experienced visual deprivation for extended periods can still acquire the ability to integrate multisensory information (Senna et al., 2021). This highlight the need for further research to fully understand the developmental process of multisensory integration. The lack of understanding in this area is especially striking in rodents, even though they have demonstrated remarkable multisensory capabilities within the primary sensory cortices (Bieler et al., 2017a; Bieler et al., 2017b; Sieben et al., 2013).

Excitatory neuronal hubs in association areas have shown to be phase-locked to multisensory inputs coordinating its integration (Kuroki et al., 2018). Multisensory integration models have suggested that the cortex initially integrates and compresses multisensory information from several sensory regions, before employing this simplified representation in higher-level association regions and more complex cognitive processes (Shadi et al., 2020). A similar model could be used to infer the cascade of regions activated in response to uni- or multisensory stimuli and how that might change across development, with a particular focus on association area maturation during early postnatal development. In the early stages of postnatal development, extensive multisensory connections between secondary and primary areas start to develop around P9, while direct connections between primary sensory areas emerge around P15 (Henschke et al., 2018). These intracortical multisensory connections are established through sensory-driven thalamocortical activity, leading to the formation of distinct sets of thalamocortical and cortico-cortical connections across sensory regions (Henschke et al., 2018). This could suggests the presence of unique integration mechanisms for different combinations of sensory modalities. Therefore, studying the development of multisensory integration using neocortex-wide calcium imaging would be key to understand the distributed nature of this type of integration, particularly focusing on the differential roles that the pyramidal and GABAergic populations might play in gating the information flow across the wider network. This would also require a more detailed measurement of the ongoing behaviour through videography and nuchal muscle electromyogram to be able to draw functional links between neural activity and behavioural state.

## 4.2 Closing remarks.

This thesis has provided valuable insights into the dynamics of neocortex-wide activity in GABAergic and pyramidal populations during early postnatal development. The observed activity patterns exhibited unique developmental trajectories, not only differing between the two neuronal populations but also varying across cortical regions. The extensive dataset gathered in this study provides an exceptional opportunity for further exploration of these dynamics and a deeper understanding of the intricate development of functional relationships within the cortex.

The use of this minimally invasive, *in vivo* technique on non-anaesthetised neonatal mice offers a promising avenue for exploring various aspects of development. It enables the investigation of interactions between spontaneous and sensory-evoked activity, taking into account the influence of brain states on this process. Additionally, it provides an opportunity to examine the cortex-wide developmental shift from synchronised to desynchronised network activity, uncovering the different trajectories across neocortical regions. By employing pharmacological interventions and optogenetics, it becomes possible to investigate the spatiotemporal actions of specific cell types, particularly focusing on the spatial extent and temporal dynamics of the excitatory effects mediated by GABA. Furthermore, this technique will be particularly valuable in studying the emergence of cognitive functions such as learning and memory, spatial navigation, and social interactions. Previous successful applications of this technique in adult studies have shed light on the distributed nature of these functions, making it a valuable tool for further exploration in developmental contexts.

Additionally, this technique provides an opportunity for a critical assessment of the applicability of rodent models in understanding early cortical development in humans. It could serve as a valuable tool to investigate alterations in functional development in animal models subjected to early-life insults and neurodevelopmental disorders, highlighting its potential for translational research.

# Annex

The annex provides essential information summarising the fit of the Linear Mixed Model (LMM) or Generalized Linear Mixed Model (GLMM) to assess significance. The details are reported as follows:

- Model and response variable: The formula used to fit the model, specifying the fixed and random effects.
- Fixed effects: The estimated $\beta$ coefficients along with their corresponding standard errors, presented at a 95% confidence interval.
- Random effects: The standard deviation values associated with the random effects.
- Model fit: The Bayesian Information Criterion (BIC), which evaluates model complexity and goodness of fit. Additionally, the p-value of the Likelihood Ratio Test (LRT) is reported, indicating the significance of the model.

These statistics and results provide a comprehensive summary of the LMM/GLMM fit, enabling an assessment of the model's performance and significance.

## Figure 2.13: Movement-induced blood volume artefacts in CAG-GFP mice across early postnatal development.

**LMM Blood volume artefacts**: 'movement correlation $\sim$ 1 + Age + (1|Sex)'. Fixed effects: Age = -0.0154 (0.00858). Random effects: Sex = 0.0759. Random effects do not significantly affect the model fit, BIC = -3.0584 (full model), -4.463 (reduced model, just fixed effects), p = 0.842.

**LMM Other artefacts**: 'movement correlation $\sim$ 1 + Age + (1|Sex)'. Fixed effects: Age = -0.0120 (0.00671). Random effects: Sex = 1.337e-17. Random effects do not significantly affect the model fit, BIC = -14.74 (full model), -17.684 (reduced model, just fixed effects), p = 0.901.

**LMM noise**: 'movement correlation ∼ 1 + Age + (1|Sex)'. Fixed effects: Age = 0.0141 (0.00698). Random effects: Sex = 1.391e-17. Random effects do not significantly affect the model fit, BIC = -13.248 (full model), -16.192 (reduced model, just fixed effects), p = 0.941.

## Figure 2.14: Evaluation of signals contributing to the spectrogram and hemodynamics.

**LMM S1 whisker trace**: 'whisker correlation ∼ 1 + Age + (1|Sex)'. Fixed effects: Age = -0.000500 (0.00124). Random effects: Sex = 1.612e-18. Random effects do not significantly affect the model fit, BIC = -41.849 (full model), -44.046 (reduced model, just fixed effects), p = 0.921.

**LMM S1 whisker trace shifted:** 'whisker correlation ∼ 1 + Age + (1|Sex)'. Fixed effects: Age = 0.004319 (5.898e-04). Random effects: Sex = 0.00611. Random effects do not significantly affect the model fit, BIC = -52.441 (full model), -52.838 (reduced model, just fixed effects), p = 0.693.

## Figure 2.16: Assessment of the effect of the chronic implant on developmental growth.

**LMM body weight**: 'weight ∼ 1 + Age + Protocol + Age*Protocol + (Age|Animal ID) + (1|Sex)'. Fixed effects: Age = 0.351 (0.0266); Protocol = 0.861 (0.663); Age*Protocol = -0.00611 (0.0557). Random effects: Age|Animal ID = 0.1072; Sex = 6.207e-10. Random effects do not significantly affect the model fit, BIC = 1862.6 (full model), 2118.4 (reduced model, just fixed effects), p = 0.178.

## Figure 2.17: Open field behaviour of the chronic implanted animals after longitudinal recordings.

**LMM distance travelled during recording**: 'distance travelled ∼ 1 + Protocol + Distance/min + (1|Age) + (1|Animal ID) + (1|Sex)'. Fixed effects: Protocol = 3574.9 (3147); Distance/min = -7069 (571.87). Random effects: Age = 10156; Animal ID = 5828.9; Sex = 7.925e-06. Random effects do not significantly affect the model fit, BIC = 2116 (full model), 2183.8 (reduced model, just fixed effects), p = 0.604.

## Figure 3.4: Stable coverage of the exposed cortex by spatial activity motifs during early postnatal development.

**LMM exposed cortex**: 'exposed cortex $\sim$ 1 + Age + (Age|Pup ID) + (1|Genotype) + (1|Sex) + (1|Litter size)'. Fixed effects: Age = 0.0019 (0.00184). Random effects: Age|Pup ID = 0.00552); Genotype = 3.515e-10; Sex = 6.535e-11; Litter size = 5.127e-11).

**GLMM (gamma distribution) spatial coverage**: 'spatial coverage $\sim$ 1 + Age + Population + (Age|Pup ID) + (1|Genotype) + (1|Sex) + (1|Litter size)'. Fixed effects: Age = -2.907e-05 (2.931e-05), Population = 3.361e-4 (0.165). Random effects: Age|Pup ID = 1.662e-4; Genotype = 6.280e-06; Sex = 2.920e-06; Litter size = 4.523e-4. Collectively, Random effects significantly affect the model fit, BIC = -1311.4 (full model), -1322.6 (reduced model, just fixed effects), p = 0.00525.

**GLMM (gamma distribution) L/R spatial coverage**: 'L/R spatial coverage $\sim$ 1 + Age + Population + (Age|Pup ID) + (1|Genotype) + (1|Sex) + (1|Litter size)'. Fixed effects: Age = 0.00121 (0.00260); Population = 0.00281 (0.02282). Random effects: Age|Pup ID = 0.00712; Genotype = 5.417e-06; Sex = 5.448e-06; Litter size = 1.899e-05. Individual random effect Age|Pup ID significantly affects model fit, BIC = -151.35 (full model), -91.652 (reduced model, fixed effects and Genotype, Sex, Litter size), p = 4.441e-16.

## Figure 3.5: Developmental trajectory of activity motif size in excitatory and GABAergic populations during early postnatal development.

**GLMM (gamma distribution) mean motif size**: 'mean motif size $\sim$ 1 + Age + Population + (Age|Pup ID) + (1|Genotype) + (1|Sex) + (1|Litter size)'. Fixed effects: Age = -1.734e-05 (1.969e-06), Population = 1.006e-04 (1.403e-05). Random effects: Age|Pup ID = 6.872e-06; Genotype = 0.185; Sex = 0.175; Litter size = 0.174. Random effects do not significantly affect the model fit, BIC = -2109.8 (full model), -2008.3 (reduced model, just fixed effects), p = 0.

**LMM KL divergence motif size distributions**: 'KL divergence motif size $\sim$ 1 + Age + Population + (Age|Pup ID) + (1|Genotype) + (1|Sex) + (1|Litter size)'. Fixed effects: Age = 0.0781 (0.00722); Population = 0.144 (0.0550). Random effects: Age|Pup ID = 0.0232; Genotype = 0.0677; Sex = 9.959e-10; Litter size = 1.0801e-09. Random effects do not significantly affect model fit, BIC = 73.043 (full model), 69.808 (reduced model, just fixed effects), p = 0.327.

## Figure 3.7: Developmental trajectory of activity motif frequency in excitatory and GABAergic populations during early postnatal development.

**GLMM (gamma distribution) mean motif frequency**: 'mean motif frequency $\sim$ 1 + Age + Population + (Age|Pup ID) + (1|Genotype) + (1|Sex) + (1|Litter size)'. Fixed effects: Age = -0.146 (0.0225), Population = -0.423 (0.0959). Random effects: Age|Pup ID = 1.960; Genotype = 1.756e-05; Sex = 6.365e-06; Litter size = 1.3028. Random effects Age|Pup ID, Genotype and Sex significantly affect the model fit, BIC = 280.04 (full model), 300.07 (reduced model, fixed effects and Litter size), p = 1.455e-05.

**LMM L/R mean motif frequency**: 'L/R mean motif frequency $\sim$ 1 + Age + Population + (Age|Pup ID) + (1|Genotype) + (1|Sex) + (1|Litter size)'. Fixed effects: Age = -9.643e-04 (6.836e-04); Population = -7.153e-04 (6.298e-03). Random effects: Age|Pup ID = 0.0223; Genotype = 7.042e-10; Sex = 0.00288; Litter size = 6.798e-11. Random effects do not significantly affect model fit, BIC = -481.64 (full model), -508.41 (reduced model, just fixed effects), p = 0.455.

**GLMM (gamma distribution) KL divergence motif frequency distributions**: 'KL divergence mean motif frequency $\sim$ 1 + Age + Population + (Age|Pup ID) + (1|Genotype) + (1|Sex) + (1|Litter size)'. Fixed effects: Age = -0.0370 (0.00503); Population = 0.127 (0.0610). Random effects: Age|Pup ID = 7.417e-12; Genotype = 3.191e-06; Sex = 2.500e-06; Litter size = 0.212. Random effects do not significantly affect model fit, BIC = 207.89 (full model), 179.31 (reduced model, just fixed effects), p = 0.984.

## Figure 3.9: Spread of the sICA motif spatial masks across cortical region boundaries.

**GLMM (gamma distribution) single region motif spread**: 'single region spread $\sim$ 1 + Age + Population + (Age|Pup ID) + (1|Genotype) + (1|Sex) + (1|Litter size)'. Fixed effects: Age = 0.157 (0.0213); Population = -0.706 (0.158). Random effects: Age|Pup ID = 0.0624; Genotype = 7.254e-05; Sex = 0.0970; Litter size = 2.771e-05. Random effects do not significantly affect model fit, BIC = 420.71 (full model), 406.32 (reduced model, just fixed effects), p = 0.0186.

**GLMM (gamma distribution) multi region motif spread**: 'multi region spread $\sim$ 1 + Age + Population + (Age|Pup ID) + (1|Genotype) + (1|Sex) + (1|Litter size)'. Fixed effects: Age = -0.0187 (0.00232); Population = 0.145 (0.0281). Random effects: Age|Pup ID = 0.00613; Genotype = 0.0617; Sex = 0.0218; Litter size = 0.0301. Random effects do not significantly affect model fit, BIC = -142.58 (full model), -162.06 (reduced model, just fixed effects), p = 0.119.

## Figure 3.10: Proportion of sICA motifs assigned to each region of interest across development.

**GLMM (gamma distribution) proportion of motifs in M2**: 'proportion motifs $\sim$ 1 + Age + Population + (Age|Pup ID) + (1|Genotype) + (1|Sex) + (1|Litter size)'. Fixed effects: Age = -0.542 (0.119); Population = 0.362 (1.470). Random effects: Age|Pup ID = 0.320; Genotype = 1.963e-04; Sex = 6.815e-04; Litter size = 1.851. Random effects do not significantly affect model fit, BIC = 1018.8 (full model), 985.05 (reduced model, just fixed effects), p = 0.997.

**LMM proportion of motifs in M1**: 'proportion motifs $\sim$ 1 + Age + Population + (Age|Pup ID) + (1|Genotype) + (1|Sex) + (1|Litter size)'. Fixed effects: Age = 0.00407 (9.0779e-04); Population = -0.0267 (0.00821). Random effects: Age|Pup ID = 0.00269; Genotype = 0.0128; Sex = 0.0142; Litter size = 6.841e-12. Random effects do not significantly affect model fit, BIC = -461.17 (full model), -473.72 (reduced model, just fixed effects), p = 0.32673.

**LMM proportion of motifs in S1t**: 'proportion motifs $\sim$ 1 + Age + Population + (Age|Pup ID) + (1|Genotype) + (1|Sex) + (1|Litter size)'. Fixed effects: Age = 0.00289 (5.147e-04); Population = 0.0161 (0.00701). Random effects: Age|Pup ID = 3.839e-04 ; Genotype = 0.0164; Sex = 1.767e-09; Litter size = 0.0361. Random effects do not significantly affect model fit, BIC = -501.21 (full model), -482.87 (reduced model, just fixed effects), p = 0.089109.

**LMM proportion of motifs in S1f**: 'proportion motifs $\sim$ 1 + Age + Population + (Age|Pup ID) + (1|Genotype) + (1|Sex) + (1|Litter size)'. Fixed effects: Age = -0.001607 (4.199e-04); Population = 0.0137 (0.00309). Random effects: Age|Pup ID = 0.00128 ; Genotype = 1.715e-10; Sex = 0.00499; Litter size = 0.0121. Random effects do not significantly affect model fit, BIC = -670.78 (full model), -666.48 (reduced model, just fixed effects), p = 0.50495.

**LMM proportion of motifs in S1b**: 'proportion motifs $\sim$ 1 + Age + Population + (Age|Pup ID) + (1|Genotype) + (1|Sex) + (1|Litter size)'. Fixed effects: Age = 0.00526 (6.4084e-04); Population = -0.0261 (0.00594). Random effects: Age|Pup ID = 0.00162 ; Genotype = 0.0181; Sex = 3.857e-09; Litter size = 3.857e-09. Random effects do not significantly affect model fit, BIC = -554.33 (full model), -536.52 (reduced model, just fixed effects), p = 0.26733.

**LMM proportion of motifs in S2**: 'proportion motifs $\sim$ 1 + Age + Population + (Age|Pup ID) + (1|Genotype) + (1|Sex) + (1|Litter size)'. Fixed effects: Age = -6.938e-05 (1.541e-04); Population = -0.00366 (0.00186). Random effects: Age|Pup ID = 4.361e-05; Genotype = 3.428e-11; Sex = 2.133e-09; Litter size = 3.606e-11. Random effects do not significantly affect model fit, BIC = -836.35 (full model), -862.95 (reduced model, just fixed effects), p = 0.55446.

**LMM proportion of motifs in V1**: 'proportion motifs ∼ 1 + Age + Population + (Age|Pup ID) + (1|Genotype) + (1|Sex) + (1|Litter size)'. Fixed effects: Age = -0.00236 (8.0067e-04); Population = 0.0175 (0.00927). Random effects: Age|Pup ID = 0.00174; Genotype = 1.044e-10; Sex = 7.0888e-11; Litter size = 1.102e-09. Random effects do not significantly affect model fit, BIC = -398.29 (full model), -417.07 (reduced model, just fixed effects), p = 0.495.

**LMM proportion of motifs in VISm**: 'proportion motifs ∼ 1 + Age + Population + (Age|Pup ID) + (1|Genotype) + (1|Sex) + (1|Litter size)'. Fixed effects: Age = -0.00311 (4.485e-04); Population = 0.00435 (0.00336). Random effects: Age|Pup ID = 0.00148; Genotype = 3.289e-12; Sex = 0.00275; Litter size = 0.0178. Random effects do not significantly affect model fit, BIC = -651.42 (full model), -668.38 (reduced model, just fixed effects), p = 0.426.

**LMM proportion of motifs in VISl**: 'proportion motifs ∼ 1 + Age + Population + (Age|Pup ID) + (1|Genotype) + (1|Sex) + (1|Litter size)'. Fixed effects: Age = -0.00152 (2.716e-04); Population = -1.186e-04 (0.00287). Random effects: Age|Pup ID = 6.678e-04; Genotype = 2.124e-11; Sex = 9.933e-11; Litter size = 0.00339. Random effects do not significantly affect model fit, BIC = -722.39 (full model), -734.37 (reduced model, just fixed effects), p = 0.485.

**LMM proportion of motifs in AUD**: 'proportion motifs ∼ 1 + Age + Population + (Age|Pup ID) + (1|Genotype) + (1|Sex) + (1|Litter size)'. Fixed effects: Age = -7.3953e-04 (1.806e-04); Population = 0.00559 (0.00235). Random effects: Age|Pup ID = 2.929e-04; Genotype = 0.00315; Sex = 7.474e-11; Litter size = 0.00359. Random effects do not significantly affect model fit, BIC = -811.83 (full model), -827.96 (reduced model, just fixed effects), p = 0.386.

**LMM proportion of motifs in PPC**: 'proportion motifs ∼ 1 + Age + Population + (Age|Pup ID) + (1|Genotype) + (1|Sex) + (1|Litter size)'. Fixed effects: Age = -0.00359 (9.255e-04); Population = 0.0137 (0.00618). Random effects: Age|Pup ID = 0.00331; Genotype = 0.00781; Sex = 1.463e-10; Litter size =1.365e-08. Random effects do not significantly affect model fit, BIC = -526.88 (full model), -537.53 (reduced model, just fixed effects), p = 0.149.

**LMM proportion of motifs in RS**: 'proportion motifs ∼ 1 + Age + Population + (Age|Pup ID) + (1|Genotype) + (1|Sex) + (1|Litter size)'. Fixed effects: Age = 0.00182 (8.145e-04); Population = -0.0163 (0.00741). Random effects: Age|Pup ID =0.00188; Genotype = 1.650e-09; Sex = 0.01037; Litter size =1.365e-08. Random effects do not significantly affect model fit, BIC = -442.43 (full model), -463.74 (reduced model, just fixed effects), p = 0.446.

## Figure 3.11: Motif size and frequency per region across development.

**LMM mean motif size MC**: 'motif size $\sim$ 1 + Age + Population + (Age|Pup ID) + (1|Genotype) + (1|Sex) + (1|Litter size)'. Fixed effects: Age = 189.11 (30.696); Population = -995.53 (239.78). Random effects: Age|Pup ID = 90.725; Genotype = 2.0871e-06; Sex = 84.371; Litter size = 421.24. Random effects do not significantly affect model fit, BIC = 2443.9 (full model), 2424.9 (reduced model, just fixed effects), p = 0.396.

**LMM mean motif size S1bod:** 'motif size $\sim$ 1 + Age + Population + (Age|Pup ID) + (1|Genotype) + (1|Sex) + (1|Litter size)'. Fixed effects: Age = 197.07 (17.36); Population = -1302 (153.41). Random effects: Age|Pup ID = 48.498; Genotype = 266.17; Sex = 4.729e-06; Litter size = 8.145e-06. Random effects do not significantly affect model fit, BIC = 2266.8 (full model), 2262.4 (reduced model, just fixed effects), p = 0.327.

**LMM mean motif size S1b**: 'motif size $\sim$ 1 + Age + Population + (Age|Pup ID) + (1|Genotype) + (1|Sex) + (1|Litter size)'. Fixed effects: Age = 236.11 (19.642); Population = -1125.3 (147.81). Random effects: Age|Pup ID = 58.198; Genotype = 2.689e-05; Sex = 7.0263e-07; Litter size = 742.69. Random effects do not significantly affect model fit, BIC = 2308.1 (full model), 2300.8 (reduced model, just fixed effects), p = 0.505.

**LMM mean motif size PPC**: 'motif size $\sim$ 1 + Age + Population + (Age|Pup ID) + (1|Genotype) + (1|Sex) + (1|Litter size)'. Fixed effects: Age = 138.58 (19.745); Population = -431.26 (188.03). Random effects: Age|Pup ID = 45.881; Genotype = 6.841e-07; Sex = 6.114e-07; Litter size = 1.0344e-06. Random effects do not significantly affect model fit, BIC = 2092.1 (full model), 2071.6 (reduced model, just fixed effects), p = 0.426.

**LMM mean motif size VC**: 'motif size $\sim$ 1 + Age + Population + (Age|Pup ID) + (1|Genotype) + (1|Sex) + (1|Litter size)'. Fixed effects: Age = 341.51 (42.586); Population = -1249.9 (200.49). Random effects: Age|Pup ID = 170.61; Genotype = 2.541e-04; Sex = 5.317e-05; Litter size = 6.307e-05. Random effects do not significantly affect model fit, BIC = 2419.1 (full model), 2416 (reduced model, just fixed effects), p = 0.248.

**LMM mean motif size RS**: 'motif size $\sim$ 1 + Age + Population + (Age|Pup ID) + (1|Genotype) + (1|Sex) + (1|Litter size)'. Fixed effects: Age = 163.8 (29.258); Population = -1210.6 (247.59). Random effects: Age|Pup ID = 96.323; Genotype = 685.63; Sex = 217.94; Litter size = 447.99. Random effects do not significantly affect model fit, BIC = 2361.1 (full model), 2347.5 (reduced model, just fixed effects), p = 0.188.

**LMM mean motif frequency MC**: 'motif frequency ∼ 1 + Age + Population + (Age|Pup ID) + (1|Genotype) + (1|Sex) + (1|Litter size)'. Fixed effects: Age = 0.0141 (0.00207); Population = 0.0784 (0.00961). Random effects: Age|Pup ID = 0.00825; Genotype = 1.341e-09; Sex = 1.0372e-09; Litter size = 2.575e-10. Random effects do not significantly affect model fit, BIC = -331.44 (full model), -311.16 (reduced model, just fixed effects), p = 0.762.

**LMM mean motif frequency S1bod**: 'motif frequency ∼ 1 + Age + Population + (Age|Pup ID) + (1|Genotype) + (1|Sex) + (1|Litter size)'. Fixed effects: Age = 0.0110 (0.00161); Population = 0.0467 (0.0113). Random effects: Age|Pup ID = 0.00616; Genotype = 0.0148; Sex = 2.01e-10; Litter size = 8.1041e-11. Random effects do not significantly affect model fit, BIC = -358.34 (full model), -343.69 (reduced model, just fixed effects), p = 0.782.

**LMM mean motif frequency S1b**: 'motif frequency ∼ 1 + Age + Population + (Age|Pup ID) + (1|Genotype) + (1|Sex) + (1|Litter size)'. Fixed effects: Age = 0.0122 (0.00163); Population = 0.0373 (0.0110). Random effects: Age|Pup ID = 0.00634; Genotype = 0.0160; Sex = 1.734e-11; Litter size = 6.111e-11. Random effects do not significantly affect model fit, BIC = -370.32 (full model), -354.27 (reduced model, just fixed effects), p = 0.762.

**LMM mean motif frequency PPC**: 'motif frequency ∼ 1 + Age + Population + (Age|Pup ID) + (1|Genotype) + (1|Sex) + (1|Litter size)'. Fixed effects: Age = 0.0107 (0.00132); Population = 0.0277 (0.00841). Random effects: Age|Pup ID = 0.00508; Genotype = 0.00880; Sex = 2.257e-10; Litter size = 1.313e-09. Random effects do not significantly affect model fit, BIC = -393.69 (full model), -385.16 (reduced model, just fixed effects), p = 0.723.

**LMM mean motif frequency VC**: 'motif frequency ∼ 1 + Age + Population + (Age|Pup ID) + (1|Genotype) + (1|Sex) + (1|Litter size)'. Fixed effects: Age = 0.0129 (0.00138); Population = 0.0332 (0.00813). Random effects: Age|Pup ID = 0.00496; Genotype = 7.442e-09; Sex = 0.00212; Litter size = 0.0169. Random effects do not significantly affect model fit, BIC = -420.98 (full model), -430.14 (reduced model, just fixed effects), p = 0.119.

**LMM mean motif frequency RS**: 'motif frequency ∼ 1 + Age + Population + (Age|Pup ID) + (1|Genotype) + (1|Sex) + (1|Litter size)'. Fixed effects: Age = 0.0129 (0.00138); Population = 0.0332 (0.00813). Random effects: Age|Pup ID = 0.00496; Genotype = 7.442e-09; Sex = 0.00212; Litter size = 0.0169. Random effects do not significantly affect model fit, BIC = -420.98 (full model), -430.14 (reduced model, just fixed effects), p = 0.188.

**LMM mean motif size excitatory population across regions**: 'mean motif size ∼ 1 + Age + Region + (Age|Pup ID) + (1|Genotype) + (1|Sex) + (1|Litter size)'. Fixed effects: Age = 203.61 (31.742); Region = -4.124 (36.246). Random effects: Age|Pup ID = 98.426; Genotype = 3.790e-05; Sex = 2.341e-05; Litter size = 5.382e-07. Random effects do not significantly affect model fit, BIC = 5620.5 (full model), 5639.5 (reduced model, just fixed effects), p = 0.495.

**LMM mean motif frequency excitatory population across regions**: 'mean motif frequency $\sim$ 1 + Age + Region + (Age|Pup ID) + (1|Genotype) + (1|Sex) + (1|Litter size)'. Fixed effects: Age = 0.0178 (0.00246); Region = 1.195e-04 (0.00202). Random effects: Age|Pup ID = 0.00842; Genotype = 9.814e-10; Sex = 3.416e-10; Litter size = 7.339e-10. Random effects do not significantly affect model fit, BIC = -795.21 (full model), -702.42 (reduced model, just fixed effects), p = 0.772.

**LMM mean motif size GABAergic population across regions**: 'mean motif size $\sim$ 1 + Age + Region + (Age|Pup ID) + (1|Genotype) + (1|Sex) + (1|Litter size)'. Fixed effects: Age = 248.81 (35.029); Region = -88.932 (44.933). Random effects: Age|Pup ID = 82.495; Genotype = 2.105e-04; Sex = 6.0567e-07; Litter size = 566.96. Random effects do not significantly affect model fit, BIC = 5539.4 (full model), 5536.8 (reduced model, just fixed effects), p = 0.525.

**LMM mean motif frequency GABAergic population across regions**: 'mean motif frequency $\sim$ 1 + Age + Region + (Age|Pup ID) + (1|Genotype) + (1|Sex) + (1|Litter size)'. Fixed effects: Age = 0.00835 (0.00136); Region = 5.470e-04 (0.00155). Random effects: Age|Pup ID = 0.00334; Genotype = 7.754e-09; Sex = 1.0808e-08; Litter size = 0.0361. Random effects do not significantly affect model fit, BIC = -939.32 (full model), -913.12 (reduced model, just fixed effects), p = 0.109.

**LMM KL divergence mean motif size excitatory population across regions**: 'mean motif size $\sim$ 1 + Age + Region'. Fixed effects: Age = -0.0168 (0.0521); Region = 0.166 (0.209).

**LMM KL divergence mean motif frequency excitatory population across regions**: 'mean motif frequency $\sim$ 1 + Age + Region'. Fixed effects: Age = 0.996 (0.211); Region = 0.233 (0.846).

**LMM KL divergence mean motif size GABAergic population across regions**: 'mean motif size $\sim$ 1 + Age + Region'. Fixed effects: Age = 0.0665 (0.0104); Region = -0.0416 (0.0417).

**LMM KL divergence mean motif frequency GABAergic population across regions**: 'mean motif frequency $\sim$ 1 + Age + Region'. Fixed effects: Age = 2.602 (0.424); Region = 2.875 (1.701).

## Figure 3.12: Developmental changes in population and region-specific variance of cortical activity.

**LMM mean motif variance MC**: 'motif variance $\sim$ 1 + Age + Population + (Age|Pup ID) + (1|Genotype) + (1|Sex) + (1|Litter size)'. Fixed effects: Age = -3.497e-07 (5.509e-08); Population = 1.0391e-06 (4.699e-07). Random effects: Age|Pup ID = 1.977e-07; Genotype = 2.392e-14;

Sex = 6.404e-14; Litter size = 9.830e-14. Random effects do not significantly affect model fit, BIC = -3144.3 (full model),-3134.4 (reduced model, just fixed effects), p = 0.307.

**LMM mean motif variance S1bod**: 'motif variance ∼ 1 + Age + Population + (Age|Pup ID) + (1|Genotype) + (1|Sex) + (1|Litter size)'. Fixed effects: Age = -3.102e-08 (4.485e-08); Population = -1.0717e-06 (4.180e-07). Random effects: Age|Pup ID = 1.420e-07; Genotype = 5.509e-07; Sex = 5.0712e-15; Litter size = 7.288e-15. Random effects do not significantly affect model fit, BIC = -3208.8 (full model),-3225.8 (reduced model, just fixed effects), p = 0.624.

**LMM mean motif variance S1b**: 'motif variance ∼ 1 + Age + Population + (Age|Pup ID) + (1|Genotype) + (1|Sex) + (1|Litter size)'. Fixed effects: Age = -1.122e-07 (1.386e-08); Population = -2.593e-07 (1.664e-07). Random effects: Age|Pup ID = 2.706e-08; Genotype = 2.118e-07; Sex = 1.210e-14; Litter size = 5.785e-07. Random effects do not significantly affect model fit, BIC = -3462 (full model), -3469 (reduced model, just fixed effects), p = 0.257.

**LMM mean motif variance PPC**: 'motif variance ∼ 1 + Age + Population + (Age|Pup ID) + (1|Genotype) + (1|Sex) + (1|Litter size)'. Fixed effects: Age = -1.406e-07 (1.3860.51734e-08); Population = -1.292e-06 (1.979e-07). Random effects: Age|Pup ID = 1.628e-07; Genotype = 7.856e-14; Sex = 1.764e-13; Litter size = 1.897e-13. Random effects do not significantly affect model fit, BIC = -2885.9 (full model), -2876.7 (reduced model, just fixed effects), p = 0.25743.

**LMM mean motif variance VC**: 'motif variance ∼ 1 + Age + Population + (Age|Pup ID) + (1|Genotype) + (1|Sex) + (1|Litter size)'. Fixed effects: Age = -8.994e-09 (4.427e-08); Population = 4.252e-08 (3.395e-07). Random effects: Age|Pup ID = 1.195e-08; Genotype = 2.704e-07; Sex = 7.510e-15; Litter size = 1.242e-07. Random effects do not significantly affect model fit, BIC = -3431.9 (full model), -3460.4 (reduced model, just fixed effects), p = 0.317.

**LMM mean motif variance RS**: 'motif variance ∼ 1 + Age + Population + (Age|Pup ID) + (1|Genotype) + (1|Sex) + (1|Litter size)'. Fixed effects: Age = -1.242e-07 (6.158e-08); Population = -5.798e-07 (4.898e-07). Random effects: Age|Pup ID = 2.0111e-07; Genotype = 1.939e-15; Sex = 1.491e-14; Litter size = 9.299e-15. Random effects do not significantly affect model fit, BIC = -3072 (full model), -3088.8 (reduced model, just fixed effects), p = 0.406.

**LMM mean motif variance excitatory population across regions**: 'mean motif size ∼ 1 + Age + Region + (Age|Pup ID) + (1|Genotype) + (1|Sex) + (1|Litter size)'. Fixed effects: Age = -7.503e-08 (2.649e-08); Region = 3.404e-07 (8.247e-08). Random effects: Age|Pup ID = 3.0405e-15; Genotype = 4.829e-07; Sex = 1.206e-14; Litter size = 4.650e-07. Random effects do not significantly affect model fit, BIC = -7451 (full model), -7479.2 (reduced model, just fixed effects), p = 0.64356.

**LMM mean motif variance GABAergic population across regions**: 'mean motif size $\sim$ 1 + Age + Region + (Age|Pup ID) + (1|Genotype) + (1|Sex) + (1|Litter size)'. Fixed effects: Age = -1.819e-07 (7.147e-08); Region = 3.232e-07 (9.864e-08). Random effects: Age|Pup ID = 1.710e-07; Genotype = 1.829e-15; Sex = 6.445e-17; Litter size = 2.513e-15. Random effects do not significantly affect model fit, BIC = -7061.9 (full model), -7065.2 (reduced model, just fixed effects), p = 0.584.

**LMM KL divergence mean motif variance excitatory population across regions**: 'mean motif variance $\sim$ 1 + Age + Region'. Fixed effects: Age = -0.00814 (0.0102); Region = -0.0683 (0.0382).

**LMM KL divergence mean motif variance GABAergic population across regions**: 'mean motif size $\sim$ 1 + Age + Region'. Fixed effects: Age = 1.948 (0.453); Region = 0.570 (1.695).

## Figure 3.13: Distinct developmental trajectories of activity motifs in excitatory and GABAergic neuronal populations.

**GLMM (gamma distribution) mean motif number**: 'mean motif number $\sim$ 1 + Age + Population + (Age|Pup ID) + (1|Genotype) + (1|Sex) + (1|Litter size)'. Fixed effects: Age = 0.00293 (1.763e-04), Population = -0.00716 (0.00128). Random effects: Age|Pup ID = 3.844e-04; Genotype = 0.00431; Sex = 1.22e-05; Litter size = 5.302e-04. The individual random effect Age|Pup ID significantly affects the model fit, BIC = -913.16 (full model), -900.99 (reduced model, fixed effects and without Age|Pup ID random effect), p = 5.971e-06.

**GLMM (gamma distribution) mean single mask motif**: 'mean single motif number $\sim$ 1 + Age + Population + (Age|Pup ID) + (1|Genotype) + (1|Sex) + (1|Litter size)'. Fixed effects: Age = 0.00353 (4.387e-04), Population = -0.0114 (0.00153). Random effects: Age|Pup ID = 0.00174; Genotype = 7.0881e-06; Sex = 2.326e-06; Litter size = 0.00328. Random effects did not significantly affect the model fit, BIC = -773.01 (full model), -790.61 (reduced model, just fixed effects), p = 0.0616.

**GLMM (gamma distribution) mean multi mask motif**: 'mean multi motif number $\sim$ 1 + Age + Population + (Age|Pup ID) + (1|Genotype) + (1|Sex) + (1|Litter size)'. Fixed effects: Age = 0.00821 (8.406e-04), Population = 0.00544 (0.00483). Random effects: Age|Pup ID = 0.00278; Genotype = 0.0194; Sex = 0.00467; Litter size = 0.0240. The individual random effect Age|Pup ID significantly affects the model fit, BIC = -511.2 (full model), -550.96 (reduced model, fixed effects and without Age|Pup ID random effect), p = 8.53e-12.

## Figure 3.14: Influence of SNR on the sICA decomposition of GCaMP6f and jRGECO1a dynamics.

**GLMM (gamma distribution) mean SNR**: 'mean SNR $\sim$ 1 + Age + Population + (Age|Pup ID) + (1|Genotype) + (1|Sex) + (1|Litter size)'. Fixed effects: Age = 8.713e-04 (1.337e-04), Population = -0.00766 (0.00132). Random effects: Age|Pup ID = 3.844e-04; Genotype = 0.00431; Sex = 1.22e-05; Litter size = 5.302e-04. The individual random effect Age|Pup ID significantly affects the model fit, BIC = -912.34 (full model), -958.74 (reduced model, fixed effects and without Age|Pup ID random effect), p = 3.255e-13.

**GLMM (gamma distribution) mean motif number**: 'mean motif number $\sim$ 1 + Age + Population + (Age|Pup ID) + (1|Genotype) + (1|Sex) + (1|Litter size)'. Fixed effects: Age = 0.00382 (4.861e-04), Population = -0.0229 (0.00179). Random effects: Age|Pup ID = 0.00156; Genotype = 1.582e-06; Sex = 2.444e-06; Litter size = 0.00129. Random effects did not significantly affect the model fit, BIC = -674.39 (full model), -699.41 (reduced model, just fixed effects), p = 0.723.

**LMM mean original/SNR motif proportion**: 'mean motif proportion $\sim$ 1 + Age + Population + (Age|Pup ID) + (1|Genotype) + (1|Sex) + (1|Litter size)'. Fixed effects: Age = 0.0181 (0.00398), Population = 0.0568 (0.0387). Random effects: Age|Pup ID = 0.00726; Genotype = 0.0495; Sex = 1.317e-08; Litter size = 0.0480. Random effects did not significantly affect the model fit, BIC = -63.189 (full model), -89.447 (reduced model, just fixed effects), p = 0.0704.

## Figure 3.15: Overlap distributions between excitatory and GABAergic sICA motifs across development.

**LMM maximum JI values distributions**: 'JI values $\sim$ 1 + Age + Age*Pup ID'. Fixed effects: Age = -0.00274 (0.00559), Animal ID = 0.00182 (0.0139), Age*Animal ID = -0.00168 (8.483e-04).

## Figure 3.17: Strengthening correlation between GABAergic and excitatory dynamics during development.

**LMM mean** $R_{1.5}$: 'mean R $\sim$ 1 + Age + (Age|Pup ID) + (1|Genotype) + (1|Sex) + (1|Litter size)'. Fixed effects: Age = -0.00542 (0.00257). Random effects: Age|Pup ID = 0.00284; Sex = 1.999e-13; Litter size = 4.336e-12. Random effects did not significantly affect the model fit, BIC = -41.778 (full model), -57.174 (reduced model, just fixed effects), p = 0.554.

**LMM mean time spent in low** $R_{1.5}$: 'mean time low R $\sim$ 1 + Age + (Age|Pup ID) + (1|Genotype) + (1|Sex) + (1|Litter size)'. Fixed effects: Age = 0.00874 (0.00365). Random effects: Age|Pup

ID = 0.00233; Sex = 1.665e-09; Litter size = 9.485e-10. Random effects did not significantly affect the model fit, BIC = -17.015 (full model), -32.871 (reduced model, just fixed effects), p = 0.446.

**GLMM (Gamma distribution) mean wasserstein distance between CDFs of $R_{1.5}$**: 'wasserstein CDF R $\sim$ 1 + Age + (Age|Pup ID) + (1|Genotype) + (1|Sex) + (1|Litter size)'. Fixed effects: Age = -1.408 (0.515). Random effects: Age|Pup ID = 0.575; Sex = 9.181e-05; Litter size = 1.278e-04. Random effects did not significantly affect the model fit, BIC = 213.82 (full model), 228.79 (reduced model, just fixed effects), p = 0.969.

## Figure 3.18: Region-specific tightening of correlation between GABAergic and excitatory dynamics.

**LMM mean $R_{1.5}$ across regions**: 'mean R region $\sim$ 1 + Age + Region + (Age|Pup ID) + (1|Genotype) + (1|Sex) + (1|Litter size)'. Fixed effects: Age = -0.00350 (0.00117), Region = 0.00621 (0.00365). Random effects: Age|Pup ID = 1.0895e-11; Sex = 3.486e-11; Litter size = 4.132e-11. Random effects did not significantly affect the model fit, BIC = -266.2 (full model), -290.34 (reduced model, just fixed effects), p = 0.0891.

**LMM mean wasserstein distance between CDFs of $R_{1.5}$ across regions**: 'wasserstein CDF R region $\sim$ 1 + Age + Region + (Age|Pup ID) + (1|Genotype) + (1|Sex) + (1|Litter size)'. Fixed effects: Age = 0.00344 (0.00108), Region = -0.00339 (0.00164). Random effects: Age|Pup ID = 0.00167; Sex = 0.00281; Litter size = 3.627e-10. Random effects did not significantly affect the model fit, BIC = -266.2 (full model), -290.34 (reduced model, just fixed effects), p = 0.0891.

## Figure 3.19: Epileptic-like activity induced by blockade of GABAergic signalling.

**LMM spatial coverage**: 'spatial coverage $\sim$ 1 + Condition + Population + (Condition|Pup ID) + (1|Genotype) + (1|Sex) + (1|Litter size)'. Fixed effects: Saline = 2.436 (1.504), PTX = 2.180 (1.850), Population = 7.842 (1.049). Random effects: Saline|Pup ID = 2.212; PTX|Pup ID = 3.763; Sex = 1.145e-08; Litter size = 1.580e-08. Random effects did not significantly affect the model fit, BIC = 330.21 (full model), 318.45 (reduced model, just fixed effects), p = 0.386.

**LMM ipsi/contra spatial coverage**: 'ipsi/contra spatial coverage $\sim$ 1 + Condition + Population + (Condition|Pup ID) + (1|Genotype) + (1|Sex) + (1|Litter size)'. Fixed effects: Saline = 0.0794 (0.0419), PTX = 0.0818 (0.0376), Population = -0.0138 (0.0300). Random effects: Saline|Pup ID = 0.0571; PTX|Pup ID = 0.0236; Sex = 0.0325; Litter size = 3.393e-09. Random effects did

not significantly affect the model fit, BIC = -19.513 (full model), -42.62 (reduced model, just fixed effects), p = 0.386.

## Figure 3.20: Shift towards higher GABAergic-excitatory correlation after blockage of GABAergic signalling.

**LMM number of motifs**: 'mean number motifs $\sim$ 1 + Condition + Population + (Condition|Pup ID) + (1|Genotype) + (1|Sex) + (1|Litter size)'. Fixed effects: Saline = 2.189 (3.642), PTX 4 min = 0.419 (4.168), PTX 40 min = -3.638 (3.595), Population = 15.781 (2.393). Random effects: Saline|Pup ID = 3.806; PTX 4 min|Pup ID = 6.179; PTX 40 min|Pup ID = 3.964; Sex = 1.145e-07; Litter size = 6.092e-08. Random effects did not significantly affect the model fit, BIC = 566.21 (full model), 555.22 (reduced model, just fixed effects), p = 0.475.

**LMM number of single mask motifs**: 'number motifs single $\sim$ 1 + Condition + Population + (Condition|Pup ID) + (1|Genotype) + (1|Sex) + (1|Litter size)'. Fixed effects: Saline = 3.125 (3.603), PTX 4 min = 2.302 (4.228), PTX 40 min = -1.961 (3.543), Population = 18.094 (2.175). Random effects: Saline|Pup ID = 5.304; PTX 4 min|Pup ID = 7.715; PTX 40 min|Pup ID = 5.284; Sex = 6.797e-09; Litter size = 2.969e-07. Random effects did not significantly affect the model fit, BIC = 554.24 (full model), 544.41 (reduced model, just fixed effects), p = 0.475.

**LMM number of multi mask motifs**: 'number motifs multi $\sim$ 1 + Condition + Population + (Condition|Pup ID) + (1|Genotype) + (1|Sex) + (1|Litter size)'. Fixed effects: Saline = -0.938 (1.389), PTX 4 min = -1.98 (1.140), PTX 40 min = 1.524 (1.566), Population = -2.3125 (0.555). Random effects: Saline|Pup ID = 3.240; PTX 4 min|Pup ID = 2.253; PTX 40 min|Pup ID = 3.858; Sex = 3.0158e-07; Litter size = 2.0543e-07. Random effects did not significantly affect the model fit, BIC = 385.12 (full model), 351.86 (reduced model, just fixed effects), p = 0.337.

**LMM number of EI partners**: 'EI partners $\sim$ 1 + Condition + (Condition|Pup ID) + (1|Genotype) + (1|Sex) + (1|Litter size)'. Fixed effects: Saline = 5.375 (3.364), PTX 4 min = 5.205 (3.930), PTX 40 min = 1.397 (4.858). Random effects: Saline|Pup ID = 5.361; PTX 4 min|Pup ID = 7.423; PTX 40 min|Pup ID = 11.37; Sex = 2.677e-08; Litter size = 9.171e-08. Random effects did not significantly affect the model fit, BIC = 296.23 (full model), 288.25 (reduced model, just fixed effects), p = 0.188.

**LMM mean $R_{1.5}$ acros conditions**: 'mean R $\sim$ 1 + Condition + Injection site + (Condition|Pup ID) + (1|Genotype) + (1|Sex) + (1|Litter size)'. Fixed effects: Saline = 0.015255 (0.011479), PTX 4 min = 0.092439 (0.012591), PTX 40 min = 0.077312 (0.013921), Injection site = -0.0019512 (0.0060075). Random effects: Saline|Pup ID = 0.021835; PTX 4 min|Pup ID = 0.026283; PTX 40 min|Pup ID = 0.03119; Sex = 6.0986e-10; Litter size = 1.2109e-09. Random effects did not

significantly affect the model fit, BIC = -178.98 (full model), -121.64 (reduced model, just fixed effects), p = 0.505.

**LMM mean wasserstein distance between CDFs of $R_{1.5}$ across conditions**: 'wasserstein mean R $\sim$ 1 + Condition + Injection site + (Condition|Pup ID) + (1|Genotype) + (1|Sex) + (1|Litter size)'. Fixed effects: Saline = 0.024583 (0.0059153), PTX 4 min = 0.092439 (0.0099377), PTX 40 min = 0.059967 (0.010717), Injection site = 0.0078304 (0.0034665). Random effects: Saline|Pup ID = 0.009363; PTX 4 min|Pup ID = 0.02445; PTX 40 min|Pup ID = 0.026956; Sex = 3.0885e-09; Litter size = 2.3056e-09. Random effects did not significantly affect the model fit, BIC = -262.7 (full model), -274.33 (reduced model, just fixed effects), p = 0.49505.

# Bibliography


Abdeladim, Lamiae, Hyeyoung Shin, Uday K Jagadisan, Mora B Ogando and Hillel Adesnik (2023). „Probing inter-areal computations with a cellular resolution two-photon holographic mesoscope“. In: *bioRxiv*, pp. 2023–03 (cit. on p. 38).

Ackman, James B, Timothy J Burbridge and Michael C Crair (2012). „Retinal waves coordinate patterned activity throughout the developing visual system“. In: *Nature* 490.7419, pp. 219–225 (cit. on pp. 14, 16, 91, 92, 109, 140, 141, 145).

Ackman, James B and Michael C Crair (2014a). „Role of emergent neural activity in visual map development“. In: *Current opinion in neurobiology* 24, pp. 166–175 (cit. on pp. 16, 17).

Ackman, James B, Hongkui Zeng and Michael C Crair (2014b). „Structured dynamics of neural activity across developing neocortex“. In: *BioRxiv*, p. 012237 (cit. on pp. 1, 2, 36, 84–86, 91, 94, 114, 140, 149).

Adelsberger, Helmuth, Olga Garaschuk and Arthur Konnerth (2005). „Cortical calcium waves in resting newborn mice“. In: *Nature neuroscience* 8.8, pp. 988–990 (cit. on p. 151).

Adesnik, Hillel and Alexander Naka (2018). „Cracking the function of layers in the sensory cortex“. In: *Neuron* 100.5, pp. 1028–1043 (cit. on pp. 5, 6).

Afrashteh, Navvab, Samsoon Inayat, Edgar Bermudez Contreras, Artur Luczak, Bruce L McNaughton et al. (2020). „Spatiotemporal structure of sensory-evoked and spontaneous activity revealed by mesoscale imaging in anesthetized and awake mice“. In: *BioRxiv*, pp. 2020–05 (cit. on p. 155).

Aggarwal, Adeeti, Connor Brennan, Jennifer Luo, Helen Chung, Diego Contreras et al. (2022). „Visual evoked feedforward–feedback traveling waves organize neural activity across the cortical hierarchy in mice“. In: *Nature Communications* 13.1, p. 4754 (cit. on p. 20).

Akerboom, Jasper, Nicole Carreras Calderón, Lin Tian, Sebastian Wabnig, Matthias Prigge et al. (2013). „Genetically encoded calcium indicators for multi-color neural activity imaging and combination with optogenetics“. In: *Frontiers in molecular neuroscience* 6, p. 2 (cit. on pp. 69, 87).

Akin, Orkun, Bryce T Bajar, Mehmet F Keles, Mark A Frye and S Lawrence Zipursky (2019). „Cell-type-specific patterned stimulus-independent neuronal activity in the Drosophila visual system during synapse formation“. In: *Neuron* 101.5, pp. 894–904 (cit. on p. 16).

Alberts, Jeffrey R (2007). „Huddling by rat pups: ontogeny of individual and group behavior“. In: *Developmental Psychobiology: The Journal of the International Society for Developmental Psychobiology* 49.1, pp. 22–32 (cit. on pp. 14, 42).

Ali, Farhan and Alex C Kwan (2020). „Interpreting in vivo calcium signals from neuronal cell bodies, axons, and dendrites: a review“. In: *Neurophotonics* 7.1, pp. 011402–011402 (cit. on p. 83).

Allen, William E, Isaac V Kauvar, Michael Z Chen, Ethan B Richman, Samuel J Yang et al. (2017). „Global representations of goal-directed behavior in distinct cell types of mouse neocortex“. In: *Neuron* 94.4, pp. 891–907 (cit. on pp. 61, 82–84, 88, 145, 147, 154).

Anastasiades, Paul G, Andre Marques-Smith, Daniel Lyngholm, Tom Lickiss, Sayda Raffiq et al. (2016). „GABAergic interneurons form transient layer-specific circuits in early postnatal neocortex“. In: *Nature communications* 7.1, p. 10584 (cit. on pp. 2, 9, 11, 36, 94).

Andalman, Aaron S, Vanessa M Burns, Matthew Lovett-Barron, Michael Broxton, Ben Poole et al. (2019). „Neuronal dynamics regulating brain and behavioral state transitions“. In: *Cell* 177.4, pp. 970–985 (cit. on p. 146).

André, Monique, M-D Lamblin, Anne-Marie d'Allest, Lilia Curzi-Dascalova, FTSNT Moussalli-Salefranque et al. (2010). „Electroencephalography in premature and full-term infants. Developmental features and glossary“. In: *Neurophysiologie clinique/Clinical neurophysiology* 40.2, pp. 59–124 (cit. on p. 19).

Antón-Bolaños, Noelia, Alejandro Sempere-Ferràndez, Teresa Guillamón-Vivancos, Francisco J Martini, Leticia Pérez-Saiz et al. (2019). „Prenatal activity from thalamic neurons governs the emergence of functional cortical maps in mice“. In: *Science* 364.6444, pp. 987–990 (cit. on pp. 7, 12, 15, 16).

Arakawa, Hiroyuki, Ayumi Suzuki, Shuxin Zhao, Vassiliy Tsytsarev, Fu-Sun Lo et al. (2014). „Thalamic NMDA receptor function is necessary for patterning of the thalamocortical somatosensory map and for sensorimotor behaviors“. In: *Journal of Neuroscience* 34.36, pp. 12001–12014 (cit. on pp. 24, 98, 109, 141).

Arandia-Romero, Iñigo, Ramon Nogueira, Gabriela Mochol and Rubén Moreno-Bote (2017). „What can neuronal populations tell us about cognition?“ In: *Current Opinion in Neurobiology* 46, pp. 48–57 (cit. on p. 33).

Arckens, Lutgarde, Georg Schweigart, Ying Qu, Griet Wouters, David V Pow et al. (2000). „Cooperative changes in GABA, glutamate and activity levels: the missing link in cortical plasticity“. In: *European Journal of Neuroscience* 12.12, pp. 4222–4232 (cit. on p. 26).

Ashby, Michael C and John TR Isaac (2011). „Maturation of a recurrent excitatory neocortical circuit by experience-dependent unsilencing of newly formed dendritic spines“. In: *Neuron* 70.3, pp. 510–521 (cit. on p. 111).

Avitan, Lilach, Zac Pujic, Jan Mölter, Matthew Van De Poll, Biao Sun et al. (2017). „Spontaneous activity in the zebrafish tectum reorganizes over development and is influenced by visual experience“. In: *Current Biology* 27.16, pp. 2407–2419 (cit. on p. 16).

Avitan, Lilach, Zac Pujic, Jan Mölter, Shuyu Zhu, Biao Sun et al. (2021). „Spontaneous and evoked activity patterns diverge over development“. In: *Elife* 10, e61942 (cit. on pp. 16, 155).

Awad, Patricia Nora, Clara Akofa Amegandjin, Joanna Szczurkowska, Josianne Nuñes Carriço, Antônia Samia Fernandes do Nascimento et al. (2018). „KCC2 regulates dendritic spine formation in a brain-region specific and BDNF dependent manner“. In: *Cerebral Cortex* 28.11, pp. 4049–4062 (cit. on p. 30).

Ayaz, Asli and Frances S Chance (2009). „Gain modulation of neuronal responses by subtractive and divisive mechanisms of inhibition“. In: *Journal of neurophysiology* 101.2, pp. 958–968 (cit. on p. 153).

Azevedo, Frederico AC, Ludmila RB Carvalho, Lea T Grinberg, José Marcelo Farfel, Renata EL Ferretti et al. (2009). „Equal numbers of neuronal and nonneuronal cells make the human brain an isometrically scaled-up primate brain“. In: *Journal of Comparative Neurology* 513.5, pp. 532–541 (cit. on pp. 2, 3).

Babij, Rachel, Camilo Ferrer, Alexander Donatelle, Sam Wacks, Amanda M Buch et al. (2023). „Gabrb3 is required for the functional integration of pyramidal neuron subtypes in the somatosensory cortex“. In: *Neuron* 111.2, pp. 256–274 (cit. on p. 36).

Baloch, Sajjad, Ragini Verma, Hao Huang, Parmeshwar Khurd, Sarah Clark et al. (2009). „Quantification of brain maturation and growth patterns in C57BL/6J mice via computational neuroanatomy of diffusion tensor images“. In: *Cerebral cortex* 19.3, pp. 675–687 (cit. on pp. 36, 150).

Barabási, Dániel L, Gregor FP Schuhknecht and Florian Engert (2022). „Nature over Nurture: Functional neuronal circuits emerge in the absence of developmental activity“. In: *bioRxiv*, pp. 2022–10 (cit. on p. 149).

Barber, Melissa, Yoko Arai, Yoshihiro Morishita, Lisa Vigier, Frederic Causeret et al. (2015). „Migration speed of Cajal-Retzius cells modulated by vesicular trafficking controls the size of higher-order cortical areas“. In: *Current Biology* 25.19, pp. 2466–2478 (cit. on p. 8).

Barkat, Tania Rinaldi, Daniel B Polley and Takao K Hensch (2011). „A critical period for auditory thalamo-cortical connectivity“. In: *Nature neuroscience* 14.9, pp. 1189–1194 (cit. on pp. 21, 24).

Barson, Daniel, Ali S Hamodi, Xilin Shen, Gyorgy Lur, R Todd Constable et al. (2020). „Simultaneous mesoscopic and two-photon imaging of neuronal activity in cortical circuits“. In: *Nature methods* 17.1, pp. 107–113 (cit. on p. 39).

Baruchin, Liad J, Filippo Ghezzi, Michael M Kohl and Simon JB Butt (2022). „Contribution of interneuron subtype-specific gabaergic signaling to emergent sensory processing in mouse somatosensory whisker barrel cortex“. In: *Cerebral Cortex* 32.12, pp. 2538–2554 (cit. on pp. 12, 13, 25, 36, 146).

Bass, John Samuel, Anney H Tuo, Linh T Ton, Miranda J Jankovic, Paarth K Kapadia et al. (2020). „On the digital psychopharmacology of valproic acid in mice“. In: *Frontiers in Neuroscience* 14, p. 594612 (cit. on p. 81).

Batista-Brito, Renata, Robert Machold, Corinna Klein and Gord Fishell (2008). „Gene expression in cortical interneuron precursors is prescient of their mature function“. In: *Cerebral cortex* 18.10, pp. 2306–2317 (cit. on p. 147).

Ben-Ari, Yehezkel and Enrico Cherubini (2022). „The GABA polarity shift and bumetanide treatment: making sense requires unbiased and undogmatic analysis“. In: *Cells* 11.3, p. 396 (cit. on p. 29).

Ben-Ari, Yehezkel, Jean-Luc Gaiarsa, Roman Tyzio and Rustem Khazipov (2007). „GABA: a pioneer transmitter that excites immature neurons and generates primitive oscillations“. In: *Physiological reviews* 87.4, pp. 1215–1284 (cit. on pp. 27, 30).

Ben-Ari, Yehezkel, Melanie A Woodin, Evelyne Sernagor, Laura Cancedda, Laurent Vinay et al. (2012). „Refuting the challenges of the developmental shift of polarity of GABA actions: GABA more exciting than ever!“ In: *Frontiers in cellular neuroscience* 6, p. 35 (cit. on pp. 29, 30).

Benders, Manon J, Kirsi Palmu, Caroline Menache, Cristina Borradori-Tolsa, Francois Lazeyras et al. (2015). „Early brain activity relates to subsequent brain growth in premature infants“. In: *Cerebral Cortex* 25.9, pp. 3014–3024 (cit. on p. 20).

Benisty, Hadas, Andrew H Moberly, Sweyta Lohani, Daniel Barson, Ronald R Coifman et al. (2021). „Rapid fluctuations in functional connectivity of cortical networks encode spontaneous behavior“. In: *bioRxiv*, pp. 2021–08 (cit. on p. 155).

Berardi, Nicoletta, Tommaso Pizzorusso and Lamberto Maffei (2000). „Critical periods during sensory development“. In: *Current opinion in neurobiology* 10.1, pp. 138–145 (cit. on pp. 12, 21, 23, 36).

Berkes, Pietro, Gergő Orbán, Máté Lengyel and József Fiser (2011). „Spontaneous cortical activity reveals hallmarks of an optimal internal model of the environment“. In: *Science* 331.6013, pp. 83–87 (cit. on p. 18).

Bherer, Louis (2015). „Cognitive plasticity in older adults: effects of cognitive training and physical exercise“. In: *Annals of the New York Academy of Sciences* 1337.1, pp. 1–6 (cit. on p. 22).

Bieler, Malte, Kay Sieben, Nicole Cichon, Sandra Schildt, Brigitte Röder et al. (2017a). „Rate and temporal coding convey multisensory information in primary sensory cortices“. In: *eneuro* 4.2 (cit. on p. 157).

Bieler, Malte, Kay Sieben, Sandra Schildt, Brigitte Röder and Ileana L Hanganu-Opatz (2017b). „Visual–tactile processing in primary somatosensory cortex emerges before cross-modal experience“. In: *Synapse* 71.6, e21958 (cit. on p. 157).

Bitzenhofer, Sebastian H, Jastyn A Pöpplau and Ileana Hanganu-Opatz (2020). „Gamma activity accelerates during prefrontal development“. In: *Elife* 9, e56795 (cit. on p. 19).

Blaesse, Peter, Matti S Airaksinen, Claudio Rivera and Kai Kaila (2009). „Cation-chloride cotransporters and neuronal function“. In: *Neuron* 61.6, pp. 820–838 (cit. on p. 27).

Blanquie, Oriane, Werner Kilb, Anne Sinning and Heiko J Luhmann (2017a). „Homeostatic interplay between electrical activity and neuronal apoptosis in the developing neocortex“. In: *Neuroscience* 358, pp. 190–200 (cit. on p. 10).

Blanquie, Oriane, Jenq-Wei Yang, Werner Kilb, Salim Sharopov, Anne Sinning et al. (2017b). „Electrical activity controls area-specific expression of neuronal apoptosis in the mouse developing cerebral cortex“. In: *Elife* 6, e27696 (cit. on pp. 10, 156).

Blumberg, Mark S (2015). „Developing sensorimotor systems in our sleep“. In: *Current directions in psychological science* 24.1, pp. 32–37 (cit. on p. 14).

Blumberg, Mark S, Cassandra M Coleman, Ashlynn I Gerth and Bob McMurray (2013). „Spatiotemporal structure of REM sleep twitching reveals developmental origins of motor synergies“. In: *Current Biology* 23.21, pp. 2100–2109 (cit. on p. 14).

Blumberg, Mark S, Cassandra M Coleman, Greta Sokoloff, Joshua A Weiner, Bernd Fritzsch et al. (2015). „Development of twitching in sleeping infant mice depends on sensory experience“. In: *Current Biology* 25.5, pp. 656–662 (cit. on p. 42).

Blumberg, Mark S, Adele MH Seelke, Steven B Lowen and Karl Æ Karlsson (2005). „Dynamics of sleep-wake cyclicity in developing rats“. In: *Proceedings of the National Academy of Sciences* 102.41, pp. 14860–14864 (cit. on p. 13).

Blundon, Jay A, Ildar T Bayazitov and Stanislav S Zakharenko (2011). „Presynaptic gating of postsynaptically expressed plasticity at mature thalamocortical synapses“. In: *Journal of Neuroscience* 31.44, pp. 16012–16025 (cit. on p. 25).

Bonifazi, Paolo, Miri Goldin, Michel A Picardo, Isabel Jorquera, A Cattani et al. (2009). „GABAergic hub neurons orchestrate synchrony in developing hippocampal networks“. In: *Science* 326.5958, pp. 1419–1424 (cit. on pp. 11, 94, 154).

Boon, Jacqueline, Emma Clarke, Nicoletta Kessaris, André Goffinet, Zoltán Molnár et al. (2019). „Long-range projections from sparse populations of GABAergic neurons in murine subplate“. In: *Journal of Comparative Neurology* 527.10, pp. 1610–1620 (cit. on pp. 11, 36, 154).

Bortone, Dante and Franck Polleux (2009). „KCC2 expression promotes the termination of cortical interneuron migration in a voltage-sensitive calcium-dependent manner“. In: *Neuron* 62.1, pp. 53–71 (cit. on p. 6).

Boyle, Maureen P, Amy Bernard, Carol L Thompson, Lydia Ng, Andrew Boe et al. (2011). „Cell-type-specific consequences of reelin deficiency in the mouse neocortex, hippocampus, and amygdala“. In: *Journal of Comparative Neurology* 519.11, pp. 2061–2089 (cit. on p. 6).

Bragg-Gonzalo, Lorena, NS De León Reyes and Marta Nieto (2021). „Genetic and activity dependent-mechanisms wiring the cortex: Two sides of the same coin“. In: *Seminars in Cell & Developmental Biology*. Vol. 118. Elsevier, pp. 24–34 (cit. on pp. 9, 12, 19).

Bregestovski, Piotr and Christophe Bernard (2012). „Excitatory GABA: how a correct observation may turn out to be an experimental artifact“. In: *Frontiers in pharmacology* 3, p. 65 (cit. on p. 29).

Brockmann, Marco D, Beatrice Pöschel, Nicole Cichon and Ileana L Hanganu-Opatz (2011). „Coupled oscillations mediate directed interactions between prefrontal cortex and hippocampus of the neonatal rat“. In: *Neuron* 71.2, pp. 332–347 (cit. on p. 16).

Bronchti, Gilles, Peter Heil, Ronen Sadka, Andreas Hess, Henning Scheich et al. (2002). „Auditory activation of ‘visual’cortical areas in the blind mole rat (Spalax ehrenbergi)“. In: *European Journal of Neuroscience* 16.2, pp. 311–329 (cit. on p. 23).

Bronchti, Gilles, Norbert Schönenberger, Egbert Welker and Hendrik Van der Loos (1992). „Barrelfield expansion after neonatal eye removal in mice.“ In: *Neuroreport* 3.6, pp. 489–492 (cit. on p. 23).

Broussard, Gerard Joey, Yajie Liang, Marina Fridman, Elizabeth K Unger, Guanghan Meng et al. (2018). „In vivo measurement of afferent activity with axon-specific calcium imaging“. In: *Nature neuroscience* 21.9, pp. 1272–1280 (cit. on p. 83).

Buckley, Ashura W and Gregory L Holmes (2016). „Epilepsy and autism“. In: *Cold Spring Harbor Perspectives in Medicine* 6.4, a022749 (cit. on p. 31).

Buonomano, Dean V and Wolfgang Maass (2009). „State-dependent computations: spatiotemporal processing in cortical networks“. In: *Nature Reviews Neuroscience* 10.2, pp. 113–125 (cit. on p. 146).

Butt, Simon JB, Marc Fuccillo, Susana Nery, Steven Noctor, Arnold Kriegstein et al. (2005). „The temporal and spatial origins of cortical interneurons predict their physiological subtype“. In: *Neuron* 48.4, pp. 591–604 (cit. on p. 5).

Butt, Simon JB, Jacqueline A Stacey, Yayoi Teramoto and Cristiana Vagnoni (2017). „A role for GABAergic interneuron diversity in circuit development and plasticity of the neonatal cerebral cortex“. In: *Current opinion in neurobiology* 43, pp. 149–155 (cit. on p. 153).

Cadwell, Cathryn R, Aparna Bhaduri, Mohammed A Mostajo-Radji, Matthew G Keefe and Tomasz J Nowakowski (2019). „Development and arealization of the cerebral cortex“. In: *Neuron* 103.6, pp. 980–1004 (cit. on pp. 3, 6–8).

Callaway, Edward M and Lawrence C Katz (1990). „Emergence and refinement of clustered horizontal connections in cat striate cortex“. In: *Journal of Neuroscience* 10.4, pp. 1134–1153 (cit. on p. 9).

Cang, Jianhua and David A Feldheim (2013). „Developmental mechanisms of topographic map formation and alignment“. In: *Annual review of neuroscience* 36, pp. 51–77 (cit. on pp. 12, 109).

Cang, Jianhua, René C Rentería, Megumi Kaneko, Xiaorong Liu and Michael P Stryker (2005). „Development of precise maps in visual cortex requires patterned spontaneous activity in the retina“. In: *Neuron* 48.5, pp. 797–809 (cit. on p. 16).

Capogna, Marco, Pablo E Castillo and Arianna Maffei (2021). „The ins and outs of inhibitory synaptic plasticity: Neuron types, molecular mechanisms and functional roles“. In: *European Journal of Neuroscience* 54.8, pp. 6882–6901 (cit. on p. 30).

Capone, Cristiano, Chiara De Luca, Giulia De Bonis, Robin Gutzen, Irene Bernava et al. (2023). „Simulations approaching data: cortical slow waves in inferred models of the whole hemisphere of mouse“. In: *Communications Biology* 6.1, p. 266 (cit. on p. 39).

Caputi, Antonio, Sarah Melzer, Magdalena Michael and Hannah Monyer (2013). „The long and short of GABAergic neurons“. In: *Current opinion in neurobiology* 23.2, pp. 179–186 (cit. on pp. 11, 36, 94, 154).

Cardin, Jessica A (2018). „Inhibitory interneurons regulate temporal precision and correlations in cortical circuits“. In: *Trends in neurosciences* 41.10, pp. 689–700 (cit. on pp. 11, 141, 143, 147).

Cardin, Jessica A, Michael C Crair and Michael J Higley (2020). „Mesoscopic imaging: shining a wide light on large-scale neural dynamics“. In: *Neuron* 108.1, pp. 33–43 (cit. on pp. 37, 40, 82, 89, 150).

Castelhano-Carlos, Magda João, Nuno Sousa, F Ohl and V Baumans (2010). „Identification methods in newborn C57BL/6 mice: a developmental and behavioural evaluation“. In: *Laboratory Animals* 44.2, pp. 88–103 (cit. on p. 78).

Caval-Holme, Franklin S, Marcos L Aranda, Andy Q Chen, Alexandre Tiriac, Yizhen Zhang et al. (2022). „The retinal basis of light aversion in neonatal mice“. In: *Journal of Neuroscience* 42.20, pp. 4101–4115 (cit. on p. 48).

Chabot, Nicole, Stéphane Robert, Robin Tremblay, Dom Miceli, Denis Boire et al. (2007). „Audition differently activates the visual system in neonatally enucleated mice compared with anophthalmic mutants“. In: *European Journal of Neuroscience* 26.8, pp. 2334–2348 (cit. on p. 23).

Changizi, MA (2007). „Scaling the brain and its connections“. In: *Evolution of nervous systems* 3, pp. 167–180 (cit. on p. 9).

Charbonneau, Valérie, Marie-Eve Laramée, Virginie Boucher, Gilles Bronchti and Denis Boire (2012). „Cortical and subcortical projections to primary visual cortex in anophthalmic, enucleated and sighted mice“. In: *European Journal of Neuroscience* 36.7, pp. 2949–2963 (cit. on p. 34).

Charvet, Christine J, Diarmuid J Cahalane and Barbara L Finlay (2015). „Systematic, cross-cortex variation in neuron numbers in rodents and primates“. In: *Cerebral Cortex* 25.1, pp. 147–160 (cit. on p. 7).

Che, Alicia, Rachel Babij, Andrew F Iannone, Robert N Fetcho, Monica Ferrer et al. (2018). „Layer I interneurons sharpen sensory maps during neonatal development“. In: *Neuron* 99.1, pp. 98–116 (cit. on pp. 12, 30, 91, 151).

Che, Alicia and Natalia V De Marco García (2021). „An in vivo Calcium Imaging Approach for the Identification of Cell-Type Specific Patterns in the Developing Cortex“. In: *Frontiers in Neural Circuits*, p. 102 (cit. on p. 89).

Chen, Jerry L, Walter C Lin, Jae Won Cha, Peter T So, Yoshiyuki Kubota et al. (2011). „Structural basis for the role of inhibition in facilitating adult brain plasticity“. In: *Nature neuroscience* 14.5, pp. 587–594 (cit. on p. 26).

Chen, Qian, Joseph Cichon, Wenting Wang, Li Qiu, Seok-Jin R Lee et al. (2012). „Imaging neural activity using Thy1-GCaMP transgenic mice“. In: *Neuron* 76.2, pp. 297–308 (cit. on p. 83).

Chen, Spencer Chin-Yu, Giacomo Benvenuti, Yuzhi Chen, Satwant Kumar, Charu Ramakrishnan et al. (2022). „Similar neural and perceptual masking effects of low-power optogenetic stimulation in primate V1“. In: *Elife* 11, e68393 (cit. on p. 40).

Chen, Tsai-Wen, Trevor J Wardill, Yi Sun, Stefan R Pulver, Sabine L Renninger et al. (2013). „Ultrasensitive fluorescent proteins for imaging neuronal activity“. In: *Nature* 499.7458, pp. 295–300 (cit. on p. 89).

Chew, Katherine CM, Vineet Kumar and Andrew YY Tan (2022). „Different Excitation–Inhibition Correlations Between Spontaneous and Tone-evoked Activity in Primary Auditory Cortex Neurons“. In: *Neuroscience* 496, pp. 205–218 (cit. on p. 143).

Cheyne, Juliette E, Nawal Zabouri, David Baddeley and Christian Lohmann (2019). „Spontaneous activity patterns are altered in the developing visual cortex of the Fmr1 knockout mouse“. In: *Frontiers in Neural Circuits* 13, p. 57 (cit. on p. 17).

Chialvo, Dante R (2010). „Emergent complex neural dynamics“. In: *Nature physics* 6.10, pp. 744–750 (cit. on p. 1).

Chini, Mattia, Sabine Gretenkord, Johanna K Kostka, Jastyn A Pöpplau, Laura Cornelissen et al. (2019). „Neural correlates of anesthesia in newborn mice and humans“. In: *Frontiers in neural circuits*, p. 38 (cit. on pp. 13, 16).

Chini, Mattia, Thomas Pfeffer and Ileana Hanganu-Opatz (2022). „An increase of inhibition drives the developmental decorrelation of neural activity“. In: *ELife* 11, e78811 (cit. on pp. 2, 18, 30, 128, 144, 153).

Chipaux, Mathilde, Matthew T Colonnese, Audrey Mauguen, Laure Fellous, Mostafa Mokhtari et al. (2013). „Auditory stimuli mimicking ambient sounds drive temporal “delta-brushes” in premature infants“. In: *PloS one* 8.11, e79028 (cit. on p. 16).

Chittajallu, Ramesh and John TR Isaac (2010). „Emergence of cortical inhibition by coordinated sensory-driven plasticity at distinct synaptic loci“. In: *Nature neuroscience* 13.10, pp. 1240–1248 (cit. on pp. 11, 18, 25).

Choleris, E, AW Thomas, M Kavaliers and FS Prato (2001). „A detailed ethological analysis of the mouse open field test: effects of diazepam, chlordiazepoxide and an extremely low frequency pulsed magnetic field“. In: *Neuroscience & Biobehavioral Reviews* 25.3, pp. 235–260 (cit. on p. 81).

Christenson Wick, Zoé, Madison R Tetzlaff and Esther Krook-Magnuson (2019). „Novel long-range inhibitory nNOS-expressing hippocampal cells“. In: *Elife* 8, e46816 (cit. on pp. 11, 154).

Chudotvorova, Ilona, Anton Ivanov, Sylvain Rama, Christian A Hübner, Christophe Pellegrino et al. (2005). „Early expression of KCC2 in rat hippocampal cultures augments expression of functional GABA synapses“. In: *The Journal of physiology* 566.3, pp. 671–679 (cit. on p. 30).

Chun, Sungkun, Ildar T Bayazitov, Jay A Blundon and Stanislav S Zakharenko (2013). „Thalamocortical long-term potentiation becomes gated after the early critical period in the auditory cortex“. In: *Journal of Neuroscience* 33.17, pp. 7345–7357 (cit. on pp. 24, 25).

Churchland, Mark M, John P Cunningham, Matthew T Kaufman, Justin D Foster, Paul Nuyujukian et al. (2012). „Neural population dynamics during reaching“. In: *Nature* 487.7405, pp. 51–56 (cit. on p. 40).

Cirelli, Chiara and Giulio Tononi (2015). „Cortical development, electroencephalogram rhythms, and the sleep/wake cycle“. In: *Biological psychiatry* 77.12, pp. 1071–1078 (cit. on p. 16).

Cisneros-Franco, J Miguel and Étienne de Villers-Sidani (2019). „Reactivation of critical period plasticity in adult auditory cortex through chemogenetic silencing of parvalbumin-positive interneurons“. In: *Proceedings of the National Academy of Sciences* 116.52, pp. 26329–26331 (cit. on p. 26).

Clancy, Barbara, Barbara L Finlay, Richard B Darlington and KJS Anand (2007). „Extrapolating brain development from experimental species to humans“. In: *Neurotoxicology* 28.5, pp. 931–937 (cit. on p. 19).

Clancy, Kelly B and Thomas D Mrsic-Flogel (2021). „The sensory representation of causally controlled objects“. In: *Neuron* 109.4, pp. 677–689 (cit. on p. 38).

Clancy, Kelly B, Ivana Orsolic and Thomas D Mrsic-Flogel (2019). „Locomotion-dependent remapping of distributed cortical networks“. In: *Nature neuroscience* 22.5, pp. 778–786 (cit. on pp. 35, 38).

Clough, Mitchell, Ichun Anderson Chen, Seong-Wook Park, Allison M Ahrens, Jeffrey N Stirman et al. (2021). „Flexible simultaneous mesoscale two-photon imaging of neural activity at high speeds“. In: *Nature Communications* 12.1, p. 6638 (cit. on p. 38).

Collignon, Olivier, Patrice Voss, Maryse Lassonde and Franco Lepore (2009). „Cross-modal plasticity for the spatial processing of sounds in visually deprived subjects“. In: *Experimental brain research* 192, pp. 343–358 (cit. on p. 34).

Colonnese, Matthew and Rustem Khazipov (2012). „Spontaneous activity in developing sensory circuits: implications for resting state fMRI“. In: *Neuroimage* 62.4, pp. 2212–2221 (cit. on p. 92).

Colonnese, Matthew T (2014). „Rapid developmental emergence of stable depolarization during wakefulness by inhibitory balancing of cortical network excitability“. In: *Journal of Neuroscience* 34.16, pp. 5477–5485 (cit. on pp. 77, 78, 88, 111, 141).

Colonnese, Matthew T, Anna Kaminska, Marat Minlebaev, Mathieu Milh, Bernard Bloem et al. (2010). „A conserved switch in sensory processing prepares developing neocortex for vision“. In: *Neuron* 67.3, pp. 480–498 (cit. on pp. 13, 16, 18, 77, 78, 88, 92, 111, 141, 144, 152).

Colonnese, Matthew T and Marnie A Phillips (2018). „Thalamocortical function in developing sensory circuits“. In: *Current opinion in neurobiology* 52, pp. 72–79 (cit. on pp. 12, 15).

Condé, Françoise, Jennifer S Lund and David A Lewis (1996). „The hierarchical development of monkey visual cortical regions as revealed by the maturation of parvalbumin-immunoreactive neurons“. In: *Developmental brain research* 96.1-2, pp. 261–276 (cit. on p. 25).

Corlew, Rebekah, Martha M Bosma and William J Moody (2004). „Spontaneous, synchronous electrical activity in neonatal mouse cortical neurones“. In: *The Journal of physiology* 560.2, pp. 377–390 (cit. on p. 17).

Costa, Marcos R and Ulrich Müller (2015). „Specification of excitatory neurons in the developing cerebral cortex: progenitor diversity and environmental influences“. In: *Frontiers in cellular neuroscience* 8, p. 449 (cit. on p. 4).

Coulson, Bramwell, Iain Hunter, Sarah Doran, Jill Parkin, Matthias Landgraf et al. (2022). „Critical periods in Drosophila neural network development: Importance to network tuning and therapeutic potential“. In: *Frontiers in Physiology* 13, p. 2566 (cit. on p. 21).

Couto, Joao, Simon Musall, Xiaonan R Sun, Anup Khanal, Steven Gluf et al. (2021). „Chronic, cortex-wide imaging of specific cell populations during behavior“. In: *Nature protocols* 16.7, pp. 3241–3263 (cit. on pp. 40, 43, 61, 71).

Crair, Michael C and Robert C Malenka (1995). „A critical period for long-term potentiation at thalamocortical synapses“. In: *Nature* 375.6529, pp. 325–328 (cit. on pp. 22, 24).

Cramer, Samuel W, Russell E Carter, Justin D Aronson, Suhasa B Kodandaramaiah, Timothy J Ebner et al. (2021). „Through the looking glass: A review of cranial window technology for optical access to the brain“. In: *Journal of neuroscience methods* 354, p. 109100 (cit. on p. 41).

Cross, Christine (2018). „Postnatal Development of Neural Networks in the Healthy and Premature Brain“. PhD thesis. University of Bristol (cit. on pp. 75, 78).

Cross, Christine M, Laura Mediavilla Santos, Nick Whiteley, Karen Luyt and Michael C Ashby (2021). „Early functional connectivity in the developing sensorimotor network that is independent of sensory experience“. In: *bioRxiv*, pp. 2021–06 (cit. on pp. 1, 35, 50, 106, 141, 149, 155).

Crowley, David E and Marie C Hepp-Reymond (1966). „Development of cochlear function in the ear of the infant rat.“ In: *Journal of comparative and physiological psychology* 62.3, p. 427 (cit. on p. 15).

Cruz-Martin, Alberto and Carlos Portera-Cailliau (2014). „In vivo imaging of axonal and dendritic structures in neonatal mouse cortex“. In: *Cold Spring Harbor Protocols* 2014.1, pdb–prot080150 (cit. on p. 50).

Cunningham, John P and Byron M Yu (2014). „Dimensionality reduction for large-scale neural recordings“. In: *Nature neuroscience* 17.11, pp. 1500–1509 (cit. on pp. 39, 86).

Daigle, Tanya L, Linda Madisen, Travis A Hage, Matthew T Valley, Ulf Knoblich et al. (2018). „A suite of transgenic driver and reporter mouse lines with enhanced brain-cell-type targeting and functionality“. In: *Cell* 174.2, pp. 465–480 (cit. on pp. 41, 42, 75, 87).

Dana, Hod, Boaz Mohar, Yi Sun, Sujatha Narayan, Andrew Gordus et al. (2016). „Sensitive red protein calcium indicators for imaging neural activity“. In: *elife* 5, e12727 (cit. on pp. 41, 46, 67, 87, 89, 96, 144).

Dana, Hod, Ondrej Novak, Michael Guardado-Montesino, James W Fransen, Amy Hu et al. (2018). „Thy1 transgenic mice expressing the red fluorescent calcium indicator jRGECO1a for neuronal population imaging in vivo“. In: *PloS one* 13.10, e0205444 (cit. on pp. 41, 52, 83, 87, 96).

Dani, Vardhan S, Qiang Chang, Arianna Maffei, Gina G Turrigiano, Rudolf Jaenisch et al. (2005). „Reduced cortical activity due to a shift in the balance between excitation and inhibition in a mouse model of Rett syndrome“. In: *Proceedings of the National Academy of Sciences* 102.35, pp. 12560–12565 (cit. on p. 26).

Daw, Michael I, Michael C Ashby and John TR Isaac (2007). „Coordinated developmental recruitment of latent fast spiking interneurons in layer IV barrel cortex“. In: *Nature neuroscience* 10.4, pp. 453–461 (cit. on pp. 11, 18, 124, 152).

De Marco García, Natalia V, Rashi Priya, Sebnem N Tuncdemir, Gord Fishell and Theofanis Karayannis (2015). „Sensory inputs control the integration of neurogliaform interneurons into cortical circuits“. In: *Nature neuroscience* 18.3, pp. 393–401 (cit. on p. 12).

Dehghani, Nima, Adrien Peyrache, Bartosz Telenczuk, Michel Le Van Quyen, Eric Halgren et al. (2016). „Dynamic balance of excitation and inhibition in human and monkey neocortex“. In: *Scientific reports* 6.1, pp. 1–12 (cit. on pp. 132, 143).

Dehorter, Nathalie, Nicolás Marichal, Oscar Marín and Benedikt Berninger (2017). „Tuning neural circuits by turning the interneuron knob“. In: *Current opinion in neurobiology* 42, pp. 144–151 (cit. on pp. 11, 152, 153).

Dehorter, Nathalie, Laurent Vinay, Constance Hammond and Yehezkel Ben-Ari (2012). „Timing of developmental sequences in different brain structures: physiological and pathological implications“. In: *European Journal of Neuroscience* 35.12, pp. 1846–1856 (cit. on pp. 2, 94, 119, 150, 152, 154).

Deidda, Gabriele, Manuela Allegra, Chiara Cerri, Shovan Naskar, Guillaume Bony et al. (2015a). „Early depolarizing GABA controls critical-period plasticity in the rat visual cortex“. In: *Nature neuroscience* 18.1, pp. 87–96 (cit. on pp. 31, 94).

Deidda, Gabriele, Martina Parrini, Shovan Naskar, Ignacio F Bozarth, Andrea Contestabile et al. (2015b). „Reversing excitatory GABAAR signaling restores synaptic plasticity and memory in a mouse model of Down syndrome“. In: *Nature medicine* 21.4, pp. 318–326 (cit. on p. 31).

Delaney, Thomas J and Cian O'Donnell (2023). „Fast-local and slow-global neural ensembles in the mouse brain“. In: *Network Neuroscience*, pp. 1–12 (cit. on pp. 132, 142).

Deliolanis, Nikolaos C, Thomas Wurdinger, Lisa Pike, Bakhos A Tannous, Xandra O Breakefield et al. (2011). „In vivo tomographic imaging of red-shifted fluorescent proteins“. In: *Biomedical optics express* 2.4, pp. 887–900 (cit. on p. 46).

Deng, Weihong, Yebin Liu, Jiani Hu and Jun Guo (2012). „The small sample size problem of ICA: A comparative study and analysis“. In: *Pattern Recognition* 45.12, pp. 4438–4450 (cit. on pp. 54, 57).

Destexhe, Alain, Michael Rudolph and Denis Paré (2003). „The high-conductance state of neocortical neurons in vivo“. In: *Nature reviews neuroscience* 4.9, pp. 739–751 (cit. on p. 28).

Detmar, Jacqui, Isidora Rovic, Jocelyn Ray, Isabella Caniggia and Andrea Jurisicova (2019). „Placental cell death patterns exhibit differences throughout gestation in two strains of laboratory mice“. In: *Cell and tissue research* 378, pp. 341–358 (cit. on p. 140).

Di Bella, Daniela J, Ehsan Habibi, Sun-Ming Yang, Robert R Stickels, Juliana Brown et al. (2020). „Molecular logic of cellular diversification in the mammalian cerebral cortex“. In: *BioRxiv*, pp. 2020–07 (cit. on p. 4).

Ding, Song-Lin, Joshua J Royall, Susan M Sunkin, Lydia Ng, Benjamin AC Facer et al. (2016). „Comprehensive cellular-resolution atlas of the adult human brain“. In: *Journal of Comparative Neurology* 524.16, pp. 3127–3481 (cit. on p. 6).

Donaldson, Preston D, Zahra S Navabi, Russell E Carter, Skylar ML Fausner, Leila Ghanbari et al. (2022). „Polymer Skulls With Integrated Transparent Electrode Arrays for Cortex-Wide Opto-Electrophysiological Recordings“. In: *Advanced Healthcare Materials* 11.18, p. 2200626 (cit. on p. 140).

Donato, Flavio, Santiago Belluco Rompani and Pico Caroni (2013). „Parvalbumin-expressing basket-cell network plasticity induced by experience regulates adult learning“. In: *Nature* 504.7479, pp. 272–276 (cit. on p. 117).

Dong, Hao-Ming, Daniel S Margulies, Xi-Nian Zuo and Avram J Holmes (2021). „Shifting gradients of macroscale cortical organization mark the transition from childhood to adolescence“. In: *Proceedings of the National Academy of Sciences* 118.28, e2024448118 (cit. on p. 20).

Dong, Yufan, Jiaqi Li, Min Zhou, Yihui Du and Danqian Liu (2022). „Cortical regulation of two-stage rapid eye movement sleep“. In: *Nature Neuroscience*, pp. 1–8 (cit. on pp. 15, 146).

Dooley, James C and Mark S Blumberg (2018). „Developmental'awakening'of primary motor cortex to the sensory consequences of movement“. In: *elife* 7, e41841 (cit. on pp. 14, 117, 150).

Dooley, James C, Greta Sokoloff and Mark S Blumberg (2019). „Behavioral states modulate sensory processing in early development“. In: *Current sleep medicine reports* 5, pp. 112–117 (cit. on pp. 13, 14, 119, 145).

– (2021). „Movements during sleep reveal the developmental emergence of a cerebellar-dependent internal model in motor thalamus“. In: *Current biology* 31.24, pp. 5501–5511 (cit. on p. 150).

Dorrn, Anja L, Kexin Yuan, Alison J Barker, Christoph E Schreiner and Robert C Froemke (2010). „Developmental sensory experience balances cortical excitation and inhibition“. In: *Nature* 465.7300, pp. 932–936 (cit. on pp. 16, 19, 128, 141, 143).

Douglas, Rodney J and Kevan AC Martin (2004). „Neuronal circuits of the neocortex“. In: *Annu. Rev. Neurosci.* 27, pp. 419–451 (cit. on p. 3).

Doupe, Allison J and Patricia K Kuhl (1999). „Birdsong and human speech: common themes and mechanisms“. In: *Annual review of neuroscience* 22.1, pp. 567–631 (cit. on p. 21).

Driscoll, Nicolette, Richard E Rosch, Brendan B Murphy, Arian Ashourvan, Ramya Vishnubhotla et al. (2021). „Multimodal in vivo recording using transparent graphene microelectrodes illuminates spatiotemporal seizure dynamics at the microscale“. In: *Communications Biology* 4.1, p. 136 (cit. on p. 140).

Duan, Zhe Ran S, Alicia Che, Philip Chu, Laura Modol, Yannick Bollmann et al. (2020). „GABAergic restriction of network dynamics regulates interneuron survival in the developing cortex“. In: *Neuron* 105.1, pp. 75–92 (cit. on pp. 10, 36, 91, 94, 95, 156).

Dzhala, Volodymyr I, Delia M Talos, Dan A Sdrulla, Audrey C Brumback, Gregory C Mathews et al. (2005). „NKCC1 transporter facilitates seizures in the developing brain“. In: *Nature medicine* 11.11, pp. 1205–1213 (cit. on p. 20).

Egawa, Kiyoshi and Atsuo Fukuda (2013). „Pathophysiological power of improper tonic GABAA conductances in mature and immature models“. In: *Frontiers in neural circuits* 7, p. 170 (cit. on p. 28).

El-Boustani, Sami, B Semihcan Sermet, Georgios Foustoukos, Tess B Oram, Ofer Yizhar et al. (2020). „Anatomically and functionally distinct thalamocortical inputs to primary and secondary mouse whisker somatosensory cortices“. In: *Nature communications* 11.1, p. 3342 (cit. on p. 8).

Elgueta, Claudio and Marlene Bartos (2019). „Dendritic inhibition differentially regulates excitability of dentate gyrus parvalbumin-expressing interneurons and granule cells“. In: *Nature communications* 10.1, p. 5561 (cit. on p. 31).

Elsayed, Gamaleldin F and John P Cunningham (2017). „Structure in neural population recordings: an expected byproduct of simpler phenomena?“ In: *Nature neuroscience* 20.9, pp. 1310–1318 (cit. on p. 35).

Erisir, Alev and Janna L Harris (2003). „Decline of the critical period of visual plasticity is concurrent with the reduction of NR2B subunit of the synaptic NMDA receptor in layer 4“. In: *Journal of Neuroscience* 23.12, pp. 5208–5218 (cit. on p. 24).

Erzurumlu, Reha S and Patricia Gaspar (2012). „Development and critical period plasticity of the barrel cortex“. In: *European Journal of Neuroscience* 35.10, pp. 1540–1553 (cit. on p. 22).

Esmaeili, Vahid, Anastasiia Oryshchuk, Reza Asri, Keita Tamura, Georgios Foustoukos et al. (2022). „Learning-related congruent and incongruent changes of excitation and inhibition in distinct cortical areas“. In: *PLoS Biology* 20.5, e3001667 (cit. on pp. 143, 152).

Espinosa, J Sebastian and Michael P Stryker (2012). „Development and plasticity of the primary visual cortex“. In: *Neuron* 75.2, pp. 230–249 (cit. on p. 15).

Esposito, Fabrizio, Tommaso Scarabino, Aapo Hyvarinen, Johan Himberg, Elia Formisano et al. (2005). „Independent component analysis of fMRI group studies by self-organizing clustering“. In: *Neuroimage* 25.1, pp. 193–205 (cit. on p. 145).

Fagiolini, Michela and Takao K Hensch (2000). „Inhibitory threshold for critical-period activation in primary visual cortex“. In: *Nature* 404.6774, pp. 183–186 (cit. on pp. 26, 94).

Failor, Samuel, Vien Nguyen, Daniel P Darcy, Jianhua Cang, Michael F Wendland et al. (2010). „Neonatal cerebral hypoxia–ischemia impairs plasticity in rat visual cortex“. In: *Journal of Neuroscience* 30.1, pp. 81–92 (cit. on p. 21).

Fair, Damien A, Alexander L Cohen, Jonathan D Power, Nico UF Dosenbach, Jessica A Church et al. (2009). „Functional brain networks develop from a “local to distributed” organization“. In: *PLoS computational biology* 5.5, e1000381 (cit. on p. 2).

Faux, Clare, Sonja Rakic, William Andrews and Joanne M Britto (2012). „Neurons on the move: migration and lamination of cortical interneurons“. In: *Neurosignals* 20.3, pp. 168–189 (cit. on pp. 5, 6).

Feese, Berquin D, Diego E Pafundo, Meredith N Schmehl and Sandra J Kuhlman (2018). „Binocular deprivation induces both age-dependent and age-independent forms of plasticity in parvalbumin inhibitory neuron visual response properties“. In: *Journal of neurophysiology* 119.2, pp. 738–751 (cit. on p. 25).

Felch, Daniel L, Arseny S Khakhalin and Carlos D Aizenman (2016). „Multisensory integration in the developing tectum is constrained by the balance of excitation and inhibition“. In: *Elife* 5, e15600 (cit. on p. 157).

Feldman, Daniel E (2009). „Synaptic mechanisms for plasticity in neocortex“. In: *Annual review of neuroscience* 32, pp. 33–55 (cit. on p. 23).

Feldman, Daniel E, Michael S Brainard and Eric I Knudsen (1996). „Newly learned auditory responses mediated by NMDA receptors in the owl inferior colliculus“. In: *Science* 271.5248, pp. 525–528 (cit. on p. 24).

Feldman, Daniel E and Michael Brecht (2005). „Map plasticity in somatosensory cortex“. In: *Science* 310.5749, pp. 810–815 (cit. on pp. 8, 23).

Feldman, DE, RA Nicoll and RC Malenka (1999). „Synaptic plasticity at thalamocortical synapses in developing rat somatosensory cortex: LTP, LTD, and silent synapses“. In: *Journal of neurobiology* 41.1, pp. 92–101 (cit. on p. 23).

Feng, Guoping, Rebecca H Mellor, Michael Bernstein, Cynthia Keller-Peck, Quyen T Nguyen et al. (2000). „Imaging neuronal subsets in transgenic mice expressing multiple spectral variants of GFP“. In: *Neuron* 28.1, pp. 41–51 (cit. on p. 83).

Ferezou, Isabelle and Thomas Deneux (2017). „How do spontaneous and sensory-evoked activities interact?“ In: *Neurophotonics* 4.3, pp. 031221–031221 (cit. on p. 155).

Ferezou, Isabelle, Florent Haiss, Luc J Gentet, Rachel Aronoff, Bruno Weber et al. (2007). „Spatiotemporal dynamics of cortical sensorimotor integration in behaving mice“. In: *Neuron* 56.5, pp. 907–923 (cit. on p. 35).

Fino, Elodie and Rafael Yuste (2011). „Dense inhibitory connectivity in neocortex“. In: *Neuron* 69.6, pp. 1188–1203 (cit. on p. 3).

Fiumelli, Hubert, Laura Cancedda and Mu-ming Poo (2005). „Modulation of GABAergic transmission by activity via postsynaptic Ca2+-dependent regulation of KCC2 function“. In: *Neuron* 48.5, pp. 773–786 (cit. on p. 27).

Florio, Marta and Wieland B Huttner (2014). „Neural progenitors, neurogenesis and the evolution of the neocortex“. In: *Development* 141.11, pp. 2182–2194 (cit. on p. 3).

Flossmann, Tom, Thomas Kaas, Vahid Rahmati, Stefan J Kiebel, Otto W Witte et al. (2019). „Somatostatin interneurons promote neuronal synchrony in the neonatal hippocampus“. In: *Cell reports* 26.12, pp. 3173–3182 (cit. on p. 29).

Foeller, Elisabeth, Tansu Celikel and Daniel E Feldman (2005). „Inhibitory sharpening of receptive fields contributes to whisker map plasticity in rat somatosensory cortex“. In: *Journal of neurophysiology* 94.6, pp. 4387–4400 (cit. on p. 151).

Fogarty, Matthew, Matthew Grist, Diego Gelman, Oscar Marín, Vassilis Pachnis et al. (2007). „Spatial genetic patterning of the embryonic neuroepithelium generates GABAergic interneuron diversity in the adult cortex“. In: *Journal of Neuroscience* 27.41, pp. 10935–10946 (cit. on p. 5).

Fox, Kevin, Bradley L Schlaggar, Stanislaw Glazewski and DD O'leary (1996). „Glutamate receptor blockade at cortical synapses disrupts development of thalamocortical and columnar organization in somatosensory cortex." In: *Proceedings of the National Academy of Sciences* 93.11, pp. 5584–5589 (cit. on p. 23).

Frye, Charles G and Jason N MacLean (2016). „Spontaneous activations follow a common developmental course across primary sensory areas in mouse neocortex". In: *Journal of neurophysiology* 116.2, pp. 431–437 (cit. on pp. 94, 150).

Fu, Yu, Jason M Tucciarone, J Sebastian Espinosa, Nengyin Sheng, Daniel P Darcy et al. (2014). „A cortical circuit for gain control by behavioral state". In: *Cell* 156.6, pp. 1139–1152 (cit. on p. 15).

Fusi, Stefano, Earl K Miller and Mattia Rigotti (2016). „Why neurons mix: high dimensionality for higher cognition". In: *Current opinion in neurobiology* 37, pp. 66–74 (cit. on p. 40).

Gabernet, Laetitia, Shantanu P Jadhav, Daniel E Feldman, Matteo Carandini and Massimo Scanziani (2005). „Somatosensory integration controlled by dynamic thalamocortical feed-forward inhibition". In: *Neuron* 48.2, pp. 315–327 (cit. on p. 11).

Gallero-Salas, Yasir, Shuting Han, Yaroslav Sych, Fabian F Voigt, Balazs Laurenczy et al. (2021). „Sensory and behavioral components of neocortical signal flow in discrimination tasks with short-term memory". In: *Neuron* 109.1, pp. 135–148 (cit. on p. 145).

Ganguly, Karunesh, Alejandro F Schinder, Scott T Wong and Mu-ming Poo (2001). „GABA itself promotes the developmental switch of neuronal GABAergic responses from excitation to inhibition". In: *Cell* 105.4, pp. 521–532 (cit. on p. 27).

Garaschuk, Olga, Jennifer Linn, Jens Eilers and Arthur Konnerth (2000). „Large-scale oscillatory calcium waves in the immature cortex". In: *Nature neuroscience* 3.5, pp. 452–459 (cit. on p. 30).

Georgopoulos, AP, JF Kalaska, R Caminiti and JT Massey (1983). „Interruption of motor cortical discharge subserving aimed arm movements". In: *Experimental Brain Research* 49.3, pp. 327–340 (cit. on p. 34).

Gerfen, Charles R, Michael N Economo and Jayaram Chandrashekar (2018). „Long distance projections of cortical pyramidal neurons". In: *Journal of neuroscience research* 96.9, pp. 1467–1475 (cit. on p. 83).

Ghanbari, Leila, Mathew L Rynes, Jia Hu, Daniel S Schulman, Gregory W Johnson et al. (2019). „Craniobot: A computer numerical controlled robot for cranial microsurgeries". In: *Scientific reports* 9.1, p. 1023 (cit. on pp. 63, 65).

Ghosh, Anirvan, Antonella Antonini, Susan K McConnell and Carla J Shatz (1990). „Requirement for subplate neurons in the formation of thalamocortical connections". In: *Nature* 347.6289, pp. 179–181 (cit. on p. 8).

Ghosh, Anirvan and Carla J Shatz (1993). „A role for subplate neurons in the patterning of connections from thalamus to neocortex". In: *Development* 117.3, pp. 1031–1047 (cit. on p. 8).

Ghosh, Kunal K, Laurie D Burns, Eric D Cocker, Axel Nimmerjahn, Yaniv Ziv et al. (2011). „Miniaturized integration of a fluorescence microscope". In: *Nature methods* 8.10, pp. 871–878 (cit. on p. 37).

Giannakakis, Emmanouil, Oleg Vinogradov, Victor Buendia and Anna Levina (2023). „Recurrent connectivity structure controls the emergence of co-tuned excitation and inhibition". In: *bioRxiv*, pp. 2023–02 (cit. on p. 143).

Gilad, Ariel and Fritjof Helmchen (2020). „Spatiotemporal refinement of signal flow through association cortex during learning". In: *Nature communications* 11.1, p. 1744 (cit. on pp. 35, 36).

Glaser, Joshua, Matthew Whiteway, John P Cunningham, Liam Paninski and Scott Linderman (2020). „Recurrent switching dynamical systems models for multiple interacting neural populations“. In: *Advances in neural information processing systems* 33, pp. 14867–14878 (cit. on p. 39).

Goel, Anubhuthi, Bin Jiang, Linda W Xu, Lihua Song, Alfredo Kirkwood et al. (2006). „Cross-modal regulation of synaptic AMPA receptors in primary sensory cortices by visual experience“. In: *Nature neuroscience* 9.8, pp. 1001–1003 (cit. on p. 24).

Golovin, Randall M, Jacob Vest, Dominic J Vita and Kendal Broadie (2019). „Activity-dependent remodeling of Drosophila olfactory sensory neuron brain innervation during an early-life critical period“. In: *Journal of Neuroscience* 39.16, pp. 2995–3012 (cit. on p. 21).

Golshani, Peyman, J Tiago Gonçalves, Sattar Khoshkhoo, Ricardo Mostany, Stelios Smirnakis et al. (2009). „Internally mediated developmental desynchronization of neocortical network activity“. In: *Journal of Neuroscience* 29.35, pp. 10890–10899 (cit. on pp. 2, 18, 92, 142, 144).

Gómez, Lex J, James C Dooley, Greta Sokoloff and Mark S Blumberg (2021). „Parallel and serial sensory processing in developing primary somatosensory and motor cortex“. In: *Journal of Neuroscience* 41.15, pp. 3418–3431 (cit. on pp. 146, 150).

Gonçalves, J Tiago, James E Anstey, Peyman Golshani and Carlos Portera-Cailliau (2013). „Circuit level defects in the developing neocortex of Fragile X mice“. In: *Nature neuroscience* 16.7, pp. 903–909 (cit. on p. 17).

Gonchar, Yuri and Andreas Burkhalter (1997). „Three distinct families of GABAergic neurons in rat visual cortex.“ In: *Cerebral cortex (New York, NY: 1991)* 7.4, pp. 347–358 (cit. on p. 6).

Graf, Jürgen, Chuanqiang Zhang, Stephan Lawrence Marguet, Tanja Herrmann, Tom Flossmann et al. (2021). „A limited role of NKCC1 in telencephalic glutamatergic neurons for developing hippocampal network dynamics and behavior“. In: *Proceedings of the National Academy of Sciences* 118.14, e2014784118 (cit. on pp. 27, 29, 30).

Grant, Eleanor, Anna Hoerder-Suabedissen and Zoltán Molnár (2016). „The regulation of corticofugal fiber targeting by retinal inputs“. In: *Cerebral Cortex* 26.3, pp. 1336–1348 (cit. on p. 8).

Greene, Abigail S, Corey Horien, Daniel Barson, Dustin Scheinost and R Todd Constable (2023). „Why is everyone talking about brain state?“ In: *Trends in Neurosciences* (cit. on p. 13).

Greig, Luciano Custo, Mollie B Woodworth, Maria J Galazo, Hari Padmanabhan and Jeffrey D Macklis (2013). „Molecular logic of neocortical projection neuron specification, development and diversity“. In: *Nature Reviews Neuroscience* 14.11, pp. 755–769 (cit. on pp. 4, 5, 9).

Gribizis, Alexandra, Xinxin Ge, Tanya L Daigle, James B Ackman, Hongkui Zeng et al. (2019). „Visual cortex gains independence from peripheral drive before eye opening“. In: *Neuron* 104.4, pp. 711–723 (cit. on pp. 1, 16, 17, 19, 36, 92, 141).

Griffen, Trevor C, Lang Wang, Alfredo Fontanini and Arianna Maffei (2013). „Developmental regulation of spatio-temporal patterns of cortical circuit activation“. In: *Frontiers in cellular neuroscience* 6, p. 65 (cit. on p. 140).

Griguoli, Marilena and Enrico Cherubini (2017). „Early correlated network activity in the hippocampus: its putative role in shaping neuronal circuits“. In: *Frontiers in cellular neuroscience* 11, p. 255 (cit. on p. 91).

Gu, Xiaonan and Nicholas C Spitzer (1997). „Breaking the code: regulation of neuronal differentiation by spontaneous calcium transients“. In: *Developmental neuroscience* 19.1, pp. 33–41 (cit. on p. 15).

Gu, Yameng, Lucas E Sainburg, Sizhe Kuang, Feng Han, Jack W Williams et al. (2021). „Brain activity fluctuations propagate as waves traversing the cortical hierarchy“. In: *Cerebral cortex* 31.9, pp. 3986–4005 (cit. on p. 20).

Guizar-Sicairos, Manuel, Samuel T Thurman and James R Fienup (2008). „Efficient subpixel image registration algorithms“. In: *Optics letters* 33.2, pp. 156–158 (cit. on p. 52).

Guy, Julien and Jochen F Staiger (2017). „The functioning of a cortex without layers“. In: *Frontiers in neuroanatomy* 11, p. 54 (cit. on p. 6).

Haery, Leila, Benjamin E Deverman, Katherine S Matho, Ali Cetin, Kenton Woodard et al. (2019). „Adeno-associated virus technologies and methods for targeted neuronal manipulation“. In: *Frontiers in Neuroanatomy*, p. 93 (cit. on p. 42).

Hafner, Georg, Mirko Witte, Julien Guy, Nidhi Subhashini, Lief E Fenno et al. (2019). „Mapping brain-wide afferent inputs of parvalbumin-expressing GABAergic neurons in barrel cortex reveals local and long-range circuit motifs“. In: *Cell reports* 28.13, pp. 3450–3461 (cit. on p. 36).

Haider, Bilal, Alvaro Duque, Andrea R Hasenstaub and David A McCormick (2006). „Neocortical network activity in vivo is generated through a dynamic balance of excitation and inhibition“. In: *Journal of Neuroscience* 26.17, pp. 4535–4545 (cit. on p. 142).

Hammelrath, Luam, Siniša Škokić, Artem Khmelinskii, Andreas Hess, Noortje van der Knaap et al. (2016). „Morphological maturation of the mouse brain: An in vivo MRI and histology investigation“. In: *Neuroimage* 125, pp. 144–152 (cit. on p. 64).

Hamodi, Ali S, Aude Martinez Sabino, N Dalton Fitzgerald, Dionysia Moschou and Michael C Crair (2020). „Transverse sinus injections drive robust whole-brain expression of transgenes“. In: *Elife* 9, e53639 (cit. on pp. 36, 42, 147).

Hanganu, Ileana L, Yehezkel Ben-Ari and Rustem Khazipov (2006). „Retinal waves trigger spindle bursts in the neonatal rat visual cortex“. In: *Journal of Neuroscience* 26.25, pp. 6728–6736 (cit. on pp. 17, 19).

Hanganu, Ileana L, Akihito Okabe, Volkmar Lessmann and Heiko J Luhmann (2009). „Cellular mechanisms of subplate-driven and cholinergic input-dependent network activity in the neonatal rat somatosensory cortex“. In: *Cerebral Cortex* 19.1, pp. 89–105 (cit. on p. 16).

Hanganu-Opatz, Ileana L (2010). „Between molecules and experience: role of early patterns of coordinated activity for the development of cortical maps and sensory abilities“. In: *Brain research reviews* 64.1, pp. 160–176 (cit. on p. 12).

Hanganu-Opatz, Ileana L, Simon JB Butt, Simon Hippenmeyer, Natalia V De Marco García, Jessica A Cardin et al. (2021). „The logic of developing neocortical circuits in health and disease“. In: *Journal of Neuroscience* 41.5, pp. 813–822 (cit. on p. 95).

Hanson, Meretta A and Jason C Wester (2022). „Advances in approaches to study cell-type specific cortical circuits throughout development“. In: *Frontiers in Cellular Neuroscience* (cit. on pp. 4, 82).

Harauzov, Alexey, Maria Spolidoro, Graziella DiCristo, Roberto De Pasquale, Laura Cancedda et al. (2010). „Reducing intracortical inhibition in the adult visual cortex promotes ocular dominance plasticity“. In: *Journal of Neuroscience* 30.1, pp. 361–371 (cit. on p. 26).

Harris, Julie A, Stefan Mihalas, Karla E Hirokawa, Jennifer D Whitesell, Hannah Choi et al. (2019). „Hierarchical organization of cortical and thalamic connectivity“. In: *Nature* 575.7781, pp. 195–202 (cit. on p. 20).

Harris, Kenneth D and Alexander Thiele (2011). „Cortical state and attention“. In: *Nature reviews neuroscience* 12.9, pp. 509–523 (cit. on p. 145).

He, Kaiwen, Emily Petrus, Nicholas Gammon and Hey-Kyoung Lee (2012). „Distinct sensory requirements for unimodal and cross-modal homeostatic synaptic plasticity“. In: *Journal of Neuroscience* 32.25, pp. 8469–8474 (cit. on p. 24).

He, Ling-jie, Nan Liu, Tian-lin Cheng, Xiao-jing Chen, Yi-ding Li et al. (2014). „Conditional deletion of Mecp2 in parvalbumin-expressing GABAergic cells results in the absence of critical period plasticity“. In: *Nature communications* 5.1, p. 5036 (cit. on p. 25).

He, Miao, Jason Tucciarone, SooHyun Lee, Maximiliano José Nigro, Yongsoo Kim et al. (2016). „Strategies and tools for combinatorial targeting of GABAergic neurons in mouse cerebral cortex“. In: *Neuron* 91.6, pp. 1228–1243 (cit. on p. 146).

He, Shuijin, Zhizhong Li, Shaoyu Ge, Yong-Chun Yu and Song-Hai Shi (2015). „Inside-out radial migration facilitates lineage-dependent neocortical microcircuit assembly“. In: *Neuron* 86.5, pp. 1159–1166 (cit. on p. 10).

Heck, Nicolas, Antje Golbs, Therese Riedemann, Jyh-Jang Sun, Volkmar Lessmann et al. (2008). „Activity-dependent regulation of neuronal apoptosis in neonatal mouse cerebral cortex“. In: *Cerebral cortex* 18.6, pp. 1335–1349 (cit. on p. 10).

Heimler, Benedetta and Amir Amedi (2020). „Are critical periods reversible in the adult brain? Insights on cortical specializations based on sensory deprivation studies“. In: *Neuroscience & Biobehavioral Reviews* 116, pp. 494–507 (cit. on p. 22).

Helassa, Nordine, Borbala Podor, Alan Fine and Katalin Török (2016). „Design and mechanistic insight into ultrafast calcium indicators for monitoring intracellular calcium dynamics“. In: *Scientific reports* 6.1, pp. 1–14 (cit. on pp. 89, 144).

Hellyer, Peter J, Barbara Jachs, Claudia Clopath and Robert Leech (2016). „Local inhibitory plasticity tunes macroscopic brain dynamics and allows the emergence of functional brain networks“. In: *NeuroImage* 124, pp. 85–95 (cit. on p. 153).

Hensch, Takao K (2003). „Controlling the critical period“. In: *Neuroscience research* 47.1, pp. 17–22 (cit. on p. 23).

– (2005). „Critical period plasticity in local cortical circuits“. In: *Nature Reviews Neuroscience* 6.11, pp. 877–888 (cit. on pp. 12, 21, 23, 94, 151–153).

Hensch, Takao K and Michela Fagiolini (2005). „Excitatory-inhibitory balance and critical period plasticity in developing visual cortex“. In: *Progress in brain research* 147, pp. 115–124 (cit. on p. 26).

Hensch, Takao K, Michela Fagiolini, Nobuko Mataga, Michael P Stryker, Steinunn Baekkeskov et al. (1998). „Local GABA circuit control of experience-dependent plasticity in developing visual cortex“. In: *Science* 282.5393, pp. 1504–1508 (cit. on p. 26).

Henschke, Julia U, Anja M Oelschlegel, Frank Angenstein, Frank W Ohl, Jürgen Goldschmidt et al. (2018). „Early sensory experience influences the development of multisensory thalamocortical and intracortical connections of primary sensory cortices“. In: *Brain Structure and Function* 223.3, pp. 1165–1190 (cit. on p. 157).

Heo, Chaejeong, Hyejin Park, Yong-Tae Kim, Eunha Baeg, Yong Ho Kim et al. (2016). „A soft, transparent, freely accessible cranial window for chronic imaging and electrophysiology“. In: *Scientific reports* 6.1, pp. 1–11 (cit. on p. 139).

Higashi, S, Z Molnár, T Kurotani and K Toyama (2002). „Prenatal development of neural excitation in rat thalamocortical projections studied by optical recording“. In: *Neuroscience* 115.4, pp. 1231–1246 (cit. on p. 17).

Higley, Michael J and Jessica A Cardin (2022). „Spatiotemporal dynamics in large-scale cortical networks“. In: *Current Opinion in Neurobiology* 77, p. 102627 (cit. on p. 34).

Hofer, Sonja B, Thomas D Mrsic-Flogel, Tobias Bonhoeffer and Mark Hübener (2006). „Prior experience enhances plasticity in adult visual cortex“. In: *Nature neuroscience* 9.1, pp. 127–132 (cit. on p. 22).

Hoffpauir, Brian K, Glen S Marrs, Peter H Mathers and George A Spirou (2009). „Does the brain connect before the periphery can direct?: A comparison of three sensory systems in mice“. In: *Brain research* 1277, pp. 115–129 (cit. on p. 15).

Holtmaat, Anthony, Linda Wilbrecht, Graham W Knott, Egbert Welker and Karel Svoboda (2006). „Experience-dependent and cell-type-specific spine growth in the neocortex“. In: *Nature* 441.7096, pp. 979–983 (cit. on p. 83).

Homma, Ryota, Bradley J Baker, Lei Jin, Olga Garaschuk, Arthur Konnerth et al. (2009). „Wide-field and two-photon imaging of brain activity with voltage and calcium-sensitive dyes“. In: *Dynamic Brain Imaging: Multi-Modal Methods and In Vivo Applications*, pp. 43–79 (cit. on p. 58).

Huang, Lawrence, Peter Ledochowitsch, Ulf Knoblich, Jérôme Lecoq, Gabe J Murphy et al. (2021). „Relationship between simultaneously recorded spiking activity and fluorescence signal in GCaMP6 transgenic mice“. In: *Elife* 10, e51675 (cit. on p. 89).

Huang, Z Josh, Alfredo Kirkwood, Tommaso Pizzorusso, Vittorio Porciatti, Bernardo Morales et al. (1999). „BDNF regulates the maturation of inhibition and the critical period of plasticity in mouse visual cortex“. In: *Cell* 98.6, pp. 739–755 (cit. on p. 25).

Hubatz, Sophie, Guillaume Hucher, Daniel E Shulz and Isabelle Férézou (2020). „Spatiotemporal properties of whisker-evoked tactile responses in the mouse secondary somatosensory cortex“. In: *Scientific reports* 10.1, pp. 1–11 (cit. on p. 35).

Hubel, David H and Torsten N Wiesel (1959). „Receptive fields of single neurones in the cat's striate cortex“. In: *The Journal of physiology* 148.3, p. 574 (cit. on p. 10).

Hui, Kelvin K, Thomas E Chater, Yukiko Goda and Motomasa Tanaka (2022). „How staying negative is good for the (adult) brain: Maintaining chloride homeostasis and the GABA-shift in neurological disorders“. In: *Frontiers in Molecular Neuroscience* 15 (cit. on p. 31).

Humphries, Mark D. (2020). „Strong and weak principles of neural dimension reduction“. In: *Neurons, Behavior, Data analysis, and Theory* (cit. on p. 40).

Hwang, Hun-Way, Yuhki Saito, Christopher Y Park, Nathalie E Blachère, Yoko Tajima et al. (2017). „cTag-PAPERCLIP reveals alternative polyadenylation promotes cell-type specific protein diversity and shifts Araf isoforms with microglia activation“. In: *Neuron* 95.6, pp. 1334–1349 (cit. on p. 96).

Hyvärinen, Aapo and Erkki Oja (2000). „Independent component analysis: algorithms and applications“. In: *Neural networks* 13.4-5, pp. 411–430 (cit. on p. 54).

Iannone, Andrew F and Natalia V De Marco García (2021). „The Emergence of Network Activity Patterns in the Somatosensory Cortex–an Early Window to Autism Spectrum Disorders“. In: *Neuroscience* 466, pp. 298–309 (cit. on pp. 2, 149).

Inan, Melis and Michael C Crair (2007). „Development of cortical maps: perspectives from the barrel cortex“. In: *The Neuroscientist* 13.1, pp. 49–61 (cit. on p. 8).

Innocenti, Giorgio M and David J Price (2005). „Exuberance in the development of cortical networks“. In: *Nature Reviews Neuroscience* 6.12, pp. 955–965 (cit. on p. 9).

Inta, Dragos, Julieta Alfonso, Jakob Von Engelhardt, Maria M Kreuzberg, Axel H Meyer et al. (2008). „Neurogenesis and widespread forebrain migration of distinct GABAergic neurons from the postnatal subventricular zone“. In: *Proceedings of the National Academy of Sciences* 105.52, pp. 20994–20999 (cit. on p. 6).

Isaacson, Jeffry S and Massimo Scanziani (2011). „How inhibition shapes cortical activity“. In: *Neuron* 72.2, pp. 231–243 (cit. on pp. 10, 143).

Isaev, Dmytro, Elena Isaeva, Rustem Khazipov and Gregory L Holmes (2005). „Anticonvulsant action of GABA in the high potassium–low magnesium model of ictogenesis in the neonatal rat hippocampus in vivo and in vitro“. In: *Journal of neurophysiology* 94.4, pp. 2987–2992 (cit. on p. 153).

Iwai, Youichi, Michela Fagiolini, Kunihiko Obata and Takao K Hensch (2003). „Rapid critical period induction by tonic inhibition in visual cortex“. In: *Journal of Neuroscience* 23.17, pp. 6695–6702 (cit. on p. 26).

Iwasato, Takuji, Akash Datwani, Alexander M Wolf, Hiroshi Nishiyama, Yusuke Taguchi et al. (2000). „Cortex-restricted disruption of NMDAR1 impairs neuronal patterns in the barrel cortex“. In: *Nature* 406.6797, pp. 726–731 (cit. on p. 24).

Iyer, Kartik K, James A Roberts, Lena Hellström-Westas, Sverre Wikström, Ingrid Hansen Pupp et al. (2015). „Cortical burst dynamics predict clinical outcome early in extremely preterm infants“. In: *Brain* 138.8, pp. 2206–2218 (cit. on p. 20).

Jabaudon, Denis (2017). „Fate and freedom in developing neocortical circuits“. In: *Nature communications* 8.1, p. 16042 (cit. on p. 9).

Jacquemin, Guillaume, Maria Benavente-Diaz, Samir Djaber, Aurélien Bore, Virginie Dangles-Marie et al. (2021). „Longitudinal high-resolution imaging through a flexible intravital imaging window“. In: *Science Advances* 7.25, eabg7663 (cit. on p. 140).

Jiang, Bin, Z Josh Huang, Bernardo Morales and Alfredo Kirkwood (2005). „Maturation of GABAergic transmission and the timing of plasticity in visual cortex“. In: *Brain Research Reviews* 50.1, pp. 126–133 (cit. on p. 25).

Jiang, Bin, Mario Trevino and Alfredo Kirkwood (2007). „Sequential development of long-term potentiation and depression in different layers of the mouse visual cortex“. In: *Journal of Neuroscience* 27.36, pp. 9648–9652 (cit. on p. 24).

Jiang, Xiaolong, Shan Shen, Cathryn R Cadwell, Philipp Berens, Fabian Sinz et al. (2015). „Principles of connectivity among morphologically defined cell types in adult neocortex“. In: *Science* 350.6264, aac9462 (cit. on p. 6).

Jiao, Yuanyuan, Chunzhao Zhang, Yuchio Yanagawa and Qian-Quan Sun (2006). „Major effects of sensory experiences on the neocortical inhibitory circuits“. In: *Journal of Neuroscience* 26.34, pp. 8691–8701 (cit. on pp. 25, 26).

Johansson, Johannes D (2010). „Spectroscopic method for determination of the absorption coefficient in brain tissue“. In: *Journal of biomedical optics* 15.5, pp. 057005–057005 (cit. on pp. 41, 62).

Jouvet-Mounier, Danièle, Liliane Astic and Daniel Lacote (1969). „Ontogenesis of the states of sleep in rat, cat, and guinea pig during the first postnatal month“. In: *Developmental Psychobiology: The Journal of the International Society for Developmental Psychobiology* 2.4, pp. 216–239 (cit. on p. 13).

Juczewski, Konrad, Jonathan A Koussa, Andrew J Kesner, Jeong O Lee and David M Lovinger (2020). „Stress and behavioral correlates in the head-fixed method: stress measurements, habituation dynamics, locomotion, and motor-skill learning in mice“. In: *Scientific reports* 10.1, pp. 1–19 (cit. on pp. 42, 90).

Kaas, Jon H (2011). „Neocortex in early mammals and its subsequent variations“. In: *Annals of the New York Academy of Sciences* 1225.1, pp. 28–36 (cit. on p. 2).

Kannan, Madhuvanthi, Garrett G Gross, Don B Arnold and Michael J Higley (2016). „Visual deprivation during the critical period enhances layer 2/3 GABAergic inhibition in mouse V1“. In: *Journal of Neuroscience* 36.22, pp. 5914–5919 (cit. on p. 26).

Karlen, Sarah J and Leah Krubitzer (2009). „Effects of bilateral enucleation on the size of visual and nonvisual areas of the brain“. In: *Cerebral Cortex* 19.6, pp. 1360–1371 (cit. on p. 23).

Karlen, SJ, DM Kahn and L Krubitzer (2006). „Early blindness results in abnormal corticocortical and thalamocortical connections“. In: *Neuroscience* 142.3, pp. 843–858 (cit. on p. 23).

Karniol-Tambour, Orren, David M Zoltowski, E Mika Diamanti, Lucas Pinto, David W Tank et al. (2022). „Modeling communication and switching nonlinear dynamics in multi-region neural activity“. In: *bioRxiv*, pp. 2022–09 (cit. on p. 39).

Kastli, Rahel, Rasmus Vighagen, Alexander van der Bourg, Ali Özgür Argunsah, Asim Iqbal et al. (2020). „Developmental divergence of sensory stimulus representation in cortical interneurons“. In: *Nature communications* 11.1, p. 5729 (cit. on pp. 13, 25, 94).

Katz, Lawrence C and Edward M Callaway (1992). „Development of local circuits in mammalian visual cortex“. In: *Annual review of neuroscience* 15.1, pp. 31–56 (cit. on p. 9).

Kätzel, Dennis and Gero Miesenböck (2014). „Experience-dependent rewiring of specific inhibitory connections in adult neocortex“. In: *PLoS biology* 12.2, e1001798 (cit. on pp. 22, 26).

Kätzel, Dennis, Boris V Zemelman, Christina Buetfering, Markus Wölfel and Gero Miesenböck (2011). „The columnar and laminar organization of inhibitory connections to neocortical excitatory cells“. In: *Nature neuroscience* 14.1, pp. 100–107 (cit. on pp. 3, 94, 146).

Kauvar, Isaac V, Timothy A Machado, Elle Yuen, John Kochalka, Minseung Choi et al. (2020). „Cortical observation by synchronous multifocal optical sampling reveals widespread population encoding of actions“. In: *Neuron* 107.2, pp. 351–367 (cit. on pp. 37, 41, 43, 57, 84, 90, 107, 139).

Keck, Tara, Volker Scheuss, R Irene Jacobsen, Corette J Wierenga, Ulf T Eysel et al. (2011). „Loss of sensory input causes rapid structural changes of inhibitory neurons in adult mouse visual cortex“. In: *Neuron* 71.5, pp. 869–882 (cit. on p. 26).

Keller, Daniel, Csaba Erö and Henry Markram (2018). „Cell densities in the mouse brain: a systematic review“. In: *Frontiers in neuroanatomy* 12, p. 83 (cit. on p. 3).

Kepecs, Adam and Gordon Fishell (2014). „Interneuron cell types are fit to function“. In: *Nature* 505.7483, pp. 318–326 (cit. on pp. 3–5, 94, 147).

Khalilov, Ilgam, Volodymyr Dzhala, Yehezkel Ben-Ari and Roustem Khazipov (1999). „Dual role of GABA in the neonatal rat hippocampus“. In: *Developmental neuroscience* 21.3-5, pp. 310–319 (cit. on p. 153).

Khalilov, Ilgam, Michel Le Van Quyen, Henri Gozlan and Yehezkel Ben-Ari (2005). „Epileptogenic actions of GABA and fast oscillations in the developing hippocampus“. In: *Neuron* 48.5, pp. 787–796 (cit. on pp. 29, 153).

Kharod, Shivani C, Seok Kyu Kang and Shilpa D Kadam (2019). „Off-label use of bumetanide for brain disorders: an overview“. In: *Frontiers in neuroscience* 13, p. 310 (cit. on p. 31).

Khazipov, Rustem and Heiko J Luhmann (2006). „Early patterns of electrical activity in the developing cerebral cortex of humans and rodents“. In: *Trends in neurosciences* 29.7, pp. 414–418 (cit. on pp. 19, 20).

Khazipov, Rustem, Anton Sirota, Xavier Leinekugel, Gregory L Holmes, Yehezkel Ben-Ari et al. (2004). „Early motor activity drives spindle bursts in the developing somatosensory cortex“. In: *Nature* 432.7018, pp. 758–761 (cit. on pp. 14, 16, 95).

Kilb, Werner (2021). „When are depolarizing GABAergic responses excitatory?“ In: *Frontiers in Molecular Neuroscience*, p. 290 (cit. on p. 28).

Kim, Tony Hyun and Mark J Schnitzer (2022). „Fluorescence imaging of large-scale neural ensemble dynamics“. In: *Cell* 185.1, pp. 9–41 (cit. on pp. 34, 36, 37, 41).

Kirischuk, Sergei, Anne Sinning, Oriane Blanquie, Jenq-Wei Yang, Heiko J Luhmann et al. (2017). „Modulation of neocortical development by early neuronal activity: physiology and pathophysiology“. In: *Frontiers in cellular neuroscience* 11, p. 379 (cit. on p. 95).

Kirkby, Lowry A, Georgeann S Sack, Alana Firl and Marla B Feller (2013). „A role for correlated spontaneous activity in the assembly of neural circuits“. In: *Neuron* 80.5, pp. 1129–1144 (cit. on pp. 15, 91, 92, 149).

Kirmse, Knut, Michael Kummer, Yury Kovalchuk, Otto W Witte, Olga Garaschuk et al. (2015). „GABA depolarizes immature neurons and inhibits network activity in the neonatal neocortex in vivo“. In: *Nature communications* 6.1, p. 7750 (cit. on pp. 29, 30, 151).

Kirmse, Knut and Chuanqiang Zhang (2022). „Principles of GABAergic signaling in developing cortical network dynamics“. In: *Cell Reports* 38.13, p. 110568 (cit. on p. 25).

Knöpfel, Thomas (2012). „Genetically encoded optical indicators for the analysis of neuronal circuits“. In: *Nature Reviews Neuroscience* 13.10, pp. 687–700 (cit. on pp. 37, 41).

Knott, Graham W, Charles Quairiaux, Christel Genoud and Egbert Welker (2002). „Formation of dendritic spines with GABAergic synapses induced by whisker stimulation in adult mice“. In: *Neuron* 34.2, pp. 265–273 (cit. on p. 23).

Kobayashi, Yohei, Zhanlei Ye and Takao K Hensch (2015). „Clock genes control cortical critical period timing“. In: *Neuron* 86.1, pp. 264–275 (cit. on p. 23).

Kohn, Adam, Amin Zandvakili and Matthew A Smith (2009). „Correlations and brain states: from electrophysiology to functional imaging“. In: *Current opinion in neurobiology* 19.4, pp. 434–438 (cit. on p. 145).

Kolbaev, Sergey N, Salim Sharopov, Paul W Dierkes, Heiko J Luhmann and Werner Kilb (2012). „Phasic GABAA-receptor activation is required to suppress epileptiform activity in the CA3 region of the immature rat hippocampus“. In: *Epilepsia* 53.5, pp. 888–896 (cit. on p. 29).

Komuro, Hitoshi and Pasko Rakic (1998). „Orchestration of neuronal migration by activity of ion channels, neurotransmitter receptors, and intracellular Ca2+ fluctuations“. In: *Journal of neurobiology* 37.1, pp. 110–130 (cit. on p. 15).

Kotak, Vibhakar C, Anne E Takesian and Dan H Sanes (2008). „Hearing loss prevents the maturation of GABAergic transmission in the auditory cortex“. In: *Cerebral Cortex* 18.9, pp. 2098–2108 (cit. on p. 25).

Kozberg, Mariel G, Ying Ma, Mohammed A Shaik, Sharon H Kim and Elizabeth MC Hillman (2016). „Rapid postnatal expansion of neural networks occurs in an environment of altered neurovascular and neurometabolic coupling“. In: *Journal of Neuroscience* 36.25, pp. 6704–6717 (cit. on pp. 52, 72, 88).

Kraft, Andrew W, Anish Mitra, Zachary P Rosenthal, Nico UF Dosenbach, Adam Q Bauer et al. (2020). „Electrically coupled inhibitory interneurons constrain long-range connectivity of cortical networks“. In: *Neuroimage* 215, p. 116810 (cit. on p. 10).

Kremkow, Jens, Laurent U Perrinet, Guillaume S Masson and Ad Aertsen (2010). „Functional consequences of correlated excitatory and inhibitory conductances in cortical networks“. In: *Journal of computational neuroscience* 28.3, pp. 579–594 (cit. on p. 153).

Kuhlman, Sandra J, Nicholas D Olivas, Elaine Tring, Taruna Ikrar, Xiangmin Xu et al. (2013). „A disinhibitory microcircuit initiates critical-period plasticity in the visual cortex“. In: *Nature* 501.7468, pp. 543–546 (cit. on p. 25).

Kuhlman, Sandra J, Elaine Tring and Joshua T Trachtenberg (2011). „Fast-spiking interneurons have an initial orientation bias that is lost with vision“. In: *Nature neuroscience* 14.9, pp. 1121–1123 (cit. on p. 12).

Kuroki, Satoshi, Takamasa Yoshida, Hidekazu Tsutsui, Mizuho Iwama, Reiko Ando et al. (2018). „Excitatory neuronal hubs configure multisensory integration of slow waves in association cortex“. In: *Cell reports* 22.11, pp. 2873–2885 (cit. on p. 157).

Labouesse, Marie A and Tommaso Patriarchi (2021). „A versatile GPCR toolkit to track in vivo neuromodulation: not a one-size-fits-all sensor“. In: *Neuropsychopharmacology* 46.12, pp. 2043–2047 (cit. on p. 37).

Lagerspetz, Kari YH (1966). „Postnatal development of thermoregulation in laboratory mice“. In: *Helgoländer Wissenschaftliche Meeresuntersuchungen* 14.1, pp. 559–571 (cit. on p. 48).

Lake, EM, Xinxin Ge, Xilin Shen, Peter Herman, Fahmeed Hyder et al. (2018). „Spanning spatiotemporal scales with simultaneous mesoscopic Ca2+ imaging and functional MRI“. In: *BioRXiv* (cit. on p. 39).

Lake, Evelyn MR and Michael J Higley (2022). „Building bridges: simultaneous multimodal neuroimaging approaches for exploring the organization of brain networks“. In: *Neurophotonics* 9.3, p. 032202 (cit. on pp. 1, 34, 38, 89).

Larkum, Matthew Evan, Jack Waters, Bert Sakmann and Fritjof Helmchen (2007). „Dendritic spikes in apical dendrites of neocortical layer 2/3 pyramidal neurons“. In: *Journal of Neuroscience* 27.34, pp. 8999–9008 (cit. on p. 84).

Larsen, Bart, Zaixu Cui, Azeez Adebimpe, Adam Pines, Aaron Alexander-Bloch et al. (2022). „A developmental reduction of the excitation: inhibition ratio in association cortex during adolescence“. In: *Science Advances* 8.5, eabj8750 (cit. on p. 21).

Le Magueresse, Corentin and Hannah Monyer (2013). „GABAergic interneurons shape the functional maturation of the cortex“. In: *Neuron* 77.3, pp. 388–405 (cit. on pp. 11, 28, 94).

Lee, Anthony T, Daniel Vogt, John L Rubenstein and Vikaas S Sohal (2014). „A class of GABAergic neurons in the prefrontal cortex sends long-range projections to the nucleus accumbens and elicits acute avoidance behavior“. In: *Journal of Neuroscience* 34.35, pp. 11519–11525 (cit. on p. 36).

Lee, Soo-Hyun, Peter W Land and Daniel J Simons (2007). „Layer-and cell-type-specific effects of neonatal whisker-trimming in adult rat barrel cortex“. In: *Journal of neurophysiology* 97.6, pp. 4380–4385 (cit. on p. 152).

Leighton, Alexandra H, Juliette E Cheyne, Gerrit J Houwen, Paloma P Maldonado, Fred De Winter et al. (2021). „Somatostatin interneurons restrict cell recruitment to retinally driven spontaneous activity in the developing cortex“. In: *Cell Reports* 36.1, p. 109316 (cit. on pp. 17, 36, 85, 146).

Leighton, Alexandra H and Christian Lohmann (2016). „The wiring of developing sensory circuits—from patterned spontaneous activity to synaptic plasticity mechanisms“. In: *Frontiers in neural circuits* 10, p. 71 (cit. on pp. 15, 91, 92, 149).

Leikos, Susanna, Anton Tokariev, Ninah Koolen, Päivi Nevalainen and Sampsa Vanhatalo (2020). „Cortical responses to tactile stimuli in preterm infants“. In: *European Journal of Neuroscience* 51.4, pp. 1059–1073 (cit. on p. 20).

Leitch, Elizabeth, Julie Coaker, Carol Young, Vandana Mehta and Evelyne Sernagor (2005). „GABA type-A activity controls its own developmental polarity switch in the maturing retina“. In: *Journal of Neuroscience* 25.19, pp. 4801–4805 (cit. on p. 27).

Lensjø, Kristian Kinden, Mikkel Elle Lepperød, Gunnar Dick, Torkel Hafting and Marianne Fyhn (2017). „Removal of perineuronal nets unlocks juvenile plasticity through network mechanisms of decreased inhibition and increased gamma activity“. In: *Journal of Neuroscience* 37.5, pp. 1269–1283 (cit. on p. 25).

Lewis, David A, Takanori Hashimoto and David W Volk (2005). „Cortical inhibitory neurons and schizophrenia“. In: *Nature Reviews Neuroscience* 6.4, pp. 312–324 (cit. on p. 26).

Li, Hong, Sofia Fertuzinhos, Ethan Mohns, Thomas S Hnasko, Matthijs Verhage et al. (2013). „Laminar and columnar development of barrel cortex relies on thalamocortical neurotransmission“. In: *Neuron* 79.5, pp. 970–986 (cit. on p. 12).

Li, Ye, Hui Lu, Pei-lin Cheng, Shaoyu Ge, Huatai Xu et al. (2012). „Clonally related visual cortical neurons show similar stimulus feature selectivity“. In: *Nature* 486.7401, pp. 118–121 (cit. on p. 10).

Lim, Lynette, Da Mi, Alfredo Llorca and Oscar Marín (2018). „Development and functional diversification of cortical interneurons“. In: *Neuron* 100.2, pp. 294–313 (cit. on pp. 5, 6, 11, 82, 94, 147, 156).

Lin, Michael Z and Mark J Schnitzer (2016). „Genetically encoded indicators of neuronal activity“. In: *Nature neuroscience* 19.9, pp. 1142–1153 (cit. on p. 37).

Linden, Nathaniel J, Dennis R Tabuena, Nicholas A Steinmetz, William J Moody, Steven L Brunton et al. (2021). „Go with the FLOW: visualizing spatiotemporal dynamics in optical widefield calcium imaging“. In: *Journal of the Royal Society Interface* 18.181, p. 20210523 (cit. on pp. 36, 91).

Lindsay, Grace W (2021). „Convolutional neural networks as a model of the visual system: Past, present, and future“. In: *Journal of cognitive neuroscience* 33.10, pp. 2017–2031 (cit. on p. 34).

Liu, Annie and Nathaniel N Urban (2017). „Prenatal and early postnatal odorant exposure heightens odor-evoked mitral cell responses in the mouse olfactory bulb“. In: *Eneuro* 4.5 (cit. on p. 15).

Liu, Guosong (2004). „Local structural balance and functional interaction of excitatory and inhibitory synapses in hippocampal dendrites“. In: *Nature neuroscience* 7.4, pp. 373–379 (cit. on p. 26).

Lo, Shun Qiang, Judy CG Sng and George J Augustine (2017). „Defining a critical period for inhibitory circuits within the somatosensory cortex“. In: *Scientific reports* 7.1, p. 7271 (cit. on pp. 25, 94).

Lodato, Simona and Paola Arlotta (2015). „Generating neuronal diversity in the mammalian cerebral cortex“. In: *Annual review of cell and developmental biology* 31, pp. 699–720 (cit. on pp. 4, 5, 9).

Lodato, Simona, Caroline Rouaux, Kathleen B Quast, Chanati Jantrachotechatchawan, Michèle Studer et al. (2011). „Excitatory projection neuron subtypes control the distribution of local inhibitory interneurons in the cerebral cortex“. In: *Neuron* 69.4, pp. 763–779 (cit. on p. 25).

Loepke, Andreas W, John C McCann, C Dean Kurth and John J McAuliffe (2006). „The physiologic effects of isoflurane anesthesia in neonatal mice“. In: *Anesthesia & Analgesia* 102.1, pp. 75–80 (cit. on p. 50).

Lohani, Sweyta, Andrew H Moberly, Hadas Benisty, Boris Landa, Miao Jing et al. (2022). „Spatiotemporally heterogeneous coordination of cholinergic and neocortical activity“. In: *Nature Neuroscience*, pp. 1–8 (cit. on p. 35).

Lokmane, Ludmilla, Rémi Proville, Nicolas Narboux-Nême, Ildiko Györy, Maryama Keita et al. (2013). „Sensory map transfer to the neocortex relies on pretarget ordering of thalamic axons“. In: *Current biology* 23.9, pp. 810–816 (cit. on p. 12).

Lombardi, Aniello, Heiko J Luhmann and Werner Kilb (2021). „Modelling the spatial and temporal constrains of the GABAergic influence on neuronal excitability“. In: *PLoS Computational Biology* 17.11, e1009199 (cit. on p. 28).

Long, Michael A, Scott J Cruikshank, Michael J Jutras and Barry W Connors (2005). „Abrupt maturation of a spike-synchronizing mechanism in neocortex“. In: *Journal of Neuroscience* 25.32, pp. 7309–7316 (cit. on p. 26).

Loos, Hendrik Van der and Thomas A Woolsey (1973). „Somatosensory cortex: structural alterations following early injury to sense organs“. In: *Science* 179.4071, pp. 395–398 (cit. on pp. 7, 22).

López-Bendito, Guillermina (2018). „Development of the thalamocortical interactions: past, present and future“. In: *Neuroscience* 385, pp. 67–74 (cit. on p. 8).

Loring, Matthew D, Eric E Thomson and Eva A Naumann (2020). „Whole-brain interactions underlying zebrafish behavior“. In: *Current Opinion in Neurobiology* 65, pp. 88–99 (cit. on p. 34).

Lu, Hung-Yun, Elizabeth S Lorenc, Hanlin Zhu, Justin Kilmarx, James Sulzer et al. (2021). „Multi-scale neural decoding and analysis“. In: *Journal of Neural Engineering* 18.4, p. 045013 (cit. on p. 37).

Lu, Jiangteng, Jason Tucciarone, Ying Lin and Z Josh Huang (2014). „Input-specific maturation of synaptic dynamics of parvalbumin interneurons in primary visual cortex“. In: *Proceedings of the National Academy of Sciences* 111.47, pp. 16895–16900 (cit. on p. 141).

Luccioli, Stefano, David Angulo-Garcia, Rosa Cossart, Arnaud Malvache, Laura Módol et al. (2018). „Modeling driver cells in developing neuronal networks“. In: *PLoS Computational Biology* 14.11, e1006551 (cit. on p. 94).

Luczak, Artur, Peter Barthó and Kenneth D Harris (2009). „Spontaneous events outline the realm of possible sensory responses in neocortical populations“. In: *Neuron* 62.3, pp. 413–425 (cit. on p. 155).

Luczak, Artur, Peter Bartho and Kenneth D Harris (2013). „Gating of sensory input by spontaneous cortical activity“. In: *Journal of Neuroscience* 33.4, pp. 1684–1695 (cit. on pp. 16, 91, 155).

Luhmann, Heiko J (2022). „Neurophysiology of the developing cerebral cortex: what we have learned and what we need to know“. In: *Frontiers in Cellular Neuroscience* 15, p. 814012 (cit. on pp. 2, 82).

Luhmann, Heiko J and Rustem Khazipov (2018). „Neuronal activity patterns in the developing barrel cortex“. In: *Neuroscience* 368, pp. 256–267 (cit. on pp. 10, 18, 92).

Luhmann, Heiko J, Werner Kilb and Sergei Kirischuk (2020). „Cajal–Retzius and subplate cells: transient cortical neurons and circuits with long-term impact“. In: *Synapse Development and Maturation*. Elsevier, pp. 485–505 (cit. on p. 2).

Luhmann, Heiko J, Anne Sinning, Jenq-Wei Yang, Vicente Reyes-Puerta, Maik C Stüttgen et al. (2016). „Spontaneous neuronal activity in developing neocortical networks: from single cells to large-scale interactions“. In: *Frontiers in neural circuits* 10, p. 40 (cit. on pp. 92, 149).

Ma, Hongtao, Samuel Harris, Redi Rahmani, Clay O Lacefield, Mingrui Zhao et al. (2014). „Wide-field in vivo neocortical calcium dye imaging using a convection-enhanced loading technique combined with simultaneous multiwavelength imaging of voltage-sensitive dyes and hemodynamic signals“. In: *Neurophotonics* 1.1, pp. 015003–015003 (cit. on p. 87).

Ma, Ying, Mohammed A Shaik, Sharon H Kim, Mariel G Kozberg, David N Thibodeaux et al. (2016). „Wide-field optical mapping of neural activity and brain haemodynamics: considerations and novel approaches“. In: *Philosophical Transactions of the Royal Society B: Biological Sciences* 371.1705, p. 20150360 (cit. on pp. 36, 71, 87).

Ma, Zilu, Yuncong Ma and Nanyin Zhang (2018). „Development of brain-wide connectivity architecture in awake rats“. In: *Neuroimage* 176, pp. 380–389 (cit. on p. 155).

MacDowell, Camden J, Brandy A Briones, Michael J Lenzi, Morgan L Gustison and Timothy J Buschman (2022). „Variability in sampling of cortex-wide neural dynamics explains individual differences in functional connectivity and behavioral phenotype“. In: *bioRxiv*, pp. 2022–01 (cit. on p. 139).

MacDowell, Camden J and Timothy J Buschman (2020). „Low-dimensional spatiotemporal dynamics underlie cortex-wide neural activity“. In: *Current Biology* 30.14, pp. 2665–2680 (cit. on pp. 40, 71, 138, 144).

MacDowell, Camden J, Alexandra Libby, Caroline I Jahn, Sina Tafazoli and Timothy J Buschman (2023). „Multiplexed Subspaces Route Neural Activity Across Brain-wide Networks“. In: *bioRxiv*, pp. 2023–02 (cit. on pp. 144, 155).

Machado, Timothy A, Isaac V Kauvar and Karl Deisseroth (2022). „Multiregion neuronal activity: the forest and the trees“. In: *Nature Reviews Neuroscience* 23.11, pp. 683–704 (cit. on pp. 33–37, 41, 82, 150).

Mackevicius, Emily L, Andrew H Bahle, Alex H Williams, Shijie Gu, Natalia I Denisenko et al. (2019). „Unsupervised discovery of temporal sequences in high-dimensional datasets, with applications to neuroscience“. In: *Elife* 8, e38471 (cit. on p. 144).

Madisen, Linda, Aleena R Garner, Daisuke Shimaoka, Amy S Chuong, Nathan C Klapoetke et al. (2015). „Transgenic mice for intersectional targeting of neural sensors and effectors with high specificity and performance“. In: *Neuron* 85.5, pp. 942–958 (cit. on pp. 41, 96).

Maffei, Arianna, Mary E Lambo and Gina G Turrigiano (2010). „Critical period for inhibitory plasticity in RodentBinocular V1“. In: *Journal of Neuroscience* 30.9, pp. 3304–3309 (cit. on p. 94).

Magno, Lorenza, Zeinab Asgarian, Valentina Pendolino, Theodora Velona, Albert Mackintosh et al. (2021). „Transient developmental imbalance of cortical interneuron subtypes presages long-term changes in behavior“. In: *Cell Reports* 35.11, p. 109249 (cit. on p. 156).

Makeig, Scott, Julie Onton et al. (2011). „ERP features and EEG dynamics: an ICA perspective“. In: *Oxford handbook of event-related potential components*, pp. 51–86 (cit. on pp. 54, 138).

Makino, Hiroshi, Chi Ren, Haixin Liu, An Na Kim, Neehar Kondapaneni et al. (2017). „Transformation of cortex-wide emergent properties during motor learning“. In: *Neuron* 94.4, pp. 880–890 (cit. on pp. 33, 35, 36, 71, 88, 139, 145).

Maravall, Miguel, Ingrid YY Koh, W Brent Lindquist and Karel Svoboda (2004). „Experience-dependent changes in basal dendritic branching of layer 2/3 pyramidal neurons during a critical period for developmental plasticity in rat barrel cortex“. In: *Cerebral cortex* 14.6, pp. 655–664 (cit. on p. 82).

Marcano-Reik, Amy Jo and Mark S Blumberg (2008). „The corpus callosum modulates spindle-burst activity within homotopic regions of somatosensory cortex in newborn rats“. In: *European Journal of Neuroscience* 28.8, pp. 1457–1466 (cit. on p. 16).

Marín, Oscar (2013). „Cellular and molecular mechanisms controlling the migration of neocortical interneurons“. In: *European Journal of Neuroscience* 38.1, pp. 2019–2029 (cit. on p. 5).

– (2016). „Developmental timing and critical windows for the treatment of psychiatric disorders“. In: *Nature medicine* 22.11, pp. 1229–1238 (cit. on p. 27).

Marín, Oscar and John LR Rubenstein (2001). „A long, remarkable journey: tangential migration in the telencephalon“. In: *Nature Reviews Neuroscience* 2.11, pp. 780–790 (cit. on pp. 5, 62, 82).

– (2003). „Cell migration in the forebrain“. In: *Annual review of neuroscience* 26.1, pp. 441–483 (cit. on p. 82).

Markicevic, Marija, Ben D Fulcher, Christopher Lewis, Fritjof Helmchen, Markus Rudin et al. (2020). „Cortical excitation: inhibition imbalance causes abnormal brain network dynamics as observed in neurodevelopmental disorders“. In: *Cerebral Cortex* 30.9, pp. 4922–4937 (cit. on pp. 18, 149).

Markicevic, Marija, Iurii Savvateev, Christina Grimm and Valerio Zerbi (2021). „Emerging imaging methods to study whole-brain function in rodent models“. In: *Translational Psychiatry* 11.1, p. 457 (cit. on p. 34).

Markram, Henry, Eilif Muller, Srikanth Ramaswamy, Michael W Reimann, Marwan Abdellah et al. (2015). „Reconstruction and simulation of neocortical microcircuitry“. In: *Cell* 163.2, pp. 456–492 (cit. on p. 6).

Marques-Smith, Andre, Daniel Lyngholm, Anna-Kristin Kaufmann, Jacqueline A Stacey, Anna Hoerder-Suabedissen et al. (2016). „A transient translaminar GABAergic interneuron circuit connects thalamo-cortical recipient layers in neonatal somatosensory cortex“. In: *Neuron* 89.3, pp. 536–549 (cit. on pp. 2, 9, 11, 18, 36, 94, 146, 147).

Martina, Marzia, Sébastien Royer and Denis Paré (2001). „Cell-type-specific GABA responses and chloride homeostasis in the cortex and amygdala“. In: *Journal of neurophysiology* 86.6, pp. 2887–2895 (cit. on p. 31).

Martini, Francisco J, Teresa Guillamón-Vivancos, Verónica Moreno-Juan, Miguel Valdeolmillos and Guillermina López-Bendito (2021). „Spontaneous activity in developing thalamic and cortical sensory networks“. In: *Neuron* 109.16, pp. 2519–2534 (cit. on pp. 12, 15, 17, 92).

Mathis, Alexander, Pranav Mamidanna, Kevin M Cury, Taiga Abe, Venkatesh N Murthy et al. (2018). „DeepLabCut: markerless pose estimation of user-defined body parts with deep learning“. In: *Nature neuroscience* 21.9, pp. 1281–1289 (cit. on p. 80).

Maya Vetencourt, José Fernando, Alessandro Sale, Alessandro Viegi, Laura Baroncelli, Roberto De Pasquale et al. (2008). „The antidepressant fluoxetine restores plasticity in the adult visual cortex.“ In: *Science* (cit. on p. 26).

Mayer, Christian, Christoph Hafemeister, Rachel C Bandler, Robert Machold, Renata Batista Brito et al. (2018). „Developmental diversification of cortical inhibitory interneurons“. In: *Nature* 555.7697, pp. 457–462 (cit. on p. 3).

Mazo, Camille, Antoine Nissant, Soham Saha, Enzo Peroni, Pierre-Marie Lledo et al. (2022). „Long-range GABAergic projections contribute to cortical feedback control of sensory processing“. In: *Nature Communications* 13.1, p. 6879 (cit. on pp. 11, 154).

McCormick, David A, Matthew J McGinley and David B Salkoff (2015). „Brain state dependent activity in the cortex and thalamus“. In: *Current opinion in neurobiology* 31, pp. 133–140 (cit. on p. 13).

McCormick, David A, Dennis B Nestvogel and Biyu J He (2020). „Neuromodulation of brain state and behavior“. In: *Annual review of neuroscience* 43, pp. 391–415 (cit. on pp. 13, 145).

McVea, David A, Majid H Mohajerani and Timothy H Murphy (2012). „Voltage-sensitive dye imaging reveals dynamic spatiotemporal properties of cortical activity after spontaneous muscle twitches in the newborn rat“. In: *Journal of Neuroscience* 32.32, pp. 10982–10994 (cit. on p. 36).

McVea, David A, Timothy H Murphy and Majid H Mohajerani (2016). „Large scale cortical functional networks associated with slow-wave and spindle-burst-related spontaneous activity“. In: *Frontiers in neural circuits* 10, p. 103 (cit. on p. 36).

– (2017). „Spontaneous activity synchronizes whisker-related sensorimotor networks prior to their maturation in the developing rat cortex“. In: *BioRxiv*, p. 176800 (cit. on pp. 1, 36, 91, 106).

Menon, Vinod (2011). „Large-scale brain networks and psychopathology: a unifying triple network model“. In: *Trends in cognitive sciences* 15.10, pp. 483–506 (cit. on p. 2).

– (2013). „Developmental pathways to functional brain networks: emerging principles“. In: *Trends in cognitive sciences* 17.12, pp. 627–640 (cit. on p. 1).

Menon, Vinod and Hyesang Chang (2021). „Emerging neurodevelopmental perspectives on mathematical learning“. In: *Developmental Review* 60, p. 100964 (cit. on p. 36).

Métin, Christine and Douglas O Frost (1989). „Visual responses of neurons in somatosensory cortex of hamsters with experimentally induced retinal projections to somatosensory thalamus.“ In: *Proceedings of the National Academy of Sciences* 86.1, pp. 357–361 (cit. on p. 8).

Mezzera, Cecilia and Guillermina Lopez-Bendito (2016). „Cross-modal plasticity in sensory deprived animal models: From the thalamocortical development point of view“. In: *Journal of chemical neuroanatomy* 75, pp. 32–40 (cit. on pp. 23, 24).

Minlebaev, Marat, Yehezkel Ben-Ari and Rustem Khazipov (2007). „Network mechanisms of spindle-burst oscillations in the neonatal rat barrel cortex in vivo“. In: *Journal of Neurophysiology* 97.1, pp. 692–700 (cit. on p. 29).

Minlebaev, Marat, Matthew Colonnese, Timur Tsintsadze, Anton Sirota and Roustem Khazipov (2011). „Early gamma oscillations synchronize developing thalamus and cortex“. In: *Science* 334.6053, pp. 226–229 (cit. on pp. 16, 17, 19, 24, 30).

Mitchell, Simon J and R Angus Silver (2003). „Shunting inhibition modulates neuronal gain during synaptic excitation“. In: *Neuron* 38.3, pp. 433–445 (cit. on p. 153).

Miyashita-Lin, Emily M, Robert Hevner, Karen Montzka Wassarman, Salvador Martinez and John LR Rubenstein (1999). „Early neocortical regionalization in the absence of thalamic innervation“. In: *Science* 285.5429, pp. 906–909 (cit. on pp. 7, 8).

Mizuno, Hidenobu, Tomoo Hirano and Yoshiaki Tagawa (2007). „Evidence for activity-dependent cortical wiring: formation of interhemispheric connections in neonatal mouse visual cortex requires projection neuron activity“. In: *Journal of Neuroscience* 27.25, pp. 6760–6770 (cit. on p. 106).

Mizuno, Hidenobu, Koji Ikezoe, Shingo Nakazawa, Takuya Sato, Kazuo Kitamura et al. (2018). „Patchwork-type spontaneous activity in neonatal barrel cortex layer 4 transmitted via thalamocortical projections“. In: *Cell reports* 22.1, pp. 123–135 (cit. on pp. 16, 18, 84, 92, 98, 109, 114, 141).

Mizuno, Hidenobu, Wenshu Luo, Etsuko Tarusawa, Yoshikazu M Saito, Takuya Sato et al. (2014). „NMDAR-regulated dynamics of layer 4 neuronal dendrites during thalamocortical reorganization in neonates“. In: *Neuron* 82.2, pp. 365–379 (cit. on pp. 18, 98, 114, 140).

Modol, Laura, Yannick Bollmann, Thomas Tressard, Agnès Baude, Alicia Che et al. (2020). „Assemblies of perisomatic GABAergic neurons in the developing barrel cortex“. In: *Neuron* 105.1, pp. 93–105 (cit. on pp. 10, 18, 19, 25, 36, 91, 92, 94, 95, 144, 156).

Mòdol, Laura, Vitor Hugo Sousa, Arnaud Malvache, Thomas Tressard, Agnes Baude et al. (2017). „Spatial embryonic origin delineates GABAergic hub neurons driving network dynamics in the developing entorhinal cortex“. In: *Cerebral Cortex* 27.9, pp. 4649–4661 (cit. on pp. 19, 36).

Mohajerani, Majid H, Allen W Chan, Mostafa Mohsenvand, Jeffrey LeDue, Rui Liu et al. (2013). „Spontaneous cortical activity alternates between motifs defined by regional axonal projections“. In: *Nature neuroscience* 16.10, pp. 1426–1435 (cit. on p. 138).

Mohan, Hemanth, Xu An, X Hermione Xu, Hideki Kondo, Shengli Zhao et al. (2023). „Cortical glutamatergic projection neuron types contribute to distinct functional subnetworks“. In: *Nature Neuroscience* 26.3, pp. 481–494 (cit. on p. 4).

Möhler, Hanns, J-M Fritschy, Florence Crestani, Takao Hensch and Uwe Rudolph (2004). „Specific GABAA circuits in brain development and therapy“. In: *Biochemical pharmacology* 68.8, pp. 1685–1690 (cit. on p. 26).

Mojtahedi, Nima, Yury Kovalchuk, Alexander Böttcher and Olga Garaschuk (2021). „Stable behavioral state-specific large scale activity patterns in the developing cortex of neonates“. In: *Cell Calcium* 98, p. 102448 (cit. on pp. 1, 14, 36, 86, 91, 141, 145).

Molnár, Zoltán and Gavin Clowry (2012). „Cerebral cortical development in rodents and primates“. In: *Progress in brain research* 195, pp. 45–70 (cit. on p. 19).

Molnár, Zoltán, Heiko J Luhmann and Patrick O Kanold (2020). „Transient cortical circuits match spontaneous and sensory-driven activity during development“. In: *Science* 370.6514, eabb2153 (cit. on pp. 16, 17).

Molyneaux, Bradley J, Paola Arlotta, Joao RL Menezes and Jeffrey D Macklis (2007). „Neuronal subtype specification in the cerebral cortex“. In: *Nature reviews neuroscience* 8.6, pp. 427–437 (cit. on pp. 4, 5).

Mongillo, Gianluigi, Simon Rumpel and Yonatan Loewenstein (2018). „Inhibitory connectivity defines the realm of excitatory plasticity“. In: *Nature neuroscience* 21.10, pp. 1463–1470 (cit. on p. 141).

Montagni, Elena, Francesco Resta, Emilia Conti, Alessandro Scaglione, Maria Pasquini et al. (2018). „Wide-field imaging of cortical neuronal activity with red-shifted functional indicators during motor task execution“. In: *Journal of Physics D: Applied Physics* 52.7, p. 074001 (cit. on p. 87).

Moore, Alexandra K, Aldis P Weible, Timothy S Balmer, Laurence O Trussell and Michael Wehr (2018). „Rapid rebalancing of excitation and inhibition by cortical circuitry“. In: *Neuron* 97.6, pp. 1341–1355 (cit. on p. 19).

Moore, Yvonne E, Leslie C Conway, Heike J Wobst, Nicholas J Brandon, Tarek Z Deeb et al. (2019). „Developmental regulation of KCC2 phosphorylation has long-term impacts on cognitive function“. In: *Frontiers in molecular neuroscience* 12, p. 173 (cit. on p. 31).

Morales, Bernardo, Se-Young Choi and Alfredo Kirkwood (2002). „Dark rearing alters the development of GABAergic transmission in visual cortex“. In: *Journal of Neuroscience* 22.18, pp. 8084–8090 (cit. on p. 25).

Moreno, Maria J, Binbing Ling and Danica B Stanimirovic (2020). „In vivo near-infrared fluorescent optical imaging for CNS drug discovery“. In: *Expert Opinion on Drug Discovery* 15.8, pp. 903–915 (cit. on p. 46).

Mori, Kensaku and Hitoshi Sakano (2011). „How is the olfactory map formed and interpreted in the mammalian brain?“ In: *Annual review of neuroscience* 34, pp. 467–499 (cit. on p. 15).

Morita, Kenji, Kunichika Tsumoto and Kazuyuki Aihara (2006). „Bidirectional modulation of neuronal responses by depolarizing GABAergic inputs“. In: *Biophysical journal* 90.6, pp. 1925–1938 (cit. on p. 28).

Mosley, Morgan, Charisma Shah, Kiriana A Morse, Stephen A Miloro, Melissa M Holmes et al. (2017). „Patterns of cell death in the perinatal mouse forebrain“. In: *Journal of Comparative Neurology* 525.1, pp. 47–64 (cit. on p. 9).

Mountcastle, Vernon B (1997). „The columnar organization of the neocortex.“ In: *Brain: a journal of neurology* 120.4, pp. 701–722 (cit. on pp. 10, 34).

Mukherjee, Didhiti, Alex J Yonk, Greta Sokoloff and Mark S Blumberg (2017). „Wakefulness suppresses retinal wave-related neural activity in visual cortex“. In: *Journal of neurophysiology* 118.2, pp. 1190–1197 (cit. on pp. 13, 14).

Mulholland, Haleigh N, Bettina Hein, Matthias Kaschube and Gordon B Smith (2021). „Tightly coupled inhibitory and excitatory functional networks in the developing primary visual cortex“. In: *Elife* 10, e72456 (cit. on pp. 105, 110, 130, 141).

Munz, Martin, Arjun Bharioke, Georg Kosche, Verónica Moreno-Juan, Alexandra Brignall et al. (2023). „Pyramidal neurons form active, transient, multilayered circuits perturbed by autism-associated mutations at the inception of neocortex“. In: *Cell* 186.9, pp. 1930–1949 (cit. on p. 30).

Murata, Yasunobu and Matthew T Colonnese (2016). „An excitatory cortical feedback loop gates retinal wave transmission in rodent thalamus“. In: *Elife* 5, e18816 (cit. on p. 16).

– (2018). „Thalamus controls development and expression of arousal states in visual cortex“. In: *Journal of Neuroscience* 38.41, pp. 8772–8786 (cit. on pp. 13, 14).

– (2019). „Regional heterogeneity of developing GABAergic interneuron excitation in vivo“. In: *bioRxiv*, p. 701862 (cit. on p. 94).

– (2020). „GABAergic interneurons excite neonatal hippocampus in vivo“. In: *Science advances* 6.24, eaba1430 (cit. on pp. 29, 30, 154).

Murphy, Timothy H, Jamie D Boyd, Federico Bolaños, Matthieu P Vanni, Gergely Silasi et al. (2016). „High-throughput automated home-cage mesoscopic functional imaging of mouse cortex“. In: *Nature communications* 7.1, p. 11611 (cit. on pp. 42, 90).

Murphy, Timothy H, Nicholas J Michelson, Jamie D Boyd, Tony Fong, Luis A Bolanos et al. (2020). „Automated task training and longitudinal monitoring of mouse mesoscale cortical circuits using home cages“. In: *Elife* 9, e55964 (cit. on p. 90).

Musall, Simon, Matthew T Kaufman, Ashley L Juavinett, Steven Gluf and Anne K Churchland (2019). „Single-trial neural dynamics are dominated by richly varied movements“. In: *Nature neuroscience* 22.10, pp. 1677–1686 (cit. on pp. 86, 88, 146).

Musall, Simon, Xiaonan R Sun, Hemanth Mohan, Xu An, Steven Gluf et al. (2023). „Pyramidal cell types drive functionally distinct cortical activity patterns during decision-making“. In: *Nature Neuroscience* 26.3, pp. 495–505 (cit. on pp. 4, 58, 86, 115, 146).

Nakamura, Mari, Patricia Valerio, Stitipragyan Bhumika and Tania Rinaldi Barkat (2020). „Sequential organization of critical periods in the mouse auditory system“. In: *Cell Reports* 32.8, p. 108070 (cit. on pp. 18, 118).

Nakazawa, Shingo and Takuji Iwasato (2021). „Spatial organization and transitions of spontaneous neuronal activities in the developing sensory cortex“. In: *Development, Growth & Differentiation* 63.6, pp. 323–339 (cit. on pp. 12, 15, 17, 19, 91–93, 150).

Nakazawa, Shingo, Yumiko Yoshimura, Masahiro Takagi, Hidenobu Mizuno and Takuji Iwasato (2020). „Developmental phase transitions in spatial organization of spontaneous activity in postnatal barrel cortex layer 4“. In: *Journal of Neuroscience* 40.40, pp. 7637–7650 (cit. on pp. 92, 109).

Narayanan, Rajeevan T, Robert Egger, Christiaan PJ de Kock and Marcel Oberlaender (2016). „Neuronal Cell Types in the Neocortex“. In: *Axons and Brain Architecture*. Elsevier, pp. 183–202 (cit. on p. 3).

Nardou, Romain, Yehezkel Ben-Ari and Ilgam Khalilov (2009). „Bumetanide, an NKCC1 antagonist, does not prevent formation of epileptogenic focus but blocks epileptic focus seizures in immature rat hippocampus“. In: *Journal of Neurophysiology* 101.6, pp. 2878–2888 (cit. on pp. 29, 153).

Nardou, Romain, Eastman M Lewis, Rebecca Rothhaas, Ran Xu, Aimei Yang et al. (2019). „Oxytocin-dependent reopening of a social reward learning critical period with MDMA“. In: *Nature* 569.7754, pp. 116–120 (cit. on p. 24).

Naskar, Shovan, Roberto Narducci, Edoardo Balzani, Andrzej W Cwetsch, Valter Tucci et al. (2019). „The development of synaptic transmission is time-locked to early social behaviors in rats“. In: *Nature communications* 10.1, p. 1195 (cit. on p. 13).

Naskar, Shovan, Jia Qi, Francisco Pereira, Charles R Gerfen and Soohyun Lee (2021). „Cell-type-specific recruitment of GABAergic interneurons in the primary somatosensory cortex by long-range inputs“. In: *Cell reports* 34.8, p. 108774 (cit. on p. 36).

Nelson, Sacha B and Vera Valakh (2015). „Excitatory/inhibitory balance and circuit homeostasis in autism spectrum disorders“. In: *Neuron* 87.4, pp. 684–698 (cit. on p. 26).

Newbold, Dillan J, Timothy O Laumann, Catherine R Hoyt, Jacqueline M Hampton, David F Montez et al. (2020). „Plasticity and spontaneous activity pulses in disused human brain circuits“. In: *Neuron* 107.3, pp. 580–589 (cit. on p. 20).

Ng, Philip, Cindy Beauchamp, Carole Evelegh, Robin Parks and Frank L Graham (2001). „Development of a FLP/frt system for generating helper-dependent adenoviral vectors“. In: *Molecular Therapy* 3.5, pp. 809–815 (cit. on p. 87).

Ni, Amy M, Douglas A Ruff, Joshua J Alberts, Jen Symmonds and Marlene R Cohen (2018). „Learning and attention reveal a general relationship between population activity and behavior“. In: *Science* 359.6374, pp. 463–465 (cit. on p. 40).

Niculescu, Dragos and Christian Lohmann (2014). „Gap junctions in developing thalamic and neocortical neuronal networks“. In: *Cerebral Cortex* 24.12, pp. 3097–3106 (cit. on p. 10).

Nietz, Angela K, Martha L Streng, Laurentiu S Popa, Russell E Carter, Evelyn Flaherty et al. (2022). „To be and not to be: Wide-field Ca2+ imaging reveals neocortical functional segmentation combines stability and flexibility“. In: *bioRxiv*, pp. 2022–09 (cit. on p. 103).

Nikolaou, Nikolas and Martin P Meyer (2015). „Lamination speeds the functional development of visual circuits“. In: *Neuron* 88.5, pp. 999–1013 (cit. on p. 6).

Nolan, Rory (2018). „Algorithms for the correction of photobleaching“. PhD thesis. University of Oxford (cit. on p. 60).

O'Connor, David, Francesca Mandino, Xilin Shen, Corey Horien, Xinxin Ge et al. (2022). „Functional network properties derived from wide-field calcium imaging differ with wakefulness and across cell type". In: *NeuroImage* 264, p. 119735 (cit. on p. 145).

Ohtaka-Maruyama, Chiaki (2020). „Subplate neurons as an organizer of mammalian neocortical development". In: *Frontiers in Neuroanatomy* 14, p. 8 (cit. on p. 8).

Okawa, Haruhisa, Mrinalini Hoon, Takeshi Yoshimatsu, Luca Della Santina and Rachel OL Wong (2014). „Illuminating the multifaceted roles of neurotransmission in shaping neuronal circuitry". In: *Neuron* 83.6, pp. 1303–1318 (cit. on p. 15).

Okun, Michael and Ilan Lampl (2008). „Instantaneous correlation of excitation and inhibition during ongoing and sensory-evoked activities". In: *Nature neuroscience* 11.5, pp. 535–537 (cit. on p. 128).

O'Leary, Dennis DM (1989). „Do cortical areas emerge from a protocortex?" In: *Trends in neurosciences* 12.10, pp. 400–406 (cit. on p. 7).

O'Leary, Dennis DM, Shen-Ju Chou and Setsuko Sahara (2007). „Area patterning of the mammalian cortex". In: *Neuron* 56.2, pp. 252–269 (cit. on p. 7).

Ota, Keisuke, Yasuhiro Oisi, Takayuki Suzuki, Muneki Ikeda, Yoshiki Ito et al. (2021). „Fast, cell-resolution, contiguous-wide two-photon imaging to reveal functional network architectures across multi-modal cortical areas". In: *Neuron* 109.11, pp. 1810–1824 (cit. on p. 38).

Owens, David F and Arnold R Kriegstein (2002). „Is there more to GABA than synaptic inhibition?" In: *Nature Reviews Neuroscience* 3.9, pp. 715–727 (cit. on p. 28).

O'Leary, Dennis DM and Setsuko Sahara (2008). „Genetic regulation of arealization of the neocortex". In: *Current opinion in neurobiology* 18.1, pp. 90–100 (cit. on p. 7).

Packer, Adam M and Rafael Yuste (2011). „Dense, unspecific connectivity of neocortical parvalbumin-positive interneurons: a canonical microcircuit for inhibition?" In: *Journal of Neuroscience* 31.37, pp. 13260–13271 (cit. on p. 25).

Pakan, Janelle MP, Scott C Lowe, Evelyn Dylda, Sander W Keemink, Stephen P Currie et al. (2016). „Behavioral-state modulation of inhibition is context-dependent and cell type specific in mouse visual cortex". In: *Elife* 5, e14985 (cit. on pp. 15, 145).

Palomero-Gallagher, Nicola and Karl Zilles (2019). „Cortical layers: Cyto-, myelo-, receptor-and synaptic architecture in human cortical areas". In: *Neuroimage* 197, pp. 716–741 (cit. on p. 6).

Panzeri, Stefano, Jakob H Macke, Joachim Gross and Christoph Kayser (2015). „Neural population coding: combining insights from microscopic and mass signals". In: *Trends in cognitive sciences* 19.3, pp. 162–172 (cit. on p. 91).

Park, Kicheon, Anuki C Liyanage, Alan P Koretsky, Yingtian Pan and Congwu Du (2021). „Optical imaging of stimulation-evoked cortical activity using GCaMP6f and jRGECO1a". In: *Quantitative Imaging in Medicine and Surgery* 11.3, p. 998 (cit. on p. 87).

Parker, Philip RL, Scott J Cruikshank and Barry W Connors (2009). „Stability of electrical coupling despite massive developmental changes of intrinsic neuronal physiology". In: *Journal of Neuroscience* 29.31, pp. 9761–9770 (cit. on p. 10).

Patterson, George H and David W Piston (2000). „Photobleaching in two-photon excitation microscopy". In: *Biophysical journal* 78.4, pp. 2159–2162 (cit. on pp. 58, 60, 61).

Peerboom, Carlijn and Corette J Wierenga (2021). „The postnatal GABA shift: a developmental perspective". In: *Neuroscience & Biobehavioral Reviews* 124, pp. 179–192 (cit. on pp. 30, 31, 154).

Penn, Anna A, Patricio A Riquelme, Marla B Feller and Carla J Shatz (1998). „Competition in retinogeniculate patterning driven by spontaneous activity“. In: *Science* 279.5359, pp. 2108–2112 (cit. on p. 15).

Perich, Matthew G and Kanaka Rajan (2020). „Rethinking brain-wide interactions through multi-region ‘network of networks’ models“. In: *Current opinion in neurobiology* 65, pp. 146–151 (cit. on p. 39).

Pessoa, Luiz (2023). „The entangled brain“. In: *Journal of Cognitive Neuroscience* 35.3, pp. 349–360 (cit. on p. 35).

Peters, Andrew J, Julie MJ Fabre, Nicholas A Steinmetz, Kenneth D Harris and Matteo Carandini (2021). „Striatal activity topographically reflects cortical activity“. In: *Nature* 591.7850, pp. 420–425 (cit. on p. 38).

Petit, Ted L, Janelle C LeBoutillier, Andrew Gregorio and Howard Libstug (1988). „The pattern of dendritic development in the cerebral cortex of the rat“. In: *Developmental Brain Research* 41.1-2, pp. 209–219 (cit. on p. 82).

Petrus, Emily, Amal Isaiah, Adam P Jones, David Li, Hui Wang et al. (2014). „Crossmodal induction of thalamocortical potentiation leads to enhanced information processing in the auditory cortex“. In: *Neuron* 81.3, pp. 664–673 (cit. on p. 24).

Picardo, Michel Aimé, Philippe Guigue, Paolo Bonifazi, Renata Batista-Brito, Camille Allene et al. (2011). „Pioneer GABA cells comprise a subpopulation of hub neurons in the developing hippocampus“. In: *Neuron* 71.4, pp. 695–709 (cit. on pp. 11, 154).

Piche, M, N Chabot, G Bronchti, D Miceli, F Lepore et al. (2007). „Auditory responses in the visual cortex of neonatally enucleated rats“. In: *Neuroscience* 145.3, pp. 1144–1156 (cit. on p. 23).

Pillow, Jonathan W and Mikio C Aoi (2017). „Is population activity more than the sum of its parts?“ In: *Nature neuroscience* 20.9, pp. 1196–1198 (cit. on pp. 33, 35).

Pines, Adam, Arielle S Keller, Bart Larsen, Maxwell Bertolero, Arian Ashourvan et al. (2023). „Development of top-down cortical propagations in youth“. In: *Neuron* 111.8, pp. 1316–1330 (cit. on pp. 20, 152).

Pines, Adam R, Bart Larsen, Zaixu Cui, Valerie J Sydnor, Maxwell A Bertolero et al. (2022). „Dissociable multi-scale patterns of development in personalized brain networks“. In: *Nature communications* 13.1, p. 2647 (cit. on pp. 1, 2).

Pinto, Lucas, Kanaka Rajan, Brian DePasquale, Stephan Y Thiberge, David W Tank et al. (2019). „Task-dependent changes in the large-scale dynamics and necessity of cortical regions“. In: *Neuron* 104.4, pp. 810–824 (cit. on p. 71).

Pisella, Lucie I, Jean-Luc Gaiarsa, Diabé Diabira, Jinwei Zhang, Ilgam Khalilov et al. (2019). „Impaired regulation of KCC2 phosphorylation leads to neuronal network dysfunction and neurodevelopmental pathology“. In: *Science signaling* 12.603, eaay0300 (cit. on p. 31).

Pnevmatikakis, Eftychios A and Andrea Giovannucci (2017). „NoRMCorre: An online algorithm for piecewise rigid motion correction of calcium imaging data“. In: *Journal of neuroscience methods* 291, pp. 83–94 (cit. on pp. 51, 52).

Polley, Daniel B, Eugen Kvašňák and Ron D Frostig (2004). „Naturalistic experience transforms sensory maps in the adult cortex of caged animals“. In: *Nature* 429.6987, pp. 67–71 (cit. on p. 23).

Poo, Cindy and Jeffry S Isaacson (2007). „An early critical period for long-term plasticity and structural modification of sensory synapses in olfactory cortex“. In: *Journal of Neuroscience* 27.28, pp. 7553–7558 (cit. on p. 24).

Porrero, Cesar, Pablo Rubio-Garrido, Carlos Avendaño and Francisco Clascá (2010). „Mapping of fluorescent protein-expressing neurons and axon pathways in adult and developing Thy1-eYFP-H transgenic mice“. In: *Brain research* 1345, pp. 59–72 (cit. on p. 62).

Pouchelon, Gabrielle, Deepanjali Dwivedi, Yannick Bollmann, Chimuanya K Agba, Qing Xu et al. (2021). „The organization and development of cortical interneuron presynaptic circuits are area specific“. In: *Cell reports* 37.6, p. 109993 (cit. on p. 143).

Pouchelon, Gabrielle, Frédéric Gambino, Camilla Bellone, Ludovic Telley, Ilaria Vitali et al. (2014). „Modality-specific thalamocortical inputs instruct the identity of postsynaptic L4 neurons“. In: *Nature* 511.7510, pp. 471–474 (cit. on pp. 8, 9).

Priya, Rashi, Mercedes Francisca Paredes, Theofanis Karayannis, Nusrath Yusuf, Xingchen Liu et al. (2018). „Activity regulates cell death within cortical interneurons through a calcineurin-dependent mechanism“. In: *Cell reports* 22.7, pp. 1695–1709 (cit. on pp. 10, 156).

Putignano, Elena, Giuseppina Lonetti, Laura Cancedda, Gianmichele Ratto, Mario Costa et al. (2007). „Developmental downregulation of histone posttranslational modifications regulates visual cortical plasticity“. In: *Neuron* 53.5, pp. 747–759 (cit. on p. 26).

Puxeddu, Maria Grazia, Joshua Faskowitz, Richard F Betzel, Manuela Petti, Laura Astolfi et al. (2020). „The modular organization of brain cortical connectivity across the human lifespan“. In: *NeuroImage* 218, p. 116974 (cit. on p. 138).

Puzerey, Pavel A and Roberto F Galán (2014). „On how correlations between excitatory and inhibitory synaptic inputs maximize the information rate of neuronal firing“. In: *Frontiers in computational neuroscience* 8, p. 59 (cit. on pp. 141, 153).

Quairiaux, Charles, Pierre Mégevand, Jozsef Z Kiss and Christoph M Michel (2011). „Functional development of large-scale sensorimotor cortical networks in the brain“. In: *Journal of Neuroscience* 31.26, pp. 9574–9584 (cit. on p. 91).

Quast, Kathleen B, Kevin Ung, Emmanouil Froudarakis, Longwen Huang, Isabella Herman et al. (2017). „Developmental broadening of inhibitory sensory maps“. In: *Nature Neuroscience* 20.2, pp. 189–199 (cit. on pp. 13, 36, 109, 141, 151).

Rahmati, Vahid, Knut Kirmse, Knut Holthoff, Lars Schwabe and Stefan J Kiebel (2017). „Developmental emergence of sparse coding: a dynamic systems approach“. In: *Scientific reports* 7.1, pp. 1–13 (cit. on pp. 18, 144).

Rahn, Rachel M, Lindsey M Brier, Annie R Bice, Matthew D Reisman, Joseph D Dougherty et al. (2022). „Functional connectivity of the developing mouse cortex“. In: *Cerebral Cortex* 32.8, pp. 1755–1768 (cit. on p. 155).

Raichle, Marcus E (2015). „The brain's default mode network“. In: *Annual review of neuroscience* 38, pp. 433–447 (cit. on p. 35).

Rakic, Pasko (1988). „Specification of cerebral cortical areas“. In: *Science* 241.4862, p. 170 (cit. on pp. 3, 7).

Rakic, Pasko, Albert E Ayoub, Joshua J Breunig and Martin H Dominguez (2009). „Decision by division: making cortical maps“. In: *Trends in neurosciences* 32.5, pp. 291–301 (cit. on p. 7).

Ramandi, Daniel, Nicholas J Michelson, Lynn A Raymond and Timothy H Murphy (2023). „Chronic multiscale resolution of mouse brain networks using combined mesoscale cortical imaging and subcortical fiber photometry“. In: *Neurophotonics* 10.1, p. 015001 (cit. on p. 39).

Ranasinghe, Sumudu, Grace Or, Eric Y Wang, Aiva Ievins, Merritt A McLean et al. (2015). „Reduced cortical activity impairs development and plasticity after neonatal hypoxia ischemia“. In: *Journal of Neuroscience* 35.34, pp. 11946–11959 (cit. on p. 22).

Ratzlaff, Eugene H and Amiram Grinvald (1991). „A tandem-lens epifluorescence macroscope: hundred-fold brightness advantage for wide-field imaging“. In: *Journal of neuroscience methods* 36.2-3, pp. 127–137 (cit. on pp. 43, 71, 85, 146).

Reetzke, Rachel, Zilong Xie, Fernando Llanos and Bharath Chandrasekaran (2018). „Tracing the trajectory of sensory plasticity across different stages of speech learning in adulthood“. In: *Current Biology* 28.9, pp. 1419–1427 (cit. on p. 22).

Reh, Rebecca K, Brian G Dias, Charles A Nelson III, Daniela Kaufer, Janet F Werker et al. (2020). „Critical period regulation across multiple timescales“. In: *Proceedings of the National Academy of Sciences* 117.38, pp. 23242–23251 (cit. on pp. 21, 22, 152).

Ren, Chi and Takaki Komiyama (2021). „Wide-field calcium imaging of cortex-wide activity in awake, head-fixed mice“. In: *STAR protocols* 2.4, p. 100973 (cit. on pp. 40, 86).

Rensing, Nicholas, Brianna Moy, Joseph L Friedman, Rafael Galindo and Michael Wong (2018). „Longitudinal analysis of developmental changes in electroencephalography patterns and sleep-wake states of the neonatal mouse“. In: *PloS one* 13.11, e0207031 (cit. on pp. 13, 42, 82, 146, 150).

Ribic, Adema (2020). „Stability in the face of change: lifelong experience-dependent plasticity in the sensory cortex“. In: *Frontiers in Cellular Neuroscience* 14, p. 76 (cit. on p. 24).

Richards, Sarah EV, Anna R Moore, Alice Y Nam, Shikhar Saxena, Suzanne Paradis et al. (2020). „Experience-dependent development of dendritic arbors in mouse visual cortex“. In: *Journal of Neuroscience* 40.34, pp. 6536–6556 (cit. on p. 82).

Richter, Daniel, Heiko J Luhmann and Werner Kilb (2010). „Intrinsic activation of GABAa receptors suppresses epileptiform activity in the cerebral cortex of immature mice“. In: *Epilepsia* 51.8, pp. 1483–1492 (cit. on p. 153).

Rochefort, Nathalie L, Olga Garaschuk, Ruxandra-Iulia Milos, Madoka Narushima, Nima Marandi et al. (2009). „Sparsification of neuronal activity in the visual cortex at eye-opening“. In: *Proceedings of the National Academy of Sciences* 106.35, pp. 15049–15054 (cit. on pp. 2, 18, 19, 142).

Roe, Anna W, Sarah L Pallas, Young H Kwon and Mriganka Sur (1992). „Visual projections routed to the auditory pathway in ferrets: receptive fields of visual neurons in primary auditory cortex“. In: *Journal of Neuroscience* 12.9, pp. 3651–3664 (cit. on p. 8).

Roerig, Birgit and Marla B Feller (2000). „Neurotransmitters and gap junctions in developing neural circuits“. In: *Brain research reviews* 32.1, pp. 86–114 (cit. on p. 16).

Romagnoni, Alberto, Matthew T Colonnese, Jonathan D Touboul and Boris S Gutkin (2020). „Progressive alignment of inhibitory and excitatory delay may drive a rapid developmental switch in cortical network dynamics“. In: *Journal of neurophysiology* 123.5, pp. 1583–1599 (cit. on p. 18).

Romero, Sandra, Ariel E Hight, Kameron K Clayton, Jennifer Resnik, Ross S Williamson et al. (2020). „Cellular and widefield imaging of sound frequency organization in primary and higher order fields of the mouse auditory cortex“. In: *Cerebral Cortex* 30.3, pp. 1603–1622 (cit. on pp. 84, 85).

Roy, Dheeraj S, Young-Gyun Park, Minyoung E Kim, Ying Zhang, Sachie K Ogawa et al. (2022). „Brain-wide mapping reveals that engrams for a single memory are distributed across multiple brain regions“. In: *Nature communications* 13.1, p. 1799 (cit. on p. 35).

Rubenstein, JLR and Michael M Merzenich (2003). „Model of autism: increased ratio of excitation/inhibition in key neural systems“. In: *Genes, Brain and Behavior* 2.5, pp. 255–267 (cit. on p. 26).

Rubino, Doug, Kay A Robbins and Nicholas G Hatsopoulos (2006). „Propagating waves mediate information transfer in the motor cortex“. In: *Nature neuroscience* 9.12, pp. 1549–1557 (cit. on p. 20).

Rudy, Bernardo, Gordon Fishell, SooHyun Lee and Jens Hjerling-Leffler (2011). „Three groups of interneurons account for nearly 100% of neocortical GABAergic neurons“. In: *Developmental neurobiology* 71.1, pp. 45–61 (cit. on pp. 3, 5).

Rupprecht, Peter, Stefano Carta, Adrian Hoffmann, Mayumi Echizen, Antonin Blot et al. (2021). „A database and deep learning toolbox for noise-optimized, generalized spike inference from calcium imaging“. In: *Nature neuroscience* 24.9, pp. 1324–1337 (cit. on pp. 58, 102).

Ruusuvuori, Eva, Ilya Kirilkin, Nikhil Pandya and Kai Kaila (2010). „Spontaneous network events driven by depolarizing GABA action in neonatal hippocampal slices are not attributable to deficient mitochondrial energy metabolism“. In: *Journal of Neuroscience* 30.46, pp. 15638–15642 (cit. on p. 29).

Rynes, Mathew L, Daniel A Surinach, Samantha Linn, Michael Laroque, Vijay Rajendran et al. (2021). „Miniaturized head-mounted microscope for whole-cortex mesoscale imaging in freely behaving mice“. In: *Nature methods* 18.4, pp. 417–425 (cit. on pp. 37, 150).

Ryugo, David K, Rebecca Ryugo, Albert Globus and Herbert P Killackey (1975). „Increased spine density in auditory cortex following visual or somatic deafferentation“. In: *Brain research* 90.1, pp. 143–146 (cit. on p. 23).

Sadeh, Sadra and Claudia Clopath (2020). „Patterned perturbation of inhibition can reveal the dynamical structure of neural processing“. In: *Elife* 9, e52757 (cit. on p. 144).

Sakata, Shuzo and Kenneth D Harris (2009). „Laminar structure of spontaneous and sensory-evoked population activity in auditory cortex“. In: *Neuron* 64.3, pp. 404–418 (cit. on p. 92).

Saleem, Aman B, Aslı Ayaz, Kathryn J Jeffery, Kenneth D Harris and Matteo Carandini (2013). „Integration of visual motion and locomotion in mouse visual cortex“. In: *Nature neuroscience* 16.12, pp. 1864–1869 (cit. on p. 35).

Särelä, Jaakko and Ricardo Vigário (2003). „Overlearning in marginal distribution-based ICA: analysis and solutions“. In: *The Journal of Machine Learning Research* 4, pp. 1447–1469 (cit. on pp. 54, 57).

Sava, Bogdan A, Rongqing Chen, Haiyan Sun, Heiko J Luhmann and Werner Kilb (2014). „Taurine activates GABAergic networks in the neocortex of immature mice“. In: *Frontiers in cellular neuroscience* 8, p. 26 (cit. on p. 29).

Saxena, Shreya and John P Cunningham (2019). „Towards the neural population doctrine“. In: *Current opinion in neurobiology* 55, pp. 103–111 (cit. on p. 33).

Saxena, Shreya, Ian Kinsella, Simon Musall, Sharon H Kim, Jozsef Meszaros et al. (2020). „Localized semi-nonnegative matrix factorization (LocaNMF) of widefield calcium imaging data“. In: *PLoS computational biology* 16.4, e1007791 (cit. on pp. 52, 61, 86, 87, 115).

Schielzeth, Holger, Niels J Dingemanse, Shinichi Nakagawa, David F Westneat, Hassen Allegue et al. (2020). „Robustness of linear mixed-effects models to violations of distributional assumptions“. In: *Methods in ecology and evolution* 11.9, pp. 1141–1152 (cit. on p. 105).

Schleicher, Axel, Katrin Amunts, Stefan Geyer, T Kowalski, T Schormann et al. (2000). „A stereological approach to human cortical architecture: identification and delineation of cortical areas“. In: *Journal of chemical neuroanatomy* 20.1, pp. 31–47 (cit. on p. 6).

Schneider, David M (2020). „Reflections of action in sensory cortex“. In: *Current opinion in neurobiology* 64, pp. 53–59 (cit. on p. 35).

Schotten, Michel Thiebaut de and Stephanie J Forkel (2022). „The emergent properties of the connected brain“. In: *Science* 378.6619, pp. 505–510 (cit. on pp. 1, 33).

Scott, Benjamin B, Stephan Y Thiberge, Caiying Guo, D Gowanlock R Tervo, Carlos D Brody et al. (2018). „Imaging cortical dynamics in GCaMP transgenic rats with a head-mounted widefield macroscope“. In: *Neuron* 100.5, pp. 1045–1058 (cit. on p. 40).

Seelke, Adele MH and Mark S Blumberg (2010). „Developmental appearance and disappearance of cortical events and oscillations in infant rats“. In: *Brain research* 1324, pp. 34–42 (cit. on p. 16).

Senna, Irene, Elena Andres, Ayelet McKyton, Itay Ben-Zion, Ehud Zohary et al. (2021). „Development of multisensory integration following prolonged early-onset visual deprivation“. In: *Current Biology* 31.21, pp. 4879–4885 (cit. on p. 157).

Seto-Ohshima, A, E Aoki, R Semba, PC Emson and CW Heizmann (1990). „Appearance of parvalbumin-specific immunoreactivity in the cerebral cortex and hippocampus of the developing rat and gerbil brain“. In: *Histochemistry* 94.6, pp. 579–589 (cit. on p. 147).

Shadi, Kamal, Eva Dyer and Constantine Dovrolis (2020). „Multisensory integration in the mouse cortical connectome using a network diffusion model“. In: *Network Neuroscience* 4.4, pp. 1030–1054 (cit. on p. 157).

Shaner, Nathan C, Michael Z Lin, Michael R McKeown, Paul A Steinbach, Kristin L Hazelwood et al. (2008). „Improving the photostability of bright monomeric orange and red fluorescent proteins“. In: *Nature methods* 5.6, pp. 545–551 (cit. on p. 69).

Sharopov, Salim, Paula Winkler, Rie Uehara, Aniello Lombardi, Lisa Halbhuber et al. (2019). „Allopregnanolone augments epileptiform activity of an in-vitro mouse hippocampal preparation in the first postnatal week“. In: *Epilepsy Research* 157, p. 106196 (cit. on p. 29).

Shemesh, Or A, Changyang Linghu, Kiryl D Piatkevich, Daniel Goodwin, Orhan Tunc Celiker et al. (2020). „Precision calcium imaging of dense neural populations via a cell-body-targeted calcium indicator“. In: *Neuron* 107.3, pp. 470–486 (cit. on p. 84).

Shen, Jing and Matthew T Colonnese (2016). „Development of activity in the mouse visual cortex“. In: *Journal of Neuroscience* 36.48, pp. 12259–12275 (cit. on p. 16).

Shenoy, Krishna V and Jonathan C Kao (2021). „Measurement, manipulation and modeling of brain-wide neural population dynamics“. In: *Nature communications* 12.1, p. 633 (cit. on p. 34).

Shepherd, Gordon M and Timothy B Rowe (2017). „Neocortical lamination: insights from neuron types and evolutionary precursors“. In: *Frontiers in neuroanatomy* 11, p. 100 (cit. on p. 6).

Sherrill, Samantha P, Nicholas M Timme, John M Beggs and Ehren L Newman (2020). „Correlated activity favors synergistic processing in local cortical networks in vitro at synaptically relevant timescales“. In: *Network Neuroscience* 4.3, pp. 678–697 (cit. on p. 153).

Shigematsu, Naoki, Akinori Nishi and Takaichi Fukuda (2019). „Gap junctions interconnect different subtypes of parvalbumin-positive interneurons in barrels and septa with connectivity unique to each subtype“. In: *Cerebral Cortex* 29.4, pp. 1414–1429 (cit. on p. 18).

Shimaoka, Daisuke, Kenneth D Harris and Matteo Carandini (2018). „Effects of arousal on mouse sensory cortex depend on modality“. In: *Cell reports* 22.12, pp. 3160–3167 (cit. on p. 35).

Shimizu-Okabe, Chigusa, Masamichi Yokokura, Akihito Okabe, Masahiko Ikeda, Kohji Sato et al. (2002). „Layer-specific expression of Cl- transporters and differential [Cl-] i in newborn rat cortex“. In: *Neuroreport* 13.18, pp. 2433–2437 (cit. on p. 27).

Sieben, Kay, Malte Bieler, Brigitte Röder and Ileana L Hanganu-Opatz (2015). „Neonatal restriction of tactile inputs leads to long-lasting impairments of cross-modal processing“. In: *PLoS biology* 13.11, e1002304 (cit. on pp. 156, 157).

Sieben, Kay, Brigitte Röder and Ileana L Hanganu-Opatz (2013). „Oscillatory entrainment of primary somatosensory cortex encodes visual control of tactile processing“. In: *Journal of Neuroscience* 33.13, pp. 5736–5749 (cit. on p. 157).

Siegel, Friederike, J Alexander Heimel, Judith Peters and Christian Lohmann (2012). „Peripheral and central inputs shape network dynamics in the developing visual cortex in vivo“. In: *Current Biology* 22.3, pp. 253–258 (cit. on pp. 16, 17, 19, 36, 85).

Siegel, Friederike and Christian Lohmann (2013). „Probing synaptic function in dendrites with calcium imaging“. In: *Experimental neurology* 242, pp. 27–32 (cit. on p. 83).

Silasi, Gergely, Dongsheng Xiao, Matthieu P Vanni, Andrew CN Chen and Timothy H Murphy (2016). „Intact skull chronic windows for mesoscopic wide-field imaging in awake mice“. In: *Journal of neuroscience methods* 267, pp. 141–149 (cit. on pp. 41, 61, 71, 82).

Simi, Alessandro and Michèle Studer (2018). „Developmental genetic programs and activity-dependent mechanisms instruct neocortical area mapping“. In: *Current opinion in neurobiology* 53, pp. 96–102 (cit. on p. 8).

Smith, Gordon B, Bettina Hein, David E Whitney, David Fitzpatrick and Matthias Kaschube (2018). „Distributed network interactions and their emergence in developing neocortex“. In: *Nature neuroscience* 21.11, pp. 1600–1608 (cit. on p. 36).

Sofroniew, Nicholas James, Daniel Flickinger, Jonathan King and Karel Svoboda (2016). „A large field of view two-photon mesoscope with subcellular resolution for in vivo imaging“. In: *elife* 5, e14472 (cit. on p. 38).

Sohal, Vikaas S, Feng Zhang, Ofer Yizhar and Karl Deisseroth (2009). „Parvalbumin neurons and gamma rhythms enhance cortical circuit performance“. In: *Nature* 459.7247, pp. 698–702 (cit. on p. 25).

Southwell, Derek G, Robert C Froemke, Arturo Alvarez-Buylla, Michael P Stryker and Sunil P Gandhi (2010). „Cortical plasticity induced by inhibitory neuron transplantation“. In: *Science* 327.5969, pp. 1145–1148 (cit. on p. 26).

Southwell, Derek G, Mercedes F Paredes, Rui P Galvao, Daniel L Jones, Robert C Froemke et al. (2012). „Intrinsically determined cell death of developing cortical interneurons“. In: *Nature* 491.7422, pp. 109–113 (cit. on pp. 9, 10, 156).

Spatazza, Julien, Henry HC Lee, Ariel A Di Nardo, Lorenzo Tibaldi, Alain Joliot et al. (2013). „Choroid-plexus-derived Otx2 homeoprotein constrains adult cortical plasticity“. In: *Cell reports* 3.6, pp. 1815–1823 (cit. on p. 26).

Srinivasan, Karpagam, Dino P Leone, Rosalie K Bateson, Gergana Dobreva, Yoshinori Kohwi et al. (2012). „A network of genetic repression and derepression specifies projection fates in the developing neocortex“. In: *Proceedings of the National Academy of Sciences* 109.47, pp. 19071–19078 (cit. on p. 9).

Staley, KEVIN J and ISTVAN Mody (1992). „Shunting of excitatory input to dentate gyrus granule cells by a depolarizing GABAA receptor-mediated postsynaptic conductance“. In: *Journal of neurophysiology* 68.1, pp. 197–212 (cit. on p. 28).

Stein, Valentin, Irm Hermans-Borgmeyer, Thomas J Jentsch and Christian A Hübner (2004). „Expression of the KCl cotransporter KCC2 parallels neuronal maturation and the emergence of low intracellular chloride“. In: *Journal of Comparative Neurology* 468.1, pp. 57–64 (cit. on p. 27).

Steinmetz, Nicholas A, Cagatay Aydin, Anna Lebedeva, Michael Okun, Marius Pachitariu et al. (2021). „Neuropixels 2.0: A miniaturized high-density probe for stable, long-term brain recordings“. In: *Science* 372.6539, eabf4588 (cit. on p. 150).

Steinmetz, Nicholas A, Christina Buetfering, Jerome Lecoq, Christian R Lee, Andrew J Peters et al. (2017). „Aberrant cortical activity in multiple GCaMP6-expressing transgenic mouse lines“. In: *eneuro* 4.5 (cit. on pp. 75, 77, 88, 90).

Stepien, Barbara K, Ronald Naumann, Anja Holtz, Jussi Helppi, Wieland B Huttner et al. (2020). „Lengthening neurogenic period during neocortical development causes a hallmark of neocortex expansion“. In: *Current Biology* 30.21, pp. 4227–4237 (cit. on p. 3).

Stern, Edward A, Miguel Maravall and Karel Svoboda (2001). „Rapid development and plasticity of layer 2/3 maps in rat barrel cortex in vivo“. In: *Neuron* 31.2, pp. 305–315 (cit. on pp. 22, 23).

Stevenson, Ian H and Konrad P Kording (2011). „How advances in neural recording affect data analysis“. In: *Nature neuroscience* 14.2, pp. 139–142 (cit. on pp. 33, 39, 40).

Stirman, Jeffrey N, Ikuko T Smith, Michael W Kudenov and Spencer L Smith (2016). „Wide field-of-view, multi-region, two-photon imaging of neuronal activity in the mammalian brain“. In: *Nature biotechnology* 34.8, pp. 857–862 (cit. on p. 38).

Stringer, Carsen, Marius Pachitariu, Nicholas Steinmetz, Matteo Carandini and Kenneth D Harris (2019a). „High-dimensional geometry of population responses in visual cortex“. In: *Nature* 571.7765, pp. 361–365 (cit. on pp. 40, 89).

Stringer, Carsen, Marius Pachitariu, Nicholas Steinmetz, Charu Bai Reddy, Matteo Carandini et al. (2019b). „Spontaneous behaviors drive multidimensional, brainwide activity“. In: *Science* 364.6437, eaav7893 (cit. on pp. 35, 155).

Suarez, Rodrigo, Laura R Fenlon, Roger Marek, Lilach Avitan, Pankaj Sah et al. (2014). „Balanced interhemispheric cortical activity is required for correct targeting of the corpus callosum“. In: *Neuron* 82.6, pp. 1289–1298 (cit. on p. 16).

Sukenik, Nirit, Oleg Vinogradov, Eyal Weinreb, Menahem Segal, Anna Levina et al. (2021). „Neuronal circuits overcome imbalance in excitation and inhibition by adjusting connection numbers“. In: *Proceedings of the National Academy of Sciences* 118.12, e2018459118 (cit. on p. 156).

Sulis Sato, Sebastian, Pietro Artoni, Silvia Landi, Olga Cozzolino, Riccardo Parra et al. (2017). „Simultaneous two-photon imaging of intracellular chloride concentration and pH in mouse pyramidal neurons in vivo“. In: *Proceedings of the National Academy of Sciences* 114.41, E8770–E8779 (cit. on p. 29).

Sych, Yaroslav, Aleksejs Fomins, Leonardo Novelli and Fritjof Helmchen (2022). „Dynamic reorganization of the cortico-basal ganglia-thalamo-cortical network during task learning“. In: *Cell Reports* 40.12, p. 111394 (cit. on pp. 35, 36).

Sydnor, Valerie J, Bart Larsen, Danielle S Bassett, Aaron Alexander-Bloch, Damien A Fair et al. (2021). „Neurodevelopment of the association cortices: Patterns, mechanisms, and implications for psychopathology“. In: *Neuron* 109.18, pp. 2820–2846 (cit. on p. 20).

Sydnor, Valerie J, Bart Larsen, Jakob Seidlitz, Azeez Adebimpe, Aaron F Alexander-Bloch et al. (2023). „Intrinsic activity development unfolds along a sensorimotor–association cortical axis in youth“. In: *Nature Neuroscience*, pp. 1–12 (cit. on pp. 20, 150).

Tabuena, Dennis R, Randy Huynh, Jenna Metcalf, Thomas Richner, Albrecht Stroh et al. (2022). „Large-scale waves of activity in the neonatal mouse brain in vivo occur almost exclusively during sleep cycles“. In: *Developmental Neurobiology* 82.7-8, pp. 596–612 (cit. on p. 36).

Tagawa, Yoshiaki, Hidenobu Mizuno and Tomoo Hirano (2008). „Activity-dependent development of interhemispheric connections in the visual cortex“. In: *Reviews in the Neurosciences* 19.1, pp. 19–28 (cit. on p. 16).

Takesian, Anne E, Luke J Bogart, Jeff W Lichtman and Takao K Hensch (2018). „Inhibitory circuit gating of auditory critical-period plasticity“. In: *Nature neuroscience* 21.2, pp. 218–227 (cit. on pp. 151, 153).

Takesian, Anne E and Takao K Hensch (2013a). „Balancing plasticity/stability across brain development“. In: *Progress in brain research* 207, pp. 3–34 (cit. on pp. 21, 24, 25, 152).

Takesian, Anne E, Vibhakar C Kotak, Neeti Sharma and Dan H Sanes (2013b). „Hearing loss differentially affects thalamic drive to two cortical interneuron subtypes“. In: *Journal of neurophysiology* 110.4, pp. 999–1008 (cit. on p. 25).

Tamamaki, Nobuaki and Ryohei Tomioka (2010). „Long-range GABAergic connections distributed throughout the neocortex and their possible function“. In: *Frontiers in neuroscience* 4, p. 202 (cit. on pp. 11, 36, 94, 154).

Tan, AYY, S Andoni and NJ Priebe (2013). „A spontaneous state of weakly correlated synaptic excitation and inhibition in visual cortex“. In: *Neuroscience* 247, pp. 364–375 (cit. on p. 143).

Tang, Lan and Michael J Higley (2020). „Layer 5 circuits in V1 differentially control visuomotor behavior“. In: *Neuron* 105.2, pp. 346–354 (cit. on p. 4).

Tang, Xin, Rudolf Jaenisch and Mriganka Sur (2021). „The role of GABAergic signalling in neurodevelopmental disorders“. In: *Nature Reviews Neuroscience* 22.5, pp. 290–307 (cit. on p. 2).

Taniguchi, Hiroki, Miao He, Priscilla Wu, Sangyong Kim, Raehum Paik et al. (2011). „A resource of Cre driver lines for genetic targeting of GABAergic neurons in cerebral cortex“. In: *Neuron* 71.6, pp. 995–1013 (cit. on pp. 4, 41, 62, 83, 146, 147).

Tarabykin, Victor, Anastassia Stoykova, Natalia Usman and Peter Gruss (2001). „Cortical upper layer neurons derive from the subventricular zone as indicated by Svet1 gene expression“. In: (cit. on p. 4).

Telley, Ludovic, Gulistan Agirman, Julien Prados, Nicole Amberg, Sabine Fièvre et al. (2019). „Temporal patterning of apical progenitors and their daughter neurons in the developing neocortex“. In: *Science* 364.6440, eaav2522 (cit. on p. 9).

Terada, Shin-Ichiro, Kenta Kobayashi, Masamichi Ohkura, Junichi Nakai and Masanori Matsuzaki (2018). „Super-wide-field two-photon imaging with a micro-optical device moving in post-objective space“. In: *Nature communications* 9.1, p. 3550 (cit. on p. 38).

Thivierge, Jean-Philippe (2009). „How does non-random spontaneous activity contribute to brain development?“ In: *Neural Networks* 22.7, pp. 901–912 (cit. on pp. 15, 92, 151).

Thomas, Cibu and Chris I Baker (2013). „Teaching an adult brain new tricks: a critical review of evidence for training-dependent structural plasticity in humans“. In: *Neuroimage* 73, pp. 225–236 (cit. on p. 22).

Thomson, Alex M and A Peter Bannister (2003). „Interlaminar connections in the neocortex“. In: *Cerebral cortex* 13.1, pp. 5–14 (cit. on p. 11).

Tiriac, Alexandre and Mark S Blumberg (2016). „Gating of reafference in the external cuneate nucleus during self-generated movements in wake but not sleep“. In: *Elife* 5, e18749 (cit. on p. 14).

Tiriac, Alexandre, Carlos Del Rio-Bermudez and Mark S Blumberg (2014). „Self-generated movements with “unexpected” sensory consequences“. In: *Current Biology* 24.18, pp. 2136–2141 (cit. on pp. 14, 16).

Tiriac, Alexandre, Brandt D Uitermarkt, Alexander S Fanning, Greta Sokoloff and Mark S Blumberg (2012). „Rapid whisker movements in sleeping newborn rats“. In: *Current biology* 22.21, pp. 2075–2080 (cit. on p. 92).

Tkatchenko, Tatiana V, Yimin Shen and Andrei V Tkatchenko (2010). „Analysis of postnatal eye development in the mouse with high-resolution small animal magnetic resonance imaging“. In: *Investigative ophthalmology & visual science* 51.1, pp. 21–27 (cit. on p. 15).

Toldi, József, Tamás Farkas and Béla Völgyi (1994). „Neonatal enucleation induces cross-modal changes in the barrel cortex of rat. A behavioural and electrophysiological study“. In: *Neuroscience letters* 167.1-2, pp. 1–4 (cit. on p. 23).

Tolner, Else A, Aminah Sheikh, Alexey Y Yukin, Kai Kaila and Patrick O Kanold (2012). „Subplate neurons promote spindle bursts and thalamocortical patterning in the neonatal rat somatosensory cortex“. In: *Journal of Neuroscience* 32.2, pp. 692–702 (cit. on pp. 17, 92).

Tomioka, Ryohei, Keiko Okamoto, Takahiro Furuta, Fumino Fujiyama, Takuji Iwasato et al. (2005). „Demonstration of long-range GABAergic connections distributed throughout the mouse neocortex“. In: *European Journal of Neuroscience* 21.6, pp. 1587–1600 (cit. on pp. 36, 94).

Tremblay, Robin, Soohyun Lee and Bernardo Rudy (2016). „GABAergic interneurons in the neocortex: from cellular properties to circuits“. In: *Neuron* 91.2, pp. 260–292 (cit. on pp. 3, 4).

Triplett, Marcus A, Lilach Avitan and Geoffrey J Goodhill (2018). „Emergence of spontaneous assembly activity in developing neural networks without afferent input“. In: *PLoS computational biology* 14.9, e1006421 (cit. on p. 91).

Tritsch, Nicolas X, Eunyoung Yi, Jonathan E Gale, Elisabeth Glowatzki and Dwight E Bergles (2007). „The origin of spontaneous activity in the developing auditory system“. In: *Nature* 450.7166, pp. 50–55 (cit. on pp. 14, 16, 91, 94).

Trujillo, Cleber A, Richard Gao, Priscilla D Negraes, Jing Gu, Justin Buchanan et al. (2019). „Complex oscillatory waves emerging from cortical organoids model early human brain network development“. In: *Cell stem cell* 25.4, pp. 558–569 (cit. on pp. 16, 19).

Tuncdemir, Sebnem N, Brie Wamsley, Floor J Stam, Fumitaka Osakada, Martyn Goulding et al. (2016). „Early somatostatin interneuron connectivity mediates the maturation of deep layer cortical circuits“. In: *Neuron* 89.3, pp. 521–535 (cit. on pp. 2, 9, 11, 18, 36, 94, 146, 147).

Turrigiano, Gina G and Sacha B Nelson (2004). „Homeostatic plasticity in the developing nervous system“. In: *Nature reviews neuroscience* 5.2, pp. 97–107 (cit. on p. 26).

Ugryumova, Nadya, Stephen John Matcher and Don P Attenburrow (2004). „Measurement of bone mineral density via light scattering“. In: *Physics in Medicine & Biology* 49.3, p. 469 (cit. on pp. 41, 62).

Ungerleider, Leslie G and James V Haxby (1994). „‘What’and ‘where’in the human brain“. In: *Current opinion in neurobiology* 4.2, pp. 157–165 (cit. on p. 34).

Urai, Anne E, Brent Doiron, Andrew M Leifer and Anne K Churchland (2022). „Large-scale neural recordings call for new insights to link brain and behavior“. In: *Nature neuroscience* 25.1, pp. 11–19 (cit. on pp. 33, 34, 36, 39, 40, 86).

Urrutia-Piñones, Jocelyn, Camila Morales-Moraga, Nicole Sanguinetti-González, Angelica P Escobar and Chiayu Q Chiu (2022). „Long-range gabaergic projections of cortical origin in brain function“. In: *Frontiers in Systems Neuroscience* 16 (cit. on pp. 11, 36, 83, 94, 154).

Vafaii, Hadi, Francesca Mandino, Gabriel Desrosiers-Gregoire, David O'Connor, Xinxin Ge et al. (2023). „Multimodal measures of spontaneous brain activity reveal both common and divergent patterns of cortical functional organization“. In: (cit. on pp. 39, 88).

Vagnoni, Cristiana, Liad J Baruchin, Filippo Ghezzi, Sara Ratti, Zoltán Molnár et al. (2020). „Ontogeny of the VIP+ interneuron sensory-motor circuit prior to active whisking“. In: *BioRxiv*, pp. 2020–07 (cit. on p. 36).

Valeeva, Guzel, Thomas Tressard, Marat Mukhtarov, Agnes Baude and Rustem Khazipov (2016). „An optogenetic approach for investigation of excitatory and inhibitory network GABA actions in mice expressing channelrhodopsin-2 in GABAergic neurons“. In: *Journal of Neuroscience* 36.22, pp. 5961–5973 (cit. on pp. 29, 153).

Valeeva, Guzel, Fliza Valiullina and Roustem Khazipov (2013). „Excitatory actions of GABA in the intact neonatal rodent hippocampus in vitro“. In: *Frontiers in cellular neuroscience* 7, p. 20 (cit. on p. 29).

Valiullina, Fliza, Dinara Akhmetshina, Azat Nasretdinov, Marat Mukhtarov, Guzel Valeeva et al. (2016). „Developmental changes in electrophysiological properties and a transition from electrical to chemical coupling between excitatory layer 4 neurons in the rat barrel cortex“. In: *Frontiers in neural circuits* 10, p. 1 (cit. on pp. 16, 18).

Valley, Matthew Taylor, Michael G Moore, Jun Zhuang, Natalia Mesa, Dan Castelli et al. (2020). „Separation of hemodynamic signals from GCaMP fluorescence measured with wide-field imaging“. In: *Journal of neurophysiology* 123.1, pp. 356–366 (cit. on pp. 52, 71, 75, 87).

Vanhatalo, Sampsa and Kai Kaila (2006). „Development of neonatal EEG activity: from phenomenology to physiology“. In: *Seminars in Fetal and Neonatal Medicine*. Vol. 11. 6. Elsevier, pp. 471–478 (cit. on pp. 16, 19, 20).

Vanni, Matthieu P, Allen W Chan, Matilde Balbi, Gergely Silasi and Timothy H Murphy (2017). „Mesoscale mapping of mouse cortex reveals frequency-dependent cycling between distinct macroscale functional modules“. In: *Journal of Neuroscience* 37.31, pp. 7513–7533 (cit. on pp. 46, 57, 86, 140).

Vanni, Matthieu P and Timothy H Murphy (2014). „Mesoscale transcranial spontaneous activity mapping in GCaMP3 transgenic mice reveals extensive reciprocal connections between areas of somatomotor cortex“. In: *Journal of Neuroscience* 34.48, pp. 15931–15946 (cit. on pp. 52, 75, 88).

Vasung, Lana, Caitlin K Rollins, Clemente Velasco-Annis, Hyuk Jin Yun, Jennings Zhang et al. (2020). „Spatiotemporal differences in the regional cortical plate and subplate volume growth during fetal development“. In: *Cerebral Cortex* 30.8, pp. 4438–4453 (cit. on p. 8).

Vickers, Neil J (2017). „Animal communication: when i'm calling you, will you answer too?“ In: *Current biology* 27.14, R713–R715 (cit. on p. 153).

Virtanen, Mari A, Pavel Uvarov, Christian A Hübner and Kai Kaila (2020). „NKCC1, an elusive molecular target in brain development: making sense of the existing data“. In: *Cells* 9.12, p. 2607 (cit. on p. 27).

Vora, Siddharth R, Esra D Camci and Timothy C Cox (2016). „Postnatal ontogeny of the cranial base and craniofacial skeleton in male C57BL/6J mice: a reference standard for quantitative analysis“. In: *Frontiers in Physiology* 6, p. 417 (cit. on pp. 63, 65).

Vue, Tou Yia, Melody Lee, Yew Ei Tan, Zachary Werkhoven, Lynn Wang et al. (2013). „Thalamic control of neocortical area formation in mice“. In: *Journal of Neuroscience* 33.19, pp. 8442–8453 (cit. on pp. 8, 9).

Vyas, Saurabh, Matthew D Golub, David Sussillo and Krishna V Shenoy (2020). „Computation through neural population dynamics“. In: *Annual review of neuroscience* 43, pp. 249–275 (cit. on p. 34).

Wang, Chang-Zheng, Jian Ma, Ye-Qian Xu, Shao-Na Jiang, Tian-Qi Chen et al. (2019). „Early-generated interneurons regulate neuronal circuit formation during early postnatal development“. In: *Elife* 8, e44649 (cit. on p. 36).

Wang, Chun-Lei, Lei Zhang, Yang Zhou, Jing Zhou, Xiu-Juan Yang et al. (2007). „Activity-dependent development of callosal projections in the somatosensory cortex“. In: *Journal of Neuroscience* 27.42, pp. 11334–11342 (cit. on pp. 16, 106).

Wang, Cong, Chigusa Shimizu-Okabe, Kazuo Watanabe, Akihito Okabe, Hideo Matsuzaki et al. (2002). „Developmental changes in KCC1, KCC2, and NKCC1 mRNA expressions in the rat brain“. In: *Developmental Brain Research* 139.1, pp. 59–66 (cit. on p. 27).

Wang, Doris D and Arnold R Kriegstein (2008). „GABA regulates excitatory synapse formation in the neocortex via NMDA receptor activation“. In: *Journal of Neuroscience* 28.21, pp. 5547–5558 (cit. on p. 30).

– (2011). „Blocking early GABA depolarization with bumetanide results in permanent alterations in cortical circuits and sensorimotor gating deficits“. In: *Cerebral cortex* 21.3, pp. 574–587 (cit. on pp. 30, 31).

Wang, Lang, Michelle Kloc, Yan Gu, Shaoyu Ge and Arianna Maffei (2013). „Layer-specific experience-dependent rewiring of thalamocortical circuits“. In: *Journal of Neuroscience* 33.9, pp. 4181–4191 (cit. on p. 24).

Wang, Quanxin, Song-Lin Ding, Yang Li, Josh Royall, David Feng et al. (2020). „The Allen mouse brain common coordinate framework: a 3D reference atlas“. In: *Cell* 181.4, pp. 936–953 (cit. on pp. 61, 86, 98, 99, 113, 140).

Wang, Xiao-Jing (2020). „Macroscopic gradients of synaptic excitation and inhibition in the neocortex“. In: *Nature Reviews Neuroscience* 21.3, pp. 169–178 (cit. on p. 142).

Wang, Yanshu, Jiangyang Zhang, Susumu Mori and Jeremy Nathans (2006). „Axonal growth and guidance defects in Frizzled3 knock-out mice: a comparison of diffusion tensor magnetic resonance imaging, neurofilament staining, and genetically directed cell labeling“. In: *Journal of Neuroscience* 26.2, pp. 355–364 (cit. on p. 83).

Wang, Yixiang, Maya Sanghvi, Alexandra Gribizis, Yueyi Zhang, Lei Song et al. (2021). „Efferent feedback controls bilateral auditory spontaneous activity“. In: *Nature communications* 12.1, p. 2449 (cit. on p. 36).

Wang, Yu-Feng, Xiao-Bing Gao and Anthony N van den Pol (2001). „Membrane properties underlying patterns of GABA-dependent action potentials in developing mouse hypothalamic neurons“. In: *Journal of Neurophysiology* 86.3, pp. 1252–1265 (cit. on p. 29).

Wang, Yundi, Jeffrey M LeDue and Timothy H Murphy (2022). „Multiscale imaging informs translational mouse modeling of neurological disease“. In: *Neuron* (cit. on pp. 34, 36, 37).

Wardle, Rinda A and Mu-ming Poo (2003). „Brain-derived neurotrophic factor modulation of GABAergic synapses by postsynaptic regulation of chloride transport“. In: *Journal of Neuroscience* 23.25, pp. 8722–8732 (cit. on p. 27).

Warm, Davide, Davide Bassetti, Jonas Schroer, Heiko J Luhmann and Anne Sinning (2022a). „Spontaneous Activity Predicts Survival of Developing Cortical Neurons“. In: *Frontiers in Cell and Developmental Biology* 10 (cit. on p. 10).

Warm, Davide, Jonas Schroer and Anne Sinning (2022b). „Gabaergic interneurons in early brain development: Conducting and orchestrated by cortical network activity“. In: *Frontiers in Molecular Neuroscience* 14, p. 807969 (cit. on p. 153).

Waters, Jack (2020). „Sources of widefield fluorescence from the brain“. In: *Elife* 9, e59841 (cit. on pp. 40, 41, 61–66, 71, 82–84, 145).

Waters, Jennifer C (2007). „Live-cell fluorescence imaging“. In: *Methods in cell biology* 81, pp. 115–140 (cit. on pp. 58, 63).

Wei, Ziqiang, Bei-Jung Lin, Tsai-Wen Chen, Kayvon Daie, Karel Svoboda et al. (2020). „A comparison of neuronal population dynamics measured with calcium imaging and electrophysiology“. In: *PLoS computational biology* 16.9, e1008198 (cit. on p. 89).

Weikum, Whitney M, Tim F Oberlander, Takao K Hensch and Janet F Werker (2012). „Prenatal exposure to antidepressants and depressed maternal mood alter trajectory of infant speech perception“. In: *Proceedings of the National Academy of Sciences* 109.supplement_2, pp. 17221–17227 (cit. on p. 26).

Weiser, Sydney C, Brian R Mullen, Desiderio Ascencio and James B Ackman (2021). „Data-driven filtration and segmentation of mesoscale neural dynamics“. In: *bioRxiv*, pp. 2020–12 (cit. on pp. 53, 54, 56, 57, 71, 86, 103, 139).

Wekselblatt, Joseph B, Erik D Flister, Denise M Piscopo and Cristopher M Niell (2016). „Large-scale imaging of cortical dynamics during sensory perception and behavior“. In: *Journal of neurophysiology* 115.6, pp. 2852–2866 (cit. on pp. 41, 91).

Welker, E, SB Rao, J Dorfl, P Melzer and H Van der Loos (1992). „Plasticity in the barrel cortex of the adult mouse: effects of chronic stimulation upon deoxyglucose uptake in the behaving animal“. In: *Journal of Neuroscience* 12.1, pp. 153–170 (cit. on p. 23).

Werker, Janet F and Takao K Hensch (2015). „Critical periods in speech perception: New directions“. In: *Annual review of psychology* 66, pp. 173–196 (cit. on p. 22).

West, Sarah L, Justin D Aronson, Laurentiu S Popa, Kathryn D Feller, Russell E Carter et al. (2022). „Wide-field calcium imaging of dynamic cortical networks during locomotion“. In: *Cerebral Cortex* 32.12, pp. 2668–2687 (cit. on pp. 88, 139).

Westneat, Mark W and Warren G Hal (1992). „Ontogeny of feeding motor patterns in infant rats: an electromyographic analysis of suckling and chewing.“ In: *Behavioral neuroscience* 106.3, p. 539 (cit. on p. 14).

White, Joshua J, Marife Arancillo, Trace L Stay, Nicholas A George-Jones, Sabrina L Levy et al. (2014). „Cerebellar zonal patterning relies on Purkinje cell neurotransmission“. In: *Journal of Neuroscience* 34.24, pp. 8231–8245 (cit. on pp. 12, 109, 141).

Whitehead, Kimberley, Ronit Pressler and Lorenzo Fabrizi (2017). „Characteristics and clinical significance of delta brushes in the EEG of premature infants“. In: *Clinical neurophysiology practice* 2, pp. 12–18 (cit. on p. 20).

Wiesel, Torsten N and David H Hubel (1963). „Effects of visual deprivation on morphology and physiology of cells in the cat's lateral geniculate body“. In: *Journal of neurophysiology* 26.6, pp. 978–993 (cit. on p. 21).

Winkler, Paula, Heiko J Luhmann and Werner Kilb (2019). „Taurine potentiates the anticonvulsive effect of the GABAA agonist muscimol and pentobarbital in the immature mouse hippocampus“. In: *Epilepsia* 60.3, pp. 464–474 (cit. on pp. 29, 153).

Winnubst, Johan, Erhan Bas, Tiago A Ferreira, Zhuhao Wu, Michael N Economo et al. (2019). „Reconstruction of 1,000 projection neurons reveals new cell types and organization of long-range connectivity in the mouse brain“. In: *Cell* 179.1, pp. 268–281 (cit. on p. 4).

Winnubst, Johan, Juliette E Cheyne, Dragos Niculescu and Christian Lohmann (2015). „Spontaneous activity drives local synaptic plasticity in vivo“. In: *Neuron* 87.2, pp. 399–410 (cit. on p. 17).

Wong, Fong Kuan, Kinga Bercsenyi, Varun Sreenivasan, Adrián Portalés, Marian Fernández-Otero et al. (2018). „Pyramidal cell regulation of interneuron survival sculpts cortical networks“. In: *Nature* 557.7707, pp. 668–673 (cit. on pp. 10, 156).

Wong, Rachel OL and Anirvan Ghosh (2002). „Activity-dependent regulation of dendritic growth and patterning“. In: *Nature reviews neuroscience* 3.10, pp. 803–812 (cit. on p. 15).

Woo, Nam-Sik, Jianming Lu, Roger England, Robert McClellan, Samuel Dufour et al. (2002). „Hyperexcitability and epilepsy associated with disruption of the mouse neuronal-specific K–Cl cotransporter gene“. In: *Hippocampus* 12.2, pp. 258–268 (cit. on p. 31).

Wosniack, Marina E, Jan H Kirchner, Ling-Ya Chao, Nawal Zabouri, Christian Lohmann et al. (2021). „Adaptation of spontaneous activity in the developing visual cortex“. In: *Elife* 10, e61619 (cit. on p. 17).

Xiao, Dongsheng, Matthieu P Vanni, Catalin C Mitelut, Allen W Chan, Jeffrey M LeDue et al. (2017). „Mapping cortical mesoscopic networks of single spiking cortical or sub-cortical neurons“. In: *Elife* 6, e19976 (cit. on pp. 38, 52, 75, 83).

Xiao, Dongsheng, Yuhao Yan and Timothy H Murphy (2023). „Mesotrode: chronic simultaneous mesoscale cortical imaging and subcortical or peripheral nerve spiking activity recording in mice.“ In: *bioRxiv*, pp. 2023–02 (cit. on p. 39).

Xu, Hong-Ping, Timothy J Burbridge, Ming-Gang Chen, Xinxin Ge, Yueyi Zhang et al. (2015). „Spatial pattern of spontaneous retinal waves instructs retinotopic map refinement more than activity frequency“. In: *Developmental neurobiology* 75.6, pp. 621–640 (cit. on p. 141).

Xu, Ning-long, Mark T Harnett, Stephen R Williams, Daniel Huber, Daniel H O'Connor et al. (2012). „Nonlinear dendritic integration of sensory and motor input during an active sensing task“. In: *Nature* 492.7428, pp. 247–251 (cit. on p. 84).

Xu, Weifeng, Siegrid Löwel and Oliver M Schlüter (2020a). „Silent synapse-based mechanisms of critical period plasticity“. In: *Frontiers in cellular neuroscience* 14, p. 213 (cit. on pp. 23, 24).

Xu, Xiaxia, Ileana L Hanganu-Opatz and Malte Bieler (2020b). „Cross-talk of low-level sensory and high-level cognitive processing: development, mechanisms, and relevance for cross-modal abilities of the brain“. In: *Frontiers in Neurorobotics* 14, p. 7 (cit. on p. 157).

Yamada, Akito, Naofumi Uesaka, Yasufumi Hayano, Toshihide Tabata, Masanobu Kano et al. (2010). „Role of pre-and postsynaptic activity in thalamocortical axon branching“. In: *Proceedings of the National Academy of Sciences* 107.16, pp. 7562–7567 (cit. on pp. 16, 92).

Yamamoto, Nobuhiko and Guillermina López-Bendito (2012). „Shaping brain connections through spontaneous neural activity“. In: *European Journal of Neuroscience* 35.10, pp. 1595–1604 (cit. on p. 92).

Yang, Jenq-Wei, Vicente Reyes-Puerta, Werner Kilb and Heiko J Luhmann (2016). „Spindle bursts in neonatal rat cerebral cortex“. In: *Neural plasticity* 2016 (cit. on p. 30).

Yao, Zizhen, Cindy TJ van Velthoven, Thuc Nghi Nguyen, Jeff Goldy, Adriana E Sedeno-Cortes et al. (2021). „A taxonomy of transcriptomic cell types across the isocortex and hippocampal formation“. In: *Cell* 184.12, pp. 3222–3241 (cit. on p. 4).

Yogev, Shaul and Kang Shen (2014). „Cellular and molecular mechanisms of synaptic specificity“. In: *Annual review of cell and developmental biology* 30, pp. 417–437 (cit. on p. 15).

Yu, Xin, Seungsoo Chung, Der-Yow Chen, Shumin Wang, Stephen J Dodd et al. (2012a). „Thalamocortical inputs show post-critical-period plasticity“. In: *Neuron* 74.4, pp. 731–742 (cit. on p. 25).

Yu, Yong-Chun, Shuijin He, She Chen, Yinghui Fu, Keith N Brown et al. (2012b). „Preferential electrical coupling regulates neocortical lineage-dependent microcircuit assembly“. In: *Nature* 486.7401, pp. 113–117 (cit. on p. 10).

Yuste, Rafael (2015). „From the neuron doctrine to neural networks“. In: *Nature reviews neuroscience* 16.8, pp. 487–497 (cit. on p. 33).

Yuste, Rafael, Alejandro Peinado and Lawrence C Katz (1992). „Neuronal domains in developing neocortex“. In: *Science* 257.5070, pp. 665–669 (cit. on p. 151).

Zehendner, Christoph M, Heiko J Luhmann and Jenq-Wei Yang (2013). „A simple and novel method to monitor breathing and heart rate in awake and urethane-anesthetized newborn rodents“. In: *PloS one* 8.5, e62628 (cit. on p. 74).

Zeng, Hongkui and Joshua R Sanes (2017). „Neuronal cell-type classification: challenges, opportunities and the path forward“. In: *Nature Reviews Neuroscience* 18.9, pp. 530–546 (cit. on p. 4).

Zhang, Jiayi, James B Ackman, Onkar S Dhande and Michael C Crair (2011a). „Visualization and manipulation of neural activity in the developing vertebrate nervous system“. In: *Frontiers in molecular neuroscience* 4, p. 43 (cit. on pp. 91, 149).

Zhang, Xiaohui, Eric C Landsness, Wei Chen, Hanyang Miao, Michelle Tang et al. (2022). „Automated sleep state classification of wide-field calcium imaging data via multiplex visibility graphs and deep learning“. In: *Journal of neuroscience methods* 366, p. 109421 (cit. on p. 146).

Zhang, Zhi, Y-Y Jiao and Q-Q Sun (2011b). „Developmental maturation of excitation and inhibition balance in principal neurons across four layers of somatosensory cortex“. In: *Neuroscience* 174, pp. 10–25 (cit. on pp. 19, 128).

Zhao, Yongxin, Satoko Araki, Jiahui Wu, Takayuki Teramoto, Yu-Fen Chang et al. (2011). „An expanded palette of genetically encoded Ca2+ indicators“. In: *Science* 333.6051, pp. 1888–1891 (cit. on p. 41).

Zhou, Feng, Weihua Zhao, Ziyu Qi, Yayuan Geng, Shuxia Yao et al. (2021). „A distributed fMRI-based signature for the subjective experience of fear“. In: *Nature communications* 12.1, p. 6643 (cit. on p. 35).

Zhou, Shanglin and Yuguo Yu (2018). „Synaptic EI balance underlies efficient neural coding“. In: *Frontiers in Neuroscience* 12, p. 46 (cit. on pp. 128, 132).

Zhuang, Jun, Lydia Ng, Derric Williams, Matthew Valley, Yang Li et al. (2017). „An extended retinotopic map of mouse cortex“. In: *elife* 6, e18372 (cit. on pp. 84, 85).

Znamenskiy, Petr, Mean-Hwan Kim, Dylan R Muir, Maria Florencia Iacaruso, Sonja B Hofer et al. (2018). „Functional selectivity and specific connectivity of inhibitory neurons in primary visual cortex“. In: *Biorxiv*, p. 294835 (cit. on p. 143).

Zucca, Stefano, Giulia D'Urso, Valentina Pasquale, Dania Vecchia, Giuseppe Pica et al. (2017). „An inhibitory gate for state transition in cortex“. In: *Elife* 6, e26177 (cit. on pp. 15, 145).

Zurita, Hector, Paul LC Feyen and Alfonso Junior Apicella (2018). „Layer 5 callosal parvalbumin-expressing neurons: a distinct functional group of GABAergic neurons“. In: *Frontiers in Cellular Neuroscience* 12, p. 53 (cit. on p. 94).